Novel roles for mTORC1-dependent translational control during synaptic homeostasis

by

Fredrick E. Henry

A dissertation submitted in partial fulfillment
of the requirements for the degree of
Doctor of Philosophy
(Neuroscience)
in the University of Michigan
2014

Doctoral Committee:

Associate Professor Michael M. A. Sutton, Chair
Associate Professor Diane C. Fingar
Associate Professor Roman Giger
Assistant Professor Ken Inoki
Professor Edward L. Stuenkel

“The man who believes that the secrets of the world are forever hidden lives in mystery and fear. Superstition will drag him down. The rain will erode the deeds of his life. But that man who sets himself the task of singling out the thread of order from the tapestry will by the decision alone have taken charge of the world and it is only by such taking charge that he will effect a way to dictate the terms of his own fate.”

― Cormac McCarthy, *Blood Meridian, or the Evening Redness in the West*

Fredrick E Henry © 2014

DEDICATION

To my family:

You people made me this way. Thank you.

ACKNOWLEDGMENTS

My participation in the work presented here would not have been possible without the gracious support of the many friends, family, and mentors who have shaped my personal and scientific development over the years. Scientific research provides myriad opportunities for failure, and I recognize my privileged position as someone who has received excellent guidance from my family and scientific colleagues, and can rely on an unshakable network of support to see me through challenging periods.

When I was young, my parents instilled in me the values of perseverance and hard work. It was by their example that I came to understand how much an individual could achieve through prolonged, determined effort. More than that, however, they encouraged me to seek my own path and find a calling in life that would ultimately provide genuine fulfillment. They each continue to inspire me, provide limitless encouragement, and sacrifice their own self-interests to better the lot of my siblings and me. I'll never be able to repay them for the opportunities they've given me, but I take heart in knowledge that my limited accomplishments have given them reason to be proud. I've also been fortunate to have close relationships with both my maternal and paternal grandparents, each of whom helped shape my natural curiosity and drive my academic progress. I may *still* not know my multiplication tables if it weren't for those critical afternoons at my grandmother's house after school. Finally, I've been lucky to be a member of a group of siblings that are genuinely interested in each other's lives. My brother and sister are two of the most interesting, intelligent people I've ever met and continue to be some of my biggest supporters.

In the years following my graduation from the University of North Carolina at Chapel Hill I had the good fortune of working in the lab of Dr. Linda Dykstra. I was relatively inexperienced with working in a lab setting, and Linda took a risk by hiring me as lab manager and technician. The Dykstra lab provided me with my first real experience in the day-to-day world of scientific research, and solidified my decision to pursue graduate training in neuroscience. Linda remained a valuable advisor to me throughout graduate school, and I sincerely believe I would not have taken the path I find myself on had she not provided that initial opportunity to try my hand at lab work.

I've come to appreciate that choosing the right advisor in graduate school is one of the most important decisions in a developing scientist's career, and I can say with confidence that I made the right choice in working with Mike Sutton. The Greek historian Plutarch stated that 'the mind is not a vessel to be filled but a fire to be kindled'. I find this nicely encapsulates the spirit of the relationship I came to have with Mike, where I was constantly pushed to think deeply about new ways to approach challenging problems. I knew from the start of my rotation in Mike's lab that he would be a fantastic mentor, and I consider myself lucky to be able to still call him a trusted advisor and valued friend after many years of working together.

Lastly, throughout my time in graduate school my friends have kept me aware of the unique moments of joy in life that can be found only once one leaves the lab. I'd likely be a much less interesting person now if it weren't for a core group of creative miscreants who occasionally had to remind me to actually experience my life as it was happening. I've made some of the truest friends I've ever known during my time in Ann Arbor, and I have no doubt their impact on my life will be felt long after I leave this place.

TABLE OF CONTENTS

DEDICATION ii

ACKNOWLEDGEMENTS iii

LIST OF FIGURES vi

LIST OF APPENDICES x

ABSTRACT xi

CHAPTER

I. Introduction: Locally mediated synaptic homeostasis in dendrites 1

II. Retrograde Changes in Presynaptic Function Driven by Dendritic mTORC1 34

III. Transynaptic signaling by BDNF as an immediate consequence of acute mTORC1 activation in dendrites 79

IV. Phospholipase D1 mediates a unique route to mTORC1 activation during synaptic homeostasis but not long term potentiation 115

V. Activity-dependent proteasome trafficking underlies state-dependent expression of synaptic homeostasis 150

VI. General Discussion 213

VII. Materials and Methods 233

APPENDICES 246

LIST OF FIGURES

2.1: Acute loss of excitatory synaptic drive activates dendritic mTORC1 signaling 56

2.2: mTORC1 is not involved in adaptive postsynaptic compensation induced by AMPAR blockade. 58

2.3: AMPAR blockade drives mTORC1-dependent enhancements in spontaneous and evoked vesicle release. 60

2.4: Postsynaptic mTORC1 activation is required for retrograde enhancement of presynaptic function 62

2.5: mTOR acts locally in dendrites to modulate presynaptic function after AMPAR blockade. 64

2.6: BDNF enhances presynaptic function downstream of mTORC1. 66

2.7: Compartmentalized enhancement in BDNF expression by AMPAR blockade requires mTORC1. 68

2.8: Sparse mTORC1 activation enhances synaptic efficacy in a cell-autonomous fashion. 70

2.9: Postsynaptic mTORC1 activation drives enhancement of presynaptic function via BDNF release. 72

3.1: Fast activation of neuronal mTORC1 via exogenous phosphatidic acid. 96

3.2: Enhanced BDNF synthesis is an immediate consequence of short-term mTORC1 activation. 98

3.3: Acute mTORC1 activation does not affect spine morphology. 100

3.4: PA enhances network activity via increases in excitatory neurotransmission.....................102

3.5: Enhanced presynaptic release emerges quickly after mTORC1 activation. 104

3.6: Functional effects of PA are sensitive to inhibitors of 4E-BP1 and p70S6K. 106

3.7: Postsynaptic BDNF expression is necessary for PA-induced changes in synaptic function. 108

4.1: PLD-dependent generation of PA during homeostatic plasticity but not cLTP 133

4.2: PLD signaling is required for adaptive presynaptic compensation 135

4.3: Altered postsynaptic function after cLTP does not require intact PLD signaling 137

4.4: PLD1 overexpression is sufficient to activate mTORC1 and drive changes in synapse function..139

4.5: PA binding to mTOR is necessary for enhanced mTORC1 kinase activity during synaptic homeostasis but not cLTP...141

4.6: PA binding to mTOR is necessary for altered synapse function during synaptic homeostasis but not cLTP. 143

4.7: Model: PLD/PA signaling is an upstream point of divergence during the activation of mTORC1 in unique forms of synapse plasticity. 145

5.1: Postsynaptic mTORC1 activation enhances presynaptic presynaptic release via synthesis of BDNF as a retrograde signal...180

5.2: RhebWT overexpression enhances mTORC1 activity in culture, and progressive loss of endogenous BDNF after siRNA magnetofection...183

5.3: Shared state-dependency of presynaptic enhancement driven by acute mTORC1 activation or loss of excitatory synaptic inputs. 185

5.4: The ubiquitin proteasome system operates presynaptically to mediate increased vesicle release after exposure to retrograde signal 187

5.5: Pharmacological inhibition of proteasome function blocks presynaptic augmentation after BDNF exposure or acute mTORC1 activation..189

5.6: Neuronal activity drives synaptic redistribution of the proteasome in axons.......................191

5.7: Spike blockade eliminates association between HA-tagged proteasome subunit and marker of presynaptic boutons...193

5.8: Active retention of proteasomes at presynaptic boutons 195

5.9: Phosphorylation of Rpt6 at S120 alters synaptic localization of the proteasome in axons. 197

5.10: HA-tagged Rpt6 WT and point mutants display unique distribution patterns in axons 199

5.11: Serine to alanine point mutation in Rpt6 eliminates activity dependent redistribution and blocks enhanced presynaptic function after loss of excitatory input or exposure to BDNF 201

5.12: Expression of Rpt6S120 eliminates homeostatic increases in spontaneous vesicle release 203

5.13: A phosphomimetic mutation in Rpt6 is sufficient to drive the proteasome to synapses and renders presynaptic compensation state-independent. 205

5.14: Expression of Rpt6 point mutants on its own does not alter vesicle pool characteristics...207

A2.1: Workflow of imaging analysis..263

A2.2: Example images of photobleaching apparent over a single 60s imaging session............264

A2.3: Example of plot produced by the function ‘bleach_correct_func’ 265

A2.4: Comparison of artifact corrected and uncorrected photobleaching timecourses 266

A2.5: Example of plot produced by the function ‘base_norm_func’ 267

A2.6: Illustration of processed used to determine rate of exocytosis 268

A2.7: Example of plot produced by the function ‘phluorin_graph_func’. 269

A2.8: Example of plot produced by the function ‘peak_norm_func’ 270

A2.9: Illustration of processed used to determine tau values for endocytosis............................271

A2.10: Example of plot produced by the function ‘phluorin_endograph_func’. 272

LIST OF APPENDICES

APPENDIX

I. A Fragile Balance at Synapses: New Evidence Supporting a Role for FMRP in Homeostatic Plasticity 246

II. Matlab as a tool for automated data analysis after optical assessment of presynaptic function....................253

ABSTRACT

Precisely tuned regulation of pre and post-synaptic communication depends on the coordinated action of protein synthesis and degradation mechanisms to shape the synaptic landscape. The mechanistic target of rapamycin complex 1 (mTORC1), a kinase involved in regulating translation initiation, has recently emerged as a critical player responsible for orchestrating dynamic changes in local protein synthesis in response to altered synaptic activity. Here we identify a novel mode of synaptic regulation conferred by local mTORC1-dependent signaling in dendrites, wherein mTORC1 activation gates a local retrograde signaling mechanism that drives changes in presynaptic function from apposed postsynaptic terminals. This unique trans-synaptic role for dendritic mTORC1 signaling is critically dependent on BDNF release, which serves to couple loss of excitatory synaptic drive with retrograde compensation of presynaptic function. Acute activation of mTORC1 signaling using the lipid second messenger phosphatidic acid (PA) or overexpression of the endogenous mTOR activation RhebGTPase is sufficient to exert a powerful influence on network function, which is also critically dependent on dendritic synthesis of BDNF as a retrograde signal. We identify an additional feature of the putative postsynaptic homeostatic sensor mechanism, showing that phospholipase D (PLD)-mediated hydrolysis of the lipid second messenger phosphatidic acid (PA) is a crucial component of the signaling pathway which relays homeostatic signals to postsynaptic mTORC1 after loss of excitatory input. Lastly, we find that mTORC1-dependent retrograde signaling acts in coordination with dynamic relocalization of the ubiquitin proteasome system to and from axonal boutons to adaptively regulate presynaptic function in the expression of synaptic homeostasis.

We show that increasing neuronal firing rates enriches proteasome accumulation at synaptic terminals, whereas inhibiting neuronal firing results in a dramatic redistribution away from synaptic terminals to non-synaptic areas. This altered localization is due, at least in part, to an activity-dependent active sequestration mechanism at presynaptic terminals. Moreover, activity-dependent phosphorylation of the Rpt6 subunit of the 19S proteasome is necessary and sufficient for axonal proteasome redistribution, and this altered localization plays a critical role in establishing mTORC1-dependent retrograde homeostatic changes in presynaptic function after loss of postsynaptic drive. Several monogenic neurodevelopmental conditions related to Autism Spectrum Disorder and Intellectual Disability share the common molecular phenotype of increased mTORC1 signaling. As such, a more thorough understanding of how mTORC1 regulates synaptic function may provide insights for targeting this signaling pathway as a therapeutic option for cognitive dysfunction.

CHAPTER I

Introduction:

Locally mediated synaptic homeostasis in dendrites

1.1 Introduction

In even the simplest of organisms, the cells of the nervous system are embedded in a complex array of individual units whose connections are subject to dynamic regulation. According to our current understanding, information is thought to be represented, processed or stored in this cellular lattice via a process that either depends on or itself elicits changes in the efficiency of signal transfer between individual synaptic contacts. We now have a detailed, if far from complete, biochemical account of various forms of synaptic plasticity that follow a positive feedback system: so-called Hebbian forms of plasticity such as long term potentiation (LTP) and long term depression (LTD) would fall into this category. Far less understood are types of plasticity involving synaptic adaptations to disruptive perturbations in baseline function, commonly described as “homeostatic”. This form of plasticity has been a topic of intensive study in recent years, and much effort has been spent in defining the phenomenon in functional terms (Turrigiano, 2008), identifying the molecular players involved in its induction and expression

(Poza and Goda, 2010), and advancing new conceptual approaches borrowed from control theory which may aid in our understanding of its proper physiological role (O'Leary and Wyllie, 2011). One defining feature of many forms of neuronal plasticity is a requirement for new protein synthesis in the implementation of persistent changes in synapse function (Kelleher et al., 2004). While altered gene expression is a critical for many aspects of long-lasting plasticity (Redondo and Morris, 2011), we now have a growing appreciation for the important role played by localized protein synthesis in dendrites (Sutton and Schuman, 2006). However, our understanding of how localized changes in protein translation may contribute to homeostatic forms of synaptic plasticity remains limited. The work presented here reflects an attempt to address a potential role for dendritic protein synthesis during the induction or maintenance of homeostatic changes in synaptic strength. Specifically, we have elucidated a novel function of the mechanistic target of rapamycin complex 1 (mTORC1) in a form of homeostatic plasticity involving fast acting, postsynaptic modulation of presynaptic function via a dendritically synthesized retrograde signal. We find that postsynaptic mTORC1 signaling regulates local translation of BDNF in dendrites, which functions to modulate neurotransmitter release from apposed presynaptic terminals. We then establish in greater mechanistic detail, the manner in which this form of synaptic homeostasis is implemented, revealing a role for postsynaptic phospholipase-D signaling in its induction, and activity dependent redistribution of the ubiquitin proteasome system in its expression. As a means of providing proper context and background for the work presented in subsequent chapters, what follows is a focused review of the cellular and molecular mechanisms involved in localized translation regulation in dendrites, an introduction to the multifaceted strategies utilized by neurons to implement synaptic homeostasis, and finally a summary of what is currently known about how local regulation of dendritic protein synthesis specifically mediates homeostatic forms of synaptic plasticity.

1.2 Localized translational control in dendrites: Mechanistic overview and cellular phenomenology

1.2.1 Translation initiation as a critical point of regulation

Protein translation occurs in three discrete stages, progressing through phases of initiation, elongation, and termination. Though there is evidence for each of these processes being highly regulated, it is generally believed that the signaling pathways which regulate translational control act on the initiation phase, which is the rate limiting step during which the ribosome is recruited to the mRNA (Roux and Topisirovic, 2012). At any given point in the life of a cell, the global population of mRNAs undergoing active translation is influenced by a wide range of intracellular and extracellular signaling cues, including nutrient availability, energy status, stress-related factors, or hormone and growth factor-induced signals (Sonenberg and Hinnebusch, 2009). Ultimately, this multitude of intra- and extracellular signals converge on a limited number of core pathways devoted to controlling translation initiation, largely via phosphorylation of numerous eukaryotic initiation factors (eIFs), of which at least 12 have been identified (Aitken and Lorch, 2012). These critical signaling pathways involve the activity of multiple interacting components, including PAK2, Cdk11, GSk3 and CK2 (Roux and Topisirovic, 2012). Among these, two pathways in particular are widely regarded as central to the dynamic control of translation initiation: the mechanistic target of rapamycin complex 1 (mTORC1), and family of mitogen-activated protein kinases (MAPKs).

The mechanistic target of rapamycin (mTOR) is a serine/threonine kinase which has a vital, evolutionarily conserved role in mediating cellular responses to stress and nutrient levels, and orchestrates cell growth and proliferation (Ma and Blenis, 2009). When associated with its binding partner raptor, mTOR operates in a collection of proteins known as mTOR complex 1 (mTORC1), other components of which include mLST8, PRAS40, and Deptor (Laplante and Sabatini, 2012). mTORC1 signaling can be influenced by a number of upstream signals emanating from phosphpoinositde 3-kinase (PI3K), AMPK, Ras/MAPK, or the RagGTPses (Hay and Sonenberg, 2004). Among the stimuli which impinge on these pathways and thus alter mTORC1-dependent control of protein translation, include growth factors, hormones, signals of energy status, and the availability of essential factors such as oxygen and amino acids (Laplante and Sabatini, 2012). Whether unique sets of stimuli recruit mTORC1 signaling in neurons is currently an open question, though one of central importance to the work presented in later chapters. mTORC1 has a number of well characterized downstream targets, including the p70S6Ks, eIF4E-binding proteins (4E-BPs), growth factor receptor-bound protein 10 (Grb10) and hATG1. Among these substrates, the effects of S6K and 4E-BP phosphorylation are the most thoroughly understood with respect to mTORC1-dependent regulation of translation initiation. When not phosphorylated, 4E-BP acts as a translational repressor, out-competing eIF4G for association with eIF4E, thus impairing formation of the eIF4F initiation complex (Pause et al., 1994). mTORC1 phosphorylates 4E-BP in a two-step process beginning at Thr37/Thr46, which biases subsequent phosphorylation at Ser65 and Thr70 (Gingras et al., 2001), resulting in the dissociation of 4E-BP from eIF4E and disinhibition of eIF4F complex formation. p70S6Ks, the other major players in mTORC1-mediated translational control, are members of the AGC kinase family and undergo mTOR-dependent phosphorylation at Thr229 and Thr389 (Fenton and Gout, 2011). S6Ks do not impinge on the translational machinery directly but instead influence the translation initiation process via phosphorylation of several downstream targets including eIF4B, programmed cell death 4 protein (PDCD4), and ribosomal protein S6. Phosphorylation of eIF4B promotes eIF4A-mediated helicase activity at secondary structures in the mRNA 5'UTR, thereby facilitating the scanning process by which 40S ribosomal subunits encounter initiation codons (Parsyan et al., 2011). PDCD4 normally serves to inhibit translation by binding to eIF4A and limiting assembly of the eIF4F preinitiation complex (Yang et al., 2003). Upon phosphorylation by p70S6K, PDCD4 is rapidly degraded by the ubiquitin proteasome system, thus releasing its inhibitory brake on translation (Dorello et al., 2006). Through phosphorylation of ribosomal protein S6 at 235/236 is a commonly used readout of mTORC1 kinase activity, the mechanism by which rpS6 influences translation initiation is not well understood. Indeed, MEFs harvested from knock-in mice containing alanine substitutions at all five phosphorylatable serine residues in rpS6 actually exhibit enhanced rates of protein synthesis (Ruvinsky et al., 2005), highlighting a complex role for rpS6 in translation initiation that require further characterization. Though mTORC1-mediated phosphorylation of p70S6K and 4E-BP are both vital for regulation of translation initiation, there is evidence to suggest divergent functional roles attributed to each, with the 4E-BPS largely playing a role in cell proliferation (Dowling et al., 2010), while activation of S6K mediates cell growth (Ohanna et al., 2005). Interestingly, while 4E-BP2 knockout mice display enhanced L-LTP resulting from disinhibited translation (Banko et al., 2005), neither S6K1 nor S6K2 knockout mice exhibit any functional alterations in protein-synthesis-dependent LTP (Antion et al., 2008), suggesting that a similar type of functional divergence in 4E-BP and S6K-mediated translational control might also be present in post-mitotic cells such as neurons.

MAPKs are ubiquitously expressed in eukaryotic cells and are involved in a variety of fundamental processes, including cell division, differentiation, motility, growth, and apoptosis (Pearson et al., 2001). The most commonly studied MAPKs, including ERK1/2, JNKs, and p38, exert their influence largely via phosphorylation of other kinases termed MAPK-activated protein kinases (MAPKAPKs). Of the multiple MAPKAPKs which have been identified, two have been directly linked to the regulation of translation initiation: MNK and RSK. MNK is believed to regulate formation of the preinitiation complex via phosphorylation of eIF4E at Ser209 (Waskiewicz et al., 1997). Though we do not have a complete understanding of how MNK's activity at eIF4E influences translation initiation, it has been suggested that phosphorylation of eIF4E changes its ability to bind the 5'-mRNA cap, given the relative location of the critical S209 residue to eIF4E's cap-binding region (Topisirovic et al., 2011). The RSK family, which is preferentially activated via ERK1/2 signaling (Carriere et al., 2008), regulates translation initiation through phosphorylation eIF4B, which enhances its affinity for the eIF3 complex (Shahbazian et al., 2006), and catalyzes eIF4A helicase activity (Rozen et al., 1990). Interestingly, RSK has also been shown to phosphorylate several core components of the mTOR signaling pathway including TSC2, Raptor, and Deptor (Mendoza et al., 2011), highlighting a potential role for shared feedback between the two major signaling arms involved in the regulation of translation initiation.

1.2.2 Local translation in dendrites: mRNA targets

Though many forms of synaptic plasticity and learning models are known to depend crucially on new protein synthesis (Huang et al., 1996), for many years research in this area historically focused on the role of changes in transcription to provide new gene products in response to plasticity-inducing stimuli. Interest in a potential role for localized control of protein synthesis at the level of translation in dendrites did not arrive until many years later with the discovery of polysomes in distal regions of dentate granule cells (Steward and Levy, 1982). This finding extended the initial discovery of ribosomes localized out in the proximal dendrites of primate spinal neurons (Bodian, 1965), and catalyzed the field to reassess the potential for local regulation of translation in the context of synaptic plasticity. Work from Schuman and colleagues provided the first functional demonstration of a requirement for local protein synthesis in dendrites in a form of synaptic plasticity in the mammalian brain (Kang and Schuman 1996). Findings from multiple labs have since verified a role for dendritic translation in various forms of synaptic plasticity, with multiple studies having provided functional evidence for the local synthesis of CamKIIa (Ouyang et al., 1999; Miller et al., 2002), AMPA receptor subunits (Grooms et al., 2006), NMDA receptor subunits (Benson, 1997), brain-derived neurotrophic factor (BDNF; Liao et al., 2012), Arc (Steward and Worley, 2001), and components of the translational machinery itself (Tsokas, et al., 2005). A comprehensive identification of the pool of dendritically localized mRNA transcripts subject to local translation regulation has been heavily sought after (Poon et al., 2006; Zhong et al., 2006), yet a comparison of recent attempts to characterize this group reveals a disconcertingly small degree of overlap among the multiple lists of putative dendritic transcripts generated by multiple labs. Recently, Schuman and colleagues (Cajigas et al., 2011) utilized an approach involving deep sequencing of extracted RNA from micro-dissected synaptic neuropil to generate what they consider to be a comprehensive list of the dendritic transcriptome in area CA1 of the rat hippocampus. In an effort to avoid spurious inclusion of any putative mRNA on the master list, the authors performed post-hoc verification and quantification of transcript concentration using a single mRNA visualization strategy. After subtracting transcripts that were experimentally determined to be enriched in glial or somatic preparations and controlling for contamination from mitochondrial or blood vessel derived genes, Schuman and colleagues were left with a group of 2550 transcripts believed to be uniquely localized to neuronal dendrites. This deep sequencing approach, which has extraordinary utility in detecting transcripts of low abundance, revealed that levels of dendritically localized transcripts differed by as much as three orders of magnitude. These results have important implications for future efforts to understand how dendrites may utilize localized translation regulation to homeostatically regulate synaptic strength.

1.3 Homeostatic plasticity: Global and local adaptive changes in synapse function

1.3.1 Achieving homeostasis: set points, sensors and feedback control

Forms of neuronal plasticity that have been deemed ‘homeostatic’ encompass a wide range of functional changes (Davis and Bezprozvanny, 2001; Marder and Goaillard, 2006; Lee et al., 2013). It will useful at the outset to define certain core features of homeostatic processes that are common to both biological and engineered systems, and to orient these features with respect to maintenance of synaptic function. As a foundational principle, homeostatic systems are those which display a constant output (Davis 2006). This output level is defined by a set point, which is either explicitly established or arises as an emergent property of many interacting forces. Taking neuronal firing properties as an example, it has been suggested that a set point for neuronal activity might be genetically defined via terminal selector transcription factors, akin to the process of cell fate specification (Davis, 2013, Hobert, 2011). However, as revealed by the pioneering work of Eve Marder’s group and others, nearly indistinguishable firing properties can arise from the combination of hugely diverse sets of neuronal conductances, which would seem to argue for an emergent, rather than precisely defined set point (Marder, 2011). Regardless of how it is defined, all homeostatic systems are equipped with sensors to detect deviations out of the appropriate output range established by the set point. Several putative homeostatic sensors have been identified in neurons, though accumulating evidence suggests that multiple sensors likely act simultaneously throughout the cell to regulate several homeostatically constrained aspects of neuronal function, as discussed below. Lastly, once outside the critical output range defined by the setpoint, homeostatic systems enact feedback control, mediated by 'effector' mechanisms, to return output levels to an acceptable range. Undoubtedly, neurons are endowed with a multitude of such effector mechanisms, the molecular identity of which corresponds to the particular feature of neural activity being regulated. Indeed, homeostatic forms of plasticity in neurons are believed to operate via three well-characterized types of changes, and as such, effector mechanisms at work in a given form of synaptic homeostasis are those that typically regulate shifts in intrinsic excitability, postsynaptic receptor content, or presynaptic release characteristics.

1.3.2 Possibility of multiple homeostatic sensors

The original characterization of the phenomenon now referred to as homeostatic plasticity were conducted by Turrigano and colleagues, who used dissociated cortical neurons to examine the impact of chronic changes in neuronal activity on synapse function driven by prolonged exposure to the voltage-gated Na-channel blocker TTX, or the ionotrpic GABA-A receptor blocker Bicuculine (Turrigiano et al., 1998). Prolonged periods of increased or decreased neuronal activity, after Bicuculine or TTX treatment, respectively, elicited a response originally referred to as 'synaptic scaling' due to the multiplicative nature of the shift in miniature excitatory postsynaptic current (mEPSC) amplitude. These initial observations implied a “global” shift in postsynaptic strength at every synapse across the cell. Conceptually, this has proven to be a logically appealing explanation for how neurons achieve the task of implementing changes in overall excitability while preserving relative synaptic weights of potentiated and depressed synapses distributed across the dendritic arbor (Turrigiano et al., 2011). Similar types of experiments utilizing pharmacological manipulation of synaptic responsiveness or spike rates have driven the field of homeostatic plasticity through much of its development. Though these types of approaches have the advantage of ease of use, they are coarse manipulations and may obscure the nature of the neuronal homeostat and the types of stimuli to which it may be sensitive. This problem is particularly relevant in experiments in dissociated cells where manipulations primarily designed to perturb spike rates (TTX, Bicuculine) also exert effects on levels of synaptic input. It has long been an assumption that homeostatic mechanisms operate in neurons in order to maintain firing rates within some defined range (Turrigiano and Nelson, 2004; Turrigiano 2008). This assumption is not without reason, as cells are clearly sensitive to prolonged changes in spike output. For example, cell-autonomous silencing of action potential firing via somatic-localized perfusion of TTX triggers compensatory increases in AMPAR content (Ibata et al., 2008). Additionally, diminished spike rate via overexpression of the inwardly rectifying K+ channel Kir2.1 results in an increase in both synapse number and function, depending on developmental time period at which experimental manipulations are performed (Burrone et al., 2002). This sensitivity to firing rate is bidirectional, as prolonged elevation of spike output via intermittent optical stimulation in ChR2 expressing cells leads to adaptive decrements in both AMPAR and NMDAR currents (Goold and Nicoll, 2010). These data suggest the existence of a cell-autonomous homeostatic sensor that is sensitive to firing rates, and utilizes changes in transcriptional output to exert cell wide changes in synapse number or function. Such a mechanism would correspond well with proposed utility of global forms of “synaptic scaling” (Turrigiano, 2008).

Likely operating in concert with homeostatic sensors of cell firing rate, powerful evidence from recent studies suggests that an additional homeostatic mechanism may be at work inside neurons; one sensitive to changes in and designed to regulate ongoing levels of synaptic input. A putative synaptic homeostat operating in neuronal dendrites would be well positioned to influence both pre and post synaptic function in an effort to align the rate and intensity of information transfer across the synaptic cleft. Indeed, it has been know for several years that the functional properties of presynaptic inputs are exquisitely sensitive to the identity and activity levels of their postsynaptic partners. For example, $Ca2^+$ influx and vesicle release properties at individual boutons from a single pyramidal cell show different characteristics depending on whether they form synapses onto bitufted or multipolar interneurons (Koester and Johnston, 2005). More recently, the release probability of axon terminals emanating from a single cell were shown to differ markedly when forming synapses on different branches of the same target cell, with synapses impinging on the same branch displaying similar rates of vesicle release (Branco et al., 2008). Remarkably, presynaptic release properties were demonstrated to adaptively compensate for branch-specific changes in depolarization, implying the existence of a locally implemented homeostatic mechanism that regulates steady-state levels of synaptic communication (Branco et al., 2008). A complementary set of experiments making use of novel genetic approaches to manipulate activity levels at individual synaptic inputs have demonstrated that single synapses can actually exhibit robust homeostatic responses. For instance, excitatory synapses in which the presynapitc terminal has been subject to diminished action potential firing via overexpression of Kir2.1, display increases in immunoreactivity against AMPAR subunits (Hou et al., 2008) and enhanced AMPAR current evoked by focal uncaging of glutamate (Beique et al., 2011). This effect is bidirectional, as repeated activation of individual excitatory synapses via light-activated glutamate receptors (LiGluR) results in NMDAR-dependent endocytosis of AMPARs and a weakening of synaptic strength (Hou et al., 2011). These experiments suggest that at least one set of mechanisms involved in responding to deviations from a putative set point are sensitive to small changes in synaptic input, perhaps via "sensors" at individual synapses or dendritic branches.

These data highlight a growing recognition of the important differences between globally and locally manifested forms of synaptic homeostasis, but it is possible to distinguish unique signaling pathways or induction paradigms that would indicate mechanistically unique sensors for synaptic input and spike rate? Work from the Chen lab suggests that Retinoic Acid (RA) synthesis might function in a pathway sensitive to synaptic blockade but not action potential (AP) inhibition. Postsynaptic adaptation produced by prolonged AP blockade (TTX, 48Hr) is blocked by transcription inhibitors such as actinomysin-D, is not sensitive to blockers of RA synthesis such as DEAB (Soden and Chen, 2010), and does not promote internal RA-synthesis (Wang et al., 2011A). In contrast, postsynaptic compensation induced via concurrent AP + excitatory synapse blockade (TTX+APV) is not sensitive to transcription inhibition, and reliably results in internal RA synthesis. Another clear indication that AP blockade alone exerts effects on synaptic strength that are mediated by a separate pathway than that utilized in response to blockade of synaptic receptors comes from the work of Hall and colleagues (Wang et al., 2011B). Neurons from transgenic mice in which the GluN2B subunit of the NMDAR is replaced with GluN2A throughout development display little indication of gross synaptic malformation or impairment in excitatory neurotransmission, yet are completely deficient in synaptic compensation under conditions of TTX+APV treatment. After prolonged periods of pike blockade with TTX, however, these cells exhibit homeostatic increases in mEPSC amplitude that are identical to responses seen in neurons from WT mice (Wang et al., 2011B). Collectively, these data point to the existence multiple components acting as part of a locally implemented homeostatic response system operating in dendrites, the molecular identities of which are just beginning to be reveled.

1.3.3 Trans-synaptic signaling by retrograde signals during HSP

The type of locally implemented, dynamic coupling between pre and postsynaptic function described by Branco et al. (2008) implies the existence of a retrograde signaling mechanism that could signal changes in postsynaptic responsiveness to the presynaptic neuron. This type of retrograde homeostatic signal has been extensively characterized at the drosophila neuromuscular junction (NMJ). For example, knockdown of GluAII subunits (DiAntonio et al., 1999; Petersen et al., 1997) or postsynaptic overexpression of a constitutively active variant of PKA (Davis et al., 1998), results in dramatically reduced responsiveness of the muscle cell to presynaptically released glutamate vesicles. After this reduction in postsynaptic responsiveness, the synapse compensates by increasing presynaptic release probability, thus restoring the total charge transfer measured in response to evoked stimulation back to control levels. Mutations in genes which regulate glutamate receptor clustering in the muscle, including the Rho-type GTPase effector gene *Pak* (Albin and Davis, 2004), NFKB and IKB (Heckscher et al., 2007), and *nanos* (Menon et al., 2009) also result in similar types of compensatory changes in presynaptic release. Recent efforts from the Davis lab have pioneered a novel pharmacological protocol for inducing a similar type of homeostatic response by using the GluA1 subtype-selective AMPA receptor antagonist Philanthotoxin-433 (PhTx) to attenuate postsynaptic responsiveness at the fly NMJ (Frank et al., 2006). This form of synaptic homeostasis is notable for the speed in which it emerges, operating on the time scale of minutes rather than hours or days. Having a pharmacological means of inducing synaptic homeostasis at this synapse has proven extremely useful in that it made feasible forward genetic screens to search for mutants with deficits in specific aspects of the homeostatic response. A number of molecules that control specific features of synaptic homeostasis have been identified using this approach in recent years, many of which serve the role of presynaptic effectors. These include, but are not limited to, Cacaphony (Frank et al, 2006), Eph (Frank et al., 2009), Ephexin (Frank et al., 2009), Cdc42 (Frank et al., 2009), Dysbindin (Dickman and Davis, 2009), Rab3-GAP (Muller et al., 2011), SNAP25 (Dickman et al., 2012), RIM (Muller et al., 2012), and Snapin (Dickman et al., 2012). However, despite its utility as an experimental model, there appear to be crucial differences in how this fast form of homeostasis is implemented compared with more chronic manipulations. Crucially, PhTx-induced homeostasis is not protein synthesis dependent and does not require presynaptic spiking for its expression (Frank et al., 2006), two factors which, as we will see, are absolutely vital for the types of similar homeostatic responses observed at mammalian central synapses.

Muscle cells are not only sensitive to changes in glutamate receptor function, however. It seems any number of manipulations that serve to reduce steady-state levels of postsynaptic depolarization will also recruit trans-synaptic homeostatic signals to increase presynaptic release and restore signal transfer across the synapse. For example, muscle-specific expression of the inwardly rectifying K+ channel Kir2.1 results in lowered input resistance and hyperpolarized resting membrane potential compared to control cells. Similar to the result seen in GluAII mutants, Kir2.1 expressing synapses exhibit a compensatory increase in presynaptic release probability (Paradis et al., 2004). When mutations in the cell adhesion molecule Fasciclin II were used to misdirect synapse formation at individual muscles, the question of whether postsynaptic cells are sensitive to relative amounts of presynaptic innervation could be addressed directly. Recording from neighboring muscle cells in the same animal, Davis and colleagues were able to show that postsynaptic cells which receive fewer synaptic connections have increased quantal content, while those with abnormally high levels of innervation exhibit a reduction in presynaptic release (Davis and Goodman, 1998). These later findings are very much in line with the previously detailed characterization of functional compensation across individual boutons along an axon in response to dendrite branch-specific changes in levels of depolarization (Branco et al., 2008). To reiterate a point introduced at the start of this section, this form of constitutive feedback between pre- and postsynaptic compartments would be ideally implemented by release of retrograde signal whose synthesis is under some degree of homeostatic control.

Accumulating evidence clearly demonstrates the general utility retrograde signaling as means of matching pre and post-synaptic efficacy (Regehr et al., 2009). Though the preceding studies were conducted at the fly NMJ, there is accumulating evidence that a similar type of homeostatic mechanism in which postsynaptic deprivation results in presynaptic augmentation also operates at mammalian central synapses. Using a combination of ultrastructural analysis and FM1-43 based assessment of presynaptic release, Murthy and colleagues provided an initial characterization of this form of plasticity, revealing increases in the number of docked vesicles and size of the readily releasable pool (RRP) after 48 Hr of AMPAR blockade with NBQX (Murthy et al., 2001). This increase in docked vesicles was shown to correspond to an increase in the frequency of spontaneous miniature excitatory postsynaptic currents (mEPSCs) in dissociated hippocampal neurons (Thiagarajan et al., 2002). Though this is contrary to the originally reported observation of no change in mEPSC frequency after chronic CNQX-treatment in cortical neurons (Turrigiano et al., 1998), similar homeostatic changes in presynaptic function have been observed after loss of AMPAR input across multiple labs and cell types (Thiagarajan et al., 2005; Gong et al., 2007; Wang et al., 2011).

Further solidifying the mechanistic link to the homeostatic phenomenon characterized at the drosophila NMJ, work from our lab and others have identified a critical role for retrograde signaling in the expression of presynaptic augmentation after AMPAR blockade (Jakawich et al., 2010; Lindskog et al., 2010; Groth et al., 2010). The specific molecular players involved in this retrograde signaling may be a point of evolutionary divergence between mammals and invertebrates, however. While BDNF has been identified as the retrograde signal at work in hippocampal neurons (Jakawch et al., 2010), orthologs of BDNF do not exist in the fly. Instead, several studies have shown that the muscle-derived BMP ligand Glass Bottom Boat (Gbb) may act as a retrograde signal via the presynaptic receptor Wishful Thinking (Wit) during forms of synaptic homeostasis induced by either PhTx or GluRIIA knockout at the fly NMJ (Haghighi et al., 2003; Goold and Davis, 2007).

1.4 Local protein synthesis during HSP: Initial findings

The first demonstration of a role for dendritic translation in homeostatic plasticity came from experiments involving simultaneous blockade of NMDA-type glutamate receptors (NMDARs) with APV and action potentials (AP) with TTX (Sutton et al., 2006). Similar to the earlier-reported effects observed in response to spike blockade alone (Turrigiano et al., 1998), simultaneous inhibition of spike activity and NMDAR function (TTX+APV) resulted in a protein synthesis-dependent increase in the amplitude of spontaneous mEPSCs in cultured hippocampal neurons as well as in acute hippocampal slices (Sutton et al, 2006). At the time, the speed at which this effect emerged was much faster than had been observed in the context of spike blockade alone (1-3 Hrs vs 24 Hrs or more; though see Ibata et al., 2008), highlighting a potential unique contribution of translation rather than transcription. Experiments utilizing local microperfusion across spatially restricted regions of the dendrite provided clear evidence for the importance of dendritc protein synthesis in this phenomenon: local perfusion of APV induced an anisomycin-sensitive increase in GluA1 subunits in the perfused region, while local perfusion of ansiomysin under conditions of bath NMDAR blockade resulted in a relative decrement in GluA1 subunit immunoreactivity in the perfused region (Sutton et al., 2006). This was the first indication that spatially restricted alterations in activity could induce homeostatic changes in synaptic protein content, and provided further support for the important role of ongoing spontaneous neurotransmission in stabilizing levels of protein synthesis at the synapse (Sutton et al., 2004).

Local synaptic homeostasis need not involve concurrent AP and synaptic blockade, however, as recent studies have demonstrated that simply removing the primary facet of excitatory input is sufficient to induce a compensatory response at mammalian central synapses. Interestingly, this manipulation has been observed to induce adaptations at both sides of the synapse: treatment of cultured hippocampal neurons with CNQX or NBQX for 3-24 hrs produces an adaptive enhancement in both pre and postsynaptic function (Jakawich et al., 2010; Groth et al., 2010; Lindskog et al., 2011). Signaling through βCaMKII plays an integral role in this process, as knocking out postsynaptic βCaMKII eliminates the increase in postsynaptic mEPSC amplitude and AMPAR subunit expression after AMPAR blockade, and overexpression of βCaMKII alone is sufficient to enhance expression of GluA1 homomeric AMPARs (Groth et al. 2010). Interestingly, removal of synaptic blockade after a period of deprivation causes $Ca2^+$ influx through these uniquely $Ca2^+$ permeable AMPARs, triggering the release of a retrograde signal to enhance presynaptic function (Groth et al., 2010; Lindskog et al., 2011). Though evidence suggests potential roles for both Nitric Oxide (NO) (Lindskog et al, 2011) and BDNF (Jakawich et al,, 2010) in retrograde signaling during this form of synaptic homeostasis, eliminating postsynaptic BDNF synthesis using RNAi completely blocked CNQX-induced increases in presynaptic function, suggesting that BDNF's action as a retrograde signal may be necessary in this context, while NO may provide a supporting role. In addition, BDNF was shown to be locally synthesized in dendrites in response to AMPAR blockade (Jakawhich et al., 2010), highlighting the importance of local translational regulation in this form of compensation. Some insight into the potential mechanism behind the augmenting effects of BDNF release on presynaptic function may be gleaned from data indicating that elimination of presynaptic spiking during AMPAR blockade-induced homeostasis or after acute BDNF application on its own is effective in completely blocking the increase in presynaptic release observed after either of these treatments (Jakawich et al, 2010). Additional data supports a role for presynaptic $Ca2^+$ influx through P/Q and N-type $Ca2^+$ channels operating in tandem with BDNF-triggered TrkB signaling to mediate changes in presynaptic function. Further characterization of the nature of this transynaptic regulation has been conducted in our lab and will be described in later chapters.

1.5 Local protein synthesis during HSP: Molecular Players

Recent efforts from multiple labs have provided an emerging view of the molecular mechanisms responsible for controlling local protein synthesis during homeostatic forms of synaptic plasticity. The majority of this work has focused on translational control of proteins responsible for modulating postsynaptic function, though additional insights into the mechanism responsible for presynaptically expressed homeostasis will be presented in subsequent chapters

eEF2K

Additional work has highlighted a role for the eukaryotic elongation factor-2 kinase (eEF2K) in mediating homeostatic responses to synaptic blockade. Phosphorylation of eEF2K, inhibits eEF2 mediated catalysis of ribosomal translocation during polypeptide elongation, thereby inhibiting translation. Initial experiments from Sutton et al., 2007 demonstrated that eEF2 phosophrylation levels significantly decrease in response to simultaneous blockade of APs and AMPA or NMDA-type glutamate receptors, concurrent with an increase in dendritic protein synthesis observed under these conditions (Sutton et al., 2004). Importantly, eEF2 phosphorylation was shown to be differentially regulated by specific forms of neurotransmission, with blockade of AP-induced vesicle release (via TTX application) leading to increased eEF2 phosphorylation and diminished translation elongation, and concurrent AP and excitatory receptor blockade having an opposite effect. Interesting research has emerged recently to suggest that Neuronatin mRNA is potential target of eEF2-mediated translational control under conditions of TTX/APV blockade (Oyang et al., 2011). One intriguing implication from these results is that spontaneous and evoked neurotransmission activate specific sets of postsynaptic receptors, each of which could have unique roles to play in controlling adaptive changes in dendritic translation during synaptic homeostasis. In line with this, experiments from a number of labs have provided experimental support for the functional segregation of postsynaptic receptors that are positioned to receive input from spontaneous over evoked neurotransmission (Sara et al., 2011; Melon et al., 2013). Coupled with the growing support for the notion of separate vesicle pools used for spontaneous or evoked neurotransmission (Chung et al., 2010; Ramirez and Kavalali, 2011; Rameriz et al. 2012), an argument may be made for unique signaling via spontaneous neurotransmission in the adaptive regulation of protein translation during in synaptic homeostasis.

Less clear, however, is the specific role (if any) played by particular families of excitatory neurotransmitter receptors in the context of synaptic blockade. While initial experiments did not show differential effects of blocking NMDA vs. NMDA+AMPAR type glutamate receptors (Sutton et al., 2004, Sutton et al., 2007), recent work has highlighted a unique facet of synaptic homeostasis that appears to involve changes in translation in response to transient NMDAR blockade. In one instance, Monteggia and colleagues demonstrated that acute blockade of NMDARs with systemically administered NMDAR antagonists, including ketamine, MK-801 and APV, drives protein synthesis through dephosphorylation of eEF2, an effect which is particularly strong in hippocampal dendrites (Autry et al., 2011). Interestingly, low doses of ketamine or other NMDAR antagonists also act as particularly strong antidepressants, with significant reductions in immobility on a forced swim test observed up to a week after initial injection (Autry et al., 2011). The authors identify BDNF as one of potentially many targets of altered translational regulation in response to low dose NMDAR-antagonists, and provide evidence suggesting that de novo BDNF synthesis enhances AMPAR currents. The finding that concurrent treatment with the AMPAR antagonist NBQX eliminates the efficacy of ketamine in the forced swim test supports the author’s assertion that an important role is played by enhanced AMPAR currents as an effector of ketamine- induced plasticity.

mTORC1

The effects of transient NMDAR blockade may not be mediated solely via eEF2 signaling, however. Work from the Duman lab has shown that acute NMDAR blockade via ketamine activates an alternative mediator of translation regulation, namely that of the mechanistic target of rapamycin (mTOR) pathway. mTOR, when assembled with its binding partner raptor, forms a complex (mTORC1) which has a well-characterized role in regulating translation initiation (Ma and Blenis, 2009). Systemic injection of low dose ketamine resulted in an increase in mTORC1 signaling in synaptoneurosomes prepared from rat prefrontal cortex (Li et al., 2010). The effect of ketamine on mTORC1 activation was shorter lived than the ketamine-induced enhancement in eEF2 signaling reported by Autry et al (2011), returning back down to baseline levels within 2 Hr post-injection. Concurrent with the change in mTORC1 signaling, ketamine produced a rapamycin-sensitive increase in levels of synaptic proteins, including PSD-95, synapsin and GluA1 AMPAR subunits, as well as an increase in spine density and frequency of spontaneous EPSCs (Li et al., 2010). Regarding specificity of the postsynaptic receptor as a relevant signaling factor in this phenomenon, it is interesting to note that ketamine-induced increases in mTORC1 singling were completely blocked by co-administration of the AMPAR blocker NBQX (Li et al., 2010), which mirrors the reduced efficacy of ketamine in the forced swim task when co-administered with NBQX (Autry et al., 2011). This suggests that it is not mere blockade of excitatory minis that elicits the antidepressant response, but potentially something unique to cessation of NMDAR signaling, as is suggested by the finding that an

NR2B-specific inhibitor replicated the effects of ketamine in terms of enhanced expression of synaptic proteins and antidepressant like effects on behavioral assays (Li et al., 2010). This is complimented by recent work using a genetic mouse model in which the GluN2B subunit of the NMDAR is replaced with GluN2A throughout development (Wang et al., 2011A). In cortical cultures prepared from these animals, lack of signaling through GluN2B containing receptors resulted in heightened mTORC1 signaling in dendrites, as well as a deficit in synaptic adaptation induced by concurrent AP and NMDAR blockade (TTX+APV), compared to WT cultures. These findings, combined with those from Li et al., suggest that spontaneous mEPSC signaling through NR2B containing NMDARs may tonically suppress mTORC1 signaling at these synapses, cessation of which may engage a form of synaptic homeostasis that depends on dendritic protein synthesis.

At the drosophila neuromuscular junction (NMJ), a well-characterized form of synaptic homeostasis elicited by deprivation of excitatory synaptic input has recently also been linked to the mechanistic target of rapamycin (mTOR) signaling pathway (Penney et al., 2012). Genetic deletion of the GluAII AMPAR subunit reduces the amplitude of spontaneous mEJCs. However, the size of evoked current remains comparable to WT levels due to a compensatory increase in quantal content, as described earlier (Petersen et al., 1997). Interestingly, double mutants for GluAII and mTOR show a 50% reduction in evoked current compared to WT levels, indicating a role for mTOR-dependent translation in the adaptive shift in quantal content (Penney et al., 2012). Restoration of mTOR function in the muscle, but not in the presynaptic motor neuron, rescues the homeostatic adaptation in quantal content, suggesting that postsynaptic mTOR mediates translation of a retrograde signal in response to loss of excitatory input. This novel role for postsynaptic mTOR emerged at roughly the same time as the initial results of the work presented here (Chapter 2), and thus establishes a remarkable evolutionary conservation for postsynaptic mTORC1 in the homeostatic regulation of presynaptic function.

Retinoic acid

Recently, work from Lu Chen's lab established a non-canonical role for all-trans-retinoic acid signaling, wherein application of RA to dissociated cultures or hippocampal slices produced a multiplicative scaling of mEPSC amplitude similar to that observed in homeostatic forms of plasticity (Aoto et al., 2008). Curiously, given the known function of RA in acting as a transcription factor, this effect was blocked by inhibitors of translation, but not by blockers of transcription. In support of RA signaling mediating a direct effect on local translation occurring in dendrites, additional experiments also revealed that RA stimulates synthesis of GulA1 subunits in synaptoneurosome preparations (Poon and Chen, 2008). Pharmacological blockade of RA synthesis or shRNA knockdown of the endogenous RA receptor RARa completely eliminated synaptic scaling induced by TTX and APV, indicating that RA-mediated stimulation of local protein synthesis in dendrites is an essential component of postsynaptic adaptation (Aoto, 2008). Critically, while RA is necessary for forms of synaptic homeostasis that emerge after synaptic blockade, via TTX+APV, TTX+CNQX or CNQX alone (Wang et al., 2008), it is completely unnecessary for the adaptive functional response observed after prolonged period of spike blockade via TTX. This finding provides further support to the earlier-stated idea that multiple homeostatic sensors operate in neurons, and that those operating at the level of individual synapses or dendritic branches use distinct methods to exert functional changes compared to those that sense changes in individual spike output. Critically, Chen and colleagues demonstrated that diminished $Ca2^+$ influx in dendrites is sufficient to trigger increases in intracellular RA synthesis (Wang et al, 2008), thereby positioning RA as a particularly attractive candidate to act as a homeostatic sensor mediating postsynaptic responsiveness in dendrites. Because RA-induced increases in postsynaptic function are mediated by de novo translation of uniquely $Ca2^+$ permeable GluA2-lacking AMPARs (Aoto et al 2008), this proposed homeostatic circuit comes equipped with a built-in feedback mechanism to dampen RA synthesis after an initial phase of postsynaptic strengthening.

FMRP

The RNA-binding protein FMRP is an additional modulator of translation regulation that has recently been determined to be involved in local homeostatic synaptic adaptations. Soden and Chen (2010) have identified FMRP as integral to a previously characterized form of homeostatic plasticity that depends on retinoic-acid (RA) mediated local protein synthesis (Aoto et al., 2008). FMRP mice show no compensation in mEPSC amplitude or synaptic GluA1 levels after 36 Hrs of treatment with TTX and APV (Soden and Chen 2010). FMRP is not necessary for RA-synthesis after TTX+APV treatment, but is necessary for RA-induced local translation of synaptic proteins (Soden and Chen, 2010). The fact that FMRP and the RA receptor RARα appear to not interact directly suggests a combinatorial action of multiple signaling pathways operating in parallel but converging at the level of specific transcript targets, thereby allowing for more finely-tuned translational regulation.

FMRP may also play a role in an alternative form of homeostasis, namely that of synaptic downregulation during sleep. Work from the labs of Cirelli and Tononi have advanced the intriguing hypothesis that a major function of slow-wave sleep is the homeostatic weakening of synapses that have become potentiated over the course of wakeful activity (Tononi and Cirelli, 2003). In both mammals (Vyazovskiy et al., 2008) and in drosophila (Gilestro et al, 2009), periods of wakefulness are associated with synaptic alterations reflecting potentiated excitatory responses, including enhanced GluA1 expression, elevated AMPAR and CaMKII phosphorylation levels, and increased amplitude of evoked responses. In contrast, slow wave sleep is associated with diminished evoked currents, and a general decrease in expression levels of synaptic proteins. Intensity of slow-wave delta band activity is tied to overall synaptic weight, and thus displays decreased amplitude over time during sleep as synapses are homeostatically weakened (Tononi and Cirelli, 2003). In drosophila, dFMR1 levels have been shown to increase markedly as a consequence of sleep deprivation, and genetic manipulation of dFMR1 exerts profound bidirectional changes in the duration of sleep bouts (Bushey et al., 2009). These effects on sleep duration in dFMR1 mutant flies were later shown to be synaptically mediated. While sleep deprivation typically results in enhanced morphological complexity of dendrites in mushroom body neurons, overexpression of dFMR1 eliminates these adaptations, effectively rendering sleep deprived flies identical to those with normal sleep patterns (Bushey et al., 2011). More work is needed to tie translation regulation by FMRP to the particular form of synaptic homeostasis observed during sleep, but these data raise the interesting possibility that translation regulation may have a pivotal role to play in a form of synaptic homeostasis observed in a ubiquitously observed behavioral phenomenon such as sleep.

1.6 Translational control by dendritic mTORC1 during state-dependent synaptic homeostasis

Here we present our efforts to characterize a novel role for dendritic mTORC1 in the regulation of transsynaptically-mediated, state-dependent homeostasis. We first present evidence that blockade of AMPA-type glutamate receptors with CNQX increases mTORC1 kinase activity in the postsynaptic domain, leading to the synthesis of BDNF as a retrograde signal (Chapter 2). Retrograde signaling through BDNF appears to emerge as an immediate consequence of mTORC1 activation, as genetic upregulation via postsynaptic Rheb GTPase overexpression or acute activation of mTORC1 with the lipid second messenger phosphatidic acid (PA) is sufficient to stimulate BDNF-dependent increases in presynaptic efficacy (Chapter 3). We further demonstrate that a pathway involving the intracellular synthesis of PA by phospholipase-D appears to serve as a homeostatic sensor mechanism, translating shifts in postsynaptic excitation to increased mTORC1 signaling and altered BDNF synthesis. Interestingly, this PLD/PA signaling mechanism is not a feature of mTORC1 activation shared with the phenomenon of chemically induced LTP (Chapter 4). Finally, we show that activity dependent relocalization of the ubiquitin proteasome system (UPS) acts as an important gate on this form of state-dependent homeostasis, wherein mTOR-dependent retrograde BDNF signaling drives changes in presynaptic function via the UPS-mediated disinhibition of vesicle release probability (Chapter 5). Understanding the molecular mechanisms involved in this evolutionarily conserved form of synaptic homeostasis contributes to our growing understanding of basic synapse function, and potentially yields insights into the contribution of dysregulated mTORC1 signaling to commonly observed circuit abnormalities in mTOR-related neurodevelopmental disorders.

1.6 Bibliography

Albin SD, Davis GW. (2004) Coordinating structural and functional synapse development: postsynaptic p21-activated kinase independently specifies glutamate receptor abundance and postsynaptic morphology. J Neurosci. Aug 4;24(31):6871-9.

Aoto J, Nam CI, Poon MM, Ting P, Chen L. (2008) Synaptic signaling by all-trans retinoic acid in homeostatic synaptic plasticity. Neuron. Oct 23;60(2):308-20.

An JJ, Gharami K, Liao GY, Woo NH, Lau AG, Vanevski F, Torre ER, Jones KR, Feng Y, Lu B, Xu B. (2008). Distinct role of long 3' UTR BDNF mRNA in spine morphology and synaptic plasticity in hippocampal neurons. Cell. Jul 11;134(1):175-87.

Antion MD, Merhav M, Hoeffer CA, Reis G, Kozma SC, Thomas G, Schuman EM, Rosenblum K, Klann E. (2008) Removal of S6K1 and S6K2 leads to divergent alterations in learning, memory, and synaptic plasticity. Learn Mem. Jan 3;15(1):29-38.

Aoto J, Nam CI, Poon MM, Ting P, Chen L. (2008). Synaptic signaling by all-trans retinoic acid in homeostatic synaptic plasticity. Neuron. Oct 23;60(2):308-20.

Aitken CE, Lorsch JR. (2012) A mechanistic overview of translation initiation in eukaryotes. Nat Struct Mol Biol. Jun 5;19(6):568-76.

Autry AE, Adachi M, Nosyreva E, Na ES, Los MF, Cheng PF, Kavalali ET, Monteggia LM. (2011). NMDA receptor blockade at rest triggers rapid behavioural antidepressant responses. Nature. Jun 15;475(7354):91-5.

Banko JL, Poulin F, Hou L, DeMaria CT, Sonenberg N, Klann E. (2005) The translation repressor 4E-BP2 is critical for eIF4F complex formation, synaptic plasticity, and memory in the hippocampus. J Neurosci. Oct 19;25(42):9581-90.

Bé̈ique JC, Na Y, Kuhl D, Worley PF, Huganir RL. (2011). Arc-dependent synapse-specific homeostatic plasticity. Proc Natl Acad Sci U S A. Jan 11;108(2):816-21.

Benson DL (1997) Dendritic compartmentation of NMDA receptor mRNA in cultured hippocampal neurons. Neuroreport 8: 823–828.

Burrone J, O'Byrne M, Murthy VN. (2002). Multiple forms of synaptic plasticity triggered by selective suppression of activity in individual neurons. Nature. Nov 28;420(6914):414-8.

Banko JL, Hou L, Poulin F, Sonenberg N, Klann E. (2006). Regulation of eukaryotic initiation factor 4E by converging signaling pathways during metabotropic glutamate receptor-dependent long-term depression. J Neurosci. Feb 22;26(8):2167-73.

Bodian B. (1965). A suggestive relationship of nerve cell RNA with specific synaptic site. Proc. Natl. Acad. Sci. USA, 53, pp. 418–425.

Branco T, Staras K, Darcy KJ, Goda Y. (2008). Local dendritic activity sets release probability at hippocampal synapses. Neuron. Aug 14;59(3):475-85.

Bushey D, Tononi G, Cirelli C. (2011). Sleep and synaptic homeostasis: structural evidence in Drosophila. Science. Jun 24;332(6037):1576-81.

Bushey D, Tononi G, Cirelli C. (2009). The Drosophila fragile X mental retardation gene regulates sleep need. J Neurosci. Feb 18;29(7):1948-61.

Cajigas IJ, Tushev G, Will TJ, tom Dieck S, Fuerst N, Schuman EM. (2012). The local transcriptome in the synaptic neuropil revealed by deep sequencing and high-resolution imaging. Neuron. May 10;74(3):453-66.

Cammalleri M, Lütjens R, Berton F, King AR, Simpson C, Francesconi W, Sanna PP. (2003). Time-restricted role for dendritic activation of the mTOR-p70S6K pathway in the induction of late-phase long-term potentiation in the CA1. Proc Natl Acad Sci U S A. Nov 25;100(24):14368-73.

Carriere A, Ray H, Blenis J, Roux PP. (2008). The RSK factors of activating the Ras/MAPK signaling cascade. Front Biosci. May 1;13:4258-75.

Chung C, Barylko B, Leitz J, Liu X, Kavalali ET. (2010). Acute dynamin inhibition dissects synaptic vesicle recycling pathways that drive spontaneous and evoked neurotransmission. J Neurosci. Jan 27;30(4):1363-76.

Darnell JC. (2011). Defects in translational regulation contributing to human cognitive and behavioral disease. Curr Opin Genet Dev. Aug;21(4):465-73.

Davis GW, DiAntonio A, Petersen SA, (1998). Goodman CS. Postsynaptic PKA controls quantal size and reveals a retrograde signal that regulates presynaptic transmitter release in Drosophila. Neuron. 1998 Feb;20(2):305-15.

Davis GW, Goodman CS. (1998). Synapse-specific control of synaptic efficacy at the terminals of a single neuron. Nature. Mar 5;392(6671):82-6..

Davis GW, Bezprozvanny I. (2001). Maintaining the stability of neural function: a homeostatic hypothesis. Annu Rev Physiol. ;63:847-69.

DiAntonio A, Petersen SA, Heckmann M, Goodman CS. (1999). Glutamate receptor expression regulates quantal size and quantal content at the Drosophila neuromuscular junction. J Neurosci. Apr 15;19(8):3023-32.

Dickman DK, Davis GW. (2009). The schizophrenia susceptibility gene dysbindin controls synaptic homeostasis. Science. Nov 20;326(5956):1127-30.

Dickman DK, Tong A, Davis GW. (2012). Snapin is critical for presynaptic homeostatic plasticity. J Neurosci. Jun 20;32(25):8716-24.

Dorrello NV, Peschiaroli A, Guardavaccaro D, Colburn NH, Sherman NE, Pagano M. (2006). S6K1- and betaTRCP-mediated degradation of PDCD4 promotes protein translation and cell growth. Science. Oct 20;314(5798):467-71.

Espinosa F, Kavalali ET. (2009). NMDA receptor activation by spontaneous glutamatergic neurotransmission. J Neurophysiol. 2009 May;101(5):2290-6.

Fenton TR, Gout IT. (2011). Functions and regulation of the 70kDa ribosomal S6 kinases. Int J Biochem Cell Biol. Jan;43(1):47-59.

Frank CA, Kennedy MJ, Goold CP, Marek KW, Davis GW. (2006). Mechanisms underlying the rapid induction and sustained expression of synaptic homeostasis. Neuron. Nov 22;52(4):663-77.

Gilestro GF, Tononi G, Cirelli C. (2009). Widespread changes in synaptic markers as a function of sleep and wakefulness in Drosophila. Science. Apr 3;324(5923):109-12.

Gingras AC, Raught B, Gygi SP, Niedzwiecka A, Miron M, Burley SK, Polakiewicz RD, Wyslouch-Cieszynska A, Aebersold R, Sonenberg N. (2011). Hierarchical phosphorylation of the translation inhibitor 4E-BP1. Genes Dev. Nov 1;15(21):2852-64.

Gong B, Wang H, Gu S, Heximer SP, Zhuo M. (2007) Genetic evidence for the requirement of adenylyl cyclase 1 in synaptic scaling of forebrain cortical neurons. Eur J Neurosci. Jul;26(2):275-88.

Goold CP, Nicoll RA. (2010). Single-cell optogenetic excitation drives homeostatic synaptic depression. Neuron. Nov 4;68(3):512-28.

Goold CP, Davis GW. (2007). The BMP ligand Gbb gates the expression of synaptic homeostasis independent of synaptic growth control. Neuron. Oct 4;56(1):109-23.

Grooms SY, Noh KM, Regis R, Bassell GJ, Bryan MK, Carroll RC, Zukin RS. (2006). Activity bidirectionally regulates AMPA receptor mRNA abundance in dendrites of hippocampal neurons. J Neurosci. Aug 9;26(32):8339-51.

Groth RD, Lindskog M, Thiagarajan TC, Li L, Tsien RW. (2011). Beta $Ca2^{+}$/CaM-dependent kinase type II triggers upregulation of GluA1 to coordinate adaptation to synaptic inactivity in hippocampal neurons. Proc Natl Acad Sci U S A. Jan 11;108(2):828-33.

Haghighi AP, McCabe BD, Fetter RD, Palmer JE, Hom S, Goodman CS. (2003). Retrograde control of synaptic transmission by postsynaptic CaMKII at the Drosophila neuromuscular junction. Neuron. Jul 17;39(2):255-67.

Heckscher ES, Fetter RD, Marek KW, Albin SD, Davis GW. (2007). NF-kappaB, IkappaB, and IRAK control glutamate receptor density at the Drosophila NMJ. Neuron. Sep 20;55(6):859-73.

Hobert O. (2011). Regulation of terminal differentiation programs in the nervous system. Annu Rev Cell Dev Biol. 27:681-96.

Hou L, Klann E. (2004). Activation of the phosphoinositide 3-kinase-Akt-mammalian target of rapamycin signaling pathway is required for metabotropic glutamate receptor-dependent long-term depression. J Neurosci. Jul 14;24(28):6352-61.

Hou Q, Gilbert J, Man HY. (2011). Homeostatic regulation of AMPA receptor trafficking and degradation by light-controlled single-synaptic activation. Neuron. Dec 8;72(5):806-18.

Hou Q, Zhang D, Jarzylo L, Huganir RL, Man HY. (2008). Homeostatic regulation of AMPA receptor expression at single hippocampal synapses. Proc Natl Acad Sci U S A. Jan 15;105(2):775-80.

Houweling AR, Bazhenov M, Timofeev I, Steriade M, Sejnowski TJ. (2005). Homeostatic synaptic plasticity can explain post-traumatic epileptogenesis in chronically isolated neocortex. Cereb Cortex. Jun;15(6):834-45.

Huang YY, Nguyen PV, Abel T, Kandel ER. (1996). Long-lasting forms of synaptic potentiation in the mammalian hippocampus. Learn Mem. Sep-Oct;3(2-3):74-85

Ibata K, Sun Q, Turrigiano GG. (2008). Rapid synaptic scaling induced by changes in postsynaptic firing. Neuron. Mar 27;57(6):819-26.

Jakawich SK, Nasser HB, Strong MJ, McCartney AJ, Perez AS, Rakesh N, Carruthers CJ, Sutton MA. (2010). Local presynaptic activity gates homeostatic changes in presynaptic function driven by dendritic BDNF synthesis. Neuron. Dec 22;68(6):1143-58.

Jourdi H, Hsu YT, Zhou M, Qin Q, Bi X, Baudry M. (2009). Positive AMPA receptor modulation rapidly stimulates BDNF release and increases dendritic mRNA translation.J Neurosci. Jul 8;29(27):8688-97.

Kang H, Schuman EM. (1996). A requirement for local protein synthesis in neurotrophin-induced hippocampal synaptic plasticity. Science. Sep 6;273(5280):1402-6.

Kelleher RJ 3rd, Govindarajan A, Tonegawa S. (2004). Translational regulatory mechanisms in persistent forms of synaptic plasticity. Neuron. Sep 30;44(1):59-73.

Koester HJ, Johnston D. (2005). Target cell-dependent normalization of transmitter release at neocortical synapses. Science. May 6;308(5723):863-6.

Laplante M, Sabatini DM. (2012). mTOR signaling in growth control and disease. Cell. Apr 13;149(2):274- 93.

Lau AG, Irier HA, Gu J, Tian D, Ku L, Liu G, Xia M, Fritsch B, Zheng JQ, Dingledine R, Xu B, Lu B, Feng Y. (2010). Distinct 3'UTRs differentially regulate activity-dependent translation of brain-derived neurotrophic factor (BDNF). Proc Natl Acad Sci U S A. Sep 7;107(36):15945-50.

Lee HY, Ge WP, Huang W, He Y, Wang GX, Rowson-Baldwin A, Smith SJ, Jan YN, Jan LY. (2011). Bidirectional regulation of dendritic voltage-gated potassium channels by the fragile X mental retardation protein. Neuron. Nov 17;72(4):630-42.

Lee KF, Soares C, Bé̈ïque JC. (2013). Tuning into diversity of homeostatic synaptic plasticity. Neuropharmacology. Mar 27. pii: S0028-3908(13)00112-3.

Li N, Lee B, Liu RJ, Banasr M, Dwyer JM, Iwata M, Li XY, Aghajanian G, Duman RS. (2010). mTOR-dependent synapse formation underlies the rapid antidepressant effects of NMDA antagonists. Science. Aug 20;329(5994):959-64.

Liao GY, An JJ, Gharami K, Waterhouse EG, Vanevski F, Jones KR, Xu B. (2012). Dendritically targeted Bdnf mRNA is essential for energy balance and response to leptin. Nat Med. Mar 18;18(4):564-71.

Lindskog M, Li L, Groth RD, Poburko D, Thiagarajan TC, Han X, Tsien RW. (2010). Postsynaptic GluA1 enables acute retrograde enhancement of presynaptic function to coordinate adaptation to synaptic inactivity. Proc Natl Acad Sci U S A. Dec 14;107(50):21806-11.

Ma XM, Blenis J. (2009). Molecular mechanisms of mTOR-mediated translational control. Nat Rev Mol Cell Biol. May;10(5):307-18

Ma T, Tzavaras N, Tsokas P, Landau EM, Blitzer RD. (2011). Synaptic stimulation of mTOR is mediated by Wnt signaling and regulation of glycogen synthetase kinase-3. J Neurosci. Nov 30;31(48):17537-46.

Marder E, Goaillard JM. (2006). Variability, compensation and homeostasis in neuron and network function. Nat Rev Neurosci. Jul;7(7):563-74.

Marder E. (2011). Variability, compensation, and modulation in neurons and circuits. Proc Natl Acad Sci U S A. Sep 13;108 Suppl 3:15542-8.

Melom JE, Akbergenova Y, Gavornik JP, Littleton JT. (2013). Spontaneous and evoked release are independently regulated at individual active zones. J Neurosci. Oct 30;33(44):17253-63.

Menon KP, Andrews S, Murthy M, Gavis ER, Zinn K. (2009). The translational repressors Nanos and Pumilio have divergent effects on presynaptic terminal growth and postsynaptic glutamate receptor subunit composition. J Neurosci. Apr 29;29(17):5558-72.

Meyuhas O, Dreazen A. (2009). Ribosomal protein S6 kinase from TOP mRNAs to cell size. Prog Mol Biol Transl Sci.;90:109-53.

Miller S, Yasuda M, Coats JK, Jones Y, Martone ME, Mayford M. (2002). Disruption of dendritic translation of CaMKIIalpha impairs stabilization of synaptic plasticity and memory consolidation.Neuron. Oct 24;36(3):507-19.

Müller M, Pym EC, Tong A, Davis GW. (2011). Rab3-GAP controls the progression of synaptic homeostasis at a late stage of vesicle release. Neuron. Feb 24;69(4):749-62.

Müller M, Liu KS, Sigrist SJ, Davis GW. (2012). RIM controls homeostatic plasticity through modulation of the readily-releasable vesicle pool. J Neurosci. Nov 21;32(47):16574-85.

Murthy VN, Schikorski T, Stevens CF, Zhu Y. (2001). Inactivity produces increases in neurotransmitter release and synapse size. Neuron. Nov 20;32(4):673-82.

Narayanan R, Johnston D. (2012). Functional maps within a single neuron. J Neurophysiol. Aug 29.

Ohanna M, Sobering AK, Lapointe T, Lorenzo L, Praud C, Petroulakis E, Sonenberg N, Kelly PA, Sotiropoulos A, Pende M. (2005). Atrophy of S6K1(-/-) skeletal muscle cells reveals distinct mTOR effectors for cell cycle and size control. Nat Cell Biol. Mar;7(3):286-94. Epub 2005 Feb 20.

O'Leary T, Wyllie DJ. (2011). Neuronal homeostasis: time for a change? J Physiol. Oct 15;589(Pt20):4811-26.

Ouyang Y, Rosenstein A, Kreiman G, Schuman EM, Kennedy MB (1999) Tetanic stimulation leads to increased accumulation of Ca(2+)/calmodulin-dependent protein kinase II via dendritic protein synthesis in hippocampal neurons. J Neurosci 19: 7823–7833.

Oyang EL, Davidson BC, Lee W, Poon MM. (2011). Functional characterization of the dendritically localized mRNA neuronatin in hippocampal neurons. PLoS One ;6(9):e24879. Epub 2011 Sep 14.

Paradis S, Sweeney ST, Davis GW. (2001). Homeostatic control of presynaptic release is triggered by postsynaptic membrane depolarization. Neuron. Jun;30(3):737-49.

Pause A, Belsham GJ, Gingras AC, Donzé O, Lin TA, Lawrence JC Jr, Sonenberg N. (1994). Insulin-dependent stimulation of protein synthesis by phosphorylation of a regulator of 5'-cap function. Nature. Oct 27;371(6500):762-7.

Pearson G, Robinson F, Beers Gibson T, Xu BE, Karandikar M, Berman K, Cobb MH. (2001). Mitogen-activated protein (MAP) kinase pathways: regulation and physiological functions. Endocr Rev. Apr;22(2):153-83.

Penney J, Tsurudome K, Liao EH, Elazzouzi F, Livingstone M, Gonzalez M, Sonenberg N, Haghighi AP. (2012). TOR is required for the retrograde regulation of synaptic homeostasis at the Drosophila neuromuscular junction. Neuron. Apr 12;74(1):166-78.

Petersen SA, Fetter RD, Noordermeer JN, Goodman CS, DiAntonio A. (1997). Genetic analysis of glutamate receptors in Drosophila reveals a retrograde signal regulating presynaptic transmitter release. Neuron. Dec;19(6):1237-48.

Poon MM, Choi SH, Jamieson CA, Geschwind DH, Martin KC (2006) Identification of process-localized mRNAs from cultured rodent hippocampal neurons. J Neurosci 26: 13390–13399.

Poon MM, Chen L. (2009). Retinoic acid-gated sequence-specific translational control by RARalpha. Proc Natl Acad Sci U S A. 2008 Dec 23;105(51):20303-8.

Pozo K, Goda Y. (2010). Unraveling mechanisms of homeostatic synaptic plasticity. Neuron. 13;66(3):337-51.

Ramirez DM, Khvotchev M, Trauterman B, Kavalali ET. (2012). Vti1a identifies a vesicle pool that preferentially recycles at rest and maintains spontaneous neurotransmission. Neuron. Jan 12;73(1):121-34.

Ramirez DM, Kavalali ET. (2011). Differential regulation of spontaneous and evoked neurotransmitter release at central synapses. Curr Opin Neurobiol. Apr;21(2):275-82.

Redondo RL, Morris RG. (2011). Making memories last: the synaptic tagging and capture hypothesis. Nat Rev Neurosci. Jan;12(1):17-30.

Regehr WG, Carey MR, Best AR. (2009). Activity-dependent regulation of synapses by retrograde messengers. Neuron. Jul 30;63(2):154-70.

Roux PP, Topisirovic I. (2012). Regulation of mRNA translation by signaling pathways. Cold Spring Harb Perspect Biol. Nov 1;4(11). pii: a012252.

Rozen F, Edery I, Meerovitch K, Dever TE, Merrick WC, Sonenberg N. (1990). Bidirectional RNA helicase activity of eucaryotic translation initiation factors 4A and 4F. Mol Cell Biol. Mar;10(3):1134-44.

Ruvinsky I, Sharon N, Lerer T, Cohen H, Stolovich-Rain M, Nir T, Dor Y, Zisman P, Meyuhas O. (2005). Ribosomal protein S6 phosphorylation is a determinant of cell size and glucose homeostasis. Genes Dev. Sep 15;19(18):2199-211.

Sara Y, Bal M, Adachi M, Monteggia LM, Kavalali ET. (2011). Use-dependent AMPA receptor block reveals segregation of spontaneous and evoked glutamatergic neurotransmission. J Neurosci. Apr 6;31(14):5378-82.

Shahbazian D, Roux PP, Mieulet V, Cohen MS, Raught B, Taunton J, Hershey JW, Blenis J, Pende M, Sonenberg N. (2006). The mTOR/PI3K and MAPK pathways converge on eIF4B to control its phosphorylation and activity. EMBO J. Jun 21;25(12):2781-91.

Soden ME, Chen L. (2010). Fragile X protein FMRP is required for homeostatic plasticity and regulation of synaptic strength by retinoic acid. J Neurosci. Dec 15;30(50):16910-21.

Sonenberg N, Hinnebusch AG. (2009). Regulation of translation initiation in eukaryotes: mechanisms and biological targets. Cell. Feb 20;136(4):731-45.

Sutton MA, Taylor AM, Ito HT, Pham A, Schuman EM. (2007). Postsynaptic decoding of neural activity: eEF2 as a biochemical sensor coupling miniature synaptic transmission to local protein synthesis. Neuron. Aug 16;55(4):648-61.

Sutton MA, Schuman EM. (2006). Dendritic protein synthesis, synaptic plasticity, and memory. Cell. Oct 6;127(1):49-58.

Sutton MA, Ito HT, Cressy P, Kempf C, Woo JC, Schuman EM. (2006). Miniature neurotransmission stabilizes synaptic function via tonic suppression of local dendritic protein synthesis. Cell. May 19;125(4):785-99.

Sutton MA, Wall NR, Aakalu GN, Schuman EM. (2004). Regulation of dendritic protein synthesis by miniature synaptic events. Science. Jun 25;304(5679):1979-83.

Steward O, Worley PF. (2001). Selective targeting of newly synthesized Arc mRNA to active synapes requires NMDA receptor activation. Neuron. Apr;30(1):227-40.

Steward O, Levy WB (1982) Preferential localization of polyribosomes under the base of dendritic spines in granule cells of the dentate gyrus. J Neurosci 2: 284–291.

Stoica L, Zhu PJ, Huang W, Zhou H, Kozma SC, Costa-Mattioli M. (2011). Selective pharmacogenetic inhibition of mammalian target of Rapamycin complex I (mTORC1) blocks long-term synaptic plasticity and memory storage. Proc Natl Acad Sci U S A. Mar 1;108(9):3791-6.

Thiagarajan TC, Piedras-Renteria ES, Tsien RW. alpha- and betaCaMKII. (2002). Inverse regulation by neuronal activity and opposing effects on synaptic strength. Neuron. Dec 19;36(6):1103-14.

Thiagarajan TC, Lindskog M, Tsien RW. (2005). Adaptation to synaptic inactivity in hippocampal neurons. Neuron. Sep 1;47(5):725-37.

Thoreen CC, Chantranupong L, Keys HR, Wang T, Gray NS, Sabatini DM. (2012). A unifying model for mTORC1-mediated regulation of mRNA translation. Nature. May 2;485(7396):109-13.

Tononi G, Cirelli C. (2003). Sleep and synaptic homeostasis: a hypothesis. Brain Res Bull. Dec 15;62(2):143-50.

Topisirovic I, Svitkin YV, Sonenberg N, Shatkin AJ. (2011). Cap and cap-binding proteins in the control of gene expression. Wiley Interdiscip Rev RNA. Mar-Apr;2(2):277-98.

Tsokas P, Grace EA, Chan P, Ma T, Sealfon SC, Iyengar R, Landau EM, Blitzer RD. (2005) Local protein synthesis mediates a rapid increase in dendritic elongation factor 1A after induction of late long-term potentiation. J Neurosci 25: 5833–5843.

Tsokas P, Ma T, Iyengar R, Landau EM, Blitzer RD. (2007). Mitogen-activated protein kinase upregulates the dendritic translation machinery in long-term potentiation by controlling the mammalian target of rapamycin pathway. J Neurosci. May 30;27(22):5885-94.

Turrigiano GG, Leslie KR, Desai NS, Rutherford LC, Nelson SB. (1998). Activity-dependent scaling of quantal amplitude in neocortical neurons. Nature. Feb 26;391(6670):892-6.

Turrigiano GG. (2008) The self-tuning neuron: synaptic scaling of excitatory synapses. Cell. 135:422-35.

Turrigiano GG, Nelson SB. (2004). Homeostatic plasticity in the developing nervous system. Nat Rev Neurosci. Feb;5(2):97-107.

Vyazovskiy VV, Cirelli C, Pfister-Genskow M, Faraguna U, Tononi G. (2008). Molecular and electrophysiological evidence for net synaptic potentiation in wake and depression in sleep. Nat Neurosci. Feb;11(2):200-8.

Wang CC, Held RG, Chang SC, Yang L, Delpire E, Ghosh A, Hall BJ. (2011). A critical role for GluN2B-containing NMDA receptors in cortical development and function. Neuron. Dec 8;72(5):789-805.

Wang HL, Zhang Z, Hintze M, Chen L. (2011). Decrease in calcium concentration triggers neuronal retinoic acid synthesis during homeostatic synaptic plasticity. J Neurosci. Dec 7;31(49):17764-71.

Waskiewicz AJ, Flynn A, Proud CG, Cooper JA. (1997). Mitogen-activated protein kinases activate the serine/threonine kinases Mnk1 and Mnk2. EMBO J. Apr 15;16(8):1909-20.

Yang HS, Jansen AP, Nair R, Shibahara K, Verma AK, Cmarik JL, Colburn NH. (2001). A novel transformation suppressor, Pdcd4, inhibits AP-1 transactivation but not NF-kappaB or ODC transactivation. Oncogene. Feb 8;20(6):669-76.

Zhong J, Zhang T, Bloch LM (2006) Dendritic mRNAs encode diversified functionalities in hippocampal pyramidal neurons. BMC Neurosci 7: 17.

CHAPTER II

Retrograde Changes in Presynaptic Function Driven by Dendritic mTORC1

2.1 Abstract

Mutations that alter signaling through the mammalian target of rapamycin complex 1 (mTORC1), a well-established regulator of neuronal protein synthesis, have been linked to autism and cognitive dysfunction. Although previous studies have established a role for mTORC1 as necessary for enduring changes in postsynaptic function, here we demonstrate that dendritic mTORC1 activation in rat hippocampal neurons also drives a retrograde signaling mechanism promoting enhanced neurotransmitter release from apposed presynaptic terminals. This novel mode of synaptic regulation conferred by dendritic mTORC1 is locally implemented, requires downstream synthesis of brain-derived neurotrophic factor as a retrograde messenger, and is engaged in an activity-dependent fashion to support homeostatic trans-synaptic control of presynaptic function. Our findings thus reveal that mTORC1-dependent translation in dendrites subserves a unique mode of synaptic regulation, highlighting an alternative regulatory pathway that could contribute to the social and cognitive dysfunction that accompanies dysregulated mTORC1 signaling.

2.2 Introduction

Although principal neurons receive many thousands of synapses, the ability to tune synaptic strength independently along specific regions of the dendritic arbor is thought to confer the increased computational capacity necessary for new learning and memory storage in neural circuits (Rabinowitch and Segev, 2008; Branco and Haüsser, 2010). The discovery of polyribosomes in the distal dendrites of dentate granule neurons (Steward and Levy, 1982) first suggested that dendritic translation might participate in controlling synaptic function on a local level, an idea that has been clearly substantiated by work in a wide range of model systems (Kang and Schuman, 1996; Martin et al., 1997; Huber et al., 2000; Sutton et al., 2006). In particular, the mammalian target of rapamycin (mTOR) is known to be an important control point for protein synthesis related to synaptic plasticity (Casadio et al., 1999; Tang et al., 2002; Cammalleri et al., 2003; Gong et al., 2006) and memory (Tischmeyer et al., 2003; Dash et al., 2006; Blundell et al., 2008).

mTOR is a serine/threonine protein kinase that integrates into two distinct protein complexes, mTOR complex 1 (mTORC1) and mTOR complex 2 (mTORC2) (Ma and Blenis, 2009). Of these, mTORC1 promotes translation of specific classes of mRNAs via phosphorylation of downstream effectors, such as eIF4E binding protein (4EBP) and p70 S6 kinase (S6K1) (Wang and Proud, 2006; Costa-Mattioli et al., 2009; Zoncu et al., 2011). A wide array of extracellular signals regulates mTORC1 signaling through the mTORC1 repressor tuberous sclerosis complex (TSC) or the small GTPase Rheb, which promotes mTORC1 activation (Yang and Guan, 2007).

Animal studies have clearly implicated mTORC1 in hippocampal synaptic plasticity and in the formation of long-term hippocampal-dependent memories (Ehninger et al., 2008; Gkogkas et al., 2010; Hoeffer and Klann, 2010). Moreover, human mutations that result in dysregulation of mTORC1 signaling have been associated with vulnerability to autism, cognitive impairment, and epilepsy (Onda et al., 2002; Butler et al., 2005; Johannessen et al., 2005; Kelleher and Bear, 2008), underscoring the importance of this signaling complex for proper neural circuit function in the human brain. At vertebrate synapses, dendritic mTORC1 has been most clearly implicated in enduring forms of long-term potentiation (LTP) and long-term depression (LTD) that are induced and expressed postsynaptically (Tang et al., 2002; Cammalleri et al., 2003, Sharma et al., 2010; Hoeffer et al., 2008), suggesting that mTORC1-dependent translational control may participate in maintaining altered AMPA receptor (AMPAR) expression at synapses, promoting structural synaptic changes, or both.

Here, we demonstrate that mTORC1-dependent translation in dendrites exerts a novel form of regulatory control over synapse function. Unlike enduring changes in postsynaptic function during LTP and LTD, we find that homeostatic enhancement of postsynaptic function induced by acute loss of excitatory synaptic drive occurs via mTORC1-independent protein synthesis. Instead, we find that dendritic mTORC1 activation is both necessary and sufficient for driving protein synthesis-dependent compensatory changes in neurotransmitter release from apposed presynaptic terminals, revealing that parallel translational control pathways operate locally in dendrites to mediate distinct homeostatic adaptations at synapses.

2.3 Results

Loss of excitatory synaptic input drives dendritic mTORC1 activation

Previous work has established that strong synaptic activation can drive mTORC1 signaling in hippocampal neurons (Tang et al., 2002; Cammalleri et al., 2003), but it is largely unclear how the activity-dependent regulation of mTORC1 signaling is sculpted by loss of synaptic drive. To explore this question, we examined the regulation of several downstream targets of mTORC1 signaling in active networks of cultured hippocampal neurons subject to acute blockade of excitatory transmission through either AMPARs or NMDARs. Treating cultured hippocampal neurons with the AMPAR antagonist CNQX (40 μM), but not the NMDAR antagonist APV (50 μM), induced a rapid time-dependent increase in phosphorylation of ribosomal protein S6 at S235/236 (Figure 2.1A–C), a downstream target of mTORC1 activation. Likewise, CNQX treatment (40 μM, 30 min) induced phosphorylation of S6K1 at Thr389 and 4EBP at Thr37/46 (Figure 1D-E), both direct mTORC1 phosphorylation sites. The mTORC1 inhibitor rapamycin (100 nM) completely suppressed both basal and enhanced S6 and S6K1 phosphorylation (Figure. 2.1C-D), as well as enhanced phosphorylation of 4EBP1 (Figure 2.1E), confirming a role for mTORC1 activation in these effects. Another AMPAR antagonist, NBQX (10 μM), produced similar rapamycin-sensitive effects on S6, S6K1, and 4EBP1 phosphorylation (data not shown). Finally, immunocytochemistry revealed that AMPAR blockade induced significant S6 phosphorylation in both the cell bodies and dendrites of hippocampal neurons (Figure 1F-G), whereas MAP2 expression from these same neurons was unchanged. Under our staining conditions, virtually all PS6 immunofluorescence was abolished by pretreatment with 100 nM rapamycin (data not shown), verifying PS6 staining as a valid readout of mTORC1 activation. These results indicate that mTORC1 signaling is activated in response to acute loss of excitatory synaptic drive as well as in response to patterned synaptic activation.

A drop in excitatory synaptic input is also known to regulate translation through dephosphorylation of eukaryotic elongation factor 2 (eEF2) at Thr56 (Sutton et al., 2007;

Nosyreva and Kavalali, 2010). eEF2 kinase can be regulated by mTORC1 activation (Wang and Proud, 2006), so we also examined eEF2 phosphorylation in response to AMPAR blockade and its reliance on intact mTORC1 signaling. While AMPAR blockade induced rapid eEF2 dephosphorylation consistent with translational activation, this effect was insensitive to coincident mTORC1 inhibition with rapamycin (Figure 2.1H-I). These results suggest that AMPAR blockade engages multiple translational regulatory pathways in hippocampal neurons.

Homeostatic enhancement of postsynaptic function is not dependent mTORC1 activation

We next examined whether activation of mTORC1 accompanying AMPAR blockade contributes to the homeostatic enhancement of postsynaptic function induced by such loss of synaptic activity, which is dependent on new protein synthesis (Sutton et al., 2006; Aoto et al., 2008). Indeed, rapid postsynaptic compensation shares with translation-dependent late-phase LTP (L-LTP) in the hippocampus a recruitment of AMPARs to synapses (Makino and Malinow, 2009), and mTORC1 signaling is known to be necessary for the enduring changes in postsynaptic function associated with L-LTP (Tang et al., 2002). Despite these similarities, we found that the increase in surface GluA1 expression at synapses following AMPAR blockade was not altered by the mTORC1 inhibitor rapamycin (100 nM; Figure 2.2A-B). Likewise, mTORC1 inhibition with either rapamycin or an mTOR active site inhibitor C-401 (10 μM; Ballou et al., 2007) did not affect the rapid compensatory increase in amplitude of mEPSCs accompanying AMPAR blockade (40 μM CNQX, 3 h), recorded immediately following CNQX washout (Figure 2.2C-D). Similar to previous reports (Thiagarajan et al., 2005; Sutton et al., 2006; Aoto et al., 2008), we found that the homeostatic increase in mEPSC amplitude is mediated by recruitment of GluA1 homomeric receptors to synapses, which, unlike GluA2-

containing AMPARs, are blocked by polyamine toxins, such as 1-napthylacetylspermine (NASPM). We found that mTORC1 inhibition coincident with AMPAR blockade also did not affect the NASPM sensitivity of scaled mEPSCs (Figure 2.2F-G), indicating that GluA1 homomeric receptors are recruited to synapses in the absence of mTORC1 signaling. The effects of NASPM in these conditions are specific for mEPSC amplitude. While coincident rapamycin and C-401 treatment each block the increase in mEPSC frequency induced by AMPAR blockade, NASPM treatment after these treatments does not further reduce mEPSC frequency below control levels (data not shown). Together, these observations suggest that, while mTORC1 activation during L-LTP and mGluR-LTD is necessary for enduring changes in postsynaptic function (Hou and Klann, 2004; Antion et al., 2008), the homeostatic enhancement of postsynaptic function driven by loss of synaptic activity does not require mTORC1 signaling.

mTORC1 is necessary for retrograde enhancement of presynaptic function

In addition to triggering rapid postsynaptic compensation, AMPAR blockade also drives compensatory increases in presynaptic function (Murthy et al., 2001; Thiagarajan et al., 2005) that depend on retrograde signaling from the postsynaptic cell (Jakawich et al., 2010; Lindskog et al., 2010; Groth et al., 2011). Thus, AMPAR blockade drives not only an increase in mEPSC amplitude, but also an increase in mEPSC frequency in hippocampal neurons. This increase in frequency reflects enhanced release probability from existing presynaptic terminals (Jakawich et al., 2010). Likewise, at the Drosophila neuromuscular junction, acute blockade of postsynaptic AMPARs triggers rapid compensatory increases in quantal content (Frank et al., 2006), suggesting an evolutionarily conserved mode of regulation whereby postsynaptic glutamate receptors exert homeostatic control over presynaptic function. Interestingly, while mTORC1 activation is not necessary for compensatory enhancement of postsynaptic function following AMPAR blockade, we found that such activation was essential for the development of homeostatic changes in presynaptic function. Thus, both rapamycin and C-401 completely suppressed the increase in mEPSC frequency induced by AMPAR blockade (Figure 2.2C-E). Similar to AMPAR blockade, chronic (>24 h) treatment with L-type $Ca2^+$ channel inhibitors induces compensatory enhancement of presynaptic and postsynaptic function (Thiagarajan et al., 2005; Gong et al., 2007), raising the question of whether mTORC1 plays a similar role during homeostatic plasticity induced by loss of L-type channel function. Indeed, we found that blocking L-type channels with 10 μM nifedipine over a 3 h period induced a significant increase in both mEPSC amplitude (mean ± SEM mEPSC amplitude: controls, 13.15 ± 0.60 pA, n = 11 cells; 3 h nifedipine, 15.38 ± 0.70 pA, n = 14 cells; $p < 0.05$; data not shown) and frequency (mean ± SEM mEPSC frequency: controls, 1.99 ± 0.33 Hz; 3 h nifedipine, 4.82 ± 0.75 Hz; $p < 0.05$; data not shown). As we observed with AMPAR blockade, coincident inhibition of mTORC1 with 100 nM rapamycin did not affect the compensatory increase in mEPSC amplitude (3 h nifedipine plus rapamycin, 15.76 ± 0.94 pA, n = 10 cells; $p < 0.05$ vs control), but strongly suppressed the increase in mEPSC frequency (3 h nifedipine plus rapamycin, 2.35 ± 0.30 Hz; not significant vs control) induced by nifedipine treatment. Thus, during homeostatic changes driven by either AMPAR blockade or loss of L-type $Ca2^+$ channel function, mTORC1 inhibition selectively suppresses compensatory enhancement of mEPSC frequency, but not mEPSC amplitude.

To ensure that these mTORC1-dependent changes in mEPSC frequency following AMPAR blockade reflect compensatory enhancement of presynaptic function, we visualized actively releasing synaptic terminals by brief (5 min) live-labeling with an antibody targeted against the lumenal domain of synaptotagmin 1 (syt-lum) followed by fixation and labeling with an antibody against the vesicular glutamate transporter, vglut1, to mark excitatory terminals. To estimate relative presynaptic function under control conditions and following AMPAR blockade, we measured the proportion of vglut1-positive terminals with detectable syt-lum staining under conditions of spontaneous vesicle release (15 min pretreatment with 2 μM TTX before labeling). Using this unambiguous readout of presynaptic function, we found that neither rapamycin nor C-401 altered basal syt-lum uptake, but each prevented the increase in syt-lum uptake induced by AMPAR blockade (Figure 2.3A-B). To confirm these observations and assess whether mTORC1 is necessary for homeostatic changes in action potential-driven vesicle release, we directly visualized evoked glutamate release by imaging activity-dependent changes in vglut1-pHluorin fluorescence at presynaptic terminals identified by coexpression of mCherry-tagged synaptophysin (Figure 2.3C). As previously reported (Voglmaier et al., 2006), basal vglut1-pHluorin fluorescence at presynaptic terminals was low due to effective quenching by the acidic environment of synaptic vesicles, allowing for optical detection of action potential-triggered synaptic vesicle fusion when the lumen of the vesicle is exposed to the neutral extracellular space. To induce action potentials across the network, we applied field stimulation via parallel platinum-iridium electrodes under conditions where individual pulses each faithfully produced an action potential, verified by the characteristic cell-wide $Ca2^+$ transient accompanying each stimulus (data not shown). In control (vehicle-treated) neurons, a 10 s train of action potentials delivered at 10 Hz induced a clear increase in vglut1-pHluorin fluorescence at presynaptic terminals, but following AMPAR blockade (40 μM CNQX, 3 h), this evoked vesicle fusion was markedly enhanced (Figure 2.3C-D). Blocking mTORC1 activation during AMPAR blockade (100 nM rapamycin) prevented this enhancement of evoked release, suggesting that, similar to effects on spontaneous neurotransmitter release, mTORC1 activation is necessary for the enhancement of evoked release following AMPAR blockade. Together, these findings suggest that mTORC1 is specifically required for homeostatic changes in presynaptic function induced by loss of AMPAR-mediated synaptic activity.

Homeostatic enhancement of presynaptic function is dependent on postsynaptic mTORC1 activation

The fact that AMPAR blockade elicits mTORC1 activation in dendrites (Figure 2.1H-I) raises the possibility that postsynaptic mTORC1 activation is necessary to drive retrograde compensation in presynaptic terminals. To address this issue, we overexpressed the tuberous sclerosis complex proteins TSC1 and TSC2, which together act as endogenous suppressors of mTORC1 activation (Inoki et al., 2002, 2003). To examine the specific role of postsynaptic mTORC1 activation, we used a low-efficiency strategy where <1% of neurons are transfected. This enabled us to examine selective mTORC1 inhibition in single transfected neurons that receive synapses from untransfected cells with unperturbed mTORC1 signaling (Figure 2.4A). As expected, phosphorylation of S6, downstream of mTORC1 activity, was substantially reduced in neurons transfected with TSC1/2 relative to both untransfected neighboring neurons (Figure 2.4B) and neurons transfected with EGFP alone (Figure 2.4C). Moreover, TSC1/2 expression also prevented mTORC1 activation induced by AMPAR blockade (Figure 2.4C). We next examined the effects of TSC1/2 expression on synaptic compensation. Consistent with our previous observations, postsynaptic knockdown of mTORC1 activation did not alter the ability of AMPAR blockade to drive postsynaptic compensation, as similar increases in mEPSC amplitude were evident in both TSC1/2-expressing neurons and untransfected neighboring control neurons after treatment with 40 μM CNQX (3 h, added 21 h post-transfection; Figure 2.4D-E). However, the enhancement of mEPSC frequency accompanying AMPAR blockade was strongly inhibited in TSC1/2-expressing neurons relative to both untransfected controls and neurons in sister cultures transfected with EGFP alone (Figure 4.4F). Importantly, TSC1/2 overexpression for 24 h did not alter basal mEPSC frequency or amplitude in the absence of AMPAR blockade (Figure 2.4D–F). Because the increase in mEPSC frequency accompanying AMPAR blockade is known to reflect an enhancement in release probability in presynaptic terminals synapsing on the recorded neuron (Jakawich et al., 2010), these results suggest that postsynaptic mTORC1 activation is necessary for retrograde changes in presynaptic function driven by AMPAR blockade.

Local mTORC1 activation in dendrites is necessary for retrograde changes in presynaptic function

We next examined whether local mTORC1 signaling in dendrites is necessary for retrograde changes in presynaptic function. To address this possibility, we used restricted microperfusion of rapamycin (200 nM) either alone or in conjunction with AMPAR blockade (bath 40 μM CNQX, 120 min; Figure 2.5A), and examined subsequent live syt-lum uptake as a readout of presynaptic changes. We found that spatially restricted inhibition of mTORC1 signaling during AMPAR blockade induced a selective inhibition of syt-lum uptake at terminals apposed to the treated dendritic segment (Figure 2.5B-C), while vglut1 immunofluorescence in those same segments was not significantly altered. By contrast, local rapamycin treatment in the absence of AMPAR blockade (Figure 2.5D) did not alter syt-lum uptake, demonstrating a specific role for local mTORC1 signaling in presynaptic compensation induced by AMPAR blockade. Importantly, the brief (5 min) syt-lum labeling period used in these microperfusion experiments argues against a major influence from the transit of synaptic vesicles between different presynaptic terminals. Indeed, we observed only minimal fluorescence recovery over a 50 min period after locally photobleaching syt-lum signal (data not shown), indicating that the signal observed in treated dendritic segments under brief labeling conditions primarily reflects uptake at synapses apposed to those segments. These results thus suggest that mTORC1 activation in dendrites plays a spatially restricted role in driving retrograde homeostatic changes in presynaptic function in response to AMPAR blockade.

mTORC1 operates upstream of BDNF synthesis during homeostatic plasticity

Postsynaptic release of BDNF is necessary for retrograde changes in presynaptic function driven by AMPAR blockade (Jakawich et al., 2010; Lindskog et al., 2010), raising the question of whether mTORC1 operates upstream or downstream of BDNF action. Indeed, exogenous BDNF application is known to activate mTORC1 signaling (Schratt et al., 2004), raising the possibility that mTORC1 activation in the context of synaptic attenuation might be secondary to BDNF release. However, contrary to this notion, we found that mTORC1 activation induced by AMPAR blockade was BDNF-independent as scavenging extracellular BDNF with TrkB-Fc (1 μg/ml) did not affect phosphorylation of mTORC1 effectors in response to CNQX treatment (Figure 2.6A-B). To explore this issue further, we examined whether presynaptic changes driven by direct BDNF application were sensitive to coincident mTORC1 inhibition with rapamycin. As shown in Figure 2.6C-D, application of BDNF (250 ng/ml) to cultured neurons for 60 min induced a sustained increase in mEPSC frequency that remained persistent following BDNF washout (mEPSCs were recorded 30–50 min following BDNF removal). Importantly, direct

BDNF application induced a similar increase in mEPSC frequency in the presence or absence of rapamycin (Figure 2.6C-D), indicating that BDNF modulates presynaptic function in an mTORC1-independent fashion. Likewise, BDNF-induced enhancement of syt-lum uptake at vglut1-positive excitatory terminals was similarly unaffected by coincident rapamycin treatment (Figure 2.6E-F), indicating that BDNF acts downstream of mTORC1 activation to drive enhancement of presynaptic function. Given the role of mTORC1 in translational control, these findings suggest that mTORC1 activation might participate in the regulation of de novo BDNF synthesis, which is necessary for retrograde homeostatic changes in presynaptic function (Jakawich et al., 2010). Consistent with this possibility, Western blots of hippocampal neuron lysates revealed that the increase in BDNF expression in response to AMPAR blockade was prevented by rapamycin (Figure 2.7A-B). To assess the cellular compartments where this mTORC1-dependent regulation of BDNF occurs, we examined BDNF expression by immunocytochemistry. Consistent with earlier reports (Jakawich et al., 2010), AMPAR blockade induced a significant increase in BDNF expression in dendrites without altering somatic BDNF levels (Fig. 7C,D). This highly compartmentalized increase in dendritic BDNF expression induced by AMPAR blockade was prevented by mTORC1 inhibition with rapamycin. These findings suggest that mTORC1 is a critical regulator of new BDNF synthesis following AMPAR blockade.

Cell-autonomous enhancement of synaptic activity accompanies postsynaptic mTORC1 activation

We next asked whether postsynaptic mTORC1 activation in the absence of AMPAR blockade is sufficient for driving retrograde changes in presynaptic function. To examine this question, we again used a sparse expression strategy while transfecting the mTORC1 activating GTPase Rheb (data not shown) or a hyperactive RhebQ64L mutant (Figure 2.8A) that is persistently in its GTP-bound state (Jiang and Vogt, 2008). In non-neuronal cells, expression of Rheb or RhebQ64L is sufficient to drive sustained cell-autonomous mTORC1 signaling (Tee et al., 2003; Long et al., 2005). Likewise, 24 h following transfection, immunocytochemistry against PS6 confirmed robust dendritic and somatic mTORC1 activation in RhebQ64L-transfected neurons relative to either surrounding untransfected neurons (Figure 2.8B) or neurons from sister cultures transfected with EGFP alone (Figure 2.8C). To examine the impact of cell-autonomous mTORC1 activation on overall excitatory synaptic drive in active networks, we compared spontaneous excitatory synaptic activity in RhebQ64L-expressing neurons with neighboring untransfected neurons in the same culture and EGFP-transfected neurons in sister cultures in the absence of TTX. Recording spontaneous EPSCs in the presence of bicuculine and APV, we found that overall excitatory network activity was significantly enhanced onto RhebQ64L-expressing neurons, reflected in >5-fold increase in charge transfer relative to untransfected neurons in the same culture (Figure 2.8D-E). To examine whether these changes in synaptic efficacy derive from growth of new synaptic connections, we examined the density of dendritic spines in response to either chronic suppression (with TSC1/2 overexpression) or hyperactivation (with RhebQ64L expression) of mTORC1. We found that alteration of mTORC1 signaling for ~24 h or 5 d failed to alter the density of dendritic spines (Figure 2.8F–H) relative to control neurons expressing GFP alone, despite clear mTORC-dependent regulation of cell soma size (5 d). While it is likely that more prolonged changes in mTORC1 signaling are sufficient to alter synaptic growth, these results suggest that the cell-autonomous increase in synaptic efficacy observed here results largely from altered function of existing synaptic connections.

Postsynaptic mTORC1 activation is sufficient to drive retrograde changes in presynaptic function

We next examined the mechanisms by which postsynaptic mTORC1 activation leads to enhanced synaptic efficacy. Given that the enhancement of dendritic BDNF expression following AMPAR blockade is dependent on mTORC1 (Figure 2.7C-D), we first assessed whether postsynaptic mTORC1 activation is sufficient to alter BDNF expression in the cell body or dendritic compartment of hippocampal neurons. Indeed, RhebQ64L-expressing neurons exhibited a striking increase in dendritic BDNF expression without altering MAP2 levels in the same neurons (Figure 2.9A-B). Moreover, the pattern of changes following mTORC1 activation was highly reminiscent of changes in BDNF expression that accompany AMPAR blockade (Figure 2.7C-D), as the change in BDNF expression was again highly compartmentalized, with no significant alteration in somatic BDNF levels (Figure 2.9A-B). A strikingly similar pattern was observed with overexpression of wild-type Rheb, where dendritic BDNF expression increased significantly (mean ± SEM percentage change in BDNF fluorescence relative to GFP expression alone, +145.7 ± 26.1; $p < 0.05$; data not shown) without concomitant changes in steady-state BDNF expression in the cell body (mean ± SEM percentage change in BDNF fluorescence relative to GFP expression alone, −13.4 ± 5.1, not significant; data not shown). These selective changes in dendritic BDNF expression are not due to compartment-selective mTORC1 activation, as expression of both Rheb (data not shown) and RhebQ64L (Figure 2.8B) enhance PS6 staining in both the cell bodies and dendrites. These observations suggest that dendritic and somatic expression of BDNF is subject to distinct compartment-specific regulatory control.

To determine how postsynaptic mTORC1 activation alters synaptic efficacy and to what extent the changes in BDNF expression contribute, we recorded mEPSCs from RhebQ64L-transfected neurons or neighboring untransfected control neurons with unaltered mTORC1 signaling. The sparse transfection conditions gave rise to isolated RhebQ64L-expressing neurons that receive nearly all their synaptic inputs from untransfected neurons with unaltered mTORC1 signaling (Figure 2.8A), enabling us to evaluate the effects of postsynaptic mTORC1 activation on both presynaptic and postsynaptic function. Despite the strong increase in synaptic drive induced by postsynaptic RhebQ64L expression (24 h post-transfection), the amplitude of mEPSCs onto these neurons was not altered relative to neighboring untransfected neurons (Figure 2.9C-D) or neurons expressing GFP alone (Figure 2.4E). However, RhebQ64L-expressing neurons exhibited a marked increase in mEPSC frequency (Figure 2.9C–E), suggesting enhanced spontaneous release from synaptic terminals that impinge on dendrites with activated mTORC1 signaling. Like the changes induced by AMPAR blockade, these retrograde changes in presynaptic function driven by postsynaptic mTORC1 activation required BDNF release, as they were completely prevented by the extracellular BDNF scavenger TrkB-Fc (1 μg/ml; Figure 2.9C–E). A very similar pattern of results was observed with postsynaptic expression of wild-type Rheb in parallel experiments, where postsynaptic Rheb expression induced a significant increase in mEPSC frequency (mean ± SEM mEPSC frequency, nontransfected controls: 1.52 ± 0.17 Hz; Rheb transfected neurons: 2.35 ± 0.40 Hz, $p < 0.05$ one-tailed; data not shown) without altering mEPSC amplitude (mean ± SEM mEPSC amplitude, nontransfected controls: 13.95 ± 0.66 pA; Rheb transfected neurons: 14.03 ± 0.65 pA, not significant; data not shown). As with RhebQ64L, the increase in mEPSC frequency with Rheb overexpression is similarly abolished by scavenging extracellular BDNF (mean ± SEM mEPSC frequency, nontransfected controls with TrkB-Fc: 1.51 ± 0.19 Hz; Rheb transfected neurons: 1.29 ± 0.15 Hz; data not shown).

To examine whether a similar enhancement of evoked neurotransmission is also established by postsynaptic mTORC1, we examined a use-dependent block of evoked NMDAR-mediated EPSCs onto RhebQ64L-expressing neurons and untransfected neurons from the same cultures with the open-channel blocker MK-801 to assess neurotransmitter release probability (Hessler et al., 1993; Rosenmund et al., 1993). Immediately before recording, evoked NMDAR EPSCs were pharmacologically isolated and elicited at a rate of 0.33 Hz with an extracellular stimulating electrode positioned near the recording neuron. Before MK-801 treatment, the kinetics of evoked NMDAR EPSCs in RhebQ64L-expressing neurons, untransfected neurons, and control GFP-expressing neurons were similar (mean ± SEM time to 50% decay, nontransfected controls: 75.40 ± 9.34 ms, n = 10 cells; GFP-expressing neurons: 81.72 ± 9.15 ms, n = 11 cells; RhebQ64L-expressing neurons: 85.09 ± 7.75 ms, n = 9 cells; F(2,27) = 0.29, not significant), suggesting similar NMDAR subunit composition in the three conditions. As expected for an increase in release probability, we found that MK-801 blockade of NMDAR currents was significantly accelerated in RhebQ64L-expressing neurons relative to untransfected neurons from the same cultures, as well as from control neurons expressing GFP in sister cultures (Figure 2.9F-G). Again, the extracellular BDNF scavenger TrkB-Fc completely eliminated the enhanced release probability onto RhebQ64L-expressing neurons, suggesting that postsynaptic mTORC1 activation controls evoked neurotransmitter release through the release of BDNF as a retrograde messenger. Together, these results suggest that postsynaptic mTORC1 activation is sufficient to drive retrograde enhancement of presynaptic function in a BDNF-dependent fashion, a manner similar to homeostatic changes in presynaptic function induced by loss of excitatory synaptic input.

2.4 Discussion

Our results identify a novel mode of synaptic regulation conferred by local mTORC1-dependent signaling in dendrites. While the role of mTORC1 in contributing to alterations in postsynaptic function during protein synthesis-dependent forms of synaptic plasticity is well established (Tang et al., 2002; Cammalleri et al., 2003; Hou and Klann, 2004), here we have shown that dendritic mTORC1 activation also gates a local retrograde signaling mechanism that drives changes in presynaptic function from apposed postsynaptic terminals. This unique trans-synaptic role for dendritic mTORC1 signaling is critically dependent on BDNF release, which serves to couple loss of excitatory synaptic drive with retrograde compensation of presynaptic function. Finally, we show that dendritic mTORC1 plays a spatially restricted role in retrograde modulation of presynaptic function induced by AMPAR blockade, revealing a unique role for mTORC1 as part of a homeostatic translational control pathway that operates locally in dendrites and underlies trans-synaptic control of presynaptic function.

Parallel translational regulatory pathways in dendrites mediate distinct homeostatic adaptations at synapses

While alterations in postsynaptic firing have been shown to exert cell-wide homeostatic changes in synaptic strength (Ibata et al., 2008; Goold and Nicoll, 2010), several groups have demonstrated that compensatory synaptic adaptations can also be implemented locally in dendrites (Sutton et al., 2006; Aoto et al., 2008; Jakawich et al., 2010), even at individual synapses (Lee et al., 2010; Bé̈ïque et al., 2011; Hou et al., 2011). Indeed, acute loss of excitatory synaptic input induces a rapid and local recruitment of GluA1 homomeric receptors to affected synapses. This recruitment is critically dependent on dendritic protein synthesis (Sutton et al., 2006; Aoto et al., 2008; Maghsoodi et al., 2008). In hippocampal neurons, this rapid postsynaptic compensation can be induced by blockade of either AMPARs or NMDARs, whereas retrograde compensation of presynaptic terminals accompanies AMPAR blockade but not NMDAR blockade (Jakawich et al., 2010). We also find that AMPAR blockade rapidly activates mTORC1 signaling in dendrites of hippocampal neurons, but NMDAR blockade over the same period does not. However, it is clear that patterned synaptic activity drives mTORC1 signaling in hippocampal neurons through an NMDAR-dependent mechanism (Tang et al., 2002; Cammalleri et al., 2003), and that loss of NMDAR activity in cortical neurons can also activate mTORC1 signaling (Li et al., 2010; Wang et al., 2011). Whether these differences reflect unique coupling of AMPARs to inactivation-induced mTORC1 signaling in hippocampal neurons or differences in the timing or context of NMDAR blockade await future studies. On the other hand, the coupling between AMPARs and mTORC1 activation that we describe in hippocampal neurons has also been recently observed at the Drosophila neuromuscular junction (NMJ). Similar to our findings, Penney and colleagues (2012) document a requirement for postsynaptic TOR activation in vivo during retrograde homeostatic plasticity driven by AMPAR blockade at the NMJ, and also find that genetic upregulation of postsynaptic TOR activity is sufficient to drive retrograde enhancement of presynaptic function. Together with our results, these findings suggest that the retrograde signaling role for mTORC1 at synapses is evolutionarily conserved.

We find that postsynaptic compensation induced by AMPAR blockade, which, in hippocampal neurons, is highly similar to that following acute loss of NMDAR activity, is insensitive to mTORC1 inhibitors or postsynaptic knockdown of mTORC1 signaling (but see Wang et al., 2011). Consistent with our results, Maghsoodi et al. (2008) found that mTORC1 inhibition with rapamycin did not disrupt postsynaptic compensation induced by retinoic acid, which is an essential intermediate in the recruitment of GluA1 homomeric receptors to synapses during NMDAR blockade (Aoto et al., 2008; Soden and Chen, 2010). These results illustrate that homeostatic plasticity of postsynaptic function differs from L-LTP and mGluR-LTD in hippocampal neurons in relying on a distinct mTORC1-independent translational control pathway in dendrites for its induction. We speculate that the dependence on unique translation regulatory events likely reflects a requirement for a distinct set of newly synthesized effector proteins in each case, despite the common regulation of synaptic AMPAR content as a mode of expression. Interestingly, we found that postsynaptic mTORC1 activation over a time-frame that encompasses L-LTP and mGluR-LTD induction was insufficient to drive changes in postsynaptic function directly. This suggests that the unique complement of postsynaptic proteins synthesized in an mTORC1-dependent fashion (Schratt et al., 2004; Slipczuk et al., 2009; Neasta et al., 2010) must interact with other activity-dependent signaling events to alter postsynaptic function in an enduring fashion. While relatively acute mTORC1 activation (<24 h) in our experiments did not alter postsynaptic function directly, there is evidence to suggest that longer, chronic hyperactivation of neuronal mTORC1, via knockdown of TSC1 or TSC2, is associated with morphological and functional changes in the postsynaptic compartment (Tavazoie et al., 2005; Bateup et al., 2011). Our findings raise the intriguing possibility that the alterations in postsynaptic structure and function that accompany more chronic postsynaptic mTORC1 activation might be secondary to altered neurotransmitter release from apposed synaptic terminals, given that these functional changes in the presynaptic compartment are the first to emerge following mTORC1 activation.

While the functional role of dendritic protein synthesis on postsynaptic function has been heavily studied, it is now clear that alteration of presynaptic function by dendrite-derived factors can exert an important additional level of regulatory control at synapses (Regehr et al., 2009). Such retrograde signaling is also known to play a pivotal role in synaptic homeostasis (Frank et al., 2006; Branco et al., 2008; Jakawich et al., 2010; Lindskog et al., 2010). For example, local activity in a specific dendritic branch has been shown to homeostatically modulate release probability from apposed presynaptic terminals (Branco et al., 2008), and similar retrograde changes in presynaptic function are dependent on local dendritic protein synthesis (Jakawich et al., 2010). Our results demonstrate an essential role for mTORC1 activation in this local retrograde modulation of presynaptic function. Hence, parallel mTORC1-dependent and mTORC1-independent translational control pathways in dendrites subserve rapid homeostatic adjustment of presynaptic and postsynaptic function.

mTORC1-dependent retrograde signaling requires BDNF as a downstream effector

We identified BDNF as a critical effector acting downstream of mTORC1 activation in driving enhancement of presynaptic function. mTORC1 signaling is necessary for enhanced BDNF expression accompanying AMPAR blockade, and postsynaptic mTORC1 activation in the absence of AMPAR blockade is sufficient to enhance dendritic BDNF expression. Given that mTORC1 is required locally in dendrites for presynaptic compensation and that AMPAR blockade drives local dendritic BDNF synthesis (Jakawich et al., 2010), our results suggest that dendritic mTORC1 likely directly controls BDNF synthesis in dendrites. Consistent with this notion, we find that mTORC1 activation induces highly compartmentalized changes in BDNF expression, with significant elevation in dendrites despite no measurable changes in the cell body from the same neurons. Presently, it is unclear what mechanisms account for the compartment-specific changes in BDNF expression accompanying mTORC1 activation, although it is known that the BDNF mRNA pool comprises up to 16–22 transcripts with unique 5′ and/or 3′ UTRs (Aid et al., 2007). Moreover, these distinct BDNF transcripts exhibit differences in activity-dependent dendritic trafficking (Pattabiraman et al., 2005; Chiaruttini et al., 2008) as well as constitutive dendritic localization (An et al., 2008; Baj et al., 2011), raising the possibility that only a small subset of these, which may comprise a greater relative proportion of the dendritic BDNF mRNA pool (Baj et al., 2011), are responsive to mTORC1 activation (Liao et al., 2012). Future studies are needed to map the mTORC1-responsive sites (or lack thereof) in each BDNF transcript to test this idea. Another unresolved question relates to the relative influence of proBDNF and mature BDNF in driving the presynaptic changes induced by dendritic mTORC1 activation. Whereas mature BDNF is clearly upregulated by AMPAR blockade in a rapamycin-sensitive fashion (Figure 2.7A-B), further studies are needed to test whether the presynaptic changes induced by dendritic mTORC1 activation require the release of proBDNF, mature BDNF, or some combination of the two.

A novel target for cognitive dysfunction caused by dysregulated mTORC1 signaling?

Several disorders resulting in cognitive impairment and mental retardation have been suggested to share dysregulation of local protein synthesis in dendrites as a common feature (Hoeffer and Klann, 2010), specifically via overactive signaling of mTORC1. Indeed, several monogenic disorders resulting in overactive mTORC1 signaling, such as tuberous sclerosis complex, neurofibramatosis type 1, and PTEN (phosphatase and tensin homolog deleted on chromosome 10) harmatoma syndrome (Kwiatkowski, 2003; Butler et al., 2005; Johannessen et al., 2005; Ehninger et al., 2008) have high comorbidity rates with autism spectrum disorders (ASDs), leading to the idea that altered protein synthesis in neurons may be a common phenotype central to the emergence of aberrant cognitive and behavioral characteristics related to ASD (Kelleher and Bear, 2008). Indeed, the well-established role for mTORC1 in supporting protein synthesis-dependent changes in postsynaptic function suggests that the resulting defects in postsynaptic adaptability stemming from dysregulated mTORC1 signaling are likely to contribute to these syndromes. Our findings reveal an integral role for dendritic mTORC1 in supporting retrograde modulation of presynaptic function, illustrating an alternative mode of synaptic regulation that may also be relevant for ASD and other disorders caused by synaptic dysfunction.

2.7 Acknowledgments

This work was supported by Grants F31MH093112 (F.E.H.) and RO1MH085798 (M.A.S.) from The National Institute of Mental Health and a grant from the Pew Biomedical Scholars Program (M.A.S.). We thank Robert Edwards for generously providing vglut1-pHluorin. We also thank Hisashi Umemori and members of the Sutton laboratory for many helpful discussions.

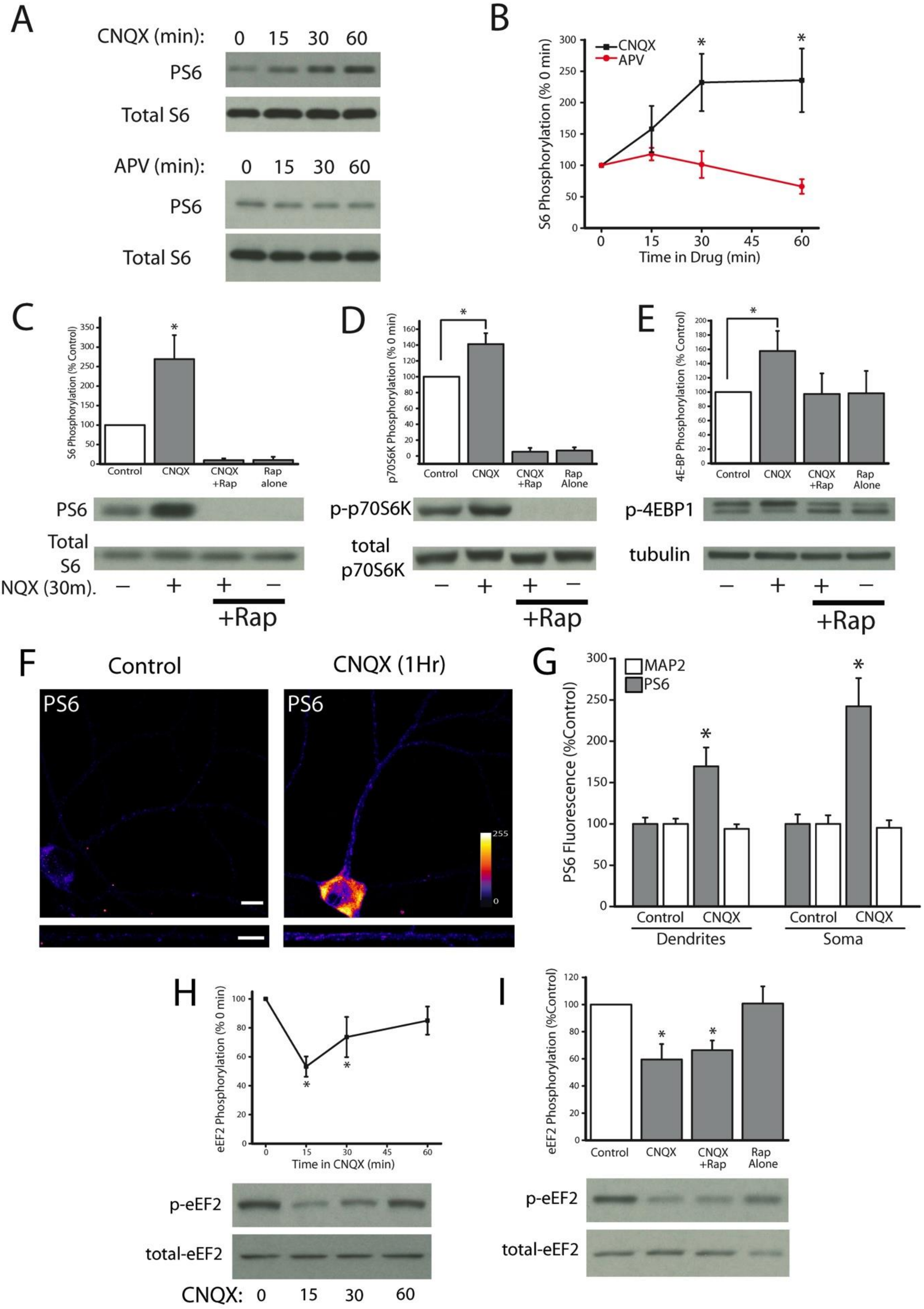
A
CNQX (min): 0 15 30 60
PS6
Total S6
APV (min): 0 15 30 60
PS6
Total S6
B
S6 Phosphorylation (% 0 min)
CNQX
APV
Time in Drug (min)
0 15 30 45 60
0 50 100 150 200 250 300
*
*
C
S6 Phosphorylation (% Control)
Control
CNQX
CNQX +Rap
Rap alone
PS6
Total S6
CNQX (30m). − + + −
+Rap
D
p70S6K Phosphorylation (% 0 min)
Control
CNQX
CNQX +Rap
Rap Alone
p-p70S6K
total p70S6K
− + + −
+Rap
E
4E-BP Phosphorylation (% Control)
Control
CNQX
CNQX +Rap
Rap Alone
p-4EBP1
tubulin
− + + −
+Rap
F
Control
CNQX (1Hr)
PS6
PS6
255
0
G
PS6 Fluorescence (%Control)
MAP2
PS6
Control
CNQX
Dendrites
Control
CNQX
Soma
*
*
H
eEF2 Phosphorylation (% 0 min)
Time in CNQX (min)
0 15 30 45 60
p-eEF2
total-eEF2
CNQX: 0 15 30 60
*
*
I
eEF2 Phosphorylation (%Control)
Control
CNQX
CNQX +Rap
Rap Alone
p-eEF2
total-eEF2
*
*

Figure 2.1: Acute loss of excitatory synaptic drive activates dendritic mTORC1 signaling. (A) Representative Western blots depicting phosphorylated (S235/236) and total ribosomal protein S6 following AMPAR blockade with 40 μM CNQX (n = 8 experiments) or NMDAR blockade with 50 μM APV (n = 6 experiments) for the indicated times. (B) Mean (±SEM) expression of PS6 in neurons subject to AMPAR or NMDAR blockade; AMPAR blockade induced a significant (*$p < 0.05$ relative to 0 min control) increase in S6 phosphorylation, whereas NMDAR blockade did not. (C–E) Representative Western blots and summary data from experiments (n = 5) where neurons were treated with CNQX (40 μM, 30 min) plus rapamycin (100 nM, 30 min pretreatment) before harvesting; *$p < 0.05$ relative to controls. AMPAR blockade stimulates phosphorylation of downstream mTORC1 effectors ribosomal protein S6 (C), p70S6K (D), and 4E-BP1 (E) (upper band) in a rapamycin-sensitive fashion. The increase in phosphorylation of S6, p70S6K, as well as 4E-BP1 accompanying AMPAR blockade is prevented by rapamycin (*$p < 0.05$ relative to untreated control). F, Representative examples of PS6 staining from cells treated with CNQX (40 μM, 60 min) or control; straightened dendrites are shown below each full-frame image. Scale bar, 10 μm. PS6 fluorescence intensity indicated by color look-up table. (G) Mean (+SEM) expression of MAP2 and PS6 in somatic and dendritic compartments, normalized to average control values, in neurons treated as indicated. PS6 fluorescence was significantly (*$p < 0.05$, relative to control) enhanced by AMPAR blockade (n = 28 cells) relative to control neurons (n = 30 cells), in both the dendritic and somatic compartments. MAP2 expression did not differ between groups. (H-I) Representative Western blots and summary data from experiments (n = 8 and 5 experiments for H and I, respectively) assessing changes in eEF2 phosphorylation as a result of AMPAR blockade. Neurons were treated with CNQX plus rapamycin as above before harvesting; *$p < 0.05$ relative to controls. AMPAR blockade elicits dephosphorylation of eEF2 (favoring translation elongation) that is insensitive to rapamycin and is characterized by kinetics distinct from mTORC1 activation.

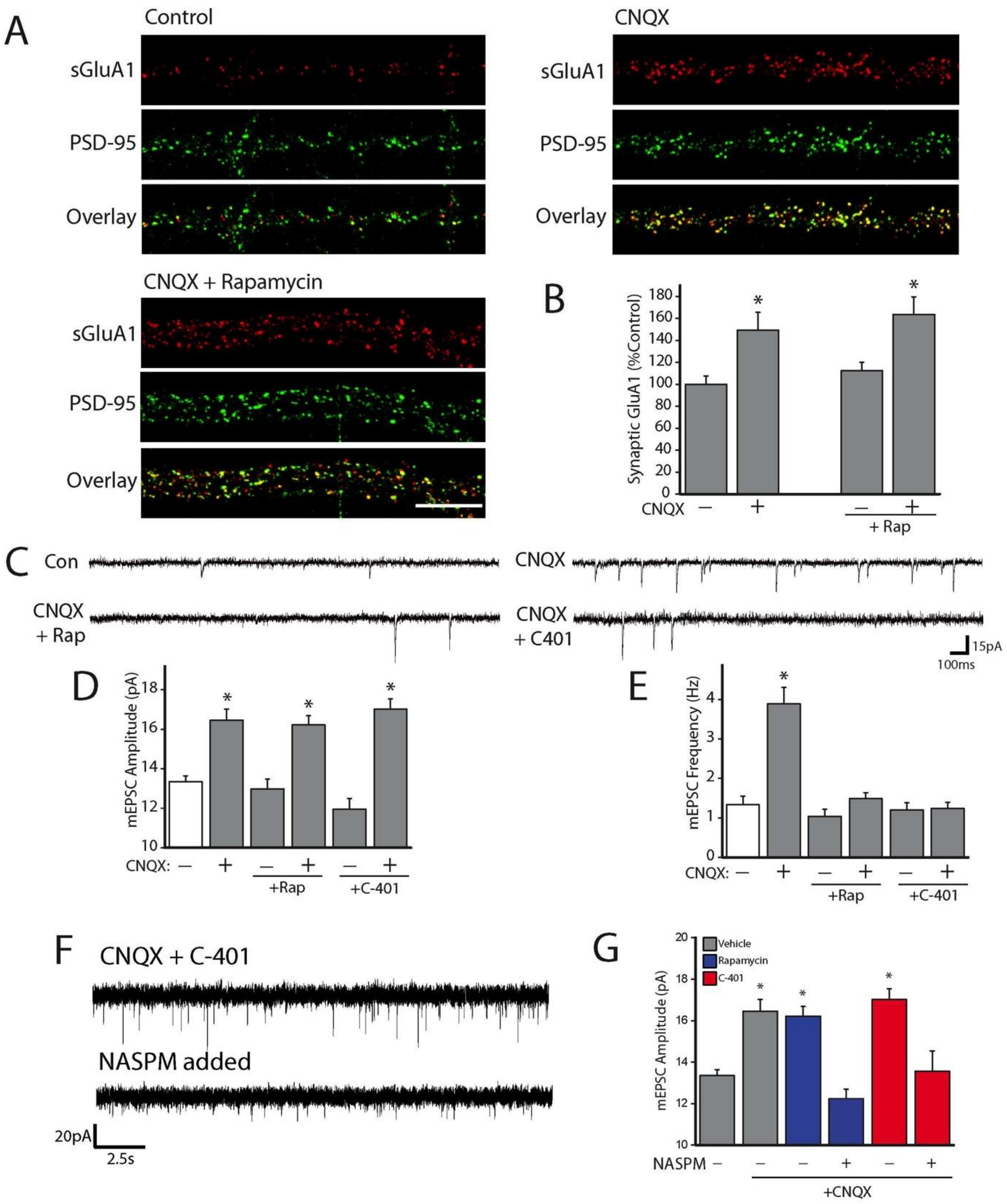
A
Control
sGluA1
PSD-95
Overlay
CNQX
sGluA1
PSD-95
Overlay
CNQX + Rapamycin
sGluA1
PSD-95
Overlay
B
Synaptic GluA1 (%Control)
0
20
40
60
80
100
120
140
160
180
*
*
CNQX
–
+
–
+
+ Rap
C
Con
CNQX
CNQX + Rap
CNQX + C401
15pA
100ms
D
mEPSC Amplitude (pA)
10
12
14
16
18
*
*
*
CNQX:
–
+
–
+
–
+
+Rap
+C-401
E
mEPSC Frequency (Hz)
0
1
2
3
4
*
CNQX:
–
+
–
+
–
+
+Rap
+C-401
F
CNQX + C-401
NASPM added
20pA
2.5s
G
Vehicle
Rapamycin
C-401
mEPSC Amplitude (pA)
10
12
14
16
18
20
*
*
*
NASPM
–
–
–
+
–
+
+CNQX

Figure 2.2: mTORC1 is not involved in adaptive postsynaptic compensation induced by AMPAR blockade. (A-B) Representative examples (A) and mean (+SEM) normalized synaptic surface GluA1 (sGluA1) expression (B) in cultured neurons treated with 40 µM CNQX for 120 min or control (n = 30 images), with or without pretreatment with rapamycin (100 nM, 30 min before CNQX) (n = 30 images/group). mTORC1 activity is not required for enhanced synaptic sGluA1 expression after AMPAR blockade. Scale bar: A, 10 µm. *p < 0.05 versus untreated control or rapamycin alone, respectively. (C–E) Representative mEPSC recordings (C) and mean (+SEM) mEPSC amplitude (D) and frequency (E) in neurons following washout of treatment with CNQX (40 µM, 3 h) with or without 30 min pretreatment with rapamycin (100 nM) or the mTOR active site inhibitor C-401 (10 µM). Cell numbers for the indicated groups: control, n = 18; CNQX, n = 19; rapamycin alone, n = 7; CNQX plus rapamycin, n = 13; C401 alone, n = 11; CNQX plus C401, n = 10. A significant (*p < 0.05 vs control) increase in mEPSC amplitude and frequency follows AMPAR blockade; treatment with either mTORC1 inhibitor blocked the increase in mEPSC frequency but not the increase in mEPSC amplitude. (F) Representative recording from an example subjected to AMPAR blockade in the presence of C-401, both before and after acute treatment with the polyamine toxin NASPM. (G) Mean (+SEM) mEPSC amplitude in neurons pretreated with either rapamycin (100 nM) or C401 (10 µM) and then subject to brief AMPAR blockade (CNQX, 40 µm, 3 h), followed by recording in the presence or absence of 10 µM NASPM. Sample sizes (# cells) for the indicated groups: control, n = 18; CNQX, n = 19; rapamycin alone, n = 7; CNQX plus rapamycin, n = 13; CNQX plus rapamycin plus NASPM, n = 12; C401 alone, n = 11; CNQX plus C401, n = 10; CNQX plus C401 plus NASPM, n = 5. Coincident mTORC1 inhibition did not affect the sensitivity of scaled mEPSCs to NASPM, indicating that the protein synthesis-dependent recruitment of GluA1 homomeric receptors to synapses is established in an mTORC1-independent manner. *p < 0.05 relative to untreated controls.

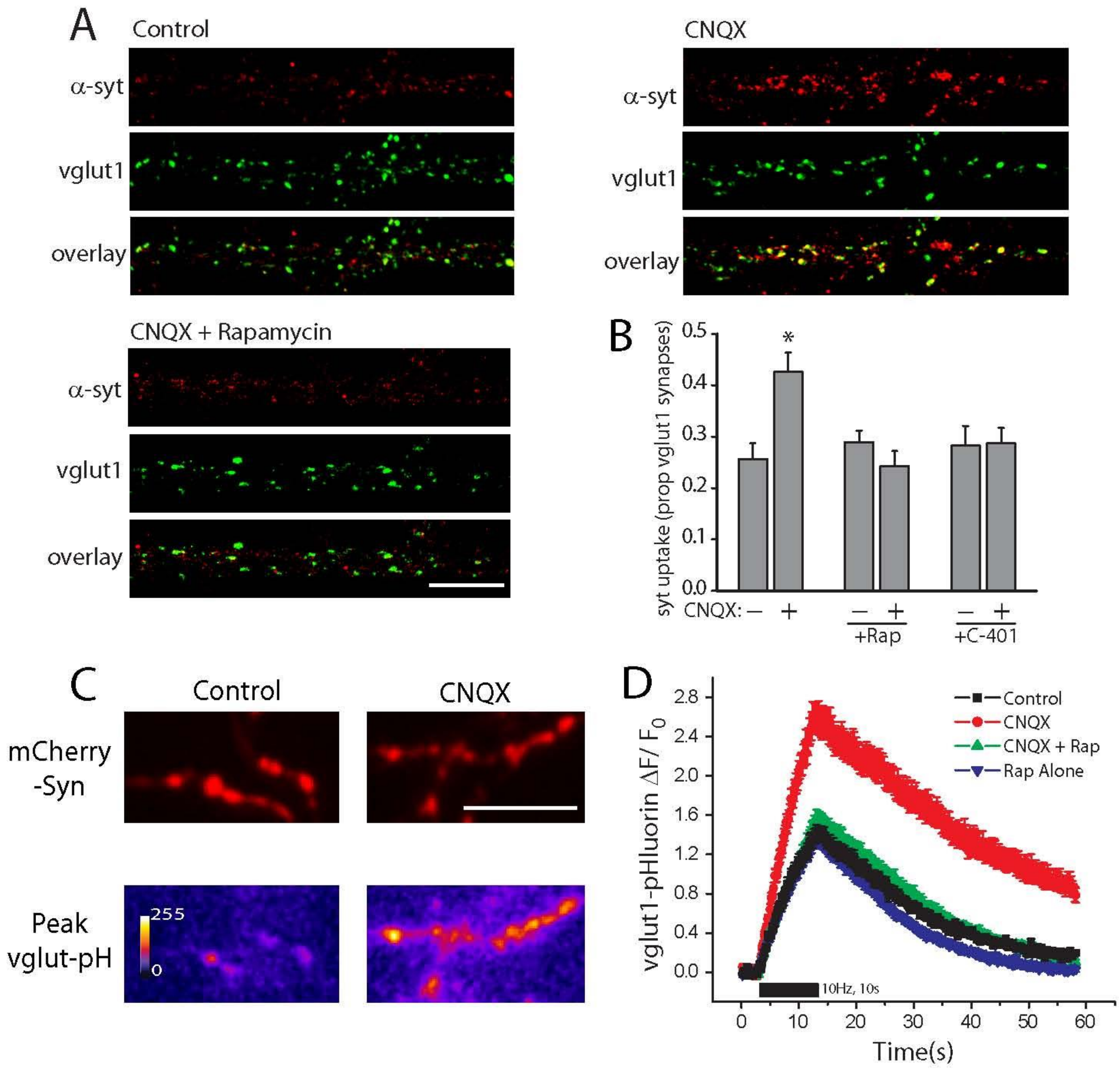
A
Control
α-syt
vglut1
overlay
CNQX
α-syt
vglut1
overlay
CNQX + Rapamycin
α-syt
vglut1
overlay
B
syt uptake (prop vglut1 synapses)
0.0
0.1
0.2
0.3
0.4
0.5
*
CNQX: – + – + – +
+Rap
+C-401
C
Control
CNQX
mCherry -Syn
Peak vglut-pH
255
0
D
vglut1-pHluorin ΔF/ F0
0.0
0.4
0.8
1.2
1.6
2.0
2.4
2.8
Control
CNQX
CNQX + Rap
Rap Alone
10Hz, 10s
0
10
20
30
40
50
60
Time(s)

Figure 2.3: AMPAR blockade drives mTORC1-dependent enhancements in spontaneous and evoked vesicle release. (A-B) Representative examples (A) and mean (+SEM) syt-lum uptake (B) from experiments where the indicated groups were pretreated (30 min before CNQX) with either rapamycin (100 nM) or C401 (10 μM) and then subject to brief AMPAR blockade (CNQX, 40 μM, 3 h) before staining. Results for indicated groups: control, n = 30 images; CNQX alone, n = 30 images; rapamycin alone, n = 30 images; CNQX plus rapamycin, n = 30 images; C401 alone, n = 30 images; CNQX plus C401, n = 30 images. AMPAR blockade induces a significant (*$p < 0.05$, relative to control) increase in syt-lum uptake prevented by coincident inhibition of mTORC1 activity. Scale bar: A, 10 μm. (C-D) Example images of axon terminals coexpressing mCherry-synaptophysin (mCh-Syn, top) as well as vglut-pHluorin (vglut-pH, bottom). Bottom, Images of the same set of synapses after termination of a 10 Hz 10 s stimulus train. Treatment with the AMPAR blocker CNQX (40 μM, 3 h) enhances the changes in vglut-pHluorin fluorescence intensity, compared with cells treated with vehicle in response to an identical stimulus train. Scale bar: C, 10 μm. (D) Relative change in vglut-pHluorin fluorescence over time in response to a 10 Hz 10 s stimulus train, recorded from cells treated with vehicle, CNQX, CNQX plus rapamycin, or rapamycin alone. Black bar represents onset of 10 s stimulus train. Black, Vehicle control (n = 579 synapses). Red, CNQX (n = 287 synapses). Green, CNQX plus rapamycin (n = 746 synapses). Blue, Rapamycin alone (n = 566 synapses). Evoked changes in vglut-pHluorin fluorescence intensity were significantly (*$p < 0.05$, relative to vehicle controls at peak fluorescence levels at immediate termination of stimulus train) enhanced by treatment with CNQX, and this effect was blocked by concurrent treatment with the mTORC1 inhibitor rapamycin.

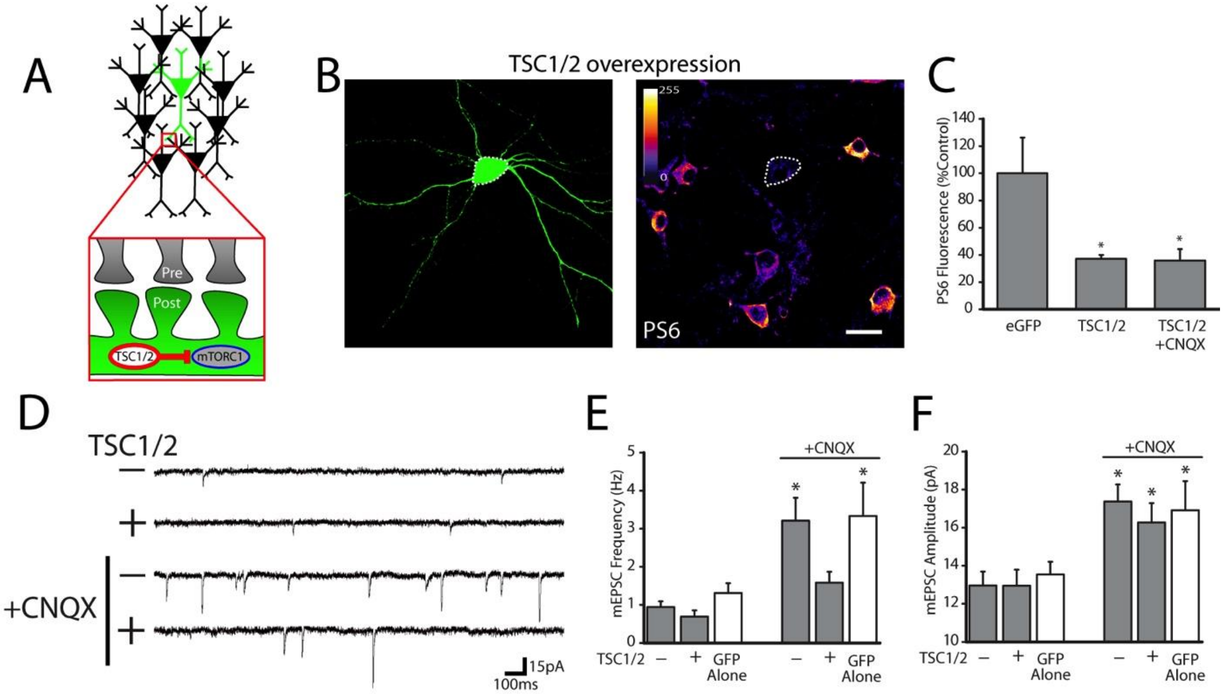
A
Pre
Post
TSC1/2
mTORC1
B
TSC1/2 overexpression
255
0
PS6
C
PS6 Fluorescence (%Control)
140
120
100
80
60
40
20
0
eGFP
TSC1/2
TSC1/2 +CNQX
*
*
D
TSC1/2
—
+
+CNQX
—
+
15pA
100ms
E
mEPSC Frequency (Hz)
5
4
3
2
1
0
+CNQX
*
*
TSC1/2
—
+
GFP Alone
—
+
GFP Alone
F
mEPSC Amplitude (pA)
20
18
16
14
12
10
+CNQX
*
*
*
TSC1/2
—
+
GFP Alone
—
+
GFP Alone

Figure 2.4: Postsynaptic mTORC1 activation is required for retrograde enhancement of presynaptic function. (A) Experimental rationale: low-efficiency transfection using calcium phosphate yields isolated transfected neurons surrounded by nontransfected cells. During recordings from TSC1/2(+) cells, mTORC1 signaling is impaired postsynaptically, while presynaptic mTORC1 activity is preserved (red insert). (B) Example of a TSC1/2-overexpressing neuron in a network of untransfected neurons depicting GFP (cotransfected with TSC1/2) and PS6 expression, as indicated; PS6 fluorescence intensity indicated by color look-up table. Scale bar, 40 μm. PS6 expression in the transfected neuron is substantially reduced relative to surrounding cells. (C) Mean (+SEM) normalized PS6 expression in transfected neurons. TSC1/2 overexpression (n = 19 neurons) significantly (*p < 0.05, t test) reduced basal PS6 levels compared with transfection with EGFP alone (n = 11 cells), and also blocked increases in PS6 by CNQX (n = 16 cells); *p < 0.05 versus EGFP alone. D–F, Representative mEPSC recordings (D) and mean (+SEM) mEPSC amplitude (E) and frequency (F) in neurons cotransfected with TSC1/2 and EGFP (n = 11) with (n = 15) or without (n = 11) treatment with CNQX (40 μM, 3 h); mEPSCs in these neurons were compared with those from untransfected neighboring cells as well as from neurons from sister cultures transfected with EGFP alone. Cells were transfected at DIV 21–25 and then used for recordings 24 h later. Postsynaptic inhibition of mTORC1 signaling via overexpression of TSC1/2 blocked the increase in mEPSC frequency but not the increase in mEPSC amplitude induced by AMPAR blockade. For the groups listed left to right in E: n = 8, 11, 16, 15, 11, 5 cells, respectively. *p < 0.05 versus control

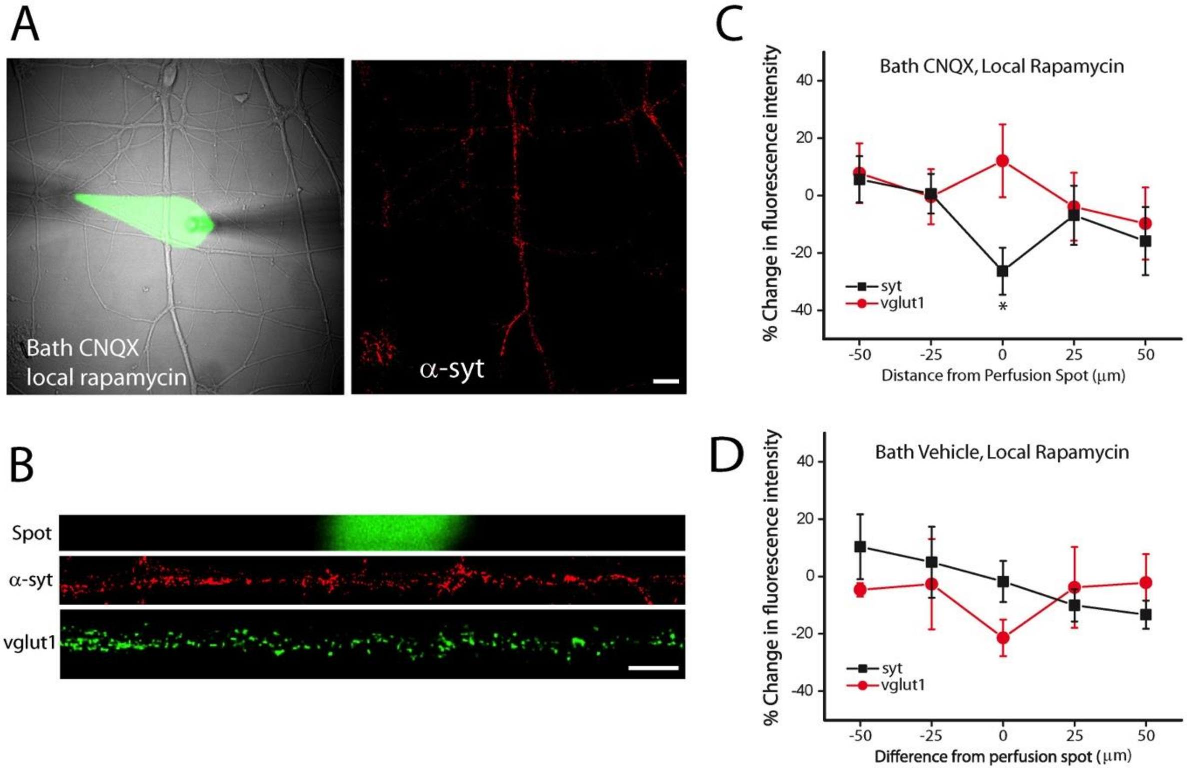
A
Bath CNQX
local rapamycin
α-syt
B
Spot
α-syt
vglut1
C
Bath CNQX, Local Rapamycin
% Change in fluorescence intensity
40
20
0
-20
-40
syt
vglut1
*
-50
-25
0
25
50
Distance from Perfusion Spot (μm)
D
Bath Vehicle, Local Rapamycin
% Change in fluorescence intensity
40
20
0
-20
-40
syt
vglut1
-50
-25
0
25
50
Difference from perfusion spot (μm)

Figure 2.5: mTOR acts locally in dendrites to modulate presynaptic function after AMPAR blockade. (A) Representative differential interference contrast image of a cultured hippocampal neuron exposed to AMPAR blockade (90 min bath application of 40 μM CNQX) with superimposed rapamycin (200 nM) perfusion spot (green) and the same neuron after staining with α-syt. (B) Linearized primary dendrite from the cell shown in A with corresponding α-syt and vglut1 staining registered to the perfusion area (green). Scale bars: 25 μm. A decrease in syt-lum uptake is evident in the perfused area, whereas vglut1 expression remains stable. C, D, Mean (±SEM) normalized syt-lum/vglut1 staining in treated and untreated dendritic segments from cells subject to local microperfusion of rapamycin (200 nM) with or without concurrent AMPAR blockade; all data are expressed as a percentage change in fluorescence relative to the average value in untreated segments. Local rapamycin perfusion significantly ($*p < 0.05$) decreased syt-lum uptake in the treated area relative to vglut1 expression in the same dendritic segment when CNQX was present (C) ($n = 10$ dendrites from 10 neurons), but not when vehicle was applied to the bath (D) ($n = 4$ dendrites from 4 neurons).

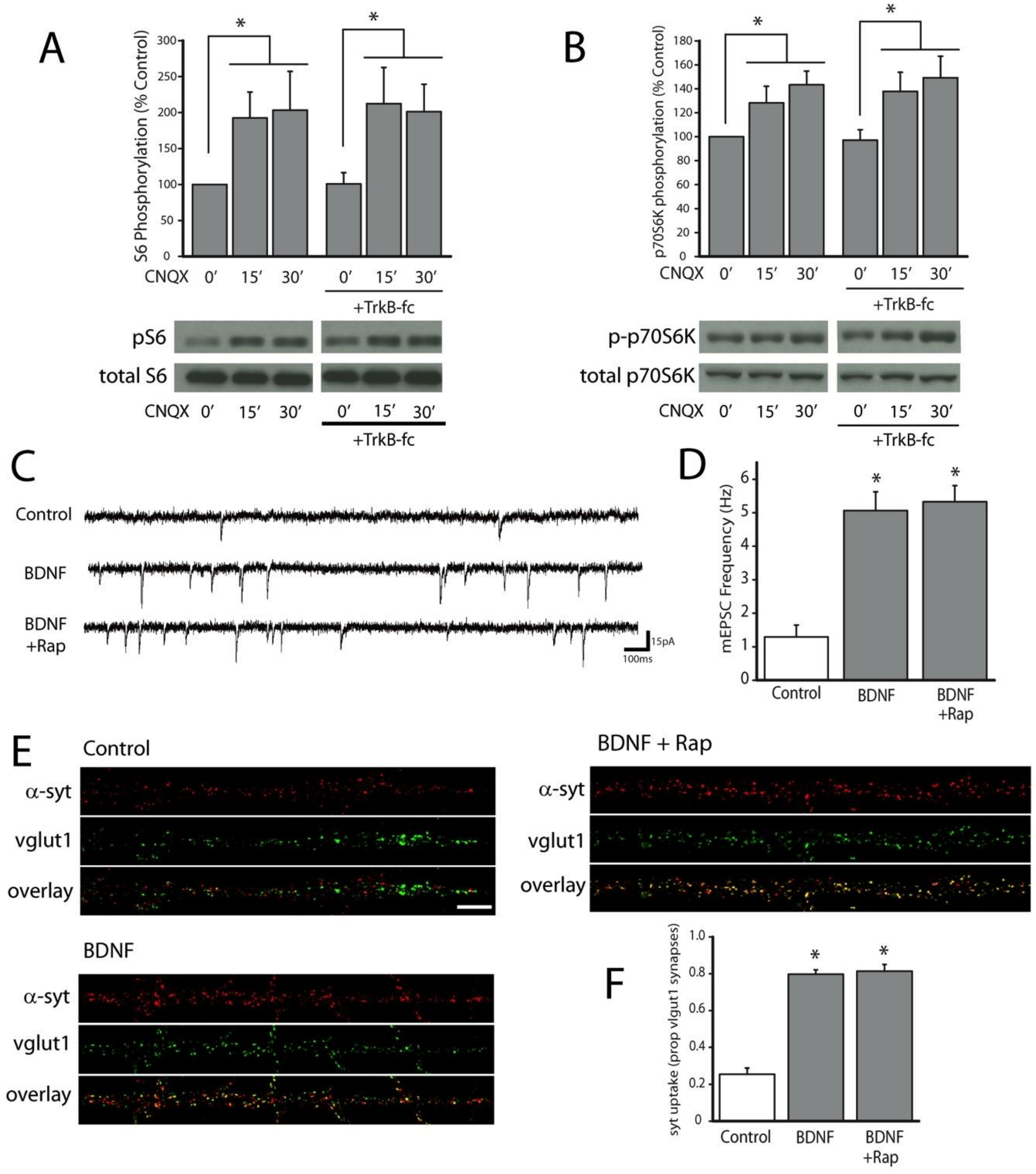
A
S6 Phosphorylation (% Control)
300
250
200
150
100
50
0
*
*
CNQX 0′ 15′ 30′ 0′ 15′ 30′
+TrkB-fc
pS6
total S6
CNQX 0′ 15′ 30′ 0′ 15′ 30′
+TrkB-fc
B
p70S6K phosphorylation (% Control)
180
160
140
120
100
80
60
40
20
0
*
*
CNQX 0′ 15′ 30′ 0′ 15′ 30′
+TrkB-fc
p-p70S6K
total p70S6K
CNQX 0′ 15′ 30′ 0′ 15′ 30′
+TrkB-fc
C
Control
BDNF
BDNF
+Rap
15pA
100ms
D
mEPSC Frequency (Hz)
6
5
4
3
2
1
0
*
*
Control
BDNF
BDNF
+Rap
E
Control
α-syt
vglut1
overlay
BDNF + Rap
α-syt
vglut1
overlay
BDNF
α-syt
vglut1
overlay
F
syt uptake (prop vlgut1 synapses)
1.0
0.8
0.6
0.4
0.2
0
*
*
Control
BDNF
BDNF
+Rap

Figure 2.6: BDNF enhances presynaptic function downstream of mTORC1. (A-B) Representative Western blots and summary data from experiments (n = 5) examining the phosphorylation of downstream mTORC1 effectors S6 (A) and p70S6K (B) during AMPAR blockade. Cultured neurons were treated with CNQX (40 μM) with or without TrkB-Fc (1 μg/ml, 30 min pretreatment) before harvesting; $*p < 0.05$ relative to 0 min control. Phosphorylation of S6 at S235/236 and p70S6K at Thr389 during AMPAR blockade is not affected by scavenging extracellular BDNF. (C-D) Representative recordings (C) and mean (+SEM) mEPSC frequency (D) after BDNF application (250 ng/ml, 2 h) in the presence or absence of rapamycin (100 nM, 30 min pretreatment). For the groups indicated left to right, n = 7, 6, and 7 cells. BDNF induces a significant ($*p < 0.05$) sustained increase in mEPSC frequency evident 30–50 min following BDNF washout. This increase is unaltered by concurrent treatment with the mTORC1 inhibitor rapamycin. (E-F) Representative examples (E) and mean (+SEM) syt-lum uptake (F) from experiments (n = 15/group) where neurons were treated with BDNF (250 ng, 60 min) with or without rapamycin (100 nM; 30 min before BDNF). Inhibiting mTORC1 signaling did not impact enhanced syt-lum uptake induced by BDNF treatment ($*p < 0.05$, relative to control). Scale bar: E, 10 μm.

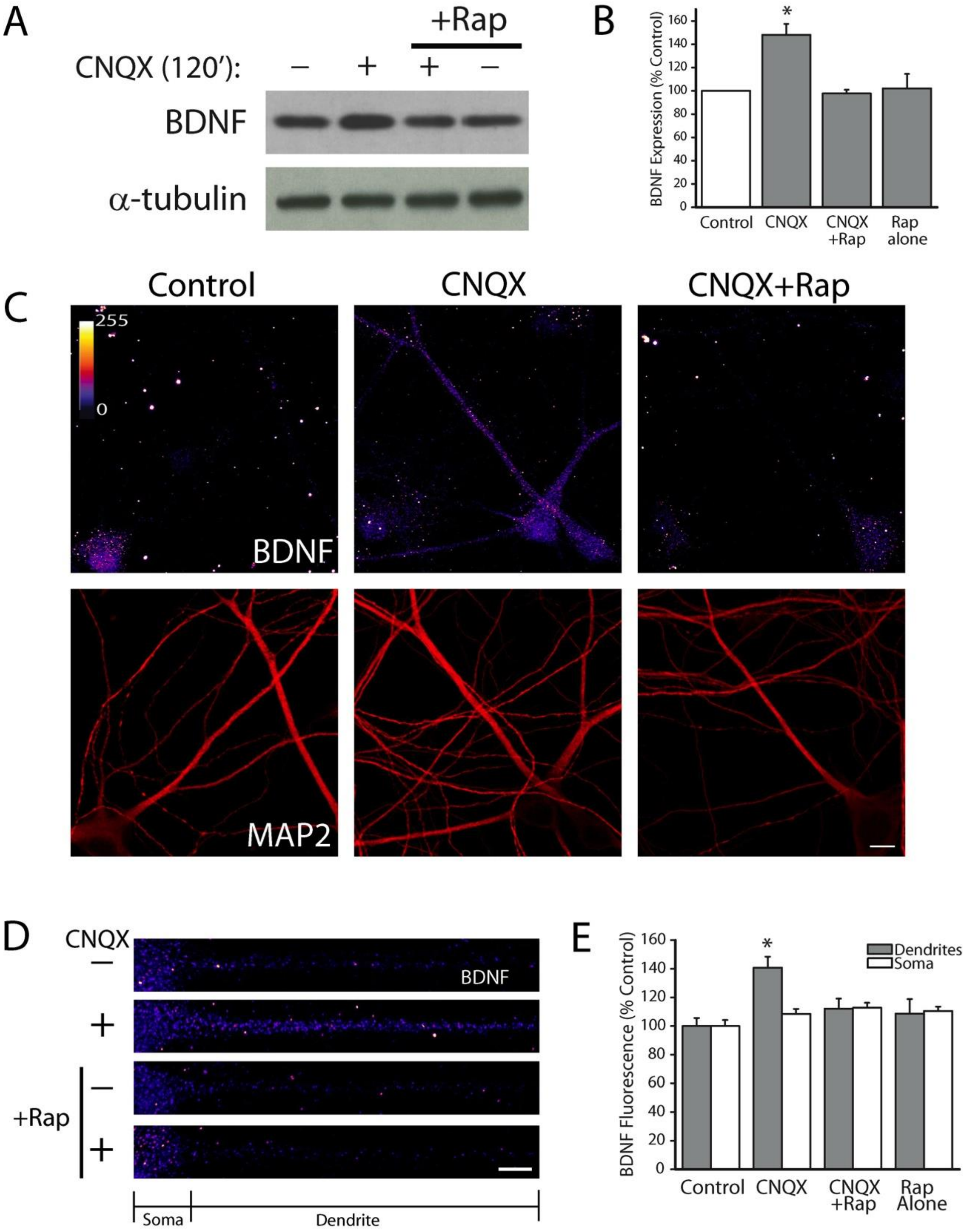
A
+Rap
CNQX (120′): – + + –
BDNF
α-tubulin
B
BDNF Expression (% Control)
0
20
40
60
80
100
120
140
160
*
Control
CNQX
CNQX +Rap
Rap alone
C
Control
CNQX
CNQX+Rap
255
0
BDNF
MAP2
D
CNQX
–
+
+Rap
–
+
BDNF
Soma
Dendrite
E
BDNF Fluorescence (% Control)
0
20
40
60
80
100
120
140
160
*
Dendrites
Soma
Control
CNQX
CNQX +Rap
Rap Alone

Figure 2.7: Compartmentalized enhancement in BDNF expression by AMPAR blockade requires mTORC1. (A-B) Representative Western blots (A) and summary data (B) in experiments (n = 6) where neurons were treated with CNQX (40 μM, 120 min) with or without rapamycin (100 nM, 30 min pretreatment) before harvesting; *p < 0.05 relative to control. The BDNF band (~14 kDa) represents mature BDNF. (C-D) BDNF expression in linearized somatic and dendritic segments and mean (+SEM) expression BDNF in somatic and dendritic compartments normalized to average control values, in neurons treated with CNQX (40 μM, 3 h) with or without rapamycin (100 nM, 30 min pretreatment). (E) AMPAR blockade significantly enhanced BDNF expression in dendrites (*p < 0.05, n = 30 neurons) compared with untreated control neurons (n = 33). This effect was blocked by pretreatment with rapamycin (100 nM; n = 31 neurons), which had no effect on BDNF expression on its own (n = 29 neurons). Somatic BDNF expression from these same cells did not change across treatment groups. Scale bar: C, 10 μm.

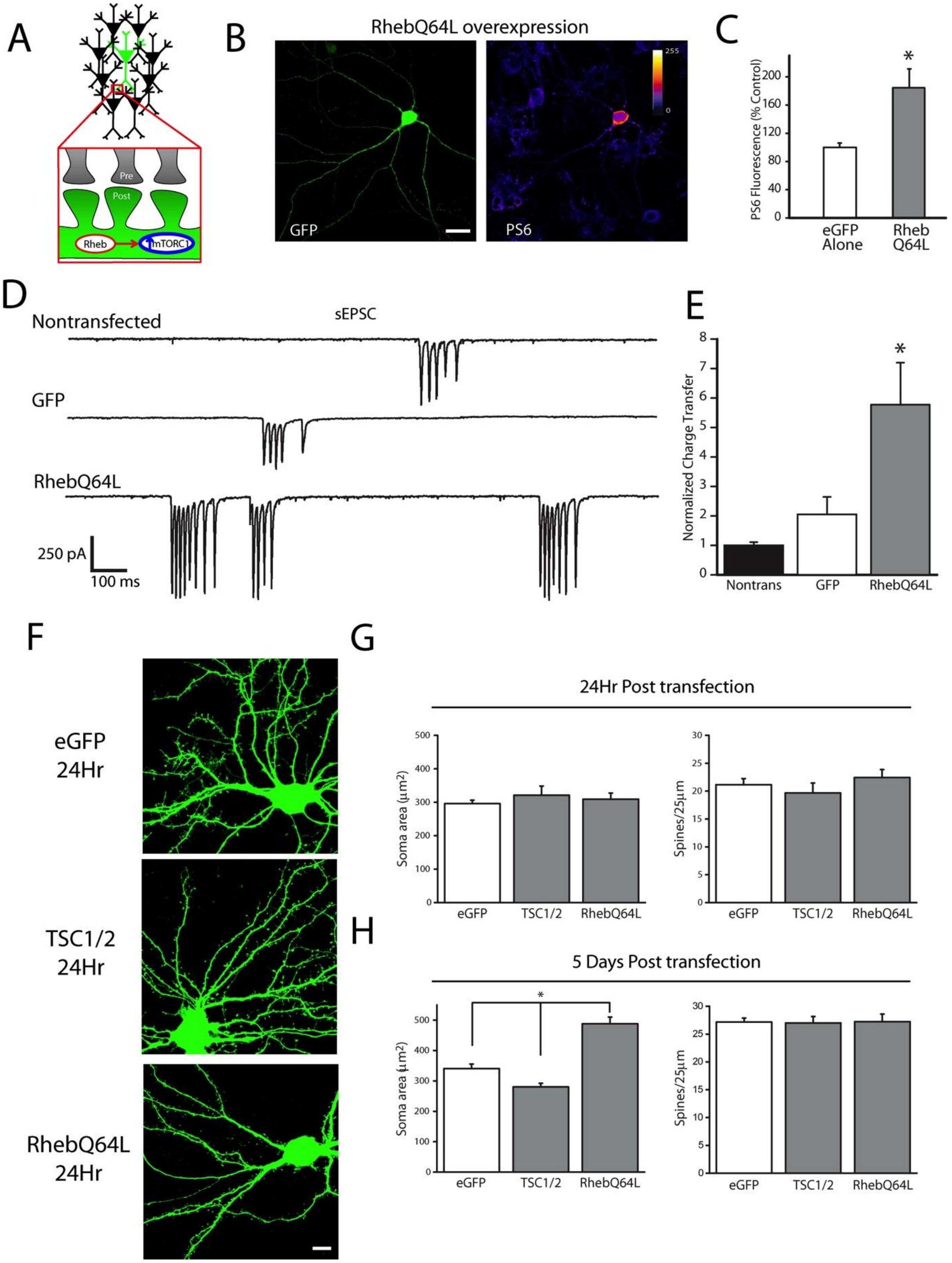
A
Pre
Post
Rheb
mTORC1
B
RhebQ64L overexpression
GFP
PS6
255
0
C
PS6 Fluorescence (% Control)
0
40
80
120
160
200
*
eGFP Alone
Rheb Q64L
D
Nontransfected
sEPSC
GFP
RhebQ64L
250 pA
100 ms
E
Normalized Charge Transfer
0
1
2
3
4
5
6
7
8
*
Nontrans
GFP
RhebQ64L
F
eGFP 24Hr
TSC1/2 24Hr
RhebQ64L 24Hr
G
24Hr Post transfection
Soma area (μm2)
0
100
200
300
400
500
eGFP
TSC1/2
RhebQ64L
Spines/25μm
0
5
10
15
20
25
30
eGFP
TSC1/2
RhebQ64L
H
5 Days Post transfection
Soma area (μm2)
*
0
100
200
300
400
500
eGFP
TSC1/2
RhebQ64L
Spines/25μm
0
5
10
15
20
25
30
eGFP
TSC1/2
RhebQ64L

Figure 2.8: Sparse mTORC1 activation enhances synaptic efficacy in a cell-autonomous fashion. (A) Experimental rationale: Low-efficiency transfection using calcium phosphate yields individual transfected neurons surrounded by nontransfected cells. During recordings from RhebQ64L(+) cells, mTORC1 signaling is enhanced postsynaptically, while presynaptic mTORC1 activity is normal (red insert). (B-C) Example images (B) and mean (+SEM) normalized PS6 expression (C) in transfected neurons. Expression of RhebQ64L (n = 14 cells) significantly (*$p < 0.05$ vs EGFP alone by t test) enhanced PS6 levels compared with transfection with EGFP alone (n = 14 cells). PS6 fluorescence intensity indicated by color look-up table. Scale bar, 40 μm. (D-E) Representative recordings of sEPSCs (D) and mean charge transfer (E) of RhebQ64L-expressing neurons (n = 17) or neighboring nontransfected neurons (n = 16), as well as EGFP-expressing neurons (n = 19) in low $Ca2^+$ (0.5 mM) extracellular solution. Quantificative analysis of spontaneous activity was performed by measuring the total charge transfer in 20 s relative to nontransfected cells. Postsynaptic expression of RhebQ64L was sufficient to induce an increase in spontaneous activity of nontransfected presynaptic neurons. *$p < 0.01$, one-way ANOVA, Tukey–Kramer post hoc. (F–H) Effects of altered mTORC1 signaling on cell growth pathways in hippocampal neurons. (F) Representative images of cultured hippocampal neurons cotransfected with GFP as well as either TSC1/2 or RhebQ64L. Scale bar, 10 μm. (G-H) After 24 h, neither TSC1/2 (n = 21) nor RhebQ64L overexpression (n = 16) has any effect on soma size or spine density when compared with cells expressing EGFP alone (n = 71). In contrast, 5 d of TSC1/2 expression yields significantly diminished soma size (n = 47) while prolonged RhebQ64L expression (n = 27) results in significantly enhanced soma size compared with control EGFP-expressing cells (n = 30); again, no significant change in spine density was observed.

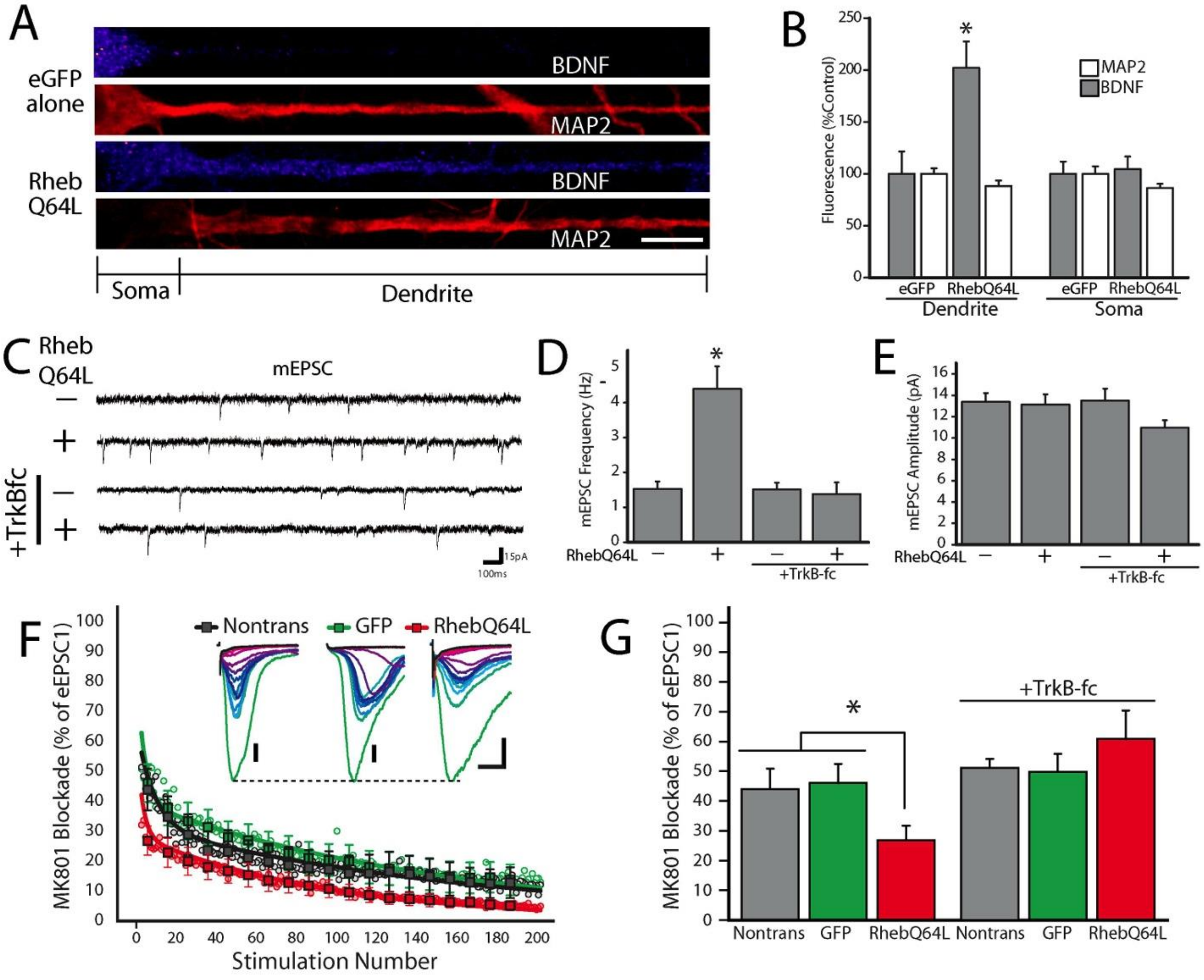
A
eGFP alone
Rheb Q64L
BDNF
MAP2
BDNF
MAP2
Soma
Dendrite
B
Fluorescence (%Control)
250
200
150
100
50
0
*
MAP2
BDNF
eGFP
RhebQ64L
eGFP
RhebQ64L
Dendrite
Soma
C
Rheb Q64L
mEPSC
−
+
+TrkBfc
−
+
15pA
100ms
D
mEPSC Frequency (Hz)
5
4
3
2
1
0
*
RhebQ64L
−
+
−
+
+TrkB-fc
E
mEPSC Amplitude (pA)
16
14
12
10
8
6
4
2
0
RhebQ64L
−
+
−
+
+TrkB-fc
F
MK801 Blockade (% of eEPSC1)
100
90
80
70
60
50
40
30
20
10
0
Nontrans
GFP
RhebQ64L
0
20
40
60
80
100
120
140
160
180
200
Stimulation Number
G
MK801 Blockade (% of eEPSC1)
100
90
80
70
60
50
40
30
20
10
0
*
+TrkB-fc
Nontrans
GFP
RhebQ64L
Nontrans
GFP
RhebQ64L

Figure 2.9: Postsynaptic mTORC1 activation drives enhancement of presynaptic function via BDNF release. (A-B) BDNF and MAP2 expression in linearized somatic and dendritic segments (A), and mean (+SEM) expression (B) of MAP2 and BDNF in somatic and dendritic compartments normalized to average control values, in neurons cotransfected with RhebQ64L and EGFP or neurons transfected with EGFP alone. While BDNF expression in dendrites was significantly (*$p < 0.05$, relative to EGFP alone) enhanced by expression of RhebQ64L (n = 22) compared with control neurons expressing EGFP alone (n = 22), somatic expression from these same cells was unchanged. MAP2 expression did not differ between groups. Scale bar: A, 10 μm. (C–E) Representative recordings (C) and mean (+SEM) mEPSC frequency (D) and amplitude (E) in nontransfected neurons (n = 9) or neurons transfected with RhebQ64L as well as EGFP (n = 7) with or without treatment with TrkB-fc (1 μg/ml applied immediately post-transfection: RhebQ64L(−) with TrkB-fc, n = 6; RhebQ64L(+) with TrkB-fc, n = 10). Cells were transfected at DIV 21–25 and then used for recordings 24 h later. Postsynaptic enhancement of mTORC1 signaling via expression of RhebQ64L was sufficient to increase mEPSC frequency compared with cells expressing EGFP alone, and this effect was blocked by scavenging extracellular BDNF with TrkB-fc. Neither RhebQ64L expression nor treatment with TrkB-fc had any effect on mEPSC amplitude. *$p < 0.05$, relative to EGFP alone. (F) Average MK801 blockade of RhebQ64L (n = 11), EGFP (n = 11), and nontransfected (n = 10) neurons. MK801 (20 μM) was applied to the bath (0 Mg2+, with CNQX and bicuculline) for 5 min, followed by 200 extracellular stimulations (0.33 Hz), while voltage-clamping the cell at −70 mV to record NMDAR-mediated currents. The amplitude of each response was measured and expressed relative to the amplitude of the first response. The mean for each response is plotted in small circles and fitted by a double-exponential curve (untransfected: $\tau1 = 8.64$, $\tau2 = 175.8$; EGFP: $\tau1 = 3.92$, $\tau2 = 157.33$; RhebQ64L: $\tau1 = 2.93$, $\tau2 = 96.97$). (G) Average percentage response of the second through eleventh stimulation relative to the first EPSC. Expression of RhebQ64L in the postsynaptic neuron was sufficient to increase the rate of MK801 blockade and extracellular incubation of TrkB-fc with RhebQ64L expression blocked the increase. *$p < 0.01$, one-way ANOVA, Tukey–Kramer post hoc.

2.9 Bibliography

Aid T, Kazantseva A, Piirsoo M, Palm K, Timmusk T (2007) Mouse and rat BDNF gene structure and expression revisited. J Neurosci Res 85:525–535.

An JJ, Gharami K, Liao GY, Woo NH, Lau AG, Vanevski F, Torre ER, Jones KR, Feng Y, Lu B, Xu B (2008) Distinct role of long 3′ UTR BDNF mRNA in spine morphology and synaptic plasticity in hippocampal neurons. Cell 134:175–187.

Antion MD, Merhav M, Hoeffer CA, Reis G, Kozma SC, Thomas G, Schuman EM, Rosenblum K, Klann E (2008) Removal of S6K1 and S6K2 leads to divergent alterations in learning, memory, and synaptic plasticity. Learn Mem 15:29–38.

Aoto J, Nam CI, Poon MM, Ting P, Chen L (2008) Synaptic signaling by all-trans retinoic acid in homeostatic synaptic plasticity. Neuron 60:308–320.

Baj G, Leone E, Chao MV, Tongiorgi E (2011) Spatial segregration of BDNF transcripts enables BDNF to differentially shape distinct dendritic compartments. Proc Natl Acad Sci U S A 108:16813–16818.

Ballou LM, Selinger ES, Choi JY, Drueckhammer DG, Lin RZ (2007) Inhibition of mammalian target of rapamycin signaling by 2-(morpholin-1-yl)pyrimido[2,1-alpha]isoquinolin-4-one. J Biol Chem 282:24463–24470.

Bateup HS, Takasaki KT, Saulnier JL, Denefrio CL, Sabatini BL (2011) Loss of Tsc1 in vivo impairs hippocampal mGluR-LTD and increases excitatory synaptic function. J Neurosci 31:8862–8869.

Bé̈ique JC, Na Y, Kuhl D, Worley PF, Huganir RL (2011) Arc-dependent synapse-specific homeostatic plasticity. Proc Natl Acad Sci U S A 108:816–821.

Blundell J, Kouser M, Powell CM (2008) Systemic inhibition of mammalian target of rapamycin inhibits fear memory reconsolidation. Neurobiol Learn Mem 90:28–35.

Branco T, Häusser M (2010) The single dendritic branch as a fundamental functional unit in the nervous system. Curr Opin Neurobiol 20:494–502.

Branco T, Staras K, Darcy KJ, Goda Y (2008) Local dendritic activity sets release probability at hippocampal synapses. Neuron 59:475–485.

Butler MG, Dasouki MJ, Zhou XP, Talebizadeh Z, Brown M, Takahashi TN, Miles JH, Wang CH, Stratton R, Pilarski R, Eng C (2005) Subset of individuals with autism spectrum disorders and extreme macrocephaly associated with germline PTEN tumour suppressor gene mutations. J Med Genet 42:318–321.

Cammalleri M, Lütjens R, Berton F, King AR, Simpson C, Francesconi W, Sanna PP (2003) Time-restricted role for dendritic activation of the mTOR-p70S6K pathway in the induction of late-phase long-term potentiation in the CA1. Proc Natl Acad Sci U S A 100:14368–14373.

Casadio A, Martin KC, Giustetto M, Zhu H, Chen M, Bartsch D, Bailey CH, Kandel ER (1999) A transient, neuron-wide form of CREB-mediated long-term facilitation can be stabilized at specific synapses by local protein synthesis. Cell 99:221–237.

Chiaruttini C, Sonego M, Baj G, Simonato M, Tongiorgi E (2008) BDNF mRNA splice variants display activity-dependent targeting to distinct hippocampal laminae. Mol Cell Neurosci 37:11–19.

Costa-Mattioli M, Sossin WS, Klann E, Sonenberg N (2009) Translational control of long-lasting synaptic plasticity and memory. Neuron 61:10–26.

Dash PK, Orsi SA, Moore AN (2006) Spatial memory formation and memory-enhancing effect of glucose involves activation of the tuberous sclerosis complex-mammalian target of rapamycin pathway. J Neurosci 26:8048–8056.

Ehninger D, Han S, Shilyansky C, Zhou Y, Li W, Kwiatkowski DJ, Ramesh V, Silva AJ (2008) Reversal of learning deficits in a Tsc2+/− mouse model of tuberous sclerosis. Nat Med 14:843–848.

Frank CA, Kennedy MJ, Goold CP, Marek KW, Davis GW (2006) Mechanisms underlying the rapid induction and sustained expression of synaptic homeostasis. Neuron 52:663–677.

Gkogkas C, Sonenberg N, Costa-Mattioli M (2010) Translational control mechanisms in long-lasting synaptic plasticity and memory. J Biol Chem 285:31913–31917.

Gong B, Wang H, Gu S, Heximer SP, Zhuo M (2007) Genetic evidence for the requirement of adenylyl cyclase 1 in synaptic scaling of forebrain cortical neurons. Eur J Neurosci 26:275–288.

Gong R, Park CS, Abbassi NR, Tang SJ (2006) Roles of glutamate receptors and the mammalian target of rapamycin (mTOR) signaling pathway in activity-dependent dendritic protein synthesis in hippocampal neurons. J Biol Chem 281:18802–18815.

Goold CP, Nicoll RA (2010) Single-cell optogenetic excitation drives homeostatic synaptic depression. Neuron 68:512–528.

Groth RD, Lindskog M, Thiagarajan TC, Li L, Tsien RW (2011) {beta} $Ca2^{+}$/CaM-dependent kinase type II triggers upregulation of GluA1 to coordinate adaptation to synaptic inactivity in hippocampal neurons. Proc Natl Acad Sci U S A 108:828–833.

Hessler NA, Shirke AM, Malinow R (1993) The probability of transmitter release at a mammalian central synapse. Nature 366:569–572.

Hoeffer CA, Klann E (2010) mTOR signaling: at the crossroads of plasticity, memory and disease. Trends Neurosci 33:67–75.

Hoeffer CA, Tang W, Wong H, Santillan A, Patterson RJ, Martinez LA, Tejada-Simon MV, Paylor R, Hamilton SL, Klann E (2008) Removal of FKBP12 enhances mTOR-Raptor interactions, LTP, memory, and perseverative/repetitive behavior. Neuron 60:832–845.

Hou L, Klann E (2004) Activation of the phosphoinositide 3-kinase-Akt-mammalian target of rapamycin signaling pathway is required for metabotropic glutamate receptor-dependent long-term depression. J Neurosci 24:6352–6361.

Hou Q, Gilbert J, Man HY (2011) Homeostatic regulation of AMPA receptor trafficking and degradation by light-controlled single-synaptic activation. Neuron 72:806–818.

Huber KM, Kayser MS, Bear MF (2000) Role for rapid dendritic protein synthesis in hippocampal mGluR-dependent long-term depression. Science 288:1254–1257.

Ibata K, Sun Q, Turrigiano GG (2008) Rapid synaptic scaling induced by changes in postsynaptic firing. Neuron 57:819–826.

Inoki K, Li Y, Zhu T, Wu J, Guan KL (2002) TSC2 is phosphorylated and inhibited by Akt and suppresses mTOR signalling. Nat Cell Biol 4:648–657.

Inoki K, Zhu T, Guan KL (2003) TSC2 mediates cellular energy response to control cell growth and survival. Cell 115:577–590.

Jakawich SK, Nasser HB, Strong MJ, McCartney AJ, Perez AS, Rakesh N, Carruthers CJ, Sutton MA (2010) Local presynaptic activity gates homeostatic changes in presynaptic function driven by dendritic BDNF synthesis. Neuron 68:1143–1158.

Jiang H, Vogt PK (2008) Constitutively active Rheb induces oncogenic transformation. Oncogene 27:5729–5740.

Johannessen CM, Reczek EE, James MF, Brems H, Legius E, Cichowski K (2005) The NF1 tumor suppressor critically regulates TSC2 and mTOR. Proc Natl Acad Sci U S A 102:8573–8578.

Kang H, Schuman EM (1996) A requirement for local protein synthesis in neurotrophin-induced hippocampal synaptic plasticity. Science 273:1402–1406.

Kelleher RJ 3rd., Bear MF (2008) The autistic neuron: troubled translation? Cell 135:401–406.

Kim SH, Ryan TA (2009) Synaptic vesicle recycling at CNS snapses without AP-2. J Neurosci 29:3865–3874.

Kwiatkowski DJ (2003) Tuberous sclerosis: from tubers to mTOR. Ann Hum Genet 67:87–96.

Lee MC, Yasuda R, Ehlers MD (2010) Metaplasticity at single glutamatergic synapses. Neuron 66:859–870.

Li N, Lee B, Liu RJ, Banasr M, Dwyer JM, Iwata M, Li XY, Aghajanian G, Duman RS (2010) mTOR-dependent synapse formation underlies the rapid antidepressant effects of NMDA antagonists. Science 329:959–964.

Liao GY, An JJ, Gharami K, Waterhouse EG, Vanevski F, Jones KR, Xu B (2012) Dendritically targeted Bdnf mRNA is essential for energy balance and response to leptin. Nat Med 18:564–571.

Lindskog M, Li L, Groth RD, Poburko D, Thiagarajan TC, Han X, Tsien RW (2010) Postsynaptic GluA1 enables acute retrograde enhancement of presynaptic function to coordinate adaptation to synaptic inactivity. Proc Natl Acad Sci U S A 107:21806–21811.

Long X, Lin Y, Ortiz-Vega S, Yonezawa K, Avruch J (2005) Rheb binds and regulates the mTOR kinase. Curr Biol 15:702–713.

Ma XM, Blenis J (2009) Molecular mechanisms of mTOR-mediated translational control. Nat Rev Mol Cell Biol 10:307–318.

Maghsoodi B, Poon MM, Nam CI, Aoto J, Ting P, Chen L (2008) Retinoic acid regulates RARalpha-mediated control of translation in dendritic RNA granules during homeostatic synaptic plasticity. Proc Natl Acad Sci U S A 105:16015–16020.

Makino H, Malinow R (2009) AMPA receptor incorporation into synapses during LTP: the role of lateral movement and exocytosis. Neuron 64:381–390.

Martin KC, Casadio A, Zhu H, Yaping E, Rose JC, Chen M, Bailey CH, Kandel ER (1997) Synapse-specific, long-term facilitation of aplysia sensory to motor synapses: a function for local protein synthesis in memory storage. Cell 91:927–938.

Murthy VN, Schikorski T, Stevens CF, Zhu Y (2001) Inactivity produces increases in neurotransmitter release and synapse size. Neuron 32:673–682.

Neasta J, Ben Hamida S, Yowell Q, Carnicella S, Ron D (2010) Role for mammalian target of rapamycin complex 1 signaling in neuroadaptations underlying alcohol-related disorders. Proc Natl Acad Sci U S A 107:20093–20098.

Nosyreva E, Kavalali ET (2010) Activity-dependent augmentation of spontaneous neurotransmission during endoplasmic reticulum stress. J Neurosci 30:7358–7368.

Onda H, Crino PB, Zhang H, Murphey RD, Rastelli L, Gould Rothberg BE, Kwiatkowski DJ (2002) Tsc2 null murine neuroepithelial cells are a model for human tuber giant cells, and show activation of an mTOR pathway. Mol Cell Neurosci 21:561–574.

Pattabiraman PP, Tropea D, Chiaruttini C, Tongiorgi E, Cattaneo A, Domenici L (2005) Neuronal activity regulates the developmental expression and subcellular localization of cortical BDNF mRNA isoforms in vivo. Mol Cell Neurosci 28:556–570.

Penney J, Tsurudome K, Liao EH, Elazzouzi F, Livingstone M, Gonzalez M, Sonenberg N, Haghighi AP (2012) TOR is required for the retrograde regulation of synaptic homeostasis at the Drosophila neuromuscular junction. Neuron 74:166–178.

Rabinowitch I, Segev I (2008) Two opposing plasticity mechanisms pulling a single synapse. Trends Neurosci 31:377–383.

Regehr WG, Carey MR, Best AR (2009) Activity-dependent regulation of synapses by retrograde messengers. Neuron 63:154–170.

Rosenmund C, Clements JD, Westbrook GL (1993) Non-uniform probability of glutamate release at a hippocampal synapse. Science 262:754–757.

Schratt GM, Nigh EA, Chen WG, Hu L, Greenberg ME (2004) BDNF regulates the translation of a select group of mRNAs by a mammalian target of rapamycin-phosphatidylinositol 3-kinase-dependent pathway during neuronal development. J Neurosci 24:7366–7377.

Sharma A, Hoeffer CA, Takayasu Y, Miyawaki T, McBride SM, Klann E, Zukin RS (2010) Dysregulation of mTOR signaling in fragile X syndrome. J Neurosci 30:694–702.

Slipczuk L, Bekinschtein P, Katche C, Cammarota M, Izquierdo I, Medina JH (2009) BDNF activates mTOR to regulate GluR1 expression required for memory formation. PLoS One 4:e6007.

Soden ME, Chen L (2010) Fragile X protein FMRP is required for homeostatic plasticity and regulation of synaptic strength by retinoic acid. J Neurosci 30:16910–16921.

Steward O, Levy WB (1982) Preferential localization of polyribosomes under the base of dendritic spines in granule cells of the dentate gyrus. J Neurosci 2:284–291.

Sutton MA, Ito HT, Cressy P, Kempf C, Woo JC, Schuman EM (2006) Miniature neurotransmission stabilizes synaptic function via tonic suppression of local dendritic protein synthesis. Cell 125:785–799.

Sutton MA, Taylor AM, Ito HT, Pham A, Schuman EM (2007) Postsynaptic decoding of neural activity: eEF2 as a biochemical sensor coupling miniature synaptic transmission to local protein synthesis. Neuron 55:648–661.

Tang SJ, Reis G, Kang H, Gingras AC, Sonenberg N, Schuman EM (2002) A rapamycin-sensitive signaling pathway contributes to long-term synaptic plasticity in the hippocampus. Proc Natl Acad Sci U S A 99:467–472.

Tavazoie SF, Alvarez VA, Ridenour DA, Kwiatkowski DJ, Sabatini BL (2005) Regulation of neuronal morphology and function by the tumor suppressors Tsc1 and Tsc2. Nat Neurosci 8:1727–1734.

Tee AR, Manning BD, Roux PP, Cantley LC, Blenis J (2003) Tuberous sclerosis complex gene products, Tuberin and Hamartin, control mTOR signaling by acting as a GTPase-activating protein complex toward Rheb. Curr Biol 13:1259–1268.

Thiagarajan TC, Lindskog M, Tsien RW (2005) Adaptation to synaptic inactivity in hippocampal neurons. Neuron 47:725–737.

Tischmeyer W, Schicknick H, Kraus M, Seidenbecher CI, Staak S, Scheich H, Gundelfinger ED (2003) Rapamycin-sensitive signalling in long-term consolidation of auditory cortex-dependent memory. Eur J Neurosci 18:942–950.

Voglmaier SM, Kam K, Yang H, Fortin DL, Hua Z, Nicoll RA, Edwards RH (2006) Distinct endocytic pathways control the rate and extent of synaptic vesicle protein recycling. Neuron 51:71–84.

Wang CC, Held RG, Chang SC, Yang L, Delpire E, Ghosh A, Hall BJ (2011) A critical role for GluN2B-containing NMDA receptors in cortical development and function. Neuron 72:789–805.

Wang X, Proud CG (2006) The mTOR pathway in the control of protein synthesis. Physiology (Bethesda) 21:362–369.

Yang Q, Guan KL (2007) Expanding mTOR signaling. Cell Res 17:666–681.

Zoncu R, Efeyan A, Sabatini DM (2011) mTOR: from growth signal integration to cancer, diabetes and ageing. Nat Rev Mol Cell Biol 12:21–35.

CHAPTER III

Transynaptic signaling by BDNF as an immediate consequence of acute mTORC1 activation in dendrites

3.1 Abstract

Spatially constrained protein synthesis within and around synaptic sites on dendrites provides an essential layer of control by which individual neurons can uniquely adapt to ongoing branch-specific changes in the pattern of afferent inputs. Further understanding of specific molecular mechanisms involved in regulating local translation of dendritic mRNAs in response to altered activity is currently an area of great interest. In particular the mammalian target of rapamycin complex 1 (mTORC1) has been implicated as an important regulator of local protein synthesis, with well-characterized roles in long lasting forms of synaptic plasticity and memory formation. Here we report that mTORC1 is activated by the lipid second messenger phosphatidic acid (PA) in hippocampal neurons, with subsequent fast acting and profound effects on synaptic function. Transient application of exogenous PA drives mTORC1 activation in hippocampal neurons, stimulates synthesis of BDNF, and also drives a protein-synthesis dependent increase in the frequency, but not amplitude of spontaneous mEPSCs. Experiments utilizing either cell specific or transient inhibition of BDNF synthesis suggest that de novo BDNF translation in the postsynaptic compartment underlies retrograde signaling driven by dendritic mTORC1 activation. As dysregulation of protein synthesis has been implicated in a number of

neurological and psychiatric disorders, a more thorough mechanistic understanding of translation regulation in dendrites has the potential to yield greater insight into the synaptic etiology of syndromes characterized by debilitating cognitive impairment.

3.2 Introduction

The regulation of localized translation at synaptic sites in dendrites has emerged as vital mechanism whereby neurons alter the protein landscape in spatially defined regions of the cell in response to particular types of stimuli (Liu-Yesucevitz et al., 2011). The ever widening range of cellular events believed to utilize this feature suggests that it may be more commonplace than once imagined, and is likely of particular use in brain regions with well defined stratified circuits such as in the hippocampus, where cells are equipped with dendritic arbors that display a high degree of functional compartmentalization (Branco and Hausser, 2010). Recent studies suggest mRNAs transcripts representing over 2500 genes are localized outside the cell body in the CA1 region of the hippocampus (Cajigas et al., 2012), revealing a broad range of alterations in cellular function that might depend on changes in dendritic translation.

One signaling pathway that has been shown to play an important role in regulating local protein synthesis in dendrites is that of the mechanistic target of rapamycin (mTOR). When bound to the regulatory protein raptor, mTOR forms a complex (mTORC1) known to regulate protein synthesis at the level of translation initiation (Ma and Blenis, 2009). mTORC1 is believed to regulate protein synthesis via phosphrylation of several components of the translational machinery, including the S6 kinases (S6Ks), the inhibitory eIF4E-binding proteins (4E-BPs), and the eIF4G initiation factors. Recent work however, suggests that 4E-BP is uniquely indispensable for mTORC1-mediated translational control, and is responsible for the selective regulation of a subset of mRNA transcripts that contain 5′ terminal oligopyrimidine (TOP) motifs (Thoreen et al., 2012). In mammalian central neurons, multiple dendritically localized mRNA transcripts have been shown to be under mTORC1-dependent translational control, changes in which can elicit profound effects on cellular structure and function (Raab-Graham et al., 2006; Lee et al., 2011; Liao et al., 2012).

From a clinical perspective, harnessing mTORC1's influence over synapse development and plasticity has emerged as a potential point of therapeutic intervention (Ehninger and Silva, 2011). Several monogenic forms of intellectual disability (ID) and Autism Spectrum Disorders (ASD) involve mutations in proteins that normally serve to inhibit mTORC1 signaling in vivo. As such, disorders including Tuberous Sclerosis, PTEN Hamartoma syndrome, and Neurofibramatosis Type 1 all share a common molecular phenotype of hyperactive mTORC1 signaling (Kelleher and Bear, 2008). Despite this clear genetic link, it has been difficult to determine the precise relationship between dysregulated mTORC1 signaling and the abnormal social and cognitive phenotypes observed in patients with ASD and ID. Previous reports have demonstrated that mTORC1 is vital for regulating proper circuit development (Nie et al., 2010; Normand et al., 2013), and mTORC1 signaling has been implicated in multiple forms of synaptic plasticity including Long Term Potentiation (Tang et al., 2002; Cammalleri et al., 2003; Stoica et al., 2011) and mGluR-dependent long term depression (Hou and Klann, 2002; Antion et al., 2008), highlighting the multifaceted role for this signaling pathway in multiple cell types and developmental stages in the brain.

Outside of an emerging consensus regarding a role for mTORC1-dependent regulation of de novo protein-synthesis in synaptic plasticity, there is much less agreement with respect to the consequences of enhanced mTORC1 signaling on basal synaptic form and function. For example, recently published studies examining the effects of conditional deletion of PTEN or mutations in either component of the tuberous sclerosis complex, have described incongruous effects of mTOR hyperactivation with respect to basic synapse function, including descriptions of no change in fEPSP input/output curve (Wang et al., 2006), deficits in fEPSP Input/output curve (Fraser et al., 2008), increases in mEPSC amplitude but not frequency (Tavazoie et al., 2005, Weston et al., 2012), increases in mEPSC frequency but not amplitude (Bateup et al, 2011, Luikart et al., 2011), no change in mEPSC characteristics at all (Sperow et al., 2012), increases in presynaptic function (Weston et al. 2012), decreases in presynaptic release (von der Brelie et al., 2006), and no change in inhibitory neurotransmission (Luikart et al., 2011), versus profound effects on inhibitory synapse function (Bateup et al., 2013). Given that the extent of genetic manipulations utilized in these studies ranged from days to months, it is possible that variability in the duration of mTORC1 hyperactivation may possibly account for the inconsistent findings. mTORC1 is embedded in a rich network of interacting biochemical signals, and chronic dysregulation of this pathway may potentially recruit feedback mechanisms that result in cellular phenotypes which may not accurately reflect the nature of the initial insult (Rodrik-Outmezguine et al., 2011).

With these issues in mind, we sought to elucidate the immediate consequences of upregulated mTORC1 signaling on synapse form and function. To address this question, we used exogenous application of the lipid second messenger phosphatidic acid (PA), which has been shown to activate mTORC1 signaling in non-neuronal cells (Fang et al., 2001; Lim et al., 2003). Treatment with PA produced rapid activation of mTORC1 signaling in cultured hippocampal neurons, with subsequent profound effects on network function. These network effects were not due to changes in excitability or inhibitory tone, but were instead a result of enhanced presynaptic vesicle release at excitatory terminals. Cell specific elimination of BDNF expression revealed that this protein functions as a retrograde signal in response to acute mTORC1 activation, acting to increase presynaptic efficacy. Understanding this change in basal synapse function in response to enhanced mTORC1 activity is important, given that several monogenic disorders resulting in intellectual disability and Autism-like phenotypes share a common feature of dysregulated mTORC1 activation at the synapse (Hoeffer and Klann, 2010).

3.3 Results

Phosphatidic acid (PA) is a lipid second messenger believed to activate mTORC1's kinase activity by binding directly to the FRB domain on mTOR itself and stabilizing the complex with its binding partner raptor (Veverka et al., 2008; Toschi et al., 2009). Consistent with observations from experiments using non-neuronal cell lines (Fang et al., 2001; Yoon et al., 2011; You et al., 2012), western blots of lysates prepared from hippocampal neuron cultures revealed that PA rapidly induced sustained phosphorylation of the immediate downstream mTORC1 effectors 4E-BP1 and p70S6K (Figure 3.1A-B). The timing of kinase activity at these two downstream targets appear slightly staggered, with levels of phosphorylated p70S6K rising dramatically within the first 15 minutes after mTORC1 stimulation with PA, and p-4EBP1 levels showing peak activation 30 minutes after PA treatment (Normalized p-4EBP1 15 min post-PA, 120.18±5.82% of Time 0, n=3; Normalized p-4EBP1 30 min post-PA, 111.69±2.99% of Time 0, n=3; Normalized p-p70S6K 15 min post-PA, 107.84±7.26% of Time 0, n=3; Normalized p-p70S6K 30 min post-PA, 125.42±18.07% of Time 0, n=3). We observed persistent increases in mTORC1 kinase activity after activation with PA (100μM), with significantly elevated levels of p-p70S6K and p-4EBP1 as long as 120m after stimulation (Normalized p-4EBP1 120 min post-

PA, 124.89±5.28% of Time 0, n=3; Normalized p-p70S6K 120 min post-PA, 129.84±9.30% of Time 0, n=3). As an additional metric of PA-induced changes in mTORC1 kinase activity (Figures 3.1C-D), we also found robust phosphorylation of ribosomal protein S6 at S235/236 in the cell bodies and dendrites of hippocampal neurons as assessed via immunocytochemistry (Normalized p-S6 Intensity Vehicle Control, 100±7.21%, n=13; Normalized p-S6 Intensity PA 60min, 177.28±25.99%, n=19). Expression of tubulin (Figure 3.1A) and microtubule associated protein 2 (MAP2) did not change significantly as a consequence of exposure to PA (Figure 3.1D).

Using PA as a tool to acutely activate mTORC1 signaling in neurons, we next examined the consequences of such activation on dendritic BDNF expression. Previous work from our lab and others has identified BDNF as a unique target of mTORC1-dependent translational regulation in dendrites (Henry et al., 2012; Liao et al., 2012). In hippocampal neurons, this dendritic synthesis of BDNF plays a vital role in the homeostatic regulation of excitatory synapses, acting as a retrograde signal to enhance the efficacy of presynaptic terminals (Jakawich et al., 2010; Lindskog et al., 2010; Henry et al, 2012). Acute mTORC1 activation (60 min PA, 100μM) enhanced dendritic BDNF staining intensity in hippocampal dendrites, while having no effect on dendritic MAP2 expression in these same neurons (Figure 3.2A-B). Coincident blockade of protein synthesis (with 40μM anisomycin, 30 min prior to PA) or mTORC1 (with 300nM rapamycin, 30 min prior to PA) completely suppressed this effect, suggesting that treatment with PA drives new synthesis of BDNF via activation of mTORC1 (Normalized BDNF Intensity Vehicle Controls, 100±15.17%, n=25; Normalized BDNF Intensity PA 60min, 220.03±29.21%, n=25; Normalized BDNF Intensity PA+Aniso, 93.92±13.92%, n=25; Normalized BDNF Intensity PA+Rap, 114.51±17.59%, n=25). We observed a slight, though statistically insignificant, effect of Anisomycin and Rapamycin on dendritic BDNF intensity when administered alone, suggesting a very limited role for steady-state BDNF synthesis under baseline conditions (Normalized BDNF Intensity Aniso alone, 77.89±11.33%, n=25; Normalized BDNF Intensity Rap alone, 86.76±22.38%, n=25). Similar effects were observed in western blots of hippocampal neuron lysates from cells treated with PA alone or in combination with Rapamycin (Figure 3.2C-D). PA elicited a time-dependent increase in BDNF expression, with an initial peak at 15min post PA treatment and significantly elevated levels observed up to 60min post treatment (Normalized BDNF expression PA 15min, 156.13±28.25% of time 0, n=3; Normalized BDNF expression PA 30min, 152.67±20.39% of time 0, n=3; Normalized BDNF expression PA 60min, 134.69±23.05% of time 0, n=3). This increase in BDNF expression was also mTORC1-dependent, as concurrent rapamycin (300nM) treatment completely eliminated PA-induced BDNF expression (Normalized BDNF expression PA+Rap 15min, 121.37±25.32% of time 0, n=3; Normalized BDNF expression PA+Rap 30min, 104.13±20.80% of time 0, n=3; Normalized BDNF expression PA+Rap 60min, 101.94±9.52% of time 0, n=3). As a final readout of PA-induced changes in BDNF expression, we took advantage of a recently developed fluorescent reporter of local BDNF synthesis in dendrites (Figure 3.2E-F). The reporter consists of the entire long Bdnf 3′ UTR (sequence ‘A*B’), alongside a myristoylation peptide (myr), destabilized d1GFP protein, and a nuclear localization sequence (nls), which in total prevents substantial intracellular movement of reporter-based fluorescence away from the area in which it was synthesized (Liao et al., 2012). BDNF transcripts with long 3’UTR have been previously shown to display preferential localization to the distal regions of dendrites (An et al., 2008), and as such the myr-d1GFP-nls–A*B reporter has been utilized recently as an effective readout of dendritic BDNF synthesis (Liao et al., 2012). We found that application of PA to neuronal cultures transfected with the BDNF-A*B reporter showed enhanced GFP fluorescence intensity in the distal regions of dendrites (located 100-200μm away from cell bodies), compared to transfected neurons treated with vehicle (Normalized reporter intensity vehicle control, 100±17.53%, n=21; Normalized reporter intensity PA 45min, 195.07±28.99% of control, n=16). In total, these experiments clearly indicate that synthesis of BDNF is an immediate consequence of acute activation of mTORC1 in hippocampal neurons.

mTORC1 signaling, long known to play an important role in regulating cell size and metabolism (Laplante and Sabatini, 2012), has been previously linked to changes in spine density and morphology after prolonged periods of hyperactivity (Tavazoie et al., 2005; Kwon et al., 2006; Fraser et al., 2008; Luikart et al., 2011; Xiong et al., 2012; but see Sperow et al., 2012; Bateup et al., 2012). To investigate potential changes in spine morphology after acute mTORC1 activation, we transfected mature hippocampal neurons (DIV 21 or older) with eGFP, then treated with PA or vehicle 24 Hrs later (Figures 3.3A-C). We found no change in soma size or spine density after 90 minutes of enhanced mTORC1 activity (soma size vehicle control, 335.07±31.73μm^2, n=8; Soma size PA 90 min, 323.61±27.96μm^2, n=10; Spine density vehicle control, 19.7±1.14 spines per 25μm, n=20; Spine density PA 90min, 20.41±0.97 spines per 25μm, n=27), indicating that cell growth pathways were not significantly recruited by this transient activation. Additionally, we found no change in spine length or head width as a consequence of PA treatment (Spine length vehicle control, 2.57±0.052μm, n=852; Spine length PA 90min, 2.56±0.04um, n=1344; Head width vehicle control, 1.07±0.02um, n=852; Head width PA 90min, 1.06±0.01um, n=1344), suggesting little if any impact on the morphological characteristics of excitatory synapses after acute mTORC1 activation with PA (Figure 3.3E-D).

In contrast to the effects on spine morphology, cell attached recordings from hippocampal neurons in culture revealed a profound impact on cell spiking behavior after treatment with PA, potentially suggesting an increase in overall network function (Figure 3.4A). Whole cell current clamp recordings revealed no difference between control and PA-treated neurons in the number of action potentials elicited by a series of depolarizing current steps (Max # evoked spikes control, 5.57±0.96, n=14; Max # evoked spikes PA45min, 6.25±0.99, n=12), suggesting that PA-induced change in spike behavior do not reflect mTORC1-dependent changes in intrinsic excitability (Figure 3.4B-D). In agreement with results indicating no effect of transient mTORC1 activation on spine head width, we found no change in the amplitude of spontaneous mEPSCs after 45 or 90 minutes treatment with PA (mEPSC Amplitude control, 12.22±0.53pA; mEPSC Amplitude PA 90 min, 12.57±0.52pA), suggesting that acute mTORC1 activation is not sufficient to alter excitatory postsynaptic function (Figure 3.4E). In contrast, we found that transient pharmacological upregulation of mTORC1 activity via PA treatment resulted in a rapid increase in mEPSC frequency (mEPSC frequency control, 1.58±0.33Hz; mEPSC frequency PA 90 min, 4.43±0.58Hz). This time-dependent increase in mEPSC frequency induced by PA was dependent on protein synthesis, mTORC1 activation, and BDNF release, as the increase in mEPSC frequency was blocked by concurrent application of anisomycin (40μM), Rapamycin (300nM) and an extracellular scavenger of released BDNF, TrkB-fc (1μg/ml) (Figure 3.4G-H). While recent reports suggest that increases in network activity in mouse models featuring enhanced mTORC1 activity may reflect selective changes in inhibitory synapse function (Bateup et al., 2013), we found no changes in the frequency or amplitude of spontaneous mIPSCs in hippocampal cultures after treatment with PA (mIPSC amplitude control, 29.49±0.75pA, n=16; mIPSC amplitude PA 45min, 27.98±1.03pA, n=20; mIPSC frequency control, 0.97±0.12Hz, n=16; mIPSC frequency PA 45min, 1.29±0.13Hz, n=20), suggesting that altered inhibitory neurotransmission is not an immediate consequence of increased mTORC1 signaling (Figures 3.4I-J). To confirm that the observed changes in mEPSC frequency reflect bona fide changes in presynaptic function, we examined the effect of PA on syt-lum uptake at vglut1-positive excitatory synapses (Figure 3.5A-B). The results of these experiments mirrored the observed changes in synaptic physiology, as transient mTORC1 activation induced a significant increase in syt-lum uptake that was blocked by anisomycin, rapamycin, and TrkB-Fc (Prop syt uptake Control, 0.40±0.04, n=52; Prop syt uptake PA 45min, 0.58±0.03, n=91; Prop syt uptake PA+Rap, 0.33±0.03, n=34; Prop syt uptake PA+Aniso, 0.44±0.06, n=30; Prop syt uptake PA+TrkB-fc, 0.28±0.04, n=30).

mTORC1 is believed to regulate translation by phosphorylating components of the translation machinery itself, including the primary targets 4EBP1 and p70S6K (Hay and Sonenberg, 2004). In light of recent findings suggesting unique synaptic and behavioral consequences resulting from disruption of p70S6K (Bhattacharya et al., 2012) or 4E-BP1 (Gkogkas et al., 2013), we were interested in determining whether either of these signaling components were uniquely responsible for mediating the effects of transient mTORC1 activation on synapse function (Figure 3.6A-C). To selectively disrupt individual elements of the signaling network downstream of mTORC1 activation, we utilized newly developed pharmacological agents including PF-4708671, a selective inhibitor of p70S6K (Pearce et al., 2010), as well as 4EGI-1, a compound that disrupts the interaction between eukaryotic initiation factors 4E and 4G (Hoeffer et al., 2011). While the amplitude of spontaneous excitatory currents was not affected by inhibition of downstream mTORC1 targets (mEPSC amplitude control, 13.38±0.50pA, n=19, mEPSC amplitude PA 45 min, 14.59±0.68pA, n=14; mEPSC amplitude PA+4EGi, 14.09±0.63pA, n=7; mEPSC amplitude PA+p70S6Ki, 12.29±0.87pA, n=13) co-application of either of these agents alongside PA disrupted the potentiating effects of PA on mEPSC frequency (mEPSC frequency control, 1.75±0.34Hz, n=19; mEPSC frequency PA 45min, 4.72±0.84Hz, n=14; mEPSC frequency PA+4EGi, 2.97±0.61Hz, n=7; mEPSC frequency PA+p70S6Ki, 2.68±0.73Hz, n=13), suggesting that transient mTORC1 activation via application of PA utilizes both 4EBP1 and p70S6K to mediate effects on presynaptic function.

The preceding results demonstrate that acute mTORC1 activation drives rapid protein synthesis-dependent increases in dendritic BDNF expression and rapid translation-dependent enhancement of presynaptic function that requires BDNF, suggesting a potential causal relationship between the two. To evaluate this possibility, we examined the specific role of postsynaptic BDNF release using sparse transfection of BDNF shRNA, which has been previously demonstrated to effectively knock down BDNF expression (Jakawich et al., 2010). 24 hrs post-transfection, neurons were exposed to PA for 45 min, and postsynaptic mEPSC recordings were made from shRNA-expressing neurons (identified by RFP, expressed by an independent cassette in each shRNA plasmid) or untransfected control neurons (Figure 3.7A). We found that whereas acute mTORC1 activation with PA resulted in robust increases in mEPSC frequency, but not mEPSC amplitude, in non-transfected neurons or neurons transfected with a scrambled control shRNA (Figure 3.7B-D), PA had no effect in BDNF shRNA expressing neurons (untransfected vehicle, 1.04±0.27Hz, n=7; scrambled siRNA vehicle, 0.81±0.22Hz, n=4; BDNF siRNA vehicle, 0.69±0.07Hz, n=8; untransfected PA 45min, 6.42±2.01Hz, n=6; scrambled siRNA PA 45 min, 5.56±1.10Hz, n=3; BDNF siRNA PA 45 min, 1.79±0.40Hz, n=9). These results indicate that a postsynaptic source of BDNF is required for the retrograde enhancement of presynaptic function driven by acute mTORC1 activation.

3.4 Discussion

These results highlight a unique mechanism of trans-synaptic communication initiated by acute mTORC1-dependent signaling in dendrites. Though mTORC1 has been shown to play an important role in multiple forms of synaptic plasticity, studies examining effects of mTORC1 hyperactivation on basal synapse form and function have produced markedly different results. Here we have shown that acute mTORC1 activation using the lipid second messenger phosphatidic acid (PA) elicits strong increases in network activity in dissociated hippocampal cultures that is not mediated by alterations in intrinsic excitability or inhibitory neurotransmission. Instead, we find that transient increases in mTORC1 signaling produce a dramatic increase in release probability from apposed postsynaptic terminals. This effect emerges rapidly, likely within 30 minutes of mTORC1 activation, based on comparing the time course of mTORC1 activation to the time needed for functional changes to appear after PA treatment. Finally, we show that these changes in presynaptic function depend fundamentally on synthesis of BDNF in the postsynaptic cell for use as a retrograde signal.

Initial observations that PA is necessary for mTOR activation came from studies examining mitogenic stimulation of mTORC1 signaling (Fang et al., 2001). Subsequent functional and structural evidence indicate that PA binds to the FKBP12-rapamycin-binding (FRB) domain of mTOR at R2109, where it is believed to directly compete with the binding of the FKBP12-rapamycin complex itself (Veverka et al., 2008; Toschi et al., 2009). In support of this, cancer cell lines with high rates of internal synthesis of PA display resistance to rapamycin-mediated inhibition of mTORC1 signaling (Chen et al., 2003), which is line with our finding that higher concentrations of rapamycin were needed to block the effects of exogenous PA on presynaptic function (300nM, vs 100nM as has been used previously in our lab to inhibit mTORC1 activity). Additional work in non-neuronal cells suggests that PA stimulates mTOR's kinase activity by promoting the stabilization between mTOR and its binding partner raptor (Toschi et al., 2009), or by enhancing mTORC1 autophosphorylation at S2481 via displacement of FK506 binding protein 38 (FKBP38)-mediated inhibition (Yoon et al., 2011). We find that in cultured hippocampal neurons, application of PA-containing vesicles rapidly stimulated mTORC1 signaling (Figure 3.1). Our observation that PA-induced increases in phosphorylation of downstream mTORC1 targets were apparent within 15 min (Figure 3.1), is similar to the timecourse of S6K activity previously observed after exogenously applied PA in Neutrophils and Monocytes (Frondorf et al., 2010). It is important to note that PA can bind to multiple targets besides mTOR, including Arf, Raf and NSF (Ktistakis et al., 2003). Additionally, PA has been shown exert a direct influence on vesicle release in chromaffin cells (Bader and Vitale, 2009) and at ribbon synapses in the CNS (Schwarz et al., 2011). While we cannot completely rule out a contribution of off-target effects, we remain confident that the enhancement in excitatory synapse function we observe after PA treatment is due to mTORC1-induced synthesis of BDNF as a retrograde signal. We support this claim with the following observations: 1) The PA-induced changes in excitatory synapse function we report here exactly mirror previously reported changes in synapse function observed after transient genetic upregulation of mTORC1 signaling via overexpression of Rheb-GTPase (Henry et al., 2012); 2) Our reported PA-induced increases in presynaptic function, assessed using an array of live-cell imaging and electrophysiology approaches, were completely blocked when PA was co-applied with anisomycin, rapamycin, or a scavenger of extracellular BDNF, TrkB-fc (Figures 3.4 and 3.5); and 3) postsynaptic knockdown of BDNF eliminated the enhancement in presynaptic function observed after PA-treatment

(Figure 3.7). In total, the results of these experiments are most parsimonious with a model in which PA activates mTORC1 and leads to the release of BDNF from dendrites as a transynaptic signal to enhancement presynaptic function.

We use a number of approaches to demonstrate BDNF expression is enhanced as a result of acute mTORC1 activation with PA. Though mTORC1 undoubtedly targets a number of other transcripts for translation control under such conditions as well, our data suggests that the synaptic and network level changes we observe after acute mTORC1 activation (Figure 3.4) are due to the dendritic synthesis and release of BDNF as a retrograde messenger to enhance presynaptic function. Of the numerous BDNF mRNA isoforms that exist in rat neurons, there is evidence for unique trafficking and subcellular localization depending on the configuration of alternatively spliced 5'UTR exons (Chiaruttini et al., 2008) or polyadenylation of the 3'UTR (An et al., 2008). We find a marked increase in levels of dendritic BDNF as assessed via immunocytochemistry (Figure 3.2A-B) as well as with a fluorescent reporter under control of the long 3'UTR variant of BDNF mRNA (Figure 3.2E-F). These findings raise the interesting possibility that acute activation of mTORC1 yields increased translation of particular BDNF mRNA species. Given the recent observation that specific transcripts mediate local BDNF synthesis in the hippocampus after pilocarpine-induced status epilepticus (Baj et al., 2013), it will be of central interest for future studies to elucidate the mechanisms by which mTORC1 signaling targets particular transcript isoforms to induce protein synthesis-dependent changes in synapse function.

An important open question is how BDNF secretion is regulated after mTORC1-dependent synthesis. Previous studies have established that dendritic BDNF release is $Ca2^+$-dependent and can be promoted through high frequency stimulation (Hartmann et al., 2001) or in response to backpropagating action potentials (Kuczewski et al., 2008). More recently, work from Chapman and colleagues suggests that particular sets of BDNF-containing vesicles are trafficked in a segregated manner out into dendritic or axonal compartments (Dean et al., 2012). It will be of interest for future work to further establish how this sorting mechanism operates in tandem with localized synthesis of BDNF to be utilized as a retrograde signal. Regardless, these data are interesting in light of the well-characterized role of BDNF in stimulating new protein synthesis via mTORC1 activation (Schratt et al., 2004). While our previous work demonstrated that blockade of excitatory input can elicit mTORC1-dependent synthesis of BDNF in the presence of extracellular scavengers of BDNF (Henry et al., 2012), the possibility remains that dendritically synthesized BDNF might exert an additional autocrine signaling effect to continuously stimulate mTORC1 activity after its initial engagement. This type of autocrine activity for BDNF release has been observed previously at developing presynaptic terminals in the hippocampus (Cheng et al., 2011). Such a mechanism might be useful for the continued propagation of a plasticity-inducing event that requires an external signal to break the positive feedback cycle, as has been observed recently at synapses in the hypothalamus (Yang et al., 2011).

Though the effects of chronic mTORC1 upregulation on basal characteristics of synapse form and function have been extremely varied, our findings mirror that of several recent publications. Specifically, we find that acute activation of mTORC1 signaling after PA treatment mirrors the effects of more prolonged activation reported previously with respect to increases in mEPSC frequency (Luikart et al., 2011; Bateup et al., 2011), and increases in presynaptic release probability (Wang et al., 2006; Weston et al., 2012). Additionally, we found no change in inhibitory neurotransmission, mEPSC amplitude, or dendritic spine morphology, similar to effects seen after hyperactivation of mTORC1 signaling resulting from mutations in PTEN or TSC1/2 (Luikart et al., Bateup et al., 2011; Sperow et al.2012). Our results differ from previous reports describing changes in inhibitory synapse connectivity (Bateup et al., 2013), increases in spine density (Fraser et al., 2008), and increases in mEPSC amplitude (Tavazoie et al., 2005). One potential source of this discrepancy may be the amount of time during which mTORC1 activity is aberrantly upregulated. A recent report indicates that mTORC1 signaling follows a biphasic trajectory in the context of gustatory learning, with peaks of activity at 15 and 180 min post-learning, which may indicate some degree of feedback or non-linearity within the pathway in vivo (Belelovsky et al., 2007). There are additional indications that particular consequences of mTORC1 activation on cell function proceed at different time scales. For instance, our previous work demonstrated that somatic hypertrophy in cultured hippocampal neurons is observed after 5 days, but not after 1 day of genetic mTORC1 hyperactivation (Henry et al., 2012). This may also suggest that the synaptic functional abnormalities we report here actually precede changes in cell morphology. Given the essential role played by synaptic activity in shaping neuronal connectivity during development (Bleckert and Wong, 2011), it is conceivable that early shifts in excitatory synapse function resulting from mTORC1 hyperactivation may drive the subsequent changes in spine density and circuit structure that have been observed after longer periods of mTORC1 hyperactivation (Nie et al., 2010; Luikart et al., 2011; Weston et al., 2012; Normand et al., 2013). With its common role in several monogenic neurodevelopmental disorders, additional insight into the consequences of mTORC1 upregulation on synapse form and function will provide a crucial link between cellular and behavioral abnormalities observed in patients with Autism and Intellectual Disability.

3.5 Acknowledgments

This work was supported by Grants F31MH093112 (F.E.H.) and RO1MH085798 (M.A.S.) from The National Institute of Mental Health and a grant from the Pew Biomedical Scholars Program (M.A.S.). We thank Robert Edwards for generously providing vglut1-pHluorin. We also thank Hisashi Umemori and members of the Sutton laboratory for many helpful discussions.

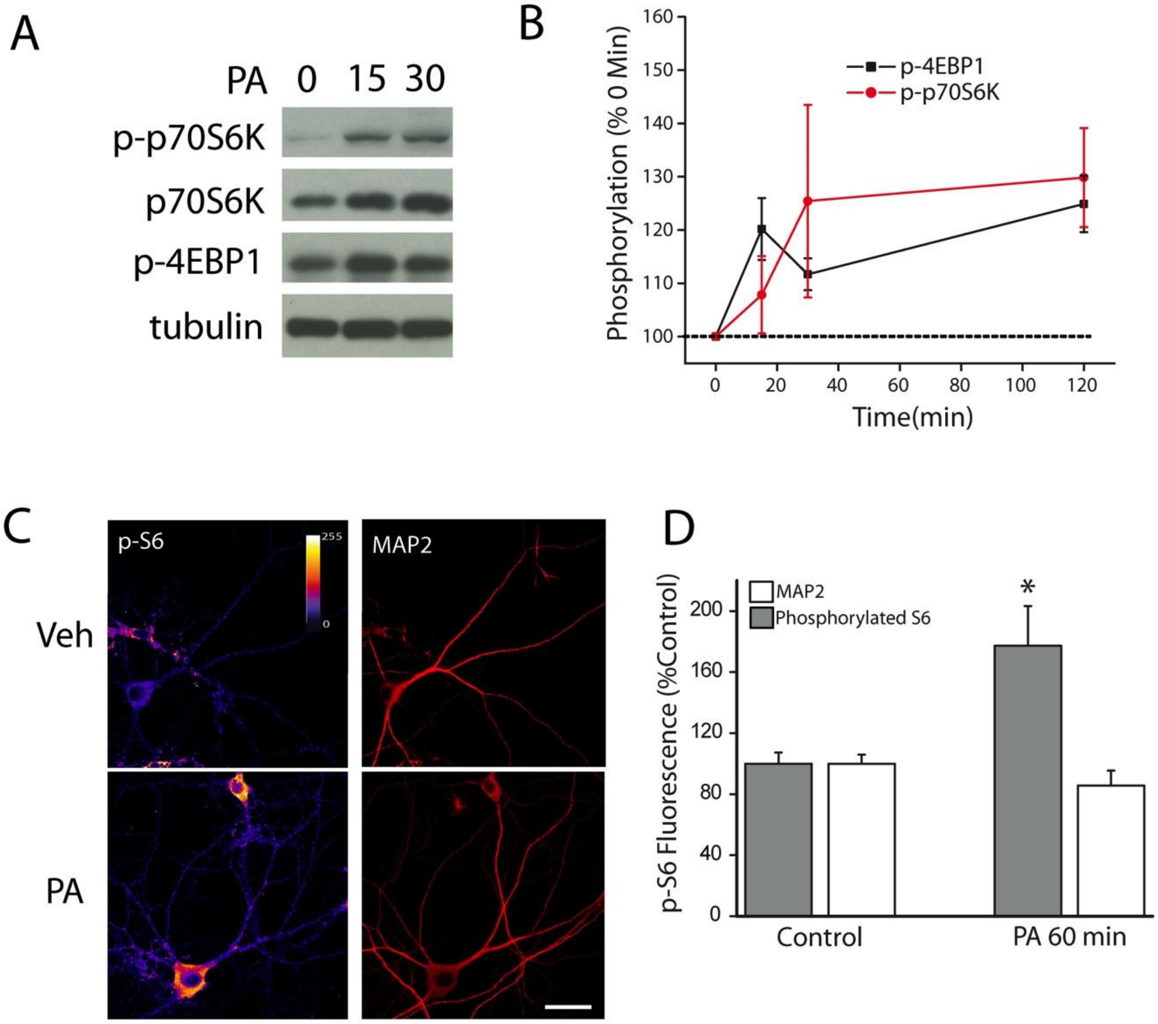
A
PA 0 15 30
p-p70S6K
p70S6K
p-4EBP1
tubulin
B
Phosphorylation (% 0 Min)
160
150
140
130
120
110
100
p-4EBP1
p-p70S6K
0 20 40 60 80 100 120
Time(min)
C
p-S6
255
0
MAP2
Veh
PA
D
p-S6 Fluorescence (%Control)
MAP2
Phosphorylated S6
*
200
160
120
80
40
0
Control
PA 60 min

Figure 3.1: Fast activation of neuronal mTORC1 via exogenous phosphatidic acid. (A) Representative Western blots depicting phosphorylated p70S6K (Thr389) and 4EBP1 (Thr37/46) following treatment with PA (100μM, n=3 exps) or vehicle for the indicated times. (B) Mean (SEM) expression of p-p70S6K and p-4EBP1in neurons subject to treatment with PA. Exogenous PA rapidly enhanced mTORC1 activity, as evidence by significant, time-dependent increases in phosphorylation of its immediate downstream targets p70S6K and 4EBP. (C) Full-frame examples of MAP2 and phosphorylated ribosomal protein S6 (Thr 235/236) staining in neurons treated with vehicle (n = 13) or phosphatidic acid (PA; 100 μM) for 60 min (n = 19). PS6 fluorescence intensity indicated by color look-up table; scale bar equals 40 μm. (D) Mean (+SEM) normalized MAP2 and PS6 expression in neurons treated as indicated. Application of PA activates mTORC1 signaling as indicated by enhanced PS6 staining. $^*p < 0.05$ (t-test), relative to vehicle treated controls.

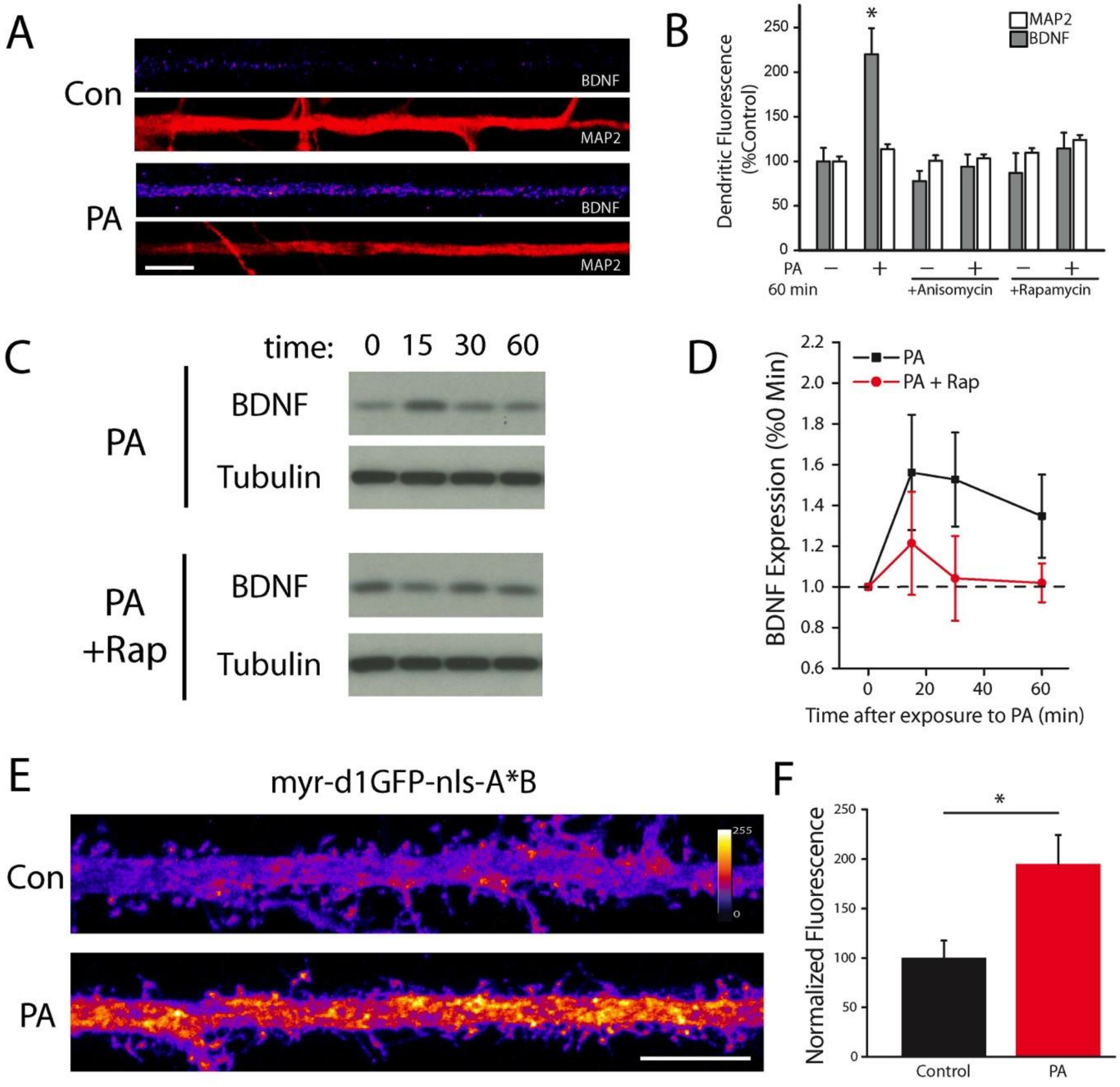
A
Con
BDNF
MAP2
PA
BDNF
MAP2
B
Dendritic Fluorescence (%Control)
250
200
150
100
50
0
*
MAP2
BDNF
PA
60 min
−
+
−
+
+Anisomycin
−
+
+Rapamycin
C
time: 0 15 30 60
PA
BDNF
Tubulin
PA +Rap
BDNF
Tubulin
D
BDNF Expression (%0 Min)
2.2
2.0
1.8
1.6
1.4
1.2
1.0
0.8
0.6
PA
PA + Rap
0
20
40
60
Time after exposure to PA (min)
E
myr-d1GFP-nls-A*B
Con
PA
255
0
F
Normalized Fluorescence
250
200
150
100
50
0
*
Control
PA

Figure 3.2: Enhanced BDNF synthesis is an immediate consequence of short-term mTORC1 activation. (A-B) BDNF and MAP2 expression in linearized dendritic segments (A), and mean (+ SEM) expression of MAP2 and BDNF (B) in dendritic compartments normalized to average control values, in neurons treated with PA (100 µM, 60 min; n = 25) or vehicle (n=25). BDNF expression in dendrites was significantly (*p < 0.05, relative to vehicle controls) enhanced by treatment with PA compared to vehicle treated controls. This effect was blockaded by pre-treatment with anisomycin (40 µM, 30 min prior to PA; n=25) or rapamycin (200 nM, 30 min prior to PA; n = 25). MAP2 expression did not differ between groups. Scale bar represents 10 µm in (A). (C) Representative western blots depicting changes in expression of BDNF or tublulin after treatment with PA (100µM) ± Rapamycin (300nM) for the indicated times. (D) Mean (SEM) expression of BDNF in cultured neurons subject to treatment with PA (n=3 experiments). Exogenous PA rapidly enhanced BDNF expression in an mTORC1 dependent manner, as the increased expression was blocked by rapamycin. (E). Representative images of hippocampal neurons expressing myr-d1GFP-nls-A*B treated with either vehicle or PA (100µM, 45 min). Scale bar, 10 µm. (F) Mean (+SEM) GFP fluorescence in dendrites of hippocampal neurons treated with PA (n=16) or vehicle (n=21). Sampled dendritic regions were located 100-200µm away from the cell body. *p < 0.05 (t-test), relative to vehicle treated controls.

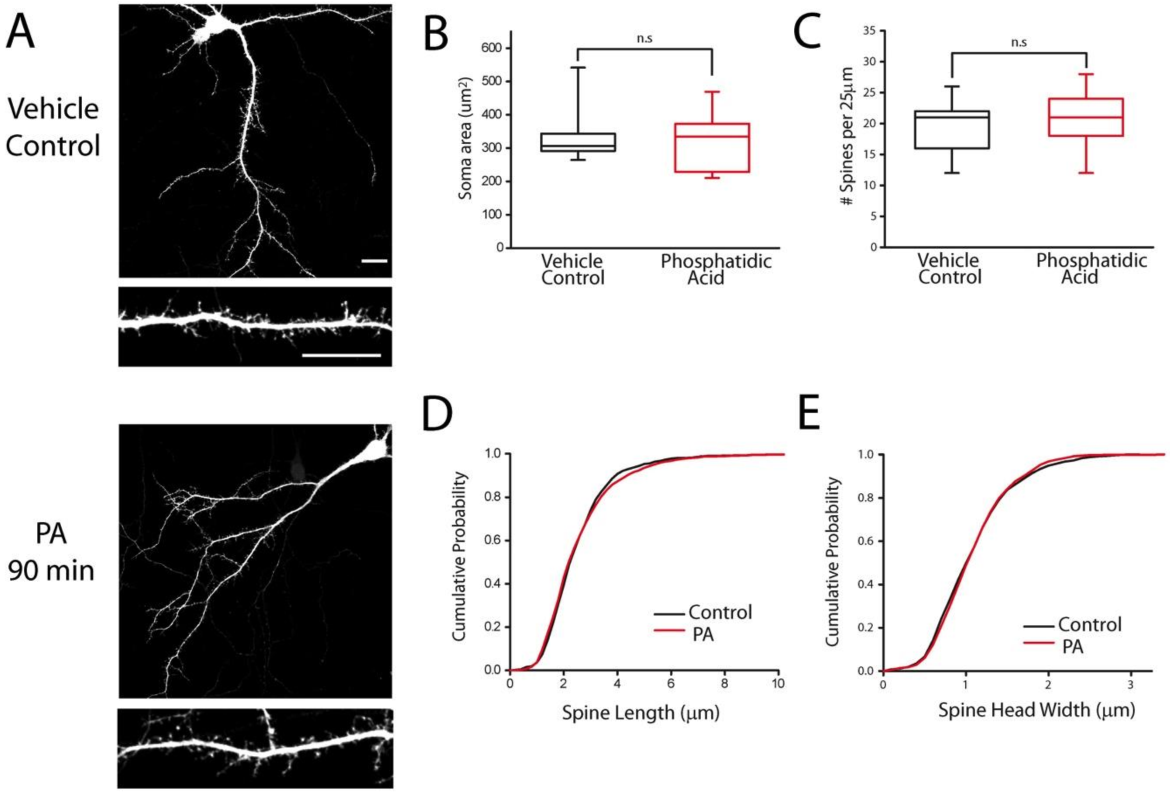
A
Vehicle Control
PA 90 min
B
n.s
Soma area (um²)
0
100
200
300
400
500
600
Vehicle Control
Phosphatidic Acid
C
n.s
# Spines per 25µm
0
5
10
15
20
25
30
35
Vehicle Control
Phosphatidic Acid
D
Cumulative Probability
0.0
0.2
0.4
0.6
0.8
1.0
Spine Length (µm)
0
2
4
6
8
10
Control
PA
E
Cumulative Probability
0.0
0.2
0.4
0.6
0.8
1.0
Spine Head Width (µm)
0
1
2
3
Control
PA

Figure 3.3: Acute mTORC1 activation does not affect spine morphology. (A) Representative full frame images and dendritc sub-regions of cultured hippocampal neurons transfected with GFP then treated with PA or vehcile for 90min at DIV 21-24. Scale bar, 10μm. (B-C) Box-plot summaries of soma area and spine density (spines per 25μm of dendrite) in cells treated with vehicle (n=20 cells) or PA (n=27 cells). (D-E) Cumulative distributions of spine length and spine head width (both in micrometers) from cells treated with vehicle (black traces, n=852 spines) or PA (red traces, n=1344 spines) for 90 min. n.s., Not significant

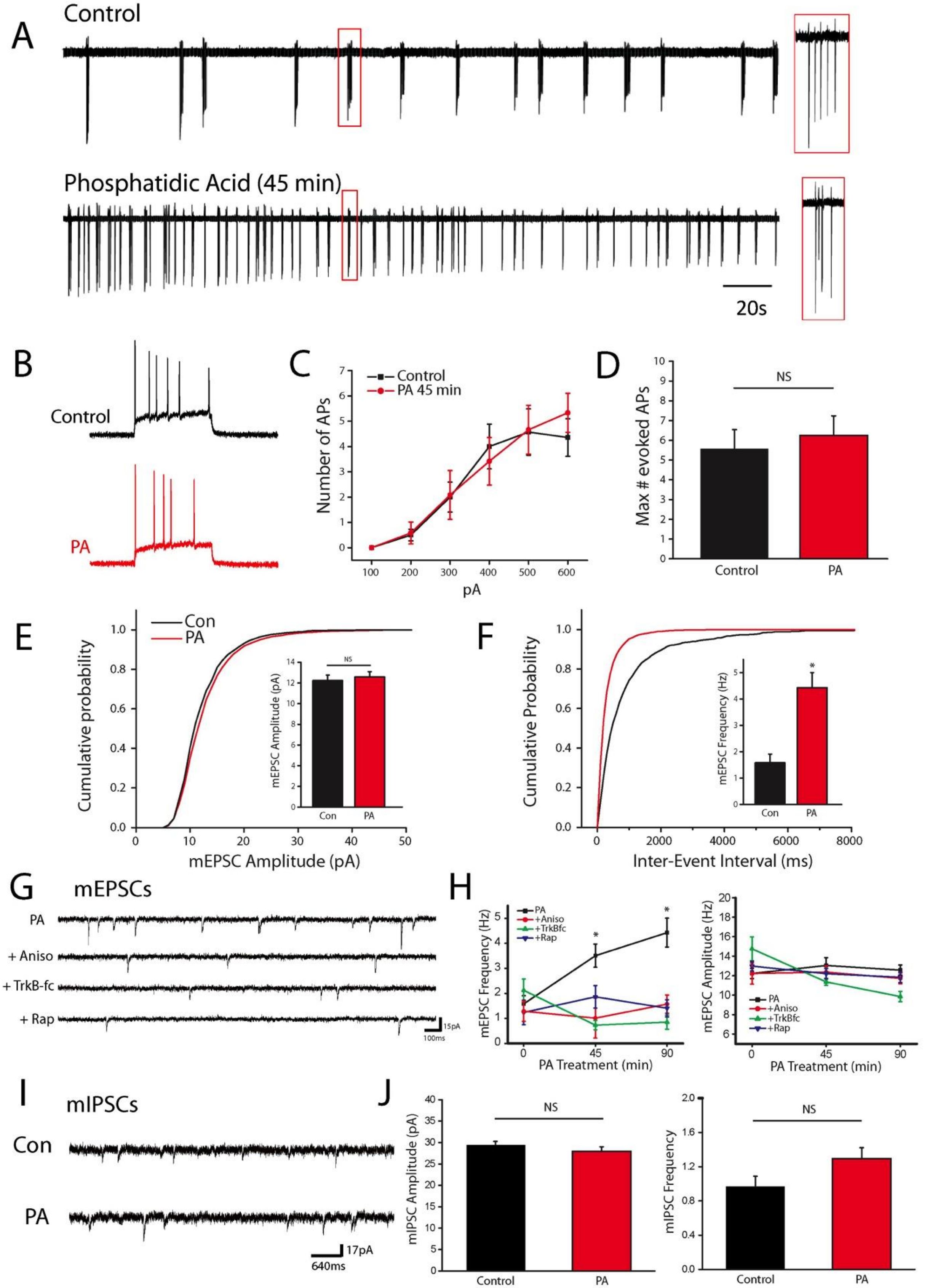
A
Control
Phosphatidic Acid (45 min)
20s
B
Control
PA
C
Control
PA 45 min
Number of APs
pA
100
200
300
400
500
600
D
NS
Max # evoked APs
Control
PA
E
Con
PA
Cumulative probability
mEPSC Amplitude (pA)
NS
Con
PA
F
Cumulative Probability
Inter-Event Interval (ms)
mEPSC Frequency (Hz)
*
Con
PA
G
mEPSCs
PA
+ Aniso
+ TrkB-fc
+ Rap
15pA
100ms
H
mEPSC Frequency (Hz)
PA
+Aniso
+TrkBfc
+Rap
PA Treatment (min)
mEPSC Amplitude (Hz)
I
mIPSCs
Con
PA
17pA
640ms
J
NS
mIPSC Amplitude (pA)
Control
PA
mIPSC Frequency

Figure 3.4: PA enhances network activity via increases in excitatory neurotransmission. **(A)** Cell attached recordings of hippocampal neurons in dissociated cultured treated with vehicle or PA (100μM, 45 min). Inset: enlarged region of recording (red box) showing individual spikes in a burst. **(B)** Whole-cell current clamp recordings showing example action potential traces from vehicle-treated control neurons (black) or cell treated with PA (red,). APs were evoked by injecting 1 s depolarizing current steps in the presence of excitatory and inhibitory synaptic blockers (CNQX 10μM, APV 50μM, Bicuculine 10μM). **(C-D)** Mean (± SEM) and maximum number of action potentials evoked by a series of depolarizing current steps in vehicle treated (n=14) or PA treated (n=12) cells. **(E-F)** Cumulative histogram of amplitude (pA) and inter-event interval (msec) of mEPSCs recorded from neurons treated with vehicle or 100 μM PA for 45 or 90 min. Inset, mean (+ SEM) mEPSC amplitude and frequency in neurons after treatment with PA (100 μM) or vehicle. **(G)** Representative recordings in neurons treated with PA (100mm, 45 min) with or without 30 min pretreatment with rapamycin (200 nM), anisomysin (40 μM) or TrkB-fc (1 μg/ml). **(H)** Timecourse of mean (+SEM) mEPSC amplitude and frequency of spontaneous mEPSCs at 45m or 90m exposure to PA with or without pretreatment, as indicated above. Sample sizes for the indicated groups: Vehicle (n = 7), PA 45 min (n = 9), PA45min + rapamycin (n = 9), PA45min +anisomycin (n = 5), PA45min +TrKB-fc (n = 6), PA90min (n = 6), PA90min + rapamycin (n = 6), PA90min + anisomycin (n = 9), PA90min+ TrkBfc (n = 3), rapamycin alone (n = 7), anisomycin alone (n = 7), TrkB-fc alone (n = 6). Acute activation of mTORC1 signaling with PA enhances mEPSC frequency in a protein synthesis, mTORC1, and TrkB dependent manner. **(I)** Representative recordings of pharmacologically isolated (TTX 1μM, CNQX 10μM, APV 50μM) spontaneous miniature inhibitory currents in cells treated with vehicle or PA. (J). Mean (+SEM) mIPSC amplitude and frequency of cultured neurons treated with vehicle or PA (100μM, 45min). ns=not significant.

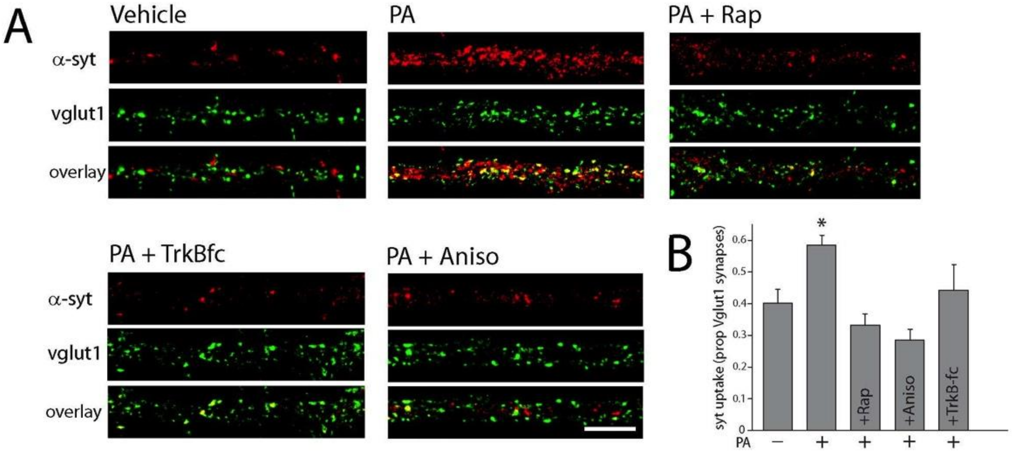
A
Vehicle
PA
PA + Rap
α-syt
vglut1
overlay
PA + TrkBfc
PA + Aniso
α-syt
vglut1
overlay
B
syt uptake (prop Vglut1 synapses)
0.6
0.5
0.4
0.3
0.2
0.1
0
*
+Rap
+Aniso
+TrkB-fc
PA
−
+
+
+
+

Figure 3.5: Enhanced presynaptic release emerges quickly after mTORC1 activation. (A-B) Representative examples (A) and mean (+ SEM) syt-lum uptake (B) from experiments where the indicated groups were treated with PA (100 μM, 90 min) in the presence or absence of rapamycin (200 nM, 30 min prior), anisomycin (40 μM, 30 min prior) or TrkB-Fc (1 μg/ml, 30 min prior). Sample sizes for the indicated groups: vehicle control (n=52), PA alone (n=91), PA+rapamycin (n=34), PA+anisomycin (n=41), or PA+TrkB-Fc (n=30 images). PA treatment induced a significant (*$p < 0.05$, relative to vehicle control) increase in syt-lum uptake that was blocked by inhibiting protein synthesis, mTORC1, or by scavenging extracellular BDNF. Scale bar represents 10 μm in (A).

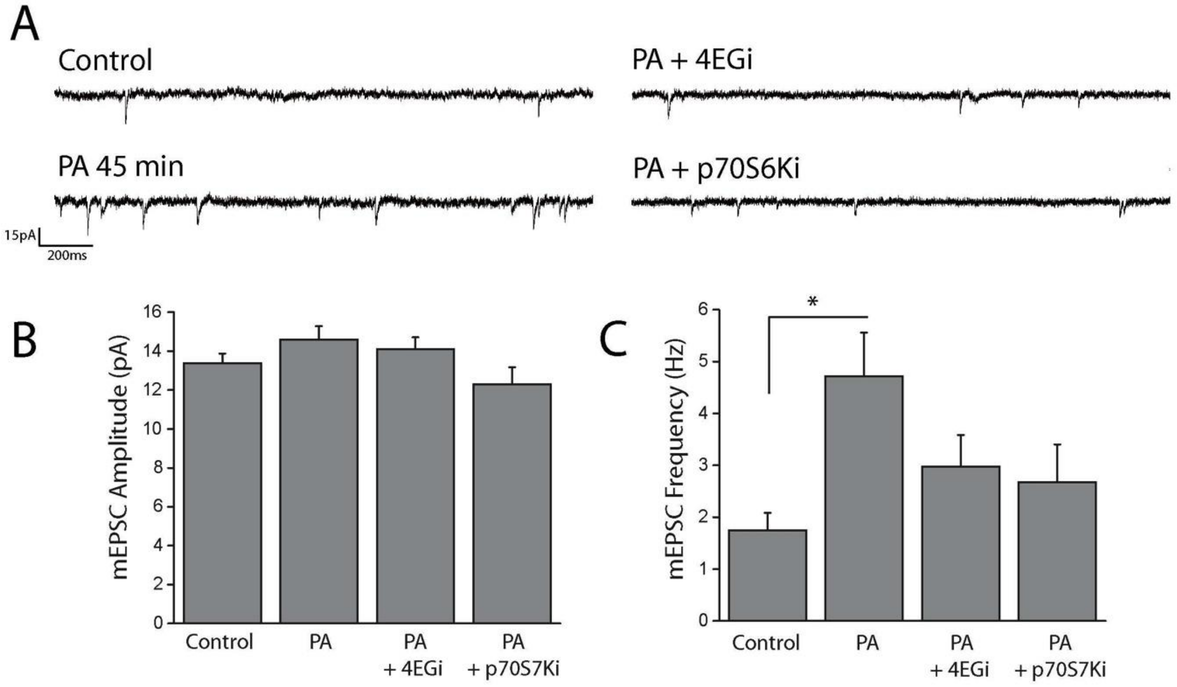
A
Control
PA + 4EGi
PA 45 min
PA + p70S6Ki
15pA
200ms
B
mEPSC Amplitude (pA)
16
14
12
10
8
6
4
2
0
Control
PA
PA + 4EGi
PA + p70S7Ki
C
mEPSC Frequency (Hz)
6
5
4
3
2
1
0
*
Control
PA
PA + 4EGi
PA + p70S7Ki

Figure 3.6: Functional effects of PA are sensitive to inhibitors of 4E-BP1 and p70S6K. Representative recordings (A) and mean (+ SEM) mEPSC amplitude (B) and frequency (C) in vehicle-treated control neurons (n = 19), as well as cells treated with PA alone (n = 14), or in combination with a pharmacological inhibitor of p70S6K (n=13) or a compound which disrupts the interaction between eukaryotic initiation factors 4E and 4G (4EGi, n=7). The decrement in PA-induced increases in mEPSC frequency after co-treatment with either inhibitor suggests that acute activation of mTORC1 does not act preferentially through phosphorylation of p70S6K or 4EBP. $p < 0.05$ versus vehicle-treated controls.

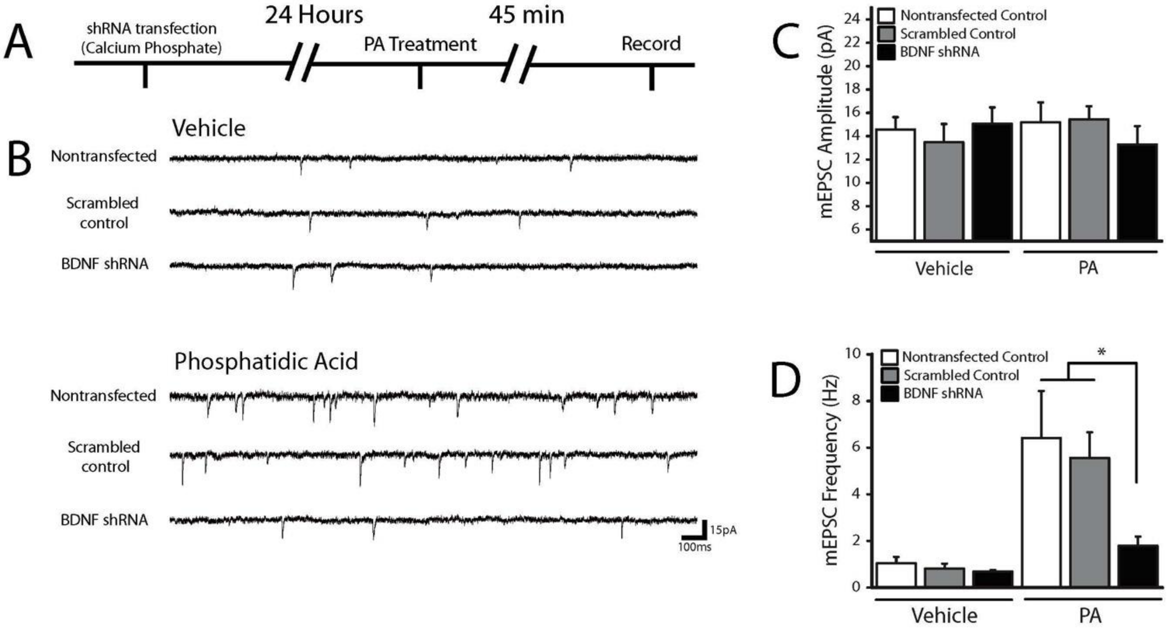
A
shRNA transfection
(Calcium Phosphate)
24 Hours
PA Treatment
45 min
Record
B
Vehicle
Nontransfected
Scrambled control
BDNF shRNA
Phosphatidic Acid
Nontransfected
Scrambled control
BDNF shRNA
15pA
100ms
C
Nontransfected Control
Scrambled Control
BDNF shRNA
mEPSC Amplitude (pA)
24
22
20
18
16
14
12
10
8
6
Vehicle
PA
D
Nontransfected Control
Scrambled Control
BDNF shRNA
*
mEPSC Frequency (Hz)
10
8
6
4
2
0
Vehicle
PA

Figure 3.7: Postsynaptic BDNF expression is necessary for PA-induced changes in synaptic function. (A) Experimental timeline: Dissociated hippocampal cultures were tranfsteced with shRNA against BDNF or scrambled control via calcium phosphate. 24 hr post transfection, cells were treated with 100 μM PA for 45 minutes before recording. (B-D) Representative recordings (B) and mean (+SEM) mEPSC amplitude (C) and frequency (D) in control nontransfected neurons (n = 7), as well as cells expressing BDNF shRNA (n = 8), or scrambled control shRNA (n = 4). The top panel in (B) contains representative traces from vehicle treated group, while the lower panel contains traces from cells subject to treatment with PA (100 μM, 45 min; n=6, 9, 3). Cells were transfected at DIV 15 then used for recordings 24 hrs later. Postsynaptic BDNF knockdown blocked the increase in mEPSC frequency observed after PA treatment $^*p < 0.05$ versus non-transfected cells and neurons transfected with scrambled shRNA.

3.7 Bibliography

An JJ, Gharami K, Liao GY, Woo NH, Lau AG, Vanevski F, Torre ER, Jones KR, Feng Y, Lu B, Xu B. (2008). Distinct role of long 3' UTR BDNF mRNA in spine morphology and synaptic plasticity in hippocampal neurons. Cell. Jul 11;134(1):175-87.

Antion MD, Hou L, Wong H, Hoeffer CA, Klann E. (2008). mGluR-dependent long-term depression is associated with increased phosphorylation of S6 and synthesis of elongation factor 1A but remains expressed in S6K-deficient mice. Mol Cell Biol. May;28(9):2996-3007.

Bader MF, Vitale N. (2009). Phospholipase D in calcium-regulated exocytosis: lessons from chromaffin cells. Biochim Biophys Acta. Sep;1791(9):936-41.

Bateup HS, Takasaki KT, Saulnier JL, Denefrio CL, Sabatini BL. (2011). Loss of Tsc1 in vivo impairs hippocampal mGluR-LTD and increases excitatory synaptic function. J Neurosci. Jun 15;31(24):8862-9.

Bateup HS, Johnson CA, Denefrio CL, Saulnier JL, Kornacker K, Sabatini BL. (2013). Excitatory/Inhibitory synaptic imbalance leads to hippocampal hyperexcitability in mouse models of tuberous sclerosis. Neuron. May 8;78(3):510-22.

Baj G, Del Turco D, Schlaudraff J, Torelli L, Deller T, Tongiorgi E. (2013). Regulation of the spatial code for BDNF mRNA isoforms in the rat hippocampus following pilocarpine-treatment: a systematic analysis using laser microdissection and quantitative real-time PCR. Hippocampus. May;23(5):413-23.

Belelovsky K, Kaphzan H, Elkobi A, Rosenblum K. (2009). Biphasic activation of the mTOR pathway in the gustatory cortex is correlated with and necessary for taste learning. J Neurosci. Jun 10;29(23):7424-31.

Bhattacharya A, Kaphzan H, Alvarez-Dieppa AC, Murphy JP, Pierre P, Klann E. (2012). Genetic removal of p70 S6 kinase 1 corrects molecular, synaptic, and behavioral phenotypes in fragile X syndrome mice. Neuron. Oct 18;76(2):325-37.

Bleckert A, Wong RO. (2011). Identifying roles for neurotransmission in circuit assembly: insights gained from multiple model systems and experimental approaches. Bioessays. Jan;33(1):61-72.

Branco T, Häusser M. (2010). The single dendritic branch as a fundamental functional unit in the nervous system. Curr Opin Neurobiol. Aug;20(4):494-502.

Branco T, Staras K, Darcy KJ, Goda Y. (2009). Local dendritic activity sets release probability at hippocampal synapses. Neuron. Aug 14;59(3):475-85.

Cajigas IJ, Tushev G, Will TJ, tom Dieck S, Fuerst N, Schuman EM. (2012). The local transcriptome in the synaptic neuropil revealed by deep sequencing and high-resolution imaging. Neuron. May 10;74(3):453-66.

Cammalleri M, Lütjens R, Berton F, King AR, Simpson C, Francesconi W, Sanna PP. (2003). Time-restricted role for dendritic activation of the mTOR-p70S6K pathway in the induction of late-phase long-term potentiation in the CA1. Proc Natl Acad Sci U S A. Nov 25;100(24):14368-73.

Chen Y, Zheng Y, Foster DA. (2003). Phospholipase D confers rapamycin resistance in human breast cancer cells. Oncogene. Jun 19;22(25):3937-42.

Cheng PL, Song AH, Wong YH, Wang S, Zhang X, Poo MM. (2011). Self-amplifying autocrine actions of BDNF in axon development. Proc Natl Acad Sci U S A. Nov 8;108(45):18430-5.

Chiaruttini C, Sonego M, Baj G, Simonato M, Tongiorgi E. (2008). BDNF mRNA splice variants display activity-dependent targeting to distinct hippocampal laminae. Mol Cell Neurosci. Jan;37(1):11-9.

Davis GW. (1995). Long-term regulation of short-term plasticity: a postsynaptic influence on presynaptic transmitter release. J Physiol Paris. 89(1):33-41.

Dean C, Liu H, Dunning FM, Chang PY, Jackson MB, Chapman ER. (2009). Synaptotagmin-IV modulates synaptic function and long-term potentiation by regulating BDNF release. Nat Neurosci. Jun;12(6):767-76.

Dean C, Liu H, Staudt T, Stahlberg MA, Vingill S, Bückers J, Kamin D, Engelhardt J, Jackson MB, Hell SW, Chapman ER. (2012). Distinct subsets of Syt-IV/BDNF vesicles are sorted to axons versus dendrites and recruited to synapses by activity. J Neurosci. Apr 18;32(16):5398-413.

Ehninger D, Silva AJ. (2011). Rapamycin for treating Tuberous sclerosis and Autism spectrum disorders. Trends Mol Med. Feb;17(2):78-87.

Fang Y, Vilella-Bach M, Bachmann R, Flanigan A, Chen J. (2001). Phosphatidic acid-mediated mitogenic activation of mTOR signaling. Science. Nov 30;294(5548):1942-5.

Frondorf K, Henkels KM, Frohman MA, Gomez-Cambronero J. (2010). Phosphatidic acid is a leukocyte chemoattractant that acts through S6 kinase signaling. J Biol Chem. May 21;285(21):15837-47.

Fraser MM, Bayazitov IT, Zakharenko SS, Baker SJ. (2008). Phosphatase and tensin homolog, deleted on chromosome 10 deficiency in brain causes defects in synaptic structure, transmission and plasticity, and myelination abnormalities. Neuroscience. Jan 24;151(2):476-88.

Futai K, Kim MJ, Hashikawa T, Scheiffele P, Sheng M, Hayashi Y. (2007). Retrograde modulation of presynaptic release probability through signaling mediated by PSD-95-neuroligin. Nat Neurosci. Feb;10(2):186-95.

Gkogkas CG, Khoutorsky A, Ran I, Rampakakis E, Nevarko T, Weatherill DB, Vasuta C, Yee S, Truitt M, Dallaire P, Major F, Lasko P, Ruggero D, Nader K,Lacaille JC, Sonenberg N. (2013). Autism-related deficits via dysregulated eIF4E-dependent translational control. Nature. Jan 17;493(7432):371-7.

Hartmann M, Heumann R, Lessmann V. (2001). Synaptic secretion of BDNF after high-frequency stimulation of glutamatergic synapses. EMBO J. Nov 1;20(21):5887-97.

Hay N, Sonenberg N. (2004). Upstream and downstream of mTOR. Genes Dev. Aug 15;18(16):1926-45.

Hoeffer CA, Cowansage KK, Arnold EC, Banko JL, Moerke NJ, Rodriguez R, Schmidt EK, Klosi E, Chorev M, Lloyd RE, Pierre P, Wagner G, LeDoux JE, Klann E. (2011). Inhibition of the interactions between eukaryotic initiation factors 4E and 4G impairs long-term associative memory consolidation but not reconsolidation. Proc Natl Acad Sci U S A. Feb 22;108(8):3383-8.

Hoeffer CA, Klann E. (2010). mTOR signaling: at the crossroads of plasticity, memory and disease. Trends Neurosci. Feb;33(2):67-75.

Hou L, Klann E. (2004). Activation of the phosphoinositide 3-kinase-Akt-mammalian target of rapamycin signaling pathway is required for metabotropic glutamate receptor-dependent long-term depression. J Neurosci. Jul 14;24(28):6352-61.

Hu Z, Hom S, Kudze T, Tong XJ, Choi S, Aramuni G, Zhang W, Kaplan JM. (2012). Neurexin and neuroligin mediate retrograde synaptic inhibition in C. elegans. Science. Aug 24;337(6097):980-4.

Jakawich SK, Nasser HB, Strong MJ, McCartney AJ, Perez AS, Rakesh N, Carruthers CJ, Sutton MA. (2010). Local presynaptic activity gates homeostatic changes in presynaptic function driven by dendritic BDNF synthesis. Neuron. Dec 22;68(6):1143-58.

Kelleher RJ 3rd, Bear MF. (2008). The autistic neuron: troubled translation? Cell. Oct 31;135(3):401-6.

Ktistakis NT, Delon C, Manifava M, Wood E, Ganley I, Sugars JM. (2003). Phospholipase D1 and potential targets of its hydrolysis product, phosphatidic acid. Biochem Soc Trans. Feb;31(Pt 1):94-7.

Kuczewski N, Porcher C, Ferrand N, Fiorentino H, Pellegrino C, Kolarow R, Lessmann V, Medina I, Gaiarsa JL. (2008). Backpropagating action potentials trigger dendritic release of BDNF during spontaneous network activity. J Neurosci. Jul 2;28(27):7013-23.

Kwon CH, Luikart BW, Powell CM, Zhou J, Matheny SA, Zhang W, Li Y, Baker SJ, Parada LF. (2006). Pten regulates neuronal arborization and social interaction in mice. Neuron. May 4;50(3):377-88.

Laplante M, Sabatini DM. (2012). mTOR signaling in growth control and disease. Cell. Apr 13;149(2):274-93.

Lee HY, Ge WP, Huang W, He Y, Wang GX, Rowson-Baldwin A, Smith SJ, Jan YN, Jan LY. (2011). Bidirectional regulation of dendritic voltage-gated potassium channels by the fragile X mental retardation protein. Neuron. Nov 17;72(4):630-42.

Liao GY, An JJ, Gharami K, Waterhouse EG, Vanevski F, Jones KR, Xu B. (2012). Dendritically targeted Bdnf mRNA is essential for energy balance and response to leptin. Nat Med. Mar 18;18(4):564-71.

Lim HK, Choi YA, Park W, Lee T, Ryu SH, Kim SY, Kim JR, Kim JH, Baek SH. (2003). Phosphatidic acid regulates systemic inflammatory responses by modulating the Akt-mammalian target of rapamycin-p70 S6 kinase 1 pathway. J Biol Chem. Nov 14;278(46):45117-27.

Lindskog M, Li L, Groth RD, Poburko D, Thiagarajan TC, Han X, Tsien RW. (2010). Postsynaptic GluA1 enables acute retrograde enhancement of presynaptic function to coordinate adaptation to synaptic inactivity. Proc Natl Acad Sci U S A. Dec 14;107(50):21806-11.

Liu-Yesucevitz L, Bassell GJ, Gitler AD, Hart AC, Klann E, Richter JD, Warren ST, Wolozin B. (2011). Local RNA translation at the synapse and in disease. J Neurosci. Nov 9;31(45):16086-93.

Luikart BW, Schnell E, Washburn EK, Bensen AL, Tovar KR, Westbrook GL. (2011). Pten knockdown in vivo increases excitatory drive onto dentate granule cells. J Neurosci. Mar 16;31(11):4345-54.

Ma XM, Blenis J. (2009). Molecular mechanisms of mTOR-mediated translational control. Nat Rev Mol Cell Biol. May;10(5):307-18.

Nie D, Di Nardo A, Han JM, Baharanyi H, Kramvis I, Huynh T, Dabora S, Codeluppi S, Pandolfi PP, Pasquale EB, Sahin M. (2010). Tsc2-Rheb signaling regulates EphA-mediated axon guidance. Nat Neurosci. Feb;13(2):163-72.

Normand EA, Crandall SR, Thorn CA, Murphy EM, Voelcker B, Browning C, Machan JT, Moore CI, Connors BW, Zervas M. (2013). Temporal and mosaic tsc1 deletion in the developing thalamus disrupts thalamocortical circuitry, neural function, and behavior. Neuron. Jun 5;78(5):895-909.

Paradis S, Sweeney ST, Davis GW. (2001). Homeostatic control of presynaptic release is triggered by postsynaptic membrane depolarization. Neuron. Jun;30(3):737-49.

Pearce LR, Alton GR, Richter DT, Kath JC, Lingardo L, Chapman J, Hwang C, Alessi DR. (2010). Characterization of PF-4708671, a novel and highly specific inhibitor of p70 ribosomal S6 kinase (S6K1). Biochem J. Oct 15;431(2):245-55.

Penney J, Tsurudome K, Liao EH, Elazzouzi F, Livingstone M, Gonzalez M, Sonenberg N, Haghighi AP. (2012). TOR is required for the retrograde regulation of synaptic homeostasis at the Drosophila neuromuscular junction. Neuron. Apr 12;74(1):166-78.

Raab-Graham KF, Haddick PC, Jan YN, Jan LY. (2006). Activity- and mTOR-dependent suppression of Kv1.1 channel mRNA translation in dendrites. Science. Oct 6;314(5796):144-8.

Regehr WG, Carey MR, Best AR. (2009). Activity-dependent regulation of synapses by retrograde messengers. Neuron. Jul 30;63(2):154-70.

Rodrik-Outmezguine VS, Chandarlapaty S, Pagano NC, Poulikakos PI, Scaltriti M, Moskatel E, Baselga J, Guichard S, Rosen N. (2011). mTOR kinase inhibition causes feedback-dependent biphasic regulation of AKT signaling. Cancer Discov. Aug;1(3):248-59.

Schratt GM, Nigh EA, Chen WG, Hu L, Greenberg ME. (2004). BDNF regulates the translation of a select group of mRNAs by a mammalian target of rapamycin-phosphatidylinositol 3-kinase-dependent pathway during neuronal development. J Neurosci. Aug 18;24(33):7366-77.

Schwarz K, Natarajan S, Kassas N, Vitale N, Schmitz F. (2011). The synaptic ribbon is a site of phosphatidic acid generation in ribbon synapses. J Neurosci. Nov 2;31(44):15996-6011.

Sperow M, Berry RB, Bayazitov IT, Zhu G, Baker SJ, Zakharenko SS.(2012). Phosphatase and tensin homologue (PTEN) regulates synaptic plasticity independently of its effect on neuronal morphology and migration. J Physiol. Feb 15;590(Pt 4):777-92.

Stoica L, Zhu PJ, Huang W, Zhou H, Kozma SC, Costa-Mattioli M. (2011). Selective pharmacogenetic inhibition of mammalian target of Rapamycin complex I (mTORC1) blocks long-term synaptic plasticity and memory storage. Proc Natl Acad Sci U S A. Mar 1;108(9):3791-6.

Tang SJ, Reis G, Kang H, Gingras AC, Sonenberg N, Schuman EM. (2002). A rapamycin-sensitive signaling pathway contributes to long-term synaptic plasticity in the hippocampus. Proc Natl Acad Sci U S A. Jan 8;99(1):467-72.

Tavazoie SF, Alvarez VA, Ridenour DA, Kwiatkowski DJ, Sabatini BL. (2005). Regulation of neuronal morphology and function by the tumor suppressors Tsc1 and Tsc2. Nat Neurosci. Dec;8(12):1727-34.

Thoreen CC, Chantranupong L, Keys HR, Wang T, Gray NS, Sabatini DM. (2012). A unifying model for mTORC1-mediated regulation of mRNA translation. Nature. May 2;485(7396):109-13.

Toschi A, Lee E, Xu L, Garcia A, Gadir N, Foster DA. (2009). Regulation of mTORC1 and mTORC2 complex assembly by phosphatidic acid: competition with rapamycin. Mol Cell Biol. Mar;29(6):1411-20.

Veverka V, Crabbe T, Bird I, Lennie G, Muskett FW, Taylor RJ, Carr MD. (2008). Structural characterization of the interaction of mTOR with phosphatidic acid and a novel class of inhibitor: compelling evidence for a central role of the FRB domain in small molecule-mediated regulation of mTOR. Oncogene. Jan 24;27(5):585-95.

Vitureira N, Letellier M, White IJ, Goda Y. (2011). Differential control of presynaptic efficacy by postsynaptic N-cadherin and β-catenin. Nat Neurosci. Dec 4;15(1):81-9.

Voglmaier SM, Kam K, Yang H, Fortin DL, Hua Z, Nicoll RA, Edwards RH. (2006). Distinct endocytic pathways control the rate and extent of synaptic vesicle protein recycling. Neuron. Jul 6;51(1):71-84.

von der Brelie C, Waltereit R, Zhang L, Beck H, Kirschstein T. (2006). Impaired synaptic plasticity in a rat model of tuberous sclerosis. Eur J Neurosci. Feb;23(3):686-92

Wang Y, Cheng A, Mattson MP. (2006). The PTEN phosphatase is essential for long-term depression of hippocampal synapses. Neuromolecular Med. 8(3):329-36.

Weston MC, Chen H, Swann JW. (2012). Multiple roles for mammalian target of rapamycin signaling in both glutamatergic and GABAergic synaptic transmission. J Neurosci. Aug 15;32(33):11441-52.

Xiong Q, Oviedo HV, Trotman LC, Zador AM. (2012). PTEN regulation of local and long-range connections in mouse auditory cortex. J Neurosci. Feb 1;32(5):1643-52.

Yang Y, Atasoy D, Su HH, Sternson SM. (2011). Hunger states switch a flip-flop memory circuit via a synaptic AMPK-dependent positive feedback loop. Cell. Sep 16;146(6):992-1003.

Yoon MS, Sun Y, Arauz E, Jiang Y, Chen J. (2011). Phosphatidic acid activates mammalian target of rapamycin complex 1 (mTORC1) kinase by displacing FK506 binding protein 38 (FKBP38) and exerting an allosteric effect. J Biol Chem. Aug 26;286(34):29568-74.

You JS, Frey JW, Hornberger TA. (2012). Mechanical stimulation induces mTOR signaling via an ERK-independent mechanism: implications for a direct activation of mTOR by phosphatidic acid. PLoS One. 7(10):e47258.

CHAPTER IV

Phospholipase D1 mediates a unique route to mTORC1 activation during synaptic homeostasis but not long term potentiation

4.1 Abstract

mTOR-dependent translational control is vital to several forms of long lasting synaptic plasticity, including long term potentiation and mGluR-dependent long term depression. We have recently reported that dendritic mTORC1 also plays a role in regulating synaptic homeostasis, where it serves to modulate presynaptic function via synthesis of a retrograde signal. The means by which these varied types of synaptic stimuli all recruit mTOR-dependent protein synthesis yet lead to widely varied functional outcomes is unclear. Here we report that PLD-mediated hydrolysis of the lipid second messenger phosphatidic acid is a crucial component of the signaling pathway that relays homeostatic signals to postsynaptic mTORC1 after loss of excitatory input. We also find that this PLD/PA mediated activation of mTORC1 is a point of divergence between homeostatic and Hebbian forms of synaptic plasticity. PLD signaling is necessary for mTORC1 activation after AMPAR blockade but not during LTP, which mirrors the pattern of intracellular PA synthesis detected under each condition. This dissociation between LTP and HSP also holds true at the functional level, as inhibition of PLD signaling, or genetic disruption of PA/mTOR interaction eliminates the well-defined presynaptic enhancement

observed after AMPAR blockade but not the postsynaptic potentiation which is a central feature LTP.

4.2 Introduction

The execution of long lasting changes in the strength of excitatory synapses is believed to be a central mechanism by which neuronal networks relay and encode information. A supply of newly synthesized proteins is vital for maintaining prolonged changes in synapse function. While altered gene expression via transcriptional regulation in the cell nucleus undoubtedly plays a vital role in mediating common forms of long-lasting plasticity, recent years have witnessed a growing appreciation for localized changes in the synaptic proteome served by dendritic translation (Sutton and Schuman, 2006). The mechanistic target of rapamycin complex 1 (mTORC1) is a critical regulator of translation initiation (Ma and Blenis, 2009) and is known to be necessary for several unique forms of synaptic plasticity, including Long term potentiation (Tang et al., 2002; Cammalleri et al., 2003; Vickers, et al., 2005), mGluR-dependent long term depression in the hippocampus (Hou and Klann, 2004) and VTA (Mameli et al., 2007), homeostatic adaptation to synaptic inactivity (Penney et al., 2012; Henry et al., 2012), and the antidepressant action of acute NMDAR blockade (Li et al., 2010). Given the apparent ubiquity of mTORC1 signaling in such phenomenologically distinct forms of synaptic plasticity, the question remains as to how mTOR-dependent changes in protein synthesis implement the expression of such markedly different functional outcomes.

mTOR signaling is embedded in an extremely complex network of interacting signaling components (Zoncu et al., 2011) and our understanding of this multifaceted pathways is under constant revision (Wang and Proud, 2011). The past decade has witnessed growing interest in a unique mechanism for regulating mTOR activity via internal synthesis of phosphatidic acid (Chen and Fang, 2002; Foster 2009). Phosphatidic acid (PA) is a lipid second messenger that was originally discovered to play important role in relaying mitogenic signals to mTOR during cell growth and proliferation (Fang et al., 2001). PA binds directly to mTOR on its FKBP12-Rapamycin Binding (FRB) domain and is thought to strengthen its association with its binding partner raptor, thus increasing mTOR’s catalytic activity (Veverka et al., 2008; Toschi et al., 2009). In post-mitotic cells such as neurons, it is possible that this mitogenic signaling mechanism could have been co-opted for an alternative purpose in mediating synaptic plasticity. This possibility is supported by previous work from our lab in which we have utilized acute application of PA to potently drive mTORC1 kinase activity in hippocampal neurons.

Here we report that intracellular synthesis of phosphatidic acid (PA) by Phospholipase-D (PLD) signaling is an integral step in mTORC1 activation in response to AMPAR blockade, but not in response to multiple forms of chemically induced LTP. Pharmacological blockade of PLD1/2 eliminates mTORC1 kinase activity in response to loss of excitatory input, but not after glycine or forskolin based cLTP. Similarly, well-characterized alterations in synapse function associated with homeostatic plasticity and LTP are differentially sensitive to elimination of PLD1/2 function. Overexpression of PLD1, but not PLD2, recapitulates these effects and is sufficient to drive changes in mTORC1 kinase activity, increase levels of dendritic, but not somatic, BDNF expression, and enhance the frequency of spontaneous mEPSCs. Lastly, we utilize a pharmacogenetic strategy to replace endogenous mTOR with point mutants which no longer bind internally synthesized PA. Inhibition of intracellular PA/mTOR interaction renders neurons insensitive to AMPAR blockade with respect to altered mTORC1 signaling or functional adaptations in presynaptic efficacy, though cLTP-induced changes in postsynaptic function remain identical to cells with normal mTOR function. These results further establish mTORC1 as a central hub which meditates multiple forms of synaptic plasticity, and identifies PLD1/PD signaling as a unique entry point in the context of homeostatic adaptation to synaptic inactivity.

4.3 Results

Intracellular Synthesis of PA is critical for mTOR signaling during HSP

Intracellular synthesis of the lipid second-messenger phosphatidic acid (PA) has emerged as an important signal in mitogenic activation of mTORC1 signaling (Foster et al., 2009), but little is known about a potential role for PA in relaying synaptic signals to mTOR in mammalian central neurons. To visualize PA synthesis in dissociated hippocampal neurons, we transfected cells with GFP-Spo20-PABD at DIV 16-18 and performed live-imaging experiments 2-3 days later. The GFP-Spo20-PABD plasmid contains the PA-binding domain of the yeast N-ethylmaleimide-sensitive factor attachment protein receptor (SNARE) protein Spo20 fused to EGFP (Zeniou-Meyer et al., 2007). Similar to previous findings in COS-7 (Frondorf et al., 2010) and PC12 cells (Zeniou-Meyer et al., 2007), we find that GFP-Spo20-PABD fluorescence is largely limited to the cell nucleus under basal conditions (Figure 4.1A). However, after subjecting neurons to AMPAR blockade (CNQX, 40μM) we observed a steady, time-dependent increase in PA-related fluorescence intensity in discrete regions around the soma and extending out into the distal regions of the dendrites by 2Hrs post-treatment (Figure 4.1A). In additional experiments we utilized a secondary fluorescence-based sensor of intracellular PA synthesis (Figure 4.1B). This reporter contained the C-terminal PA-binding module of human Raf1 fused to EGFP (GFP-Raf1-PABD). Previous characterizations of this reporter indicate that it can associate with various negatively charged lipids, but displays a strong bias for binding to PA

(Schwarz et al., 2011). Similar to our findings using GFP-Spo20-PABD, we observed the presence of discrete regions of intracellular clustering of the GFP-Raf1-PABD reporter after subjecting neurons to a brief period of AMPAR blockade (CNQX, 40μM, 3Hrs). These clustered regions of fluorescence intensity did not appear in cells treated with a vehicle control, indicating low or extremely transient levels of intracellular PA synthesis under baseline conditions (Figure 4.1B).

Together, our reporter data suggest that intracellular synthesis of PA may be a mechanism utilized by neurons to activate mTORC1 signaling in the context of homeostatic adaptation to synaptic inactivity. Given previous findings that mTORC1 activity is required during other well-studied forms of plasticity such as LTP (Tang et al., 2002; Cammalleri et al., 2003), we also wanted to examine a potential role for intracellular PA synthesis in LTP. Using a glycine-based chemical LTP (cLTP) paradigm which has been previously used to induce long-lasting, mTOR-dependent changes in synaptic strength in dissociated cultures (Lu et al., 2001), we found no difference in the distribution of the GFP-Raf1-PABD reporter between cells subject to a cLTP paradigm vs vehicle-treated controls (Figure 4.1B). The markedly different responses of the GFP-Raf1-PABD reporter to cLTP and AMPAR blockade raised the possibility that these two forms of plasticity differ in the means by which mTORC1 signaling is engaged, with intracellular synthesis of PA acting as an important point of divergence. Intracellular PA can arise from multiple sources, including lysophosphatidic acid (LPA), diacylglycerol (DG) and phosphatidylcholine (Foster 2009). Previous reports suggest that the primary source of intracellularly generated PA in cancer cells is via hydrolysis of phosphatidylcholine by phospholipase-D (Jenkins and Frohman, 2005). To explore a role for phospholipase-D (PLD) signaling in the activation of mTORC1 during LTP or synaptic homeostasis, we utilized a newly developed small molecule inhibitor of PLD, 5-fluoro-2-indolyl des-chlorohalopemide (FIPI), which inhibits both PLD1 and PLD2 activity and blocks intracellular PA accumulation at subnanomolar concentrations (Su et al., 2009). We found that pretreatment with FIPI either completely eliminated or severely reduced the number of GFP-Raf1-PABD puncta after treatment with CNQX (Figure 4.1B).

To examine the effect of PLD signaling on mTORC1 activation during different forms of synaptic plasticity, we performed immunocytochemical analysis of phosphorylated ribosomal protein S6 (p-S6) at S235/236, a commonly used readout of mTORC1 kinase activity (Henry et al., 2012). We observed significant increases in somatic p-S6 intensity after both a glycine (cLTP1, 227.73±17.43% over control, n=39) and forskolin-based (cLTP2, 275.19±15.60% over controls, n=40) stimulation paradigm (Figure 4.1C-E). Synaptic deprivation via AMPAR blockade (CNQX, 40μM, 3Hr) also produced a significant increase in S6 phosphorylation (CNQX, 127.75±6.63% above control, n=73) as we have reported previously (Henry et al., 2012). Interestingly, co-application of the PLD1/2 inhibitor FIPI (100nM, 30 min pre-treatment) had no effect on increased p-S6 levels induced by glycine (cLTP1+FIPI, 235.08±20.74% above control, n=40) or forskolin (cLTP2+FIPI, 295.28±24.08% above controls, n=37), but completely eliminated CNQX-induced increases in mTORC1 kinase activity (CNQX+FIPI, 102.93±5.50% of control, n=71). Cells treated with FIPI alone showed no significant difference in p-S6 levels compared to controls, suggesting minimal contribution of steady state PLD signaling to baseline levels of mTORC1 activity. Together these data suggest that PLD/PA signaling is uniquely engaged in mediating an intracellular response to AMPAR blockade and is an essential signaling component leading to mTORC1 activation during homeostatic plasticity, but not during the activation of mTORC1 in the context of long-term potentiation.

PLD signaling mediates Functional Changes during HSP

We next used whole-cell patch-clamp electrophysiology to examine a potential role for PLD signaling in the functional changes that emerge at excitatory synapses during homeostatic plasticity or LTP. Previous efforts from our lab and others have revealed an adaptive, mTORC1-dependent increase in presynaptic function that emerges after subjecting synapses to postsynaptic deprivation of AMPAR-mediated inputs (Penney et al., 2012, Henry et al., 2012). We replicate those effects here (Figure 4.2A-C), demonstrating a homeostatic increase in mEPSC frequency that emerges roughly 3 Hrs after subjecting cells to AMPAR blockade (Control, 1.27±0.14Hz, n=22; CNQX, 3.61±0.38Hz, n=9). Notably, this effect was completely blocked by co-application of the PLD1/2 inhibitor FIPI (Figure 4.2C), though FIPI had no effect on mEPSC frequency on its own (CNQX+FIPI, 1.43±0.17Hz, n=14; FIPI Alone, 1.61±0.22Hz, n=18). A similar requirement for PLD signaling was observed for homeostatic changes in presynaptic function engaged by blockade of L-type voltage gated calcium channels (Figure 4.2D-F). As reported previously (Henry et al., 2012), Nifedpine (10μM, 2Hr) elicits an mTORC1-dependent increase in mEPSC frequency when applied for >3Hrs. This increase in presynaptic function was blocked by concurrent treatment with FIPI (Control, 3.75±0.81Hz, n=6; Nifedpine, 11.88±2.82 Hz, n=8; Nifedipine+FIPI, 2.34±0.524Hz, n=6; FIPI Alone, 3.521±1.09Hz, n=6), indicating a similar mechanism at work to that utilized during AMPAR blockade. In mammalian central neurons, this adaptive increase in presynaptic function after AMPAR blockade depends on the mTORC1-dependent synthesis of BDNF as a retrograde signal (Henry et al., 2012). In line with a role for PLD/PA signaling operating upstream of mTORC1 in mediating this effect, immunocytochemical analysis revealed enhanced BDNF intensity in dendrites after AMPAR blockade (Figure 4.2G-H), which was completely blocked by co-application of FIPI (Control, 100±10.98%, n=63; CNQX, 200.67±26.43% of control, n=75; CNQX+FIPI, 63.12±7.15% of control, n=70; FIPI Alone, 75.10±10.47% of control, n=56). The homeostatic increase in postsynaptic function after seen AMPAR blockade (Figure 4.2A-C), which previous reports have indicated is mTORC1-independent and may depend on intracellular Retinoic acid signaling (Aoto et al., 2008; Wang et al., 2011; Henry et al, 2012), is unaffected by concurrent PLD1/2 blockade (Control, 12.80±0.42pA, n=22; CNQX, 15.82±1.35pA, n=9; CNQX+FIPI, 14.90±0.62pA, n=14; FIPI Alone, 13.06±0.70pA, n=17), suggesting that this pathway is uniquely involved in mediating adaptive changes in presynaptic function during loss of excitatory input.

Similar to previous reports (Lu et al., 2001) we found that a glycine-based cLTP stimulus produced a significant increase in both the amplitude and frequency of spontaneous mEPSCs when assessed 2Hrs after stimulation (Figure 4.3A-D). Though the increase in mEPSC frequency was slightly attenuated by co-application of the mTORC1 inhibitor rapamycin (100nM, 30min pre-treatment), event frequency remained markedly elevated above controls levels (Control, 0.90 ±0.24Hz, n=12; Glycine, 4.76±1.35Hz, n=11; Glycine+Rap, 3.20±0.88Hz, n=8), indicating the non-mTOR dependent nature of this functional change. In contrast, glycine-induced increases in mEPSC amplitude were completely blocked by co-application of rapamycin (Control, 12.87±0.55pA, n=12; Glycine, 16.80±0.77pA, n=11; Glycine+Rap, 13.05±0.64pA, n=8), which is in line with a role for de novo translation of additional AMPARs in this form of plasticity. Interestingly, we found a dissociation between the requirement for mTORC1 activity and PLD1/2 signaling in the potentiation of excitatory synapses during LTP (Figure 4.3A-D). In marked contrast to its effect on homeostatic increases in presynaptic function after AMPAR blockade (Figure 4.2A-C), co-application of FIPI had no effect on glycine-induced increases in mEPSC amplitude (Glycine+FIPI, 15.77±1.03pA, n=11, $P<0.05$ compared to control), suggesting that PLD1/2 signaling is not necessary for mTORC1-dependent changes in postsynaptic function at excitatory synapses during chemically-induced LTP.

PLD1 contributes to PA-induced activation of mTORC1

There are two PLD genes expressed in the mammalian brain, PLD1 and PLD2, each of which show unique localization profiles and activation criterion. Given that PA, the product of PLD activity, is a transient messenger which signals within a very limited spatial range of the membrane compartment from which it is generated, unique sites of PLD-mediated PA synthesis could have feasibly have markedly different functional consequences (Cockcroft 2001). To examine if PLD1 and PLD2 exhibit unique subcellular localization patterns in the mammalian CNS, we expressed HA-tagged human PLD1 (hPLD1) or PLD2 (hPLD2) in dissociated hippocampal cultures and assessed HA localization via immunocytochemistry 24-48 Hrs later (Figure 4.4A). In previously published reports using non-neuronal cells, overexpressed HA-PLD1 was primarily localized to late endosomes or the golgi complex, while overexpressed HA-PLD2 was found mainly along the plasma membrane (Du et al., 2004). We observed a similar pattern of HA staining in neurons expressing hPLD1 or hPLD2, with HA-tagged hPLD1 localized to discrete intracellular puncta, and hPLD2 localized to the plasma membrane (Figure 4.4A).

Using phosphorylated ribosomal protein S6 as a readout of mTORC1 activity, we found significantly elevated levels of somatic p-S6 in cells expressing hPLD1, compared to cells expressing GFP as a control, indicating potent activation of mTORC1 signaling via PLD1 overexpression (Figure 4.4A-B). In contrast, neurons expressing either human or rat versions of PLD2 showed no significant change in somatic p-S6 levels compared to GFP expressing controls (GFP, 100±11.53%, n=29; hPLD1, 286.90±37.27% of control, n=19; hPLD2, 139.69±19.91% of control, n=26; rPLD2, 88.71±9.63% of control, n=25). Given recent reports that PLD1 signaling influences dendrite arborization during neuronal development (Zhu et al., 2012) we wanted to assess any potential changes to excitatory synapse morphology that result from PLD manipulations in mature cells (Figure 4.4C-D). We found that the density of dendritic spines was unaffected as a result of 24hrs of overexpression of PLD1 or PLD2 (GFP, 23.19±1.6 spines/25μm, n=16; hPLD1, 24.18±1.11 spines per 25μm, n=17; hPLD2, 24.86±1.87 spines per 25μm, n=14). To characterize the effects of PLD overexpression on excitatory synapse function, we recorded mEPSCs from dissociated hippocampal neurons expressing hPLD1 or hPLD2 at DIV21-23 (Figure 4.54E-G). Similar to our previous results using overexpression of Rheb-GTPase to constitutively drive mTORC1 signaling (Henry et al., 2012), neurons expressing hPLD1 displayed a significant increase in mEPSC frequency compared to cells expressing GFP alone (Figure 4.4E-G). Cells expressing hPLD2 were not significantly different from GFP controls with respect to mEPSC frequency (GFP, 0.54±0.10Hz, n=13; hPLD1, 2.12±0.44Hz, n=11; hPLD2, 0.43±0.08Hz, n=8). The amplitude of spontaneous mEPSCs did not change as a function of PLD1 or PLD2 overexpression (GFP, 20.58±1.99pA, n=13; hPLD1, 22.16±2.42pA, n=11; hPLD2, 21.72±2.71pA, n=8). Previous efforts in our lab have also shown that genetic upregulation of mTORC1 activity by Rheb overexpression is sufficient to enhance BDNF levels in the dendrites of cultured hippocampal neurons (Henry et al., 2012). Given recent reports that PLD1 is required for Rheb-mediated activation of mTORC1 (Sun et al., 2008); we next asked whether expression of PLD1 would also induce changes in BDNF expression. Compared to

GFP-expressing control cells, neurons expressing hPLD1 exhibited significantly higher BDNF intensity in the dendritic, but not somatic, subcompartment (Figure 4.5H-I). No such change in dendritic BDNF expression was observed in neurons expressing human or rat PLD2 (GFP dendrites, 100±12.99%, n=23; hPLD1 dendrites, 141.72±11.36% of control, n=38; hPLD2 dendrites, 103.65±9.74% of control, n=26; rPLD2 dendrites 111.81±10.97% of control, n=25). Somatic BDNF intensity was not significantly increased as a result of PLD1 or PLD2 overexpression (GFP soma, 100±6.24%, n=23; hPLD1 soma, 84.26±4.04% of control, n=38; hPLD2 soma, 78.67±4.346% of control, n=26; rPLD2 soma, 95.54±5.69% of control, n=25). Collectively, these results suggest that overexpression of PLD1, but not PLD2, is sufficient to increase intracellular levels of PA, which acts as a potent activator of mTORC1 signaling leading to increased BDNF expression as a retrograde signal. In line with our previous work, this dendritically released BDNF acts to enhance the efficacy of opposed presynaptic terminals, here reflected as an increase in the frequency of spontaneous mEPSCs.

PA binding to mTOR is essential for homeostatic adaptation

Previous work has established that the positively charged Arg2109 residue in the FRB domain of mTOR is vital for the binding of PA to mTOR (Fang et al., 2001). This site exhibits a high degree of evolutionary conservation (Rodriguez Camargo et al., 2012), suggesting an important role for PA/mTOR signaling across multiple species. Substituting this positively charged Arginine residue with Alanine severely impairs the hydrophobic interaction between mTOR and PA. We took advantage to this fact to develop a pharmacogenetic approach with the aim of reducing intracellular PA binding to mTOR in a select group of neurons in culture. Neurons were transfected with a variant of mTOR carrying a point mutation in the rapamycin binding domain (S2035T), which eliminates binding between mTOR and the rapamycin-FKB12 complex, thus rendering neurons expressing this mutant insensitive to rapamycin-induced inhibition of mTORC1 function (Brown et al., 1995). An additional set of cells were made to express a mutant form of mTOR carrying both the S2035T and R2109A point mutations, which renders these cells insensitive to both rapamycin and PA. All neurons were co-transfected with GFP as a cell fill and treated with rapamycin (100nM) to eliminate endogenous mTOR signaling, resulting in a one condition in which a small group of cells were left with intact mTOR activity due to rapamycin resistance, and a second group of cells with intact mTORC1 signaling but significantly reduced PA binding (Figure 4.5A). Using levels of p-S6 staining intensity as a readout of mTORC1 kinase activity, we found that disruption of PA-mTOR binding had no impact on mTORC1 activation during LTP (Figure 4.5B-5C). In contrast, while neurons expressing the rapamycin-resistant (S2035T) mTOR point mutant showed significant increases in somatic p-S6 intensity after AMPAR blockade (CNQX, 40μM, 3Hrs), cells in which PA/mTOR binding was disrupted showed no change in somatic p-S6 intensity after loss of excitatory input compared to controls (S2035T Control 100±9.35%, n=37; S2035 cLTP, 217.87±27.77% of control, n=22; S2035 CNQX, 283.32±72.10% of control, n=15; S2035T/R2109A Control, 100±13.78% of control, n=26; S2035T/R2109A cLTP, 250.13±72.23% of control, n=22; S2035T/R2109A CNQX, 114.42±15.62% of control, n=16). This indicates that binding of PA to mTOR's FRB domain is critical for increases in mTORC1 kinase activity engaged during homeostatic adaptation to synaptic inactivity, but not during chemically induced LTP.

To assess the impact of reduced PA/mTOR binding on synaptic plasticity, we assessed functional characteristics of spontaneous mEPSCs, using amplitude and frequency as a proxies of postsynaptic and presynaptic function, respectively. We utilized an identical strategy to that described for the proceeding set of experiments (Figure 4.5A), in which rapamycin was used to eliminate endogenous mTORC1 function under conditions of rapamycin and/or PA resistant mTOR mutant expression. In keeping with our previously published results (Jakawich et al., 2011; Henry et al., 2012), 'control' neurons expressing the rapamycin-resistant version of mTOR (S2035T Control) showed a significant increase in mEPSC frequency in response to AMPAR blockade (Figure 4.6A-B). In contrast, under conditions in which the postsynaptic neuron expressed a form of mTOR which was resistant to PA binding (R2109A), treatment with CNQX no longer had any effect on mEPSC frequency compared to vehicle treated controls (S2035T Control, 0.66±0.12Hz, n=26; S2035 CNQX, 1.92±0.32Hz, n=14; S2035T/R2109A Control, 1.14±0.31Hz, n=9; S2035T/R2109A CNQX, 0.98±0.15Hz, n=16). Similar results were obtained after subjecting cells to L-type voltage gated Calcium channel blockade (Figure 4.6C-D): Nifedipine-induced increases in mEPSC frequency were completely blocked under conditions of reduced intracellular PA/mTOR binding (S2035T Control, 0.35±0.08Hz, n=6; S2035 Nifedpine, 1.53±0.35Hz, n=9; S2035T/R2109A Control, 0.44±0.15Hz, n=8; S2035T/R2109A Nifedpine, 0.73±0.19Hz, n=11). While PA/mTOR binding appears to be essential for homeostatic increases in presynaptic function during AMPAR or VGCC blockade, the same was not true for cLTP-induced increases in postsynaptic function (Figure 4.6E-F). Indeed, we found largely identical levels of postsynaptic potentiation when assessed 2Hrs post cLTP stimulation in cells with or without impaired postsynaptic PA/mTOR binding (S2035T Control, 15.86±1.13pA, n=12; S2035T cLTP, 21.90±1.80pA, n=9; S2035T/R2109A Control, 16.71±0.76pA, n=10; S2035T/R2109A cLTP, 21.95±2.013pA, n=8). Together, these data reveal an essential role for intracellular PA/mTOR binding in the postsynaptic domain for the expression of functional changes at excitatory synapses during homeostatic plasticity but not LTP.

4.4 Discussion

Here we report that PLD-mediated hydrolysis of the lipid second messenger PA is a crucial component of the signaling pathway which relays homeostatic signals to postsynaptic mTORC1 after loss of excitatory input (Figure 4.7). Critically, our data reveal that this PLD/PA mediated activation of mTORC1 is a point of divergence between homeostatic and Hebbian forms of synaptic plasticity. We find that PLD signaling is necessary for mTORC1 activation after AMPAR blockade but not during LTP, which mirrors the pattern of intracellular PA synthesis detected under each condition (Figure 4.1). This dissociation between LTP and HSP also holds true at the functional level, as inhibition of PLD signaling, or genetic disruption of PA/mTOR interaction eliminates the well-defined presynaptic enhancement observed after AMPAR blockade but not the postsynaptic potentiation which is a central feature LTP.

How is PLD/PA signaling engaged?

Steady state levels of PA are believed to be quite low under normal conditions; with some estimates showing baseline levels of intracellular PA roughly 5% of that shown for its precursor, phosphatidylcholine (Fang et al., 2003). While there is evidence to support a role for constitutive regulation of mTORC1 and mTORC2 complex integrity by steady-state levels of PA (Toschi et al., 2009), more recent work suggests that actively synthesized PA may directly stimulate mTORC1, but not mTORC2, kinase activity by displacing the inhibitory FK506 binding protein 38 then serving to allosterically modulate complex 1-related mTOR autophosphorylation (Yoon et al., 2011a). In non-neuronal cells, recent reports have demonstrated that PLD/PA signaling plays an important role in signaling nutrient availability to mTOR. Specifically, amino acid availability is believed to act as a signal which causes the Rag-dependent translocation of mTOR (Sancak et al., 2008) and hVps34-dependent translocation of PLD1 (Yoon et al., 2011b) to the late endosomal/lysosomal membrane. It is after this amino-acid induced translocation occurs that Rheb activates PLD1-induced synthesis of PA to activate mTORC1 signaling. Besides Rheb, PLD1 can also be activated by protein kinase C, select Rho-GTPases, and members of the ADP-ribosylation factor (Arf) family (Ktistakis et al., 2003). Interestingly, recent work has implicated postsynaptic action of the RhoGTPase Cdc42 in the expression of presynaptic homeostasis at the drosophila NMJ (Pilgram et al., 2011). Further experiments are needed to explore the possibility that neurons utilize PLD/PA signaling as a mechanism similar to that implemented by mitotic cells in relaying nutrient signals to mTOR, or if instead an alternative manner of activating PLD signaling is utilized, perhaps involving a member of the RhoGTPase family, during synaptic homeostasis.

How do unique types of activation lead to different function outcomes?

The increased postsynaptic strength observed during LTP (Figure 4.3) and presynaptic enhancement which emerges after AMPAR blockade (Figure 4.2, Henry et al., 2012), are both mTORC1-dependent phenomena. Given mTOR's prominent role in orchestrating protein translation necessary for many forms of synapse plasticity and learning (Hoeffer and Klann, 2010), we were interested to uncover an upstream point of divergence by which mTOR is activated in these two forms of plasticity. While our data suggest that PLD/PA signaling is uniquely necessary and sufficient for mTOR-mediated synthesis of BDNF for use as a retrograde signal during synaptic homeostasis (Figure 4.2E, Figure 4.5), it remains unclear how this route to mTOR activation results in this unique synaptic phenotype. It is possible that these two different mTORC1-dependent functional outcomes arise as a consequence of mTOR's action at unique sets of dendritically localized transcripts. If this is indeed the case, a possible explanation is that mTORC1 acts to regulate the translation of mRNAs in close proximity to the stimulated complex, and the spatial locale of cLTP or PLD/PA-induced mTOR activation occurs in subcellular regions with unique compositions of potential mRNA targets. Previous work has identified mTOR distribution at the cell nucleus (Kim and Chen, 2000), at late endosomes/lysosomes (Sancak et al., 2008; Flinn et al., 2010), along the golgi apparatus (Nartia et al., 2011) as well as in the endoplasmic reticulum (Drenan et al., 2004). It is conceivable that stimulation of mTORC1 signaling at the late endosome/lysosome would potentially lead to the translation of specific mRNA transcripts, and hence produce different functional outcomes, than would be observed when mTOR is activated in another subcellular compartment such as the endoplasmic reticulum. The complex ER network in neuronal dendrites contains rich sites of polyribosome accumulation, and acts as a critical region of local translation for membrane-bound proteins such as AMPARs during LTP (Cui-Wang et al., 2012), a form of plasticity which is known to be mTORC1-dependent (Tang et al., 2002). Additionally, there is growing evidence for mRNA localization at late endosomes/lysosomes (Gibbings and Voinnet, 2010), though little is known about the potential cadre of uniquely localized transcripts that might occupy this subcellular locale in neurons. Further experiments will be necessary to determine if activation of mTORC1 at distinct subcellular compartments can explain the unique aspects of PLD/PA-mediated activation we observe in the context of synaptic homeostasis.

Isoform specific effects on mTORC1 activation and synapse function

Our experiments involving overexpression of either PLD1 or PLD2 reveal an interesting degree of specificity with respect to the influence each of these isoforms exerts over neuronal mTORC1 activation and synapse function. The finding that overexpression of PLD1, but not PLD2, causes an increase in mTORC1 activation (Figure 4.4C) was somewhat surprising given previous work showing that overexpression of either PLD isoform is sufficient to activate mTORC1 signaling in non-neuronal cell lines (Fang et al., 2003; Chen et al., 2003). Part of this discrepancy could be a result of the different ways in which post-mitotic cells such as neurons make use of signaling pathways which normally serve a role in mitogenic signaling. Additionally, PLD1 and PLD2 are known to exhibit markedly different patterns of subcellular localization, with PLD1 present at late endosomes/ lysosomes (Todo et al., 1999) or the golgi apparatus (Freyberg et al., 2001), and PLD2 occupying lipid raft sites along the plasma membrane (Colley et al., 1997). Our finding that PLD1 overexpression dramatically increases dendritic BDNF expression and mEPSC frequency (Figure 4.5) mirrors our previously reported effects on BDNF expression and presynaptic function after overexpression of a constitutively active version of Rheb GTPase (Henry et al., 2012). This is perhaps not surprising, given previous reports that Rheb, mTOR, and PLD1 share a similar subcellular localization (Todo et al.,1999; Sancak et al., 2008) and that Rheb directly binds to and activates PLD1 (Sun et al., 2008). If PLD1 is directly implicated in certain aspects of Rheb-induced changes in synaptic function, it could serve as an important point of entry of future therapeutic interventions for neurodevelopmental disorders which share upregulated mTORC1 signaling as a common phenotype, including PTEN hamartoma syndrome and Tuberous sclerosis.

4.6 Acknowledgments

This work was supported by Grants F31MH093112 (F.E.H.) and RO1MH085798 (M.A.S.) from The National Institute of Mental Health and a grant from the Pew Biomedical Scholars Program (M.A.S.). We thank Robert Edwards for generously providing vglut1-pHluorin. We also thank Hisashi Umemori and members of the Sutton laboratory for many helpful discussions. Human HA-PLD1, human HA-PLD2, rat HA-PLD2, and pEGFP-Spo20PABD-WT were provided by Dr. Michael Frohman (SUNY Stony Brook). GFP-Rap1-PABD was provided by Dr. Frank Schmitz (Universität des Saarlandes Medizinische Fakultät). Rapamycin-resistant (S2035T) and Rapamycin/Phosphatic acid resistant (32035T/R2109A) mTOR point mutants were provided by Dr. Jie Chen (University of Illinois at Urbana-Champaign).

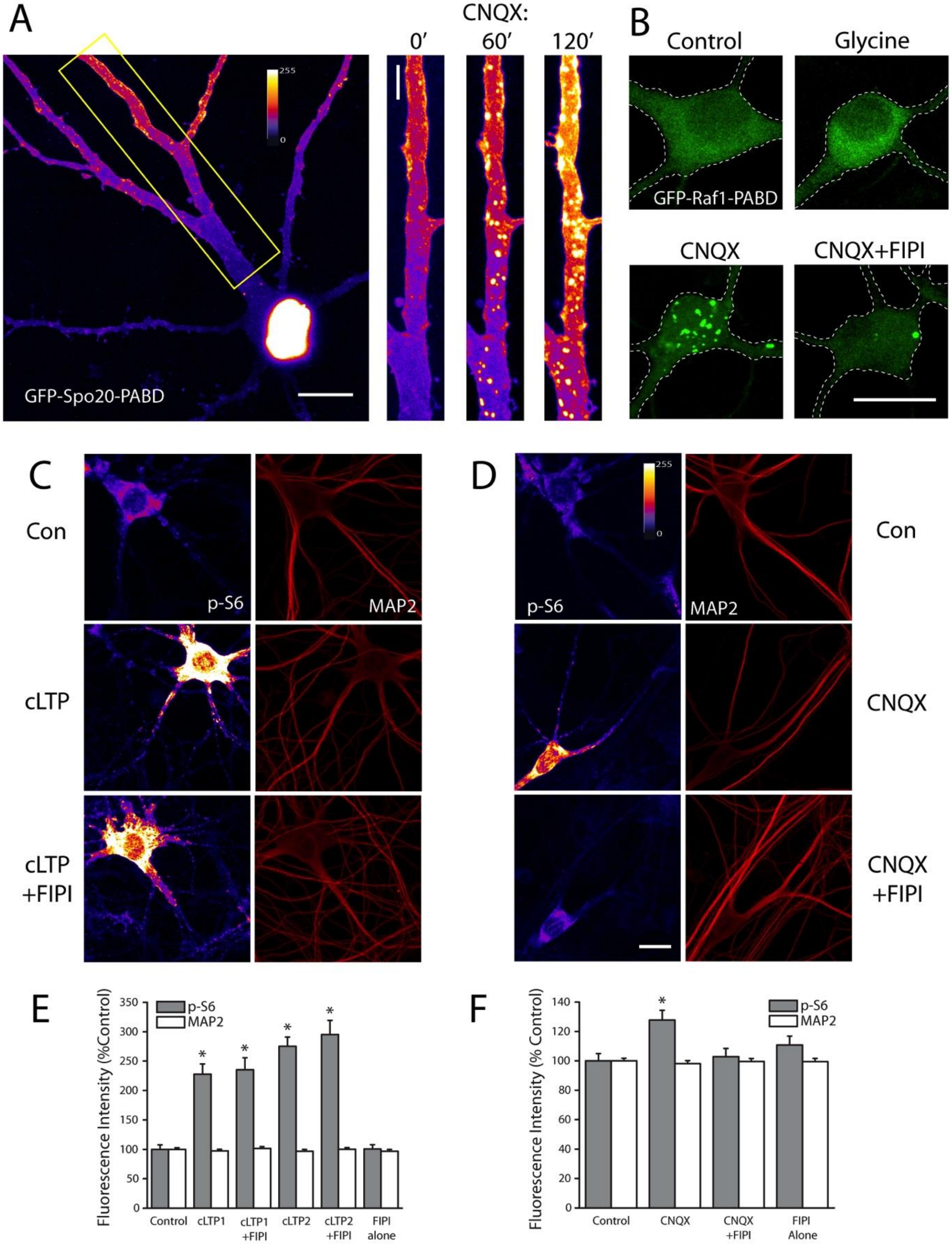
A
CNQX:
0′
60′
120′
255
0
GFP-Spo20-PABD
B
Control
Glycine
GFP-Raf1-PABD
CNQX
CNQX+FIPI
C
Con
cLTP
cLTP
+FIPI
p-S6
MAP2
D
255
0
Con
CNQX
CNQX
+FIPI
p-S6
MAP2
E
Fluorescence Intensity (%Control)
350
300
250
200
150
100
50
0
p-S6
MAP2
*
Control
cLTP1
cLTP1
+FIPI
cLTP2
cLTP2
+FIPI
FIPI
alone
F
Fluorescence Intensity (% Control)
140
120
100
80
60
40
20
0
p-S6
MAP2
*
Control
CNQX
CNQX
+FIPI
FIPI
Alone

Figure 4.1: PLD-dependent generation of PA during homeostatic plasticity but not cLTP (A) Hippocampal neuron expressing the fluorescent PA reporter GFP-Spo20-PABD in culture (left). Right, expanded section of dendrite highlighted in left panel under baseline conditions, and after 60 or 120 minutes of exposure to CNQX (40μM). (B) Example images of neurons expressing an alternate fluorescent reporter of PA synthesis, GFP-Raf1-PABD, under control conditions or after treatment with glycine, CNQX, or CNQX + FIPI. Intracellular accumulation of PA-associated GFP fluorescence was regularly observed after CNQX, but not glycine treatment. FIPI significantly reduced the number of PA-positive punta after CNQX treatment. (C-D) Representative images (C-D) and mean (+ SEM) fluorescence intensity (E-F) of MAP2 and phosphorylated ribosomal protein S6 (p-S6) signal in somatic regions under baseline conditions, or under conditions of cLTP or AMPAR blockade with or without concurrent inhibition of PLD signaling (FIPI, 100nM, 30 min pretreatment). FIPI blocks enhanced mTORC1 kinase activity after AMPAR blockade but not during cLTP. Scale bar = 10μm in A, B and C.

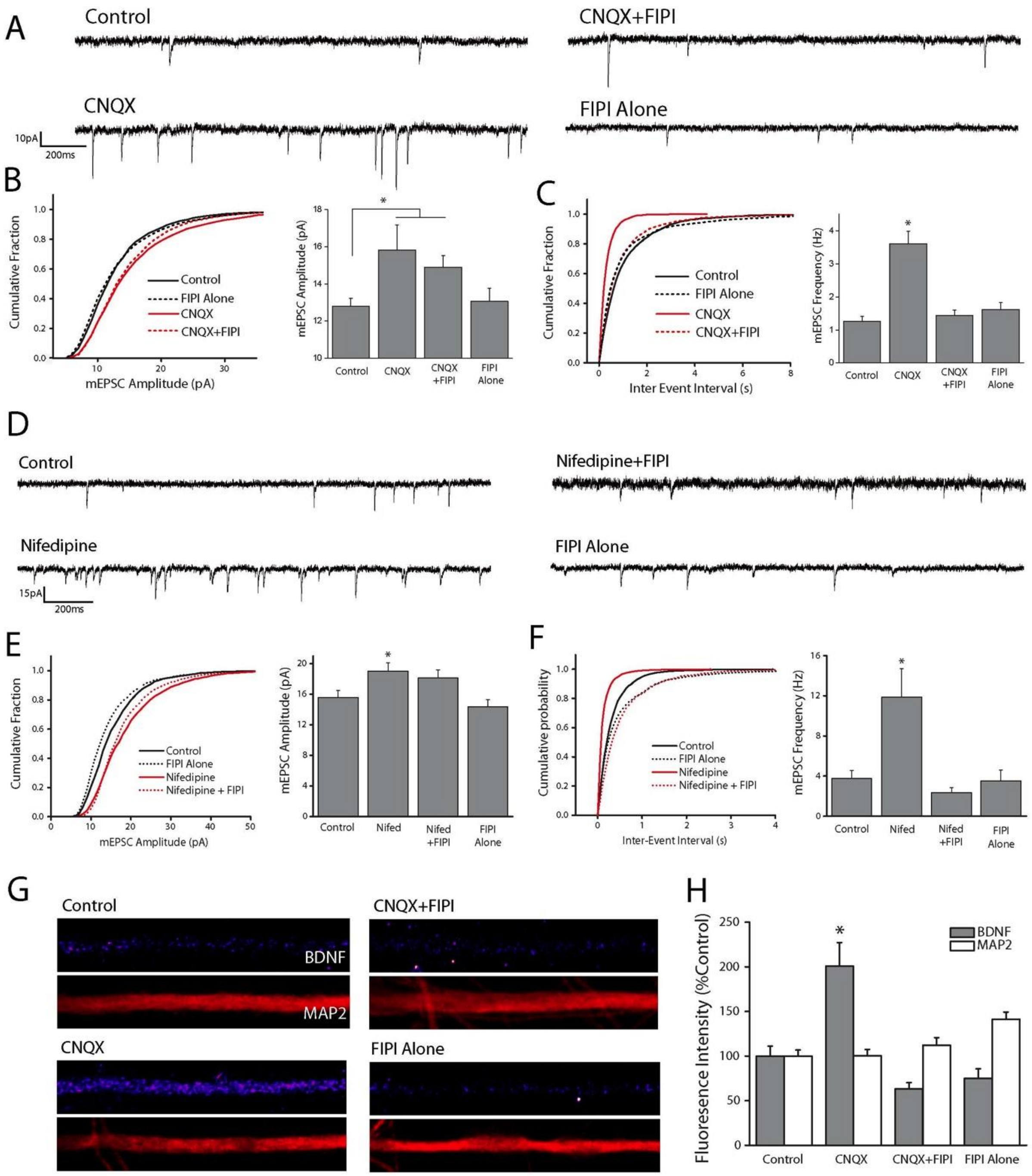
A
Control
CNQX+FIPI
CNQX
FIPI Alone
10pA
200ms
B
Cumulative Fraction
mEPSC Amplitude (pA)
Control
FIPI Alone
CNQX
CNQX+FIPI
mEPSC Amplitude (pA)
*
Control
CNQX
CNQX +FIPI
FIPI Alone
C
Cumulative Fraction
Inter Event Interval (s)
Control
FIPI Alone
CNQX
CNQX+FIPI
mEPSC Frequency (Hz)
*
Control
CNQX
CNQX +FIPI
FIPI Alone
D
Control
Nifedipine+FIPI
Nifedipine
FIPI Alone
15pA
200ms
E
Cumulative Fraction
mEPSC Amplitude (pA)
Control
FIPI Alone
Nifedipine
Nifedipine + FIPI
mEPSC Amplitude (pA)
*
Control
Nifed
Nifed +FIPI
FIPI Alone
F
Cumulative probability
Inter-Event Interval (s)
Control
FIPI Alone
Nifedipine
Nifedipine + FIPI
mEPSC Frequency (Hz)
*
Control
Nifed
Nifed +FIPI
FIPI Alone
G
Control
BDNF
MAP2
CNQX+FIPI
CNQX
FIPI Alone
H
Fluoresence Intensity (%Control)
*
BDNF
MAP2
Control
CNQX
CNQX+FIPI
FIPI Alone

Figure 4.2: PLD signaling is required for adaptive presynaptic compensation (A-C) Representative recordings (A) and mean (+SEM) mEPSC amplitude (B) and frequency (C) recorded from cells treated with vehicle control or CNQX (40μM, 3Hr) with or without the PLD1/2 inhibitor FIPI (100nM, 30m pretreatment). Summary graphs presented on left and cumulative probability distribution shown on right. (*p<0.05 relative to vehicle controls). PLD is necessary for CNQX-induced in mEPSC frequency but not amplitude. (D-F) Representative recordings (D) and mean (+SEM) mEPSC amplitude (E) and frequency (F) recorded from cells treated with vehicle control or Nifedipine (10uM, 2Hr) with or without the PLD1/2 inhibitor FIPI (100nM, 30m pretreatment). Summary graphs presented on left and cumulative probability distribution shown on right. (*p<0.05 relative to vehicle controls). (G-H) Examples images of BDNF and MAP2 expression in linearized dendritic segments (G), and mean (+SEM) expression (H) of MAP2 and BDNF in dendritic compartments normalized to average control values, in neurons treated with CNQX (40mM, 3Hr) with or without the PLD1/2 inhibitor FIPI (100nM, 30 min pre-treatment). BDNF expression in dendrites was significantly enhanced by AMPAR blockade compared with control neurons. This effect was completely blocked by concurrent inhibition of PLD signaling. (*p<0.05, relative to controls).

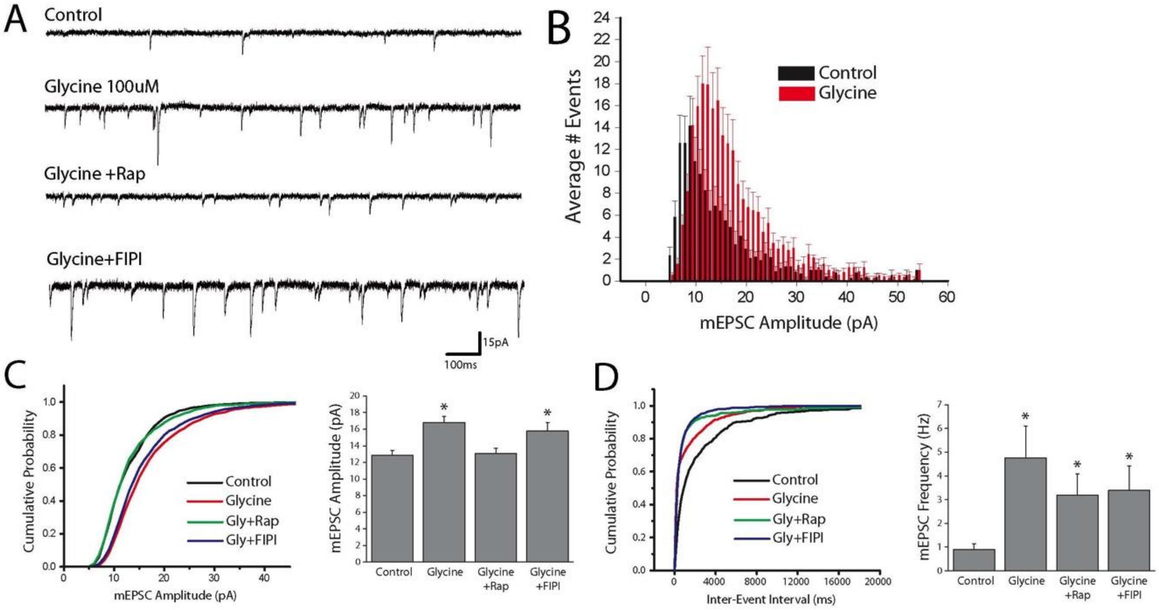
A
Control
Glycine 100uM
Glycine +Rap
Glycine+FIPI
15pA
100ms
B
Average # Events
0 2 4 6 8 10 12 14 16 18 20 22 24
Control
Glycine
0 10 20 30 40 50 60
mEPSC Amplitude (pA)
C
Cumulative Probability
0.0 0.2 0.4 0.6 0.8 1.0
0 10 20 30 40
mEPSC Amplitude (pA)
Control
Glycine
Gly+Rap
Gly+FIPI
mEPSC Amplitude (pA)
0 2 4 6 8 10 12 14 16 18 20
*
*
Control
Glycine
Glycine +Rap
Glycine +FIPI
D
Cumulative Probability
0.0 0.2 0.4 0.6 0.8 1.0
0 4000 8000 12000 16000 20000
Inter-Event Interval (ms)
Control
Glycine
Gly+Rap
Gly+FIPI
mEPSC Frequency (Hz)
0 1 2 3 4 5 6 7
*
*
*
Control
Glycine
Glycine +Rap
Glycine +FIPI

Figure 4.3: Altered postsynaptic function after cLTP does not require intact PLD signaling (A-D) Representative recordings (A), population distribution (B) and mean (+SEM) mEPSC amplitude (C) and frequency (D) recorded from cells treated with vehicle control or Glycine based cLTP stimulus (100µM glycine) with or without the PLD1/2 inhibitor FIPI (100nM, 30m pretreatment). Summary graphs presented on left and cumulative probability distribution shown on right in C and D. (*p<0.05 relative to vehicle controls). PLD signaling is not necessary for cLTP-induced changes in mPESC Amplitude.

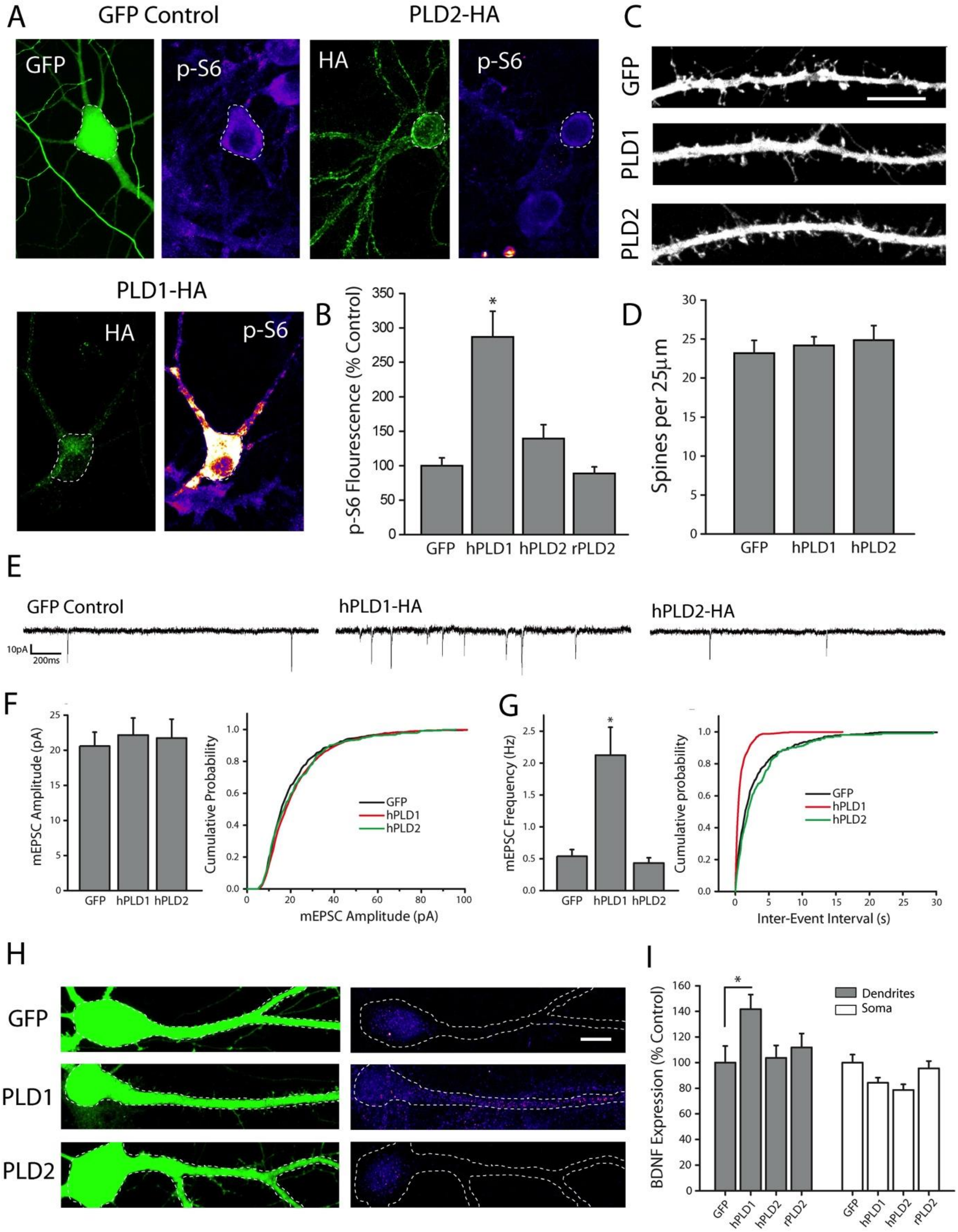
A
GFP Control
GFP
p-S6
PLD2-HA
HA
p-S6
PLD1-HA
HA
p-S6
B
p-S6 Flourescence (% Control)
0
50
100
150
200
250
300
350
*
GFP
hPLD1
hPLD2
rPLD2
C
GFP
PLD1
PLD2
D
Spines per 25μm
0
5
10
15
20
25
30
GFP
hPLD1
hPLD2
E
GFP Control
hPLD1-HA
hPLD2-HA
10pA
200ms
F
mEPSC Amplitude (pA)
0
5
10
15
20
25
GFP
hPLD1
hPLD2
Cumulative Probability
0.0
0.2
0.4
0.6
0.8
1.0
0
20
40
60
80
100
mEPSC Amplitude (pA)
GFP
hPLD1
hPLD2
G
mEPSC Frequency (Hz)
0.0
0.5
1.0
1.5
2.0
2.5
*
GFP
hPLD1
hPLD2
Cumulative probability
0.0
0.2
0.4
0.6
0.8
1.0
0
5
10
15
20
25
30
Inter-Event Interval (s)
GFP
hPLD1
hPLD2
H
GFP
PLD1
PLD2
I
BDNF Expression (% Control)
0
20
40
60
80
100
120
140
160
*
Dendrites
Soma
GFP
hPLD1
hPLD2
rPLD2
GFP
hPLD1
hPLD2
rPLD2

Figure 4.4: PLD1 overexpression is sufficient to activate mTORC1 and drive changes in synapse function. (A-B) Representative images (A) and mean intensity (+SEM,B) of somatic p-S6 staining in neurons expressing HA-tagged hPLD1, hPLD2, or GFP control. Expression of hPLD1, but not hPLD2 or rPLD2, significantly (*$p<0.05$ relative to GFP expressing control neurons) increases p-S6 staining. (C) Representative dendritic sub-regions of cultured hippocampal neurons expressing GFP alone or in combination with hPLD1 or hPLD2. (D) Mean (+SEM) number of spines per 25μm in groups as indicated. Spine density was unaffected by overexpression of either PLD isoform. Scale bar = 10μm in (B). (E-G) Representative recordings (E) and mean (+SEM) mEPSC amplitude (F) and frequency (G) recorded from cells expressing hPLD1, hPLD2 or GHFP control. Summary graphs presented on left and cumulative probability distribution shown on right. (*$p<0.05$ relative to vehicle controls). Overexpression of hPLD1, but not hPLD2, is sufficient to elevate mEPSC frequency after 24 Hrs compared to GFP expressing controls. (H-I) GFP and BDNF expression in somatodendritic segments (H), and mean (+SEM) expression (I) of BDNF in somatic and dendritic compartments normalized to average GFP control values, in neurons cotransfected with GFP as well as hPLD1 or hPLD2. BDNF expression in dendrites was significantly (*$p<0.05$, relative to GFP alone) enhanced by expression of hPLD1 compared with control neurons expressing GFP alone, while neurons expressing hPLD2 showed no difference in dendritic BDNF levels compared to control. hPLD1 or hPLD2 overexpression did not increase somatic BDNF intensity compared to controls. Scale bar in H = 10μm.

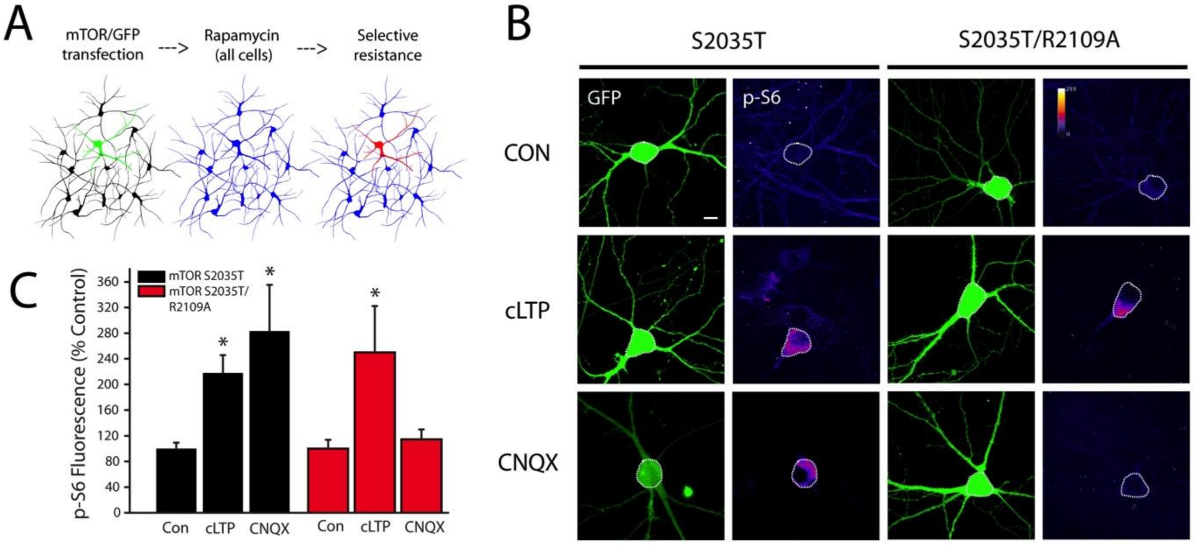
A
mTOR/GFP transfection
--->
Rapamycin (all cells)
--->
Selective resistance
B
S2035T
S2035T/R2109A
GFP
p-S6
CON
cLTP
CNQX
C
p-S6 Fluorescence (% Control)
360
320
280
240
200
160
120
80
40
0
mTOR S2035T
mTOR S2035T/R2109A
*
*
*
Con
cLTP
CNQX
Con
cLTP
CNQX

Figure 4.5: PA binding to mTOR is necessary for enhanced mTORC1 kinase activity during synaptic homeostasis but not cLTP. (A) Schematic of experimental design: Neurons were transfected with GFP as well as one of two mutant versions of mTOR (S2035T = Rapamycin resistant; S2035T/R2109A = Rapamycin and PA resistant). Cultures were then treated with rapamycin (100nM) to eliminate endogenous mTORC1 activity. (B) Full frame example images of GFP and p-S6 staining in neurons expressing GFP alongside either mTOR point mutant, under conditions of AMPAR blockade (CNQX, 40μM, 3Hr), cLTP (Forskolin-based stimulus, 50μM), or vehicle control. (C) Mean (+SEM) somatic intensity of p-S6 staining in groups as indicated. Inhibition of PA/mTOR interaction (via R2109A mutation) eliminates increased mTORC1 kinase activity in the context of AMPAR blockade, but not during cLTP. Scale bar = 10μm in (B). ($p<0.05$ compared to vehicle controls in each group)

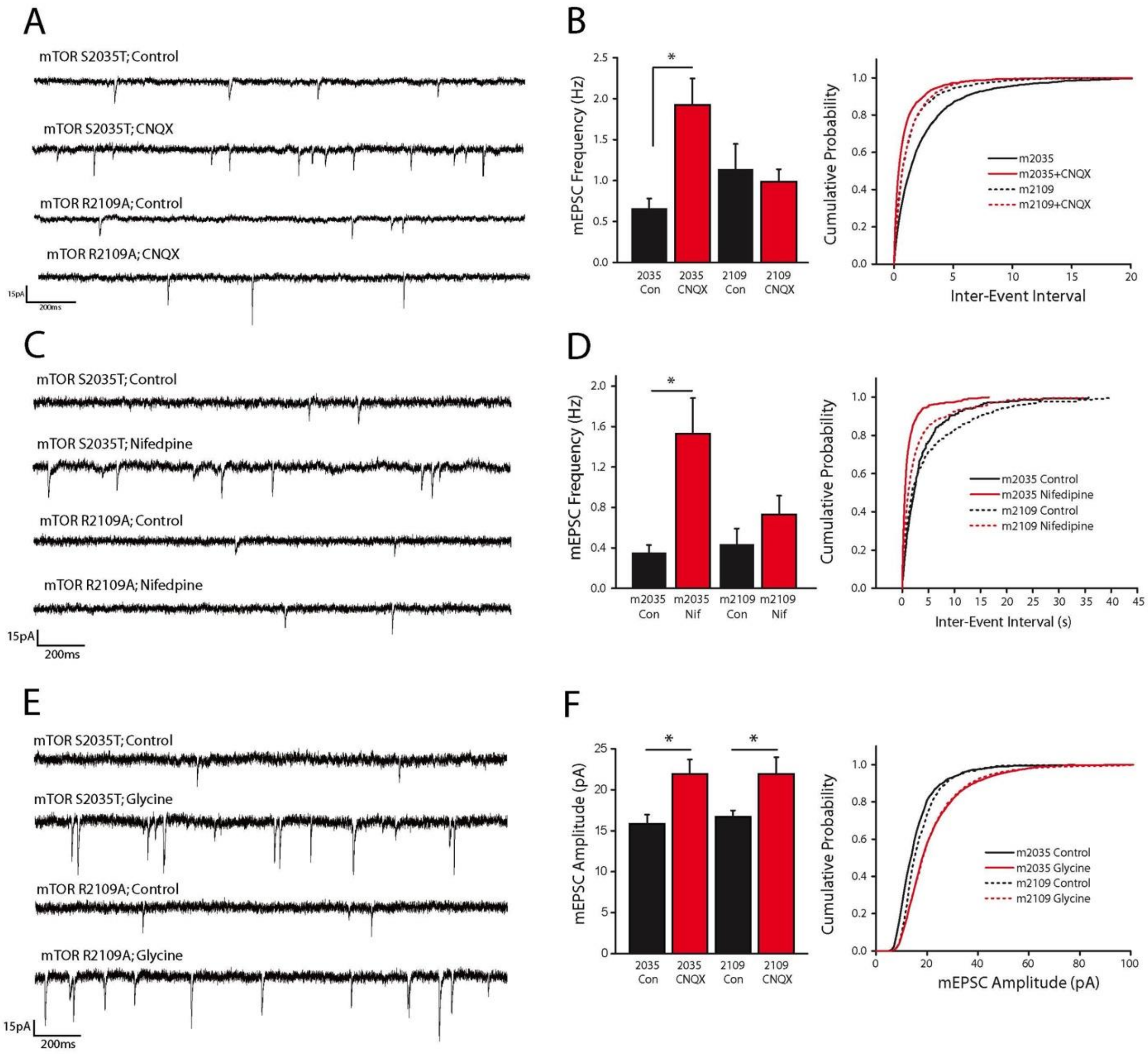
A
mTOR S2035T; Control
mTOR S2035T; CNQX
mTOR R2109A; Control
mTOR R2109A; CNQX
15pA
200ms
B
*
mEPSC Frequency (Hz)
2.5
2.0
1.5
1.0
0.5
0.0
2035 Con
2035 CNQX
2109 Con
2109 CNQX
Cumulative Probability
1.0
0.8
0.6
0.4
0.2
0.0
0
5
10
15
20
Inter-Event Interval
m2035
m2035+CNQX
m2109
m2109+CNQX
C
mTOR S2035T; Control
mTOR S2035T; Nifedpine
mTOR R2109A; Control
mTOR R2109A; Nifedpine
15pA
200ms
D
*
mEPSC Frequency (Hz)
2.0
1.6
1.2
0.8
0.4
0.0
m2035 Con
m2035 Nif
m2109 Con
m2109 Nif
Cumulative Probability
1.0
0.8
0.6
0.4
0.2
0.0
0
5
10
15
20
25
30
35
40
45
Inter-Event Interval (s)
m2035 Control
m2035 Nifedipine
m2109 Control
m2109 Nifedipine
E
mTOR S2035T; Control
mTOR S2035T; Glycine
mTOR R2109A; Control
mTOR R2109A; Glycine
15pA
200ms
F
*
*
mEPSC Amplitude (pA)
25
20
15
10
5
0
2035 Con
2035 CNQX
2109 Con
2109 CNQX
Cumulative Probability
1.0
0.8
0.6
0.4
0.2
0.0
0
20
40
60
80
100
mEPSC Amplitude (pA)
m2035 Control
m2035 Glycine
m2109 Control
m2109 Glycine

Figure 4.6: PA binding to mTOR is necessary for altered synapse function during synaptic homeostasis but not cLTP. (A-B) Representative recordings (A) and mean (+SEM) mEPSC frequency (B) recorded from cells expressing GFP as well as Rap-resistant (mTOR S2035T) or PA-resistant (mTOR R2109A) mTOR point mutants under treatment conditions as indicated. Summary graphs presented on left and cumulative probability distribution shown on right. (*p<0.05 relative to vehicle controls). Inhibition of PA/mTOR interaction (via R2109A mutation) eliminates increased mEPSC frequency after AMPAR blockade. (C-D) Representative recordings (C) and mean (+SEM) mEPSC frequency (D) recorded from cells expressing GFP as well as Rap-resistant (mTOR S2035T) or PA-resistant (mTOR R2109A) mTOR point mutants under treatment conditions as indicated. Summary graphs presented on left and cumulative probability distribution shown on right. (*p<0.05 relative to vehicle controls). Inhibition of PA/mTOR interaction (via R2109A mutation) eliminates increased mEPSC frequency after L-type VGCC blockade. (E-F) Representative recordings (E) and mean (+SEM) mEPSC amplitude (F) recorded from cells expressing GFP as well as Rap-resistant (mTOR S2035T) or PA-resistant (mTOR R2109A) mTOR point mutants under treatment conditions as indicated. Summary graphs presented on left and cumulative probability distribution shown on right. (*p<0.05 relative to vehicle controls). Inhibition of PA/mTOR interaction (via R2109A mutation) has no effect on enhanced mEPSC amplitude after cLTP induction.

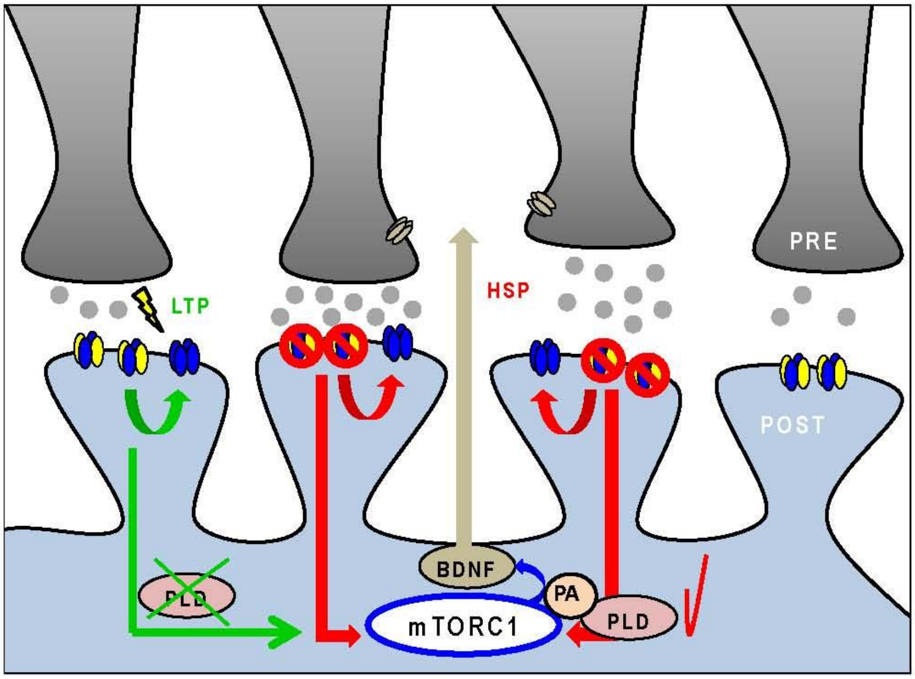
LTP
HSP
PRE
POST
PLD
BDNF
PA
mTORC1
PLD

Figure 4.7: Model: PLD/PA signaling is an upstream point of divergence during the activation of mTORC1 in unique forms of synapse plasticity PLD1-mediated synthesis of PA is essential for mTORC1 activation, and subsequent release of BDNF as a retrograde signal, as an adaptive response to loss of excitatory input via CNQX treatment. Not such role is found for PLD1/PA signaling in the context of mTORC1 activation during cLTP, whose functional effects are completely insensitive to elimination of PLD signaling or inhibition of PA/mTOR binding.

4.8 Bibliography

Aoto J, Nam CI, Poon MM, Ting P, Chen L. (2008). Synaptic signaling by all-trans retinoic acid in homeostatic synaptic plasticity. Neuron. Oct 23;60(2):308-20.

Brown EJ, Beal PA, Keith CT, Chen J, Shin TB, Schreiber SL. (1995). Control of p70 s6 kinase by kinase activity of FRAP in vivo. Nature. Oct 5;377(6548):441-6.

Cammalleri M, Lütjens R, Berton F, King AR, Simpson C, Francesconi W, Sanna PP. (2003). Time-restricted role for dendritic activation of the mTOR-p70S6K pathway in the induction of late-phase long-term potentiation in the CA1. Proc Natl Acad Sci U S A. Nov 25;100(24):14368-73.

Chen Y, Zheng Y, Foster DA. (2003). Phospholipase D confers rapamycin resistance in human breast cancer cells. Oncogene. Jun 19;22(25):3937-42.

Cockcroft S. (2001). Signalling roles of mammalian phospholipase D1 and D2. Cell Mol Life Sci. Oct;58(11):1674-87.

Colley WC, Sung TC, Roll R, Jenco J, Hammond SM, Altshuller Y, Bar-Sagi D, Morris AJ, Frohman MA. (1997). Phospholipase D2, a distinct phospholipase D isoform with novel regulatory properties that provokes cytoskeletal reorganization. Curr Biol. Mar 1;7(3):191-201.

Cui-Wang T, Hanus C, Cui T, Helton T, Bourne J, Watson D, Harris KM, Ehlers MD. (2012). Local zones of endoplasmic reticulum complexity confine cargo in neuronal dendrites. Cell. Jan 20;148(1-2):309-21.

Drenan RM, Liu X, Bertram PG, Zheng XF. (2004). FKBP12-rapamycin-associated protein or mammalian target of rapamycin (FRAP/mTOR) localization in the endoplasmic reticulum and the Golgi apparatus. J Biol Chem. Jan 2;279(1):772-8.

Du G, Huang P, Liang BT, Frohman MA. (2004). Phospholipase D2 localizes to the plasma membrane and regulates angiotensin II receptor endocytosis. Mol Biol Cell. Mar;15(3):1024-30.

Fang Y, Vilella-Bach M, Bachmann R, Flanigan A, Chen J.(2001). Phosphatidic acid-mediated mitogenic activation of mTOR signaling. Science. Nov 30;294(5548):1942-5.

Fang Y, Park IH, Wu AL, Du G, Huang P, Frohman MA, Walker SJ, Brown HA, Chen J. (2003). PLD1 regulates mTOR signaling and mediates Cdc42 activation of S6K1. Curr Biol. Dec 2;13(23):2037-44.

Flinn RJ, Yan Y, Goswami S, Parker PJ, Backer JM. (2010). The late endosome is essential for mTORC1 signaling. Mol Biol Cell. Mar 1;21(5):833-41.

Foster DA. (2009). Phosphatidic acid signaling to mTOR: signals for the survival of human cancer cells. Biochim Biophys Acta. Sep;1791(9):949-55. Mar 2.

Freyberg Z, Sweeney D, Siddhanta A, Bourgoin S, Frohman M, Shields D. (2001). Intracellular localization of phospholipase D1 in mammalian cells. Mol Biol Cell. Apr;12(4):943-55.

Frondorf K, Henkels KM, Frohman MA, Gomez-Cambronero J. (2010). Phosphatidic acid is a leukocyte chemoattractant that acts through S6 kinase signaling. J Biol Chem. May 21;285(21):15837-47.

Gibbings D, Voinnet O. (2010). Control of RNA silencing and localization by endolysosomes. Trends Cell Biol. Aug;20(8):491-501.

Henry FE, McCartney AJ, Neely R, Perez AS, Carruthers CJ, Stuenkel EL, Inoki K, Sutton MA. (2012). Retrograde changes in presynaptic function driven by dendritic mTORC1. J Neurosci. Nov 28;32(48):17128-42.

Hoeffer CA, Klann E. (2010). mTOR signaling: at the crossroads of plasticity, memory and disease. Trends Neurosci. Feb;33(2):67-75.

Hou L, Klann E. (2004). Activation of the phosphoinositide 3-kinase-Akt-mammalian target of rapamycin signaling pathway is required for metabotropic glutamate receptor-dependent long-term depression. J Neurosci. Jul 14;24(28):6352-61.

Jakawich SK, Nasser HB, Strong MJ, McCartney AJ, Perez AS, Rakesh N, Carruthers CJ, Sutton MA. (2010). Local presynaptic activity gates homeostatic changes in presynaptic function driven by dendritic BDNF synthesis. Neuron. Dec 22;68(6):1143-58.

Jenkins GM, Frohman MA. (2005). Phospholipase D: a lipid centric review. Cell Mol Life Sci. Oct;62(19-20):2305-16.

Kim JE, Chen J. (2000). Cytoplasmic-nuclear shuttling of FKBP12-rapamycin-associated protein is involved in rapamycin-sensitive signaling and translation initiation. Proc Natl Acad Sci U S A. Dec 19;97(26):14340-5.

Li N, Lee B, Liu RJ, Banasr M, Dwyer JM, Iwata M, Li XY, Aghajanian G, Duman RS. (2010). mTOR-dependent synapse formation underlies the rapid antidepressant effects of NMDA antagonists. Science. Aug 20;329(5994):959-64.

Lu W, Man H, Ju W, Trimble WS, MacDonald JF, Wang YT. (2001). Activation of synaptic NMDA receptors induces membrane insertion of new AMPA receptors and LTP in cultured hippocampal neurons. Neuron. Jan;29(1):243-54.

Ma XM, Blenis J. (2009). Molecular mechanisms of mTOR-mediated translational control. Nat Rev Mol Cell Biol. May;10(5):307-18.

Mameli M, Balland B, Luján R, Lüscher C. (2007). Rapid synthesis and synaptic insertion of GluR2 for mGluR-LTD in the ventral tegmental area. Science. Jul 27;317(5837):530-3.

Narita M, Young AR, Arakawa S, Samarajiwa SA, Nakashima T, Yoshida S, Hong S, Berry LS, Reichelt S, Ferreira M, Tavaré S, Inoki K, Shimizu S, Narita M. (2011). Spatial coupling of mTOR and autophagy augments secretory phenotypes. Science. May 20;332(6032):966-70.

Penney J, Tsurudome K, Liao EH, Elazzouzi F, Livingstone M, Gonzalez M, Sonenberg N, Haghighi AP. (2012). TOR is required for the retrograde regulation of synaptic homeostasis at the Drosophila neuromuscular junction. Neuron. Apr 12;74(1):166-78.

Pilgram GS, Potikanond S, van der Plas MC, Fradkin LG, Noordermeer JN. (2011). The RhoGAP crossveinless-c interacts with Dystrophin and is required for synaptic homeostasis at the Drosophila neuromuscular junction. J Neurosci. Jan 12;31(2):492-500.

Rodriguez Camargo DC, Link NM, Dames SA. (2012). The FKBP-rapamycin binding domain of human TOR undergoes strong conformational changes in the presence of membrane mimetics with and without the regulator phosphatidic acid. Biochemistry. Jun 19;51(24):4909-21.

Sancak Y, Peterson TR, Shaul YD, Lindquist RA, Thoreen CC, Bar-Peled L, Sabatini DM. (2008). The Rag GTPases bind raptor and mediate amino acid signaling to mTORC1. Science. Jun 13;320(5882):1496-501.

Schwarz K, Natarajan S, Kassas N, Vitale N, Schmitz F. (2011). The synaptic ribbon is a site of phosphatidic acid generation in ribbon synapses. J Neurosci. Nov 2;31(44):15996-6011.

Su W, Yeku O, Olepu S, Genna A, Park JS, Ren H, Du G, Gelb MH, Morris AJ, Frohman MA. (2009). 5-Fluoro-2-indolyl des-chlorohalopemide (FIPI), a phospholipase D pharmacological inhibitor that alters cell spreading and inhibits chemotaxis. Mol Pharmacol. Mar;75(3):437-46.

Sutton MA, Schuman EM. (2006). Dendritic protein synthesis, synaptic plasticity, and memory. Cell. Oct 6;127(1):49-58.

Sun Y, Fang Y, Yoon MS, Zhang C, Roccio M, Zwartkruis FJ, Armstrong M, Brown HA, Chen J. (2008). Phospholipase D1 is an effector of Rheb in the mTOR pathway. Proc Natl Acad Sci U S A. Jun 17;105(24):8286-91.

Tang SJ, Reis G, Kang H, Gingras AC, Sonenberg N, Schuman EM. (2002). A rapamycin-sensitive signaling pathway contributes to long-term synaptic plasticity in the hippocampus. Proc Natl Acad Sci U S A. Jan 8;99(1):467-72.

Toda K, Nogami M, Murakami K, Kanaho Y, Nakayama K. (1999). Colocalization of phospholipase D1 and GTP-binding-defective mutant of ADP-ribosylation factor 6 to endosomes and lysosomes. FEBS Lett. Jan 15;442(2-3):221-5.

Toschi A, Lee E, Xu L, Garcia A, Gadir N, Foster DA. (2009). Regulation of mTORC1 and mTORC2 complex assembly by phosphatidic acid: competition with rapamycin. Mol Cell Biol. Mar;29(6):1411-20.

Veverka V, Crabbe T, Bird I, Lennie G, Muskett FW, Taylor RJ, Carr MD. (2008). Structural characterization of the interaction of mTOR with phosphatidic acid and a novel class of inhibitor: compelling evidence for a central role of the FRB domain in small molecule-mediated regulation of mTOR. Oncogene. Jan 24;27(5):585-95.

Vickers CA, Dickson KS, Wyllie DJ. (2005). Induction and maintenance of late-phase long-term potentiation in isolated dendrites of rat hippocampal CA1 pyramidal neurones. J Physiol. Nov 1;568(Pt 3):803-13.

Wang HL, Zhang Z, Hintze M, Chen L. (2011). Decrease in calcium concentration triggers neuronal retinoic acid synthesis during homeostatic synaptic plasticity. J Neurosci. Dec 7;31(49):17764-71.

Wang X, Proud CG. (2011). mTORC1 signaling: what we still don't know. J Mol Cell Biol. Aug;3(4):206-20.

Foster DA, Xu L. (2003). Phospholipase D in cell proliferation and cancer. Mol Cancer Res. Sep;1(11):789-800.

Yoon MS, Sun Y, Arauz E, Jiang Y, Chen J. (2011). Phosphatidic acid activates mammalian target of rapamycin complex 1 (mTORC1) kinase by displacing FK506 binding protein 38 (FKBP38) and exerting an allosteric effect. J Biol Chem. Aug 26;286(34):29568-74.

Yoon MS, Du G, Backer JM, Frohman MA, Chen J. (2011). Class III PI-3-kinase activates phospholipase D in an amino acid-sensing mTORC1 pathway. J Cell Biol. Oct 31;195(3):435-47.

Zeniou-Meyer M, Zabari N, Ashery U, Chasserot-Golaz S, Haeberlé AM, Demais V, Bailly Y, Gottfried I, Nakanishi H, Neiman AM, Du G, Frohman MA, Bader MF, Vitale N. (2007). Phospholipase D1 production of phosphatidic acid at the plasma membrane promotes exocytosis of large dense-core granules at a late stage. J Biol Chem. Jul 27;282(30):21746-57.

Zhu YB, Kang K, Zhang Y, Qi C, Li G, Yin DM, Wang Y. (2012). PLD1 Negatively Regulates Dendritic Branching. J Neurosci. Jun 6;32(23):7960-9.

Zoncu R, Efeyan A, Sabatini DM. (2011). mTOR: from growth signal integration to cancer, diabetes and ageing. Nat Rev Mol Cell Biol. Jan;12(1):21-35.

CHAPTER V

Activity-dependent proteasome trafficking underlies state-dependent expression of synaptic homeostasis

5.1 Abstract

Precisely tuned regulation of pre and post-synaptic communication depends on the ability to adjust synaptic protein levels via coordinated protein synthesis and degradation mechanisms. Recent work has demonstrated activity-dependent proteasome recruitment into dendritc spines in response to synaptic stimulation, indicating that remodeling the synaptic landscape via active degradation is likely an important aspect of postsynaptic functional plasticity. In axons, where the abundance of proteasomes is dramatically lower than in dendrites, the redistribution of the proteasome to appropriate synaptic terminals could be a critical mechanism governing protein degradation in the presynaptic compartment. Indeed, we report here that intrinsic firing governs activity-dependent proteasome trafficking to and from synaptic terminals in axons of cultured hippocampal neurons, and this dynamic proteasome localization is critical for trans-synaptic signaling to homeostatically adjust presynaptic neurotransmitter release. Using epitope- and fluorescently-tagged subunits of the 19S proteasome, we find that increasing neuronal firing rates enriches prtoteasome accumulation at synaptic terminals, whereas inhibiting neuronal firing results in a dramatic redistribution away from synaptic terminals to non-synaptic areas. This altered localization is due, at least in part, to an activity-dependent active sequestration mechanism at presynaptic terminals, as revealed by live monitoring of fluorescence persistence after synaptic photoactivation of GFP-tagged proteasomal subunits. Moreover, we find that

activity dependent phosphorylation of the Rpt6 subunit of the 19S proteasome is necessary and sufficient for axonal proteasome redistribution, and that this altered localization plays a critical role in establishing retrograde homeostatic changes in presynaptic function after loss of postsynaptic drive which are selectively implemented at active boutons. Together, our data reveal dynamic redistribution of the proteasome as a novel mechanism whereby the activity-dependent “state” of synaptic compartments determines the specific forms of plasticity they can exhibit.

5.2 Introduction

The synaptic proteome is vastly complex space, with connections between particular cells types consisting of unique combinations of pre and postsynaptic constituents that are highly dynamic in space and time (O'Rourke et al., 2012). Given recent interest in the synapse as a primary locus of disruption for a range of neurological and psychiatric disorders including schizophrenia, Autism Spectrum Disorders, and Intellectual Disability (Bayés et al., 2011), it is vital to understand the mechanisms by which synapse form and function are modified in the healthy and diseased brain. Accumulating evidence suggests that precisely tuned regulation of pre- and post-synaptic communication depends on the ability to adjust synaptic protein levels via coordinated protein synthesis and degradation mechanisms (Cajigas et al., 2010). Considerable work has been devoted to understanding how these processes modify synapse function on an individual basis, but specific examples of cooperative synthesis and degradation operating in a specific form of synaptic plasticity are rare.

In the mammalian hippocampus, there is evidence that UPS-dependent degradation proceeds alongside mechanisms which regulate protein synthesis to elicit the functional changes that emerge in the context of long-term potentiation (LTP) at excitatory synapses. These processes appear to operate in tandem but on distinct sets of proteins, such that pharmacological inhibition of either de novo protein synthesis or activity of the ubiquitin proteasome system (UPS) blocks the expression of synaptic potentiation, but simultaneous inhibition of both processes restores LTP to control levels (Fonseca et al., 2006). Additional work has shown that expression of LTP at CA3-CA1 synapses in the hippocampus requires proteasome dependent degradation operating in concert with mechanistic target of rapamycin (mTOR)-dependent protein synthesis (Karpova et al., 2006). This is notable, given that hyperactivated mTORC1 signaling is a common feature of several neurodevelopmental disorders, including PTEN Hamartoma syndrome, Tuberous Sclerosis, and Neurofibramatosis type 1 (Hoeffer and Klann, 2009). Though mTORC1-dependent protein translation is likely pivotal for the altered postsynaptic function observed in the context of LTP (Tang et al., 2002; Cammalleri et al., 2003; Ma et al., 2011) and mGluR-LTD (Hou and Klann, 2004; Banko et al., 2006), recent work has also characterized a novel role for mTORC1 involving the enhancement of presynaptic function via a postsynaptically synthesized retrograde signal (Penney et al., 2012; Henry et al., 2012). Strikingly, this phenomenon was observed in the context of adaptive synaptic compensation after loss of excitatory input, as well as after transient genetic or pharmacological upregulation of mTORC1 function. While BDNF was identified as the retrograde signal which is released after acute mTORC1 activation (Henry et al., 2012), the precise mechanisms responsible for maintaining the subsequent long-lasting enhancement in presynaptic function are unknown.

Though transcription-dependent, cell-wide changes in both pre- and postsynaptic proteins are well documented during crucial developmental periods and in the context of activity dependent plasticity (Deisseroth et al., 1996; Nayak et al., 1998; Graef et al., 2003; Deppmann et al., 2008), accumulating evidence suggests that the synaptic proteome can also be regulated in spatially discrete regions of the cell in response to more subtle changes in input. Initial insights into locally regulated protein synthesis in the mammalian CNS came from the discovery of polyribosomes in the distal dendrites of dentate granule cells (Steward and Levy, 1982). These core components of the translation machinery were later shown to relocalize from dendritic shafts into spines after stimuli that induce LTP (Ostroff et al., 2001). More recently, several groups have demonstrated a similar form of activity-dependent redistribution of the proteasome into dendritic spines in response to strong synaptic stimulation (Bingol and Schuman, 2006; Bingol et al., 2010).

In axons, where the abundance of the UPS is lower than in dendrites, the redistribution of proteasomes to particular synaptic terminals could be a critical mechanism governing protein degradation in the presynaptic compartment, but thus far no such mechanism has been demonstrated. We report here that intrinsic firing governs activity-dependent proteasome redistribution to and from synaptic terminals in axons of cultured hippocampal neurons, and this dynamic relocalization is critical for trans-synaptic signaling to homeostatically adjust presynaptic neurotransmitter release. Using epitope- and fluorescently-tagged subunits of the 19S proteasome, we find that increasing neuronal firing rates enriches proteasome accumulation at synaptic terminals, whereas inhibiting neuronal firing results in a dramatic redistribution away from synaptic terminals to non-synaptic areas. This altered localization is due, at least in part, to an activity-dependent active sequestration mechanism at presynaptic terminals, as revealed by live monitoring of fluorescence persistence after synaptic photoactivation of GFP-tagged proteasomal subunits. Moreover, we find that activity dependent phosphorylation of the Rpt6 subunit of the 19S proteasome is necessary and sufficient for axonal proteasome redistribution, and that this altered localization plays a critical role in the selective expression of enhanced presynaptic release after postsynaptic mTORC1 activation or loss of postsynaptic drive. Together, our data reveal dynamic redistribution of the proteasome as a novel mechanism whereby the activity-dependent “state” of synaptic compartments determines the specific forms of plasticity they can exhibit.

5.3 Results

Postsynaptic mTORC1 activation drives state-dependent changes in presynaptic function

Previously, we have established that mTORC1 signaling participates in a unique, trans-synaptically mediated form of plasticity involving the dendritic synthesis and release of BDNF as a retrograde signal (Henry et al., 2012). In our previous efforts we utilized overexpression of a constitutively active form of Rheb-GTPase to activate mTORC1 signaling. To assess consequences of mTORC1 activation under less physiologically unrealistic conditions, we expressed WT Rheb in cultured hippocampal neurons and assessed levels of mTORC1 activation 24 Hrs later (Figure 5.2A). Similar to our previously reported findings, RhebWT expression enhanced mTORC1 kinase activity, as assessed via changes in the phosphorylation of ribosomal protein S6 (eGFP Controls, 100±13.16%, n=28; RhebWT, 266.78±28.85, n=29). In line with previous reports of BDNF as a target of mTORC1-mediated translational regulation (Henry et al., 2012; Liao et al., 202), we found enhanced BDNF expression in neurons expressing RhebWT compared to neurons expressing eGFP alone. Notably, this effect was limited to dendritic subcompartments, and no difference in BDNF intensity was observed in somatic regions between groups (eGFP dendritic BDNF Intensity, 100±16.48%, n=35, RhebWT dendritic BDNF Intensity, 245.71±26.13%, n=35; eGFP somatic BDNF Intensity, 100±5.76%, n=30; RhebWT somatic BDNF Intensity, 91.45±5.21%, n=32). Voltage-clamp recordings of miniature spontaneous excitatory postsynaptic currents (mEPSCs) revealed alterations in synaptic function as a consequence of enhanced dendritic BDNF release (Figure 5.1B). Neurons expressing RhebWT exhibited enhanced mEPSC frequency compared to cells expressing GFP alone. This effect was dependent on dendritically released BDNF, as application of the extracellular BDNF scavenger TrkB-fc (1μg/ml) completely eliminated increases spontaneous release as a consequence of Rheb expression (eGFP Control, 1.52±0.17Hz, n=25; RhebWT, 2.44±0.44Hz, n=27; eGFP + TrkB-fc, 1.51±0.19Hz, n=10; RHebWT+TrkB-fc, 1.29±0.15Hz, n=12). The amplitude of spontaneous excitatory currents was unchanged as a consequence of postsynaptic mTORC1 activation via RhebWT overexpression (eGFP Control, 13.95±0.66pA, n=25; RhebWT, 14.03±0.65pA, n=27; eGFP + TrkB-fc, 13.51±1.12pA, n=10; RHebWT+TrkB-fc, 15.31±1.05pA, n=12).

We next assessed the impact of mTORC1-dependent retrograde signaling on evoked glutamatergic neurotransmission. First, we directly visualized evoked glutamate release by imaging activity-dependent changes in vglut1-pHluorin fluorescence at presynaptic terminals identified by co-expression of mCherry-tagged synaptophysin (mCh-Syn). As previously reported (Voglmaier et al., 2006), basal vglut1-pHluorin fluorescence at presynaptic terminals was low due to effective quenching by the acidic environment of synaptic vesicles, allowing for optical detection of action potential-triggered synaptic vesicle fusion when the lumen of the vesicle is exposed to the neutral extracellular space. To induce action potentials across the network, we applied field stimulation via parallel platinum-iridium electrodes under conditions where individual pulses each faithfully produced an action potential, verified by a characteristic cell wide $Ca2^{+}$ transient accompanying each stimulus (not shown). We used exogenous application of the lipid second messenger phosphatidic acid (PA) to acutely activate mTORC1 signaling (as seen in Chapter 3). In control (vehicle-treated) neurons, a 10-s train of action potentials delivered at 10 Hz induced a clear increase in vglut1-pHluorin fluorescence at presynaptic terminals, but following acute mTORC1 activation with PA (100 μM; 45 min), this evoked vesicle fusion was markedly enhanced (Figure 5.1C). Scavenging extracellular BDNF with TrkB-fc (1 μg/ml) during PA application prevented this enhancement of evoked release, suggesting that acute mTORC1 activation drives increases in evoked glutamate release in a manner dependent on BDNF release (Vehicle Control peak DF = 0.79±0.05, n=567; PA peak DF = 1.68±0.10, n=802; PA+TrkB-fc peak DF = 0.96±0.02, n=652; TrkB-fc Alone peak DF = 0.84±0.02, n=750). As another means of assessing evoked neurotransmitter release, and to examine if mTORC1-dependent changes in evoked release are evident in a preparation where intrinsic hippocampal circuitry is preserved, we examined paired-pulse facilitation (PPF, negatively correlated with release probability) at CA3-CA1 synapses in acute hippocampal slices prepared from P18-24 rats. Following preparation and recovery, slices were treated with PA (100 μM; 45 min), either alone or coincident with the protein synthesis inhibitor anisomycin (40 μM), the mTORC1 inhibitor rapamycin (300 nM), or the Trk receptor inhibitor k252a (300 nM). Relative to control (vehicle-treated) slices, acute mTORC1 activation with PA resulted in significantly diminished PPF (Figure 5.1D), consistent with an increase in release probability at these synapses. This effect of PA required new protein synthesis, mTORC1 activation, and Trk receptor activation (Figure 5.1D), suggesting that the diminished PPF that accompanies mTORC1 activation in slices, shares core mechanistic features with the retrograde regulation of presynaptic function by dendritic mTORC1 observed in cultured hippocampal neurons. Importantly, these inhibitors have no intrinsic effect on PPF when applied on their own (Figure

5.1D). Taken together, these results demonstrate that postsynaptic mTORC1 activation exerts retrograde control over evoked neurotransmitter release, as it does over spontaneous neurotransmitter release. To verify a role for de novo synthesis of BDNF in PA-induced enhancement of presynaptic function, we used magnetofection to rapidly deliver siRNA targeting BDNF to specifically block new BDNF synthesis without loss of existing BDNF expression (Figure 5.2E). BDNF siRNA was visible inside neurons immediately following magnetofection (Figure 5.2B), and as expected, a time-dependent decrease in basal levels of BDNF expression ensued (Figures 5.2C-D). Importantly, we found that dendritic BDNF expression was similar between neurons receiving BDNF siRNA and those receiving a non-targeting control siRNA 90min following magnetofection (Relative change in BDNF Intensity- Control siRNA 90 min, 0±6.09%, n=33; Relative change in BDNF Intensity- BDNF siRNA 90 min, -3.09±4.54%, n=21; Relative change in BDNF Intensity- Control siRNA 48 Hr, 4.16%, n=32; Relative change in BDNF Intensity- BDNF siRNA 48Hr, -41.69±4.34%, n=21). In contrast, BDNF siRNA magnetofection completely suppressed the increase in dendritic BDNF expression induced by PA treatment (BDNF Intensity Vehicle-treated control siRNA, 100±9.51%, n=55; BDNF Intensity PA-treated control siRNA, 181.12±12.70% of control, n=62; BDNF Intensity Vehicle-treated BDNF siRNA, 100±13.01%, n=49; BDNF Intensity PA-treated BDNF siRNA, 90.91±5.91% of control, n=60) suggesting a relatively specific effect on new BDNF synthesis due to limited BDNF turnover over this interval. We next explored the functional consequences of suppressing new BDNF synthesis. Whereas PA treatment induced robust increases in mEPSC frequency in neurons receiving control siRNA magnetofection (Figure 5.1F), this effect was completely blocked in neurons receiving BDNF siRNA magnetofection (Vehicle -treated control siRNA, 1.68±0.34Hz, n=8; PA-treated control siRNA, 6.65±1.65Hz, n=6; Vehicle-treated BDNF siRNA, 1.52±0.19Hz, n=5; PA-treated BDNF siRNA, 2.36±0.47Hz, n=7). These results indicate that de novo BDNF synthesis is required for retrograde changes in presynaptic function driven by mTORC1 activation. Taken together, our findings reveal that dendritic mTORC1 locally regulates the function of opposed presynaptic terminals by controlling BDNF synthesis in dendrites.

Our previous characterization of locally-mediated homeostatic plasticity driven by AMPAR blockade uncovered an unexpected yet critical role for presynaptic spike activity in the expression of adaptive increases in spontaneous vesicle release (Jakawich et al., 2010). We replicate those findings here, using changes in vglut-pH fluorescence to assess a potential requirement for neuronal spiking in the expression of homeostatic shifts in evoked vesicle release after loss of excitatory input (Figure 5.3A-D). In line with our previous findings, we find that loss of excitatory input via AMPAR blockade (CNQX, 40μM, 3Hr) results in a substantial increase in vglut1-pH fluorescence intensity evoked from a 10s 10Hz stimulus train (Figure 5.3A-2D). However, we also find that simultaneous application of the voltage-gated Na+-channel blocker TTX completely eliminates CNQX-induced increases in evoked neurotransmission, without eliciting significant effects on presynaptic function when applied alone (Vehicle Control peak DF = 1.51±0.11, n=262; CNQX peak DF = 2.31±0.27, n=120; CNQX+TTX peak DF = 1.15±0.05, n=349; TTX Alone peak DF = 1.60±0.08, n=343). We next examined a potential role for ongoing spike activity in the presynaptic changes which emerge after acute mTORC1 activation with PA (Figure 5.1D-F). Using changes in the frequency of mEPSCs as a readout of presynaptic function, we found that application of PA (100μM, 45min) significantly enhanced the frequency of spontaneous mEPSCs. However, when PA was applied alongside the voltage-gated NA channel blocker TTX to inhibit neuronal spiking, PA induced changes in mEPSC frequency were completely ablated (Vehicle Controls, 1.48±0.27Hz, n=9; PA, 4.89±1.17Hz, n=11; PA+TTX, 1.16±0.31Hz, n=13; TTX Alone, 2.21±0.72Hz, n=8). Comparable increases in postsynaptic function, using changes in mEPSC Amplitude as a readout, were not observed as a consequence of PA or TTX treatment (Vehicle Controls, 17.67±1.54pA, n=9; PA, 16.19±0.76pA, n=11; PA+TTX, 14.04±0.99pA, n=13; TTX Alone, 15.39±0.96pA, n=8). Together these data clearly indicate an important role for ongoing spike activity in the expression of altered presynaptic function driven by acute mTORC1 activation or loss of excitatory input.

Critical role for presynaptic UPS function during homeostatic plasticity

Active protein turnover driven by UPS-dependent degradation has been implicated in several forms of synaptic plasticity, and recent work indicates that protein breakdown might act in concert with new protein synthesis to dynamically shape the synaptic proteome. To examine a potential role for proteasomal degradation in synaptic homeostasis after loss of excitatory input, we subjected neurons to pharmacological blockade of UPS function using Lactacystin (Lac, 10μM), and assessed changes in spontaneous synaptic current after blockade of AMPA receptors (CNQX, 40μM 3Hrs, followed by washout). Similar to our previous results (Jakawich et al., 2010; Henry et al., 2012), we found that transient loss of synaptic drive elicits a robust compensatory increase in both the amplitude and frequency of spontaneous mEPSCs (Figure 5.4A). Interestingly, while the change in mEPSC amplitude was unaltered by concurrent blockade of UPS function with Lac (Control, 13.10±0.69pA, n=11; CNQX, 15.16±0.61pA, n=14; CNQX+Lac, 14.06±0.66pA, n=9), we found that homeostatic increases in mEPSC Frequency were completely blocked under conditions of co-application of CNQX and Lac

(Control, 2.9±0.67Hz, n=11; CNQX, 4.47±0.85Hz, n=14; CNQX+Lac, 1.53±0.51Hz, n=9). To verify that this Lac-sensitive change in mEPSC frequency reflects an alteration in presynaptic function, we performed live imaging experiments with cultured hippocampal neurons expressing vglut-pH-mCH (Figure 5.4B). In line with our previous results (Figure 5.3), brief loss of excitatory input (CNQX, 40μM, 3 Hr) elicits a compensatory increase in the peak levels of fluorescence intensity evoked by a 10Hz, 10s field stimulus (Control peak DF = 1.34±0.06, n=628; CNQX peak DF = 2.31±0.27, n=120). Concurrent inhibition of proteasome function via pre-treatment of Lactacystin (10μM) or MG132 (10μM) completely eliminated this CNQX-induced increase in presynaptic function (CNQX+MG132 peak DF = 1.38±0.07, n=400; CNQX+Lac peak DF = 1.71±0.18, n=57). Collectively, these data indicate that UPS function is vital for the emergence of presynaptic functional homeostasis after loss of excitatory input.

We next examined whether UPS function is necessary in the pre- or postsynaptic compartment for the expression of presynaptic homeostasis. To perturb proteasome activity in specific synaptic compartments, we expressed a WT or mutant version of ubiquitin carrying a K48R point mutation. The formation of polyubiquitinated chains at this K48 residue serves as a canonical signal for proteasome mediated degradation, and overexpression of K48R ubiquitin thus acts as a dominant negative to eliminate UPS function without altering other aspects of ubiquitin-mediated signaling. We first performed whole cell voltage clamp recordings of spontaneous excitatory currents from neurons expressing WT or K48R ubiquitin. Recording from sparsely transfected cultures assures manipulation of postsynaptic UPS function, while presynaptic proteasome activity remains normal in the vast majority of synapses impinging on the recorded neuron (Figure 5.4C). Compared to neurons expressing GFP alone, expression of dominant negative K48R ubiquitin had no effect on the extent to which mEPSC frequency increased in response to CNQX treatment (GFP Vehicle, 0.53±0.13Hz, n=16; GFP CNQX, 1.77±0.55Hz, n=14; K48R vehicle, 0.41±0.11Hz, n=10; K48R CNQX, 1.61±0.59Hz, n=12). In contrast to our previously reported role for postsynaptic mTOR (Henry et al., 2012), these data suggest that postsynaptic UPS function is dispensable for presynaptic alterations during synaptic homeostasis. The same was not true under conditions of presynaptic UPS inhibition, however. Here, we expressed WT or K48R ubiquitin alongside vglut-pH-mCH to assess changes in presynaptic function directly after loss of excitatory input (Figure 5.4D). Compared to neurons expressing WT ubiquitin, cells exhibiting impaired UPS function in the presynaptic domain displayed no compensation in evoked neurotransmission after AMPAR blockade (WT Vehicle Peak DF, 1.26±0.09, n=442; WT CNQX Peak DF, 1.85±0.12, n=496; K48R Vehicle Peak DF, 1.13±0.04, n=238; K48R CNQX Peak DF, 1.14±0.04, n=792), suggesting that proteasomal degradation is required presynaptically for homeostatic changes to emerge in this synaptic compartment.

A critical feature of this form of synaptic homeostasis induced by loss of excitatory input is the postsynaptic synthesis and release of BDNF as a retrograde signal (Jakawich et al., 2010; Henry et al., 2012). The finding that postsynaptic UPS function is nonessential for the expression of presynaptic changes under such conditions suggests that BDNF release operates upstream of the proteasome. As such, the effects of exogenous BDNF application on presynaptic function should be sensitive to inhibition of UPS function. Similar to previous reports, we find that acute application of BDNF (250ng/ml, 2Hrs), significantly increases presynaptic function, using changes in mEPSC frequency (Vehicle Control, 2.27±0.71Hz, n=7; BDNF, 5.98±1.27Hz, n=7), a-syt antibody uptake and evoked changes in vglut-pH fluorescence intensity (Vehicle Control peak DF, 1.22±0.038, n=724 synapses; BDNF peak DF, 1.79±0.05, n=808 synapses) as a readout

(Figure 5.4E-3F, 5.5A). Notably, we found that pharmacological inhibition of proteasome activity completely blocked BDNF-induced increases in presynaptic release as assessed via changes in mEPSC frequency (Lact Alone, 1.92±0.17Hz, n=5; BDNF + Lac, 2.88±0.83Hz, n=7; MG132 alone, 2.07±0.42Hz, n=6; BDNF+MG132, 2.49±1.04Hz, n=7), proportion of a-syt uptake or evoked changes in vglut-pH intensity (BDNF + Lac, 1.18±0.04Hz, n=715; BDNF+MG132, 1.18±0.05, n=305), indicating that UPS activity is essential for BDNF-induced changes in presynaptic function.

Our previous work shows that activation of postsynaptic mTORC1 via genetic upregulation of Rheb or application of the lipid second messenger PA is sufficient to drive dendritic synthesis of BDNF, resulting in a state-dependent enhancement in presynaptic efficacy (Figures 5.1, 5.3). Critically, this change in presynaptic function after acute activation of mTORC1 signaling operates through an identical pathway to that utilized during homeostatic increases in presynaptic function after loss of excitatory input (Henry et al., 2012). To assess, whether the effects of acute mTORC1 activation on presynaptic function are also sensitive to proteasome inhibition, we performed whole cell recordings in cultured neurons subject to UPS blockade with MG132 or Lactacystin, then exposed to PA containing vesicles (100μM, 45 min) to acutely drive increased mTORC1 kinase activity (Figure 5.5B). In line with a conserved pathway shared between CNQX-driven presynaptic homeostasis and the effects of acute mTORC hyperactivation, we found that proteasome inhibition eliminated increased mEPSC frequency after PA treatment (Vehicle control, 1.0±0.15Hz, n=10; PA, 3.20±0.74Hz, n=10; PA+MG132, 1.71±0.42Hz, n=12; PA+Lac, 0.60±0.15Hz, n=10). Nether PA administered alone, nor in combination, exerted a significant effect on the amplitude of spontaneous excitatory currents (Vehicle control, 15.97±0.76pA, n=10; PA, 15.51±0.99pA, n=10; PA+MG132, 14.08±0.83pA, n=12; PA+Lac, 15.91±1.03pA, n=10).

Activity-dependent redistribution of the presynaptic UPS

Recent work has demonstrated the striking phenomenon of proteasomal sequestration at synaptic regions in dendritic spines in response to strong neuronal depolarization or NMDA receptor stimulation (Bingol and Schuman, 2006; Bingol et al., 2010). Given the dual necessity for presynaptic UPS function and ongoing spike activity for adaptive presynaptic homeostasis after loss of excitatory input, we next examined the possibility that altered neuronal activity could impact proteasome distribution in axons, and whether this altered localization could impact the expression of functional homeostasis. To assess a potential contribution of neuronal activity to presynaptic localization of the UPS, we expressed a FLAG-tagged subunit of the 19S regulatory cap of the proteasome (FLAG-Rpt3) alongside mCherry-synaptophysn (mCH-Syn) to label presynaptic terminals. Neurons were treated with the GABA-A blocker Bicuculine or the voltage-gated sodium channel blocker TTX to increase or decrease neuronal activity for 2 hours, respectively (Figure 5.6A). After this brief period of activity manipulation, we found a remarkable increase in the intensity of FLAG signal at mCH-Syn positive regions in neurons treated with Bicuculine. Conversely, in cells subject to action potential blockade with TTX, we observed a significant loss of proteasome-related fluorescence signal at synaptic boutons (Nomalized Control FLAG-Rpt3 Intensity, 100±22.17%, n=12 images; Normalized Bicuculine FLAG-Rpt3 Intensity, 176.10±50.72% of control, n=11 images; Normalized TTX FLAG-Rpt3 Intensity, 56.82±12.86% of control, n=12 images). In a separate set of experiments, we assessed changes in presynaptic localization of an alternate proteasome subunit (Ha-Rpt6) in response to loss of synaptic input with CNQX (Figure 5.7A). While AMPAR blockade (CNQX, 40μM, 3Hrs) did not significantly change proteasome-related fluorescence signal at presynaptic boutons, concurrent blockade of action potentials with TTX produced a similar loss of synaptically localized proteasome during CNQX as we previously observed during TTX treatment alone. This suggests that AMPAR blockade with CNQX does not completely block spiking activity in dissociated cultures, as reported previously (Jakawich et al., 2010), and provides potential insight into the mechanism responsible for why action blockade eliminates CNQX-induced presynaptic homeostasis.

The proceeding set of experiments provided an analysis of steady state presynaptic proteasome localization under different activity manipulations, but did not provide information regarding the timing of proteasome relocalization during activity manipulations. To assess activity-dependent proteasome redistribution in real time, we performed live-imaging experiments of GFP-tagged proteasome subunits (GFP-Rpt6) under conditions of activity blockade with TTX (1μM). We observed a progressive loss of proteasome-related GFP signal in synaptic boutons over the course of a 30 min exposure to TTX (Figure 5.6C, Yellow box). Interestingly, we found a similar increase in extrasnaptically localized GFP signal in the same set of axons over the course of action potential blockade (Figure 5.6C, red box). This suggests intrinsic spiking activity drives the relocalization of the UPS into and out of synaptic regions in axons. Strikingly, brief depolarization (60mM K+, 5 min) resulted in an immediate reversal of GFP-Rpt6 localization, such that synaptic proteasome levels were comparable to pre TTX levels and extrasynaptic regions were largely devoid of UPS-related fluorescence signal (Relative change in synaptic GFP Fluorescence 15 min-post TTX, -11.82±4.21%, n=32; 30 min post-TTX,

-22.39±5.45%; 5 min post-60mM K+, 22.29±5.42%; Relative change in extrasynaptic GFP Fluorescence 15 min-post TTX, 16.43±8.03%, n=32; 30 min post-TTX, 23.50±11.66%).

Though the preceding experiments provide compelling evidence for activity-dependent redistribution of the UPS in axons, it is unclear whether this relocalization proceeds as a course of microtubule based cargo transport or instead occurs due the paired action of free proteasomal diffusion and active sequestration, as has been suggested to occur in dendritic spines (Bingol and Schuman, 2006). To address the mechanisms behind altered UPS localization in axons, we performed live imaging experiments in neurons expressing mCH-Syn as well as the 19S proteasome subunit Rpt6 fused to photoactivatable GFP (PAGFP-Rpt6). In one set of experiments we targeted extrasynaptic regions for photoactivation and monitored movement of Rtp6-associated fluorescence throughout the axon. The example experiment shown in Figure 5.8A is representative of our repeated observations, wherein extrasynaptic photoactivation elicits a brief rise in fluorescence intensity in the targeted extrasynaptic region, which then rapidly spreads into nearby regions of the axon, displaying both retrograde and anterograde patterns of movement. We found striking differences in the longevity of fluorescence intensity in extrasynaptic regions compared to synaptic regions of interest over the course of the imaging session. After photoactivation, PAGFP signal intensity rapidly diminishes back down to baseline levels in extrasynaptic regions, indicating movement of Rpt6 away from this region of the axon (Figure 5.8B, black trace). In contrast, after invasion of nearby synaptic regions, Rpt6-PAGFP intensity tends to remain steady for much longer periods of time, here failing to reach baseline levels within the 200s imaging session (Figure 5.8B, blue and red traces). This suggests the existence of an active tethering mechanism at work to preserve proteasome localization at synaptic regions that is not present in axonal shafts. Group data averaged across multiple experiments supports this notion (Figure 5.8C), with striking differences in the decay rates between extrasynaptic and synaptic regions. To examine whether this tethering mechanism at synaptic boutons could be influenced by neuronal spike activity, we performed similar sets of experiments but targeted synaptic, rather than extrasynaptic, regions for photoactivation and monitored loss of PAGFP-Rpt6 fluorescence over time (Figure 5.8D). Compared with vehicle-treated control cells, neurons subject to increased spike activity for a period of 2 Hrs (Bicuculine, 10μM) showed a dramatic increase in the longevity of PAGFP fluorescence intensity remaining at boutons after photoactivation (Figure 5.8E-5.8F), indicating that sequestration of proteasomes at presynaptic regions in the axon is subject to modulation via changes in spike output.

Phosphorylation of the 19S Rpt6 subunit is critical for activity-driven UPS redistribution and presynaptic functional homeostasis

How do changes in spike activity lead to altered proteasome longevity at presynaptic terminals? Recent work has identified a serine residue on the Rpt6 subunit of the 19S cap, phosphorylation of which influences the synaptic localization of the proteasome at postsynaptic regions in dendritic spines (Bingol et al., 2010). Phosphorylation of Rpt6 at S120 is regulated by neuronal activity, and overexpression of Rpt6 point mutants at this site can have profound effect on postsynaptic function (Djakovic et al., 2012). Given the strong influence spike activity exerts over proteasome localization in axons and retention rates at presynaptic boutons, we next examined whether manipulations of the Rpt6 phosphorylation at S120 could impact UPS localization and synapse function presynaptically. We first examined how overexpression of phosphor-dead (S120A) or phospho-mimetic (S120D) Rpt6 mutants alters retention rates of photoactivated proteasomal subunits at presynaptic boutons. Neurons were transfected with mCh-Syn to label presynaptic regions, as well as either WT, S120A or S120D Rpt6 fused to PAGFP (Figure 5.9A). Representative examples of time-dependent loss of PAGFP intensity for each group can be seen in Figure 5.9B. Fluorescence decay rates differed markedly as a consequence of S120 phosphorylation status (Figure 5.9C). Compared to cells expressing WT-Rpt6, S120A-Rpt6 overexpression significantly increased the speed of UPS-related fluorescence loss after photoactivation at presynaptic boutons (WT-Rpt6 time to reach ½ max, 57.8±8.29s, n=15 boutons; S120A-Rpt6 time to reach ½ max, 37.62±3.11s, n=13). This effect was bidirectional, as overexpression of the phosphomimetic S120D Rpt6 point mutant resulted in a significant increase in the longevity of photoactivated proteasomes at synapses (S120D-Rpt6 time to reach ½ max, 90.21±12.55s, n=14 boutons). In line with our previous data in which activity manipulations exert similar influence over UPS retention rates ad steady state levels at presynaptic boutons, we found that manipulation of Rpt6S120 phosphorylation was also sufficient to alter steady state levels of the proteasome at synaptic regions. Here, we expressed HA-tagged Rpt6 variants (WT, S120A, S120D) with mCH-Syn to assess proteasome localization at presynaptic regions (Figure 5.10). We found that alterations in S120 phosphorylation exert effects on steady-state UPS localization in axons that mirror those seen after activity manipulation with Bicuculine or TTX, such that the S120A mutation reduces HA-tagged Rpt6 localization, and the S120D mutation increases HA-tagged Rpt6 levels at mCH-Syn positive regions in axons (Normalized control HA Intensity, 100±17.68%, n=30; Normalixzed S120A HA Intensity, 58.34±11.68% of control, n=30; Normalized S120D HA Intensity, 151.78±32.66% of control, n=20). Operating under the assumption that exogenously expressed Rpt6 mutants become incorporated into endogenous proteasomes, overexpression of S120A or S120D-Rpt6 should be sufficient to alter the localization of other proteasomal subunits within the same complex. To examine this, we expressed WT, S120A or S120D-Rpt6 alongside mCh-Syn, and assessed intensity of co-expressed FLAG-tagged Rpt1 signal at presynaptic boutons (Figure 5.9D). Similar to our findings with altered localization of HA-tagged Rpt6 mutants alone (Figure 5.10), we found that expression of S120A-Rpt6 resulted in a significant decrease in presynaptic FLAG-Rpt1 signal, while expression of S120D-Rpt6 caused a significant increase in presynaptic FLAG-Rpt1 signal compared to neurons expressing WT-Rpt6 (Normalized control FLAG Intensity, 100±12.74%, n=26; Normalixzed S120A FLAG Intensity, 60.23±9.66% of control, n=20; Normalized S120D FLAG Intensity, 153.69±27.83% of control, n=9). Together these data indicate that phosphorylation of the 19S Rpt6 subunit at S120 exerts a powerful influence over presynaptic UPS localization and retention rates at boutons.

Under conditions of baseline Rpt6 phosphorylation, increased neuronal activity via GABA-A receptor inhibition (Bicuculline, 10μM, 2Hr) results in elevated co-localization of FLAG-tagged Rpt3 at presynaptic boutons (Figure 5.6A-B). If the activity-dependent phosphorylation of Rpt6 at S120 is important from this redistribution of the UPS after enhanced spike output, then overexpression of the phospho-dead S120A Rpt6 mutant should block this change in presynaptic proteasomal accumulation. In neurons expressing GFP-tagged WT Rpt6, we repeat our earlier described observation of enhanced localization of UPS components at presynaptic terminals after treatment increased spiking activity (Figure 5.11A-B). However, under conditions of S120A-Rpt6 overexpression, GFP fluorescence intensity in mCH-Syn positive regions was indistinguishable between neurons treated with Bicuculine and vehicle-treated controls, suggesting that phosphorylation of Rpt6 at S120 is a necessary component of the mechanism by which proteasome distribution is regulated by neuronal activity. The experiments described in Figures 5.3-5.6 indicate the necessity of neuronal spike activity as well as functional UPS-mediated degradation for the expression of functional homeostasis at presynaptic terminals after loss of excitatory input. However, thus far a direct link between proteasome localization and adaptive changes in presynaptic function has not been made. As such, we next utilized overexpression of S120A-Rpt6 to shift the distribution of proteasomes away from synaptic boutons and examined what, if any, effect the resultant lack of UPS activity in presynaptic regions would have on CNQX-mediated changes in vesicle release (Figure 5.12C-D). In line with our earlier observations, evoked changes in vglut-pH intensity were dramatically enhanced after a brief period of AMPAR blockade (CNQX, 40μM, 3Hrs) in neurons expressing WT-Rpt6 (WT-Rpt6 Vehicle Peak DF, 1.23±0.07, n=248 boutons; WT-Rpt6 CNQX Peak DF, 2.51±0.14, n=287 boutons). Conversely, neurons expressing the phospho-dead S120A-Rpt6 point mutant showed significantly reduced changes in evoked neurotransmission after synaptic deprivation (S120A-Rpt6 Vehicle Peak DF, 1.23±0.09, n=237 boutons; S120A-Rpt6 CNQX Peak DF, 1.75±0.12, n=331 boutons). The slight, but statistically significant compared to controls, increase in vglut-pH fluorescence intensity which remains in S120A expressing cells (Figure 5.12D) is likely due to a failure of the S120A-Rpt6 mutant subunit to incorporate in all endogenous proteasome complexes. We observe a similar dependence on Rpt6 S120 phosphorylation for the expression of functional changes in spontaneous neurotransmission after AMPAR blockade (Figure 5.12). When expressing WT-Rpt6, neurons live labeled with an antibody against the lumenal domain of synaptotagmin show increased spontaneous vesicle release at excitatory synapses in response to CNQX treatment (Proportion of a-syt uptake in WT-Rpt6 controls, 0.26±0.05, n=23; proportion of a-syt uptake in WT-Rpt6 CNQX, 0.46±0.07, n=23; proportion of a-syt uptake in S120A-Rpt6 controls, 0.19±0.06, n=27; proportion of a-syt uptake in S120A-Rpt6 CNQX, 0.25±0.05, n=27). Given that presynaptic adaptations after

AMPAR blockade are driven by dendritically released BDNF (Jakawich et al., 2010; Henry et al, 2012), the effects of acute BDNF on presynaptic function should also be sensitive to altered distribution of the UPS in axons. We took advantage of the relatively fast-acting effects of exogenously applied BDNF to assess within-synapse changes in evoked neurotransmission in cells expressing WT or S120A-Rpt6. We collected vglut-pH responses to two identical stimuli, one administered prior to BDNF treatment and another 30 min after BDNF exposure (Figure 5.11E). Under conditions of WT-Rpt6 expression, acute BDNF treatment (250ng/μl, 30 min) produced a dramatic increase in evoked vlgut-pH fluorescence intensity (WT-Rpt6 Vehicle, 68.02±6.69% of max response to stim 1, n=139 boutons; WT-Rpt6 BDNF, 179.39±9.26% of max response to stim 1, n=217). However, driving proteasome distribution away from synaptic boutons by overexpression of S120A-Rpt6 completely eliminated BDNF-induced increases in evoked neurotransmission (S120A-Rpt6 Vehicle, 67.53±7.50% of max response to stim 1, n=35; S120A-Rpt6 BDNF, 51.59±2.47% of max response to stim 1, n=365), signaling that activity dependent phosphorylation of Rpt6 acts an important precondition for this form of plasticity.

Our previous results suggest that the mechanisms responsible for altered proteasome localization at presynaptic terminals are sensitive to baseline rates of spike activity, such that action potential inhibition with TTX drives an altered distribution away from synaptic boutons (Figure 5.6). If phosphorylation of Rpt6 at S120 is an important component of this mechanism, then overexpression of the phosphomimentic S120D point mutant of Rpt6 should obviate the requirement of neuronal activity for increased UPS localization at synapses. In neurons expressing GFP-tagged WT Rpt6, we replicate our earlier finding of diminished proteasome localization of at presynaptic terminals after a brief period of spike blockade with TTX (Figure 5.13A-B). However, under conditions of S120D-Rpt6 overexpression, GFP fluorescence intensity in mCH-Syn positive regions was not statistically different between neurons treated with TTX and vehicle-treated controls (Normalized GFP intensity WT-Rpt6 Control, 100±16.09%, n=13; Normalized GFP intensity WT-Rpt6 TTX, 59.79±10.67% of control, n=21; Normalized GFP intensity S120D-Rpt6 Control, 100±19.93%, n=16; Normalized GFP intensity S120D-Rpt6 TTX, 98.37±21.46%, n=19). This supports the notion that neuronal activity drives altered proteasome localization through a process involving the phosphorylation of Rpt6 at S120, and that mimicking phosphorylation at this site is sufficient to bypass the need for enhanced spike activity in driving the UPS to synaptic terminals. We have shown that state-dependent presynaptic homeostasis can be blocked by pharmacological disruption of neuronal spiking (Figure 5.3). As such, driving proteasomes to synaptic boutons via overexpression of S120D-Rpt6 should render functional changes in presynaptic release impervious to TTX blockade of CNQX-induced adaptation. We assessed changes in evoked neurotransmission under conditions of simultaneous AMPAR blockade and spike inhibition in neurons expressing S120D-Rpt6 (Figure 5.13C-D), and found that these synapses exhibited equivalent levels of augmented presynaptic release under conditions of AMPAR blockade alone or AMPAR blockade paired with spike inhibition (S120D-Rpt6 Vehicle Peak DF, 0.89±0.05, n=515 boutons; S120D-Rpt6 CNQX Peak DF, 1.65±0.08, n=622; S120D-Rpt6 CNQX+TTX Peak DF, 1.76±0.08, n=571; S120D-Rpt6 TTX ALone Peak DF, 1.24±0.09, n=208). Critically, these results are not due to more generalized changes in vesicle pool dynamics, as overexpression of S120A-Rpt6 or S120D-Rpt6 does not alter the recycling pool or total release pool of vesicles (Figure 5.14), as assessed using previously established methods (Kim and Ryan, 2010).

5.4 Discussion

Presynaptic UPS and synapse function

Previous reports suggest that manipulations of UPS function can impact presynaptic release properties, wherein inhibition of protesome activity on its own is sufficient to increase neurotransmitter release (Willeumier et al., 2006; Rinetti and Schweizer, 2010). While we do not find similar changes in presynaptic release driven by manipulations of UPS function alone, our work adds to a growing body of evidence indicating that proteasomal degradation can fine tune presynaptic function. Our finding of an activity-dependent role for UPS-mediated degradation in axons shares some commonality with recent reports of activity-dependent "presynaptic silencing", wherein prolonged depolarization leads to an increase in proteasome enzymatic activity at presynaptic terminals (Jiang et al., 2010). However, rather than enhanced presynaptic UPS activity eliciting an increase in presynaptic efficacy as we observe here, Jiang et al. report a decrease in the number of active synapses and reduced size of the recycling pool. It is possible that these divergent findings are a result of the different methods of enhancing neuronal activity, using pharmacological silencing of GABA-A receptors or field stimulation in the experiments described here versus several hours of exposure to a high K+ solution (Jiang et al., 2010). It seems likely that these different functional outcomes arise in response to the degradation of unique sets of presynaptic proteins in each condition. While chronic depolarization with a high K+ solution has been shown to lead to the degradation of Rim-1 and Munc13-1 (Jiang et al. 2010), the target of UPS-mediated degradation which mediates our observed increase in presynaptic function remains unidentified.

Previously verified presynaptic targets of activity-dependent proteasomal degradation include scaffolding proteins such as Bassoon, liprin-a, and liprin-a2 (Lazarevic et al., 2011;

Spangler et al., 2013), components of the vesicle release machinery including syntaxin 1 (Chin et al., 2002), synaptophysin (Wheeler et al., 2002), UNC-13 (Aravamudan and Broadie, 2003; Speese et al., 2003), and SNAP-25 (Sharma et al., 2011) as well as presynaptic voltage-gated ion channels such as Cav2.2 (Waithe et al., 2011; Marangoudakis et al., 2012). It will be of crucial interest for future work to identify the target of presynaptic degradation in the type of plasticity we describe here. Given the nature of the change in presynaptic function we observe, wherein degradation of a presynaptic protein results in an increase in synaptic release, it is sensible to assume that the target is a protein which normally serves to constrain vesicle release. Such a mechanism would share similar features to previously reported instances of the UPS operating in the context of synaptic plasticity through the degradation of proteins that normally serve to constrain synapse strength (Zhao et al., 2003), including the R subunit of PKA (Hegde et al., 1993) and the CREB repressor, CREB1b (Upadhya et al., 2004). Potential candidate targets of presynaptic degradation which could fit such a model include Slp4-A, which inhibits vesicle release via an interaction with the small GTPase Rab27 (Fukada 2003), and tomosyn, a syntaxin1-binding protein that has been shown to exert an inhibitory effect on vesicle fusion (Fujita et al., 1998; Yizhar et al., 2004; Gracheva et al., 2007).

The mechanisms by which specific proteins are targeted for degradation are complex, and subject to a high degree of activity-dependent modification (Hegde, 2010). Attachment of an ubiquitin protein to a degradation target occurs in a multistep process, involving the action of E1, E2 and E3 classes of enzymes. However, specificity of substrate targeting is achieved primarily via action of the E3 ubiquitin ligase. Thus, the identity of the specific presynaptic proteins targeted for proteasomal degradation here could potentially be linked to the identity of the specific E3 ligase at work. Relatively few ubiquitin ligases have been localized to presynaptic subdomains in neurons. Among the identified examples include SCRAPPER, which targets RIM1 (Yao et al., 2007), Siah, which targets synaptophysin, β-catenin, α-synuclein, and synphilin-1 (Waites et al., 2013), Phr1, which targets DLK (Lewcock et al., 2007), and staring, which is believed to regulate degradation of syntaxin 1 (Chin et al., 2002). It will be important for future studies to investigate a potential role for these or other as yet unidentified E3 ligases in mediating the type of state-dependent presynaptic compensation we describe here.

Activity dependent relocalization of the proteasome

Studies performed in yeast (Russell et al., 1999) and mammalian cells lines (Brooks et al., 2000) suggest that the proteasome occupies a predominantly nuclear subcellular localization under baseline conditions in many cells types. However, biochemical analyses of proteasome activity in specific neuronal subcellular compartments have indicated that UPS-mediated degradation is higher in synaptic regions than in the nucleus (Upadhya et al., 2006), which suggests a role for activity-dependent redistribution. Previous work in neuronal cells suggests that activation of PKC or treatment with the GABA-A receptor blocker Bicuculline causes the translocation of the 20S proteasome from the nucleus into the cytoplasm and dendritic subdomains (Shen et al., 2007). Notably, deletion of the cocaine-regulated protein NAC1 has been found to prevent proteasome translocation after Bicuculine but has no effect on PKC-mediated relocalization. These data provided an initial indication that neurons utilize multiple mechanisms of proteasomal redistribution, one of which may involve direct phosphorylation of the proteasome itself (Glickman and Raveh, 2005).

In vitro studies suggest that phosphorylation of the Rpt6 subunit of the 19S regulatory complex is essential for assembly and proper function of the 26S proteasome (Satoh et al., 2001).

This work has been supported by findings in neuronal cultures, wherein phosphorylation of Rpt6 at S120 has also been reported to enhance proteasome activity (Djakovic et al, 2009, Bingol et al., 2010). The findings described here add to the complexity of activity dependent regulation of proteasome function, by demonstrating that phosphorylation of the 19S regulatory subunit Rpt6 at S120 also plays an important role in the redistribution of proteasomes into presynaptic regions. A similar role for Rpt6 phosphorylation has recently been demonstrated in activity-dependent postsynaptic redistribution (Djakovic et al., 2012). Given the importance of phosphorylation of Rpt6 in guiding redistribution of the proteasome to presynaptic terminals, an important remaining question regards the identity of the upstream kinase at work. To date, both PKA and CaMKII have been shown to phosphorylate Rpt6 at S120 (Zhang et al., 2007; Djakovic et al., 2009), though only CAMKII has been directly implicated in activity-dependent phosphorylation of Rpt6 resulting in altered synaptic function (Djakovic et al., 2012). Interesting recent evidence suggests that phosphorylation of Rpt6 at S120 in the amygdala by CaMKII, but not PKA, is critical for the formation of long-term fear memories (Jarome et al., 2013), though from these data it is not possible to ascertain whether this depends predominantly on either pre- or postsynaptic phosphorylation of Rpt6.

Interaction between UPS and BDNF signaling in expression of functional changes

Phosphorylation of Rpt6, while clearly important for activity-dependent proteasome redistribution in axons, cannot fully account for the functional changes we observe after AMPAR blockade. Overexpression of the phospho-dead S120A point mutant of Rpt6, while sufficient to significantly alter proteasome localization at presynaptic terminals (Figure 5.10D) and rates of retention after photoactivation (Figure 5.10C), had no effect on evoked neurotransmission on its own when compared to cells expressing Rpt6WT (Figure 5.12D). Similar results were observed in cells expressing the phospho-mimetic S120D mutation of Rpt6, wherein increased localization of proteasomes to synaptic boutons was not sufficient to exert changes on presynaptic function on its own (Figure 5.10, Figure 5.14). A crucial component of the changes in presynaptic function we observe after AMPAR blockade or treatment with PA is the synthesis and release of BDNF from the postsynaptic compartment as a retrograde signal (Henry et al., 2012). In line with this model, we find that a brief (2Hr) treatment with BDNF results in a marked increase in neurotransmitter release (Figure 5.4E-F, 5.5B, 5.12F), an effect which has been reported previously in hippocampal cultures (Lessmann and Heumann, 1998; Jakawich et al., 2010) and slices (Gottschalk et al., 1998) and has been shown to depend on intact presynaptic TrkB receptor signaling (Li et al., 1998). We build upon this work, demonstrating that this effect can be inhibited by blocking presynaptic UPS function (Figure 5.4) or inhibiting synaptic proteasome localization (Figure 5.11). However, it is not clear how BDNF signaling interacts with presynaptically localized UPS to result in enhanced neurotransmitter release. BDNF activation of TrkB can elicit changes in cellular function through three major routes, which include the MAPK/ERK, PI3K, and PLCγ signaling pathways (Patapoutian and Reichardt, 2001). It is conceivable that the activity of one of these pathways may exert an influence on the target specificity or activation properties of presynaptically localized UPS. The most well characterized peptidase actions of the 20S proteasome include trypsin-like, chymotrypsin-like, and peptidyIgIutamyl-peptide hydrolyzing (PGPH) activity (Coux et al., 1996). Manipulations of specific peptidase actions can have unique effects on cell function, as, for example, inhibition of chymotrypsin-like, but not trypsin-like or PGPH activity, induces neurite outgrowth in Neuro2A cells (Fenteany and Schreiber, 1996). Interestingly, previous assessments of proteasome activity in specific neuronal subcompartments have identified that MAPK signaling enhances chymotrypsin-like activity in synaptosomal, but not nuclear, fractions from mouse brain homogenates (Upadhya et al., 2006). An intriguing, though as yet untested, possibility is that BDNF/TrkB-mediated activation of presynaptic MAPK signaling leads to an increase in presynaptic chymotrypsin activity, which in turn mediates enhanced vesicle release through the degradation of a specific protein or sets of proteins.

Altered longevity at boutons vs active trafficking

Our data does not appear to support a role for activity-dependent redistribution of the proteasome as a consequence of active transport of cargo along microtubules. Instead, it appears more likely that the presynaptic terminal somehow acts as diffusion sink similar to the proposed role of the postsynaptic density of excitatory synapses in tethering AMPA receptors (Bressloff and Earnshaw, 2007). Our photoactivation data (Figure 5.8) shows that photoactivated proteasome subunits travel from the site of photoactivation to nearby synaptic regions quite rapidly. This movement is much faster than what would be expected for microtubule based transport of cytosolic proteins in the axon, which have been reported to travel at speeds of ~2-8mm/day (Brown, 2003). Additionally, previous work examining microtubule based trafficking of cytosolic proteins tagged with PA-GFP have identified a distinct anterograde bias to this type of transport in axons (Scott et al., 2011), an effect which is clearly not seen after photoactivation of PAGFP-Rpt6 in our experiments (Figure 5.8A). Rather than relying on microtubule-based transport, our data suggest a model wherein proteasomes are able to diffusely move through the axon, and are eventually captured and retained at presynaptic boutons in response to activity. Our results indicate that this sequestration mechanism is activity dependent (Figure 5.6), and suggest that it is likely to be specific for proteasomes in which the S120 residue on the Rpt6 regulatory subunit is phosphorylated, based on the fact that expression of phospho-memetic or phospho-dead point mutants of Rpt6 are sufficient to exert profound changes on proteasome localization and functional adaptation to AMPAR blockade (Figure 5.9-5.12). If it is indeed the case that phosphorylated proteasome are captured and retained at presynaptic terminals, the question remains as to the mechanism by which proteasomes are sequestered. In keeping with notion that proteasomes become bound to the actin cytoskeleton in spines in response to strong synaptic stimulation (Bingol and Schuman, 2006), recent evidence shows that phosphorylation at S120 of the 19S RPT6 subunit enhances proteasome resistance to detergent extraction, suggesting increased association with cytoskeleton or scaffolding proteins (Djakovic et al., 2012). Our data is parsimonious with a similar model in which proteasomes diffuse throughout axons and become tightly associated with actin-rich boutons upon activity dependent phosphorylation of the Rpt6 subunit. Further experiments will be necessary to determine if proteasome redistribution to presynaptic regions depends on an interaction with the actin cytoskeleton, or perhaps with another as yet unidentified scaffolding protein.

5.7 Acknowledgements

This work was supported by Grants F31MH093112 (F.E.H.) and RO1MH085798 (M.A.S.) from The National Institute of Mental Health and a grant from the Pew Biomedical Scholars Program (M.A.S.). We also thank Hisashi Umemori and members of the Sutton laboratory for many helpful discussions. We thank Robert Edwards for generously providing vglut1-pHluorin. Plasmids encoding FLAG-Rpt3, HA-Rpt6, GFP-Rpt6, HA-Rpt6 S120A, HA-

Rpt6 S120D, PAGFP-Rpt6 WT, PAGFP-Rpt6 S120A, and PAGFP-Rpt6 S120D were all generously provided by Dr. Gentry Patrick (USCD).

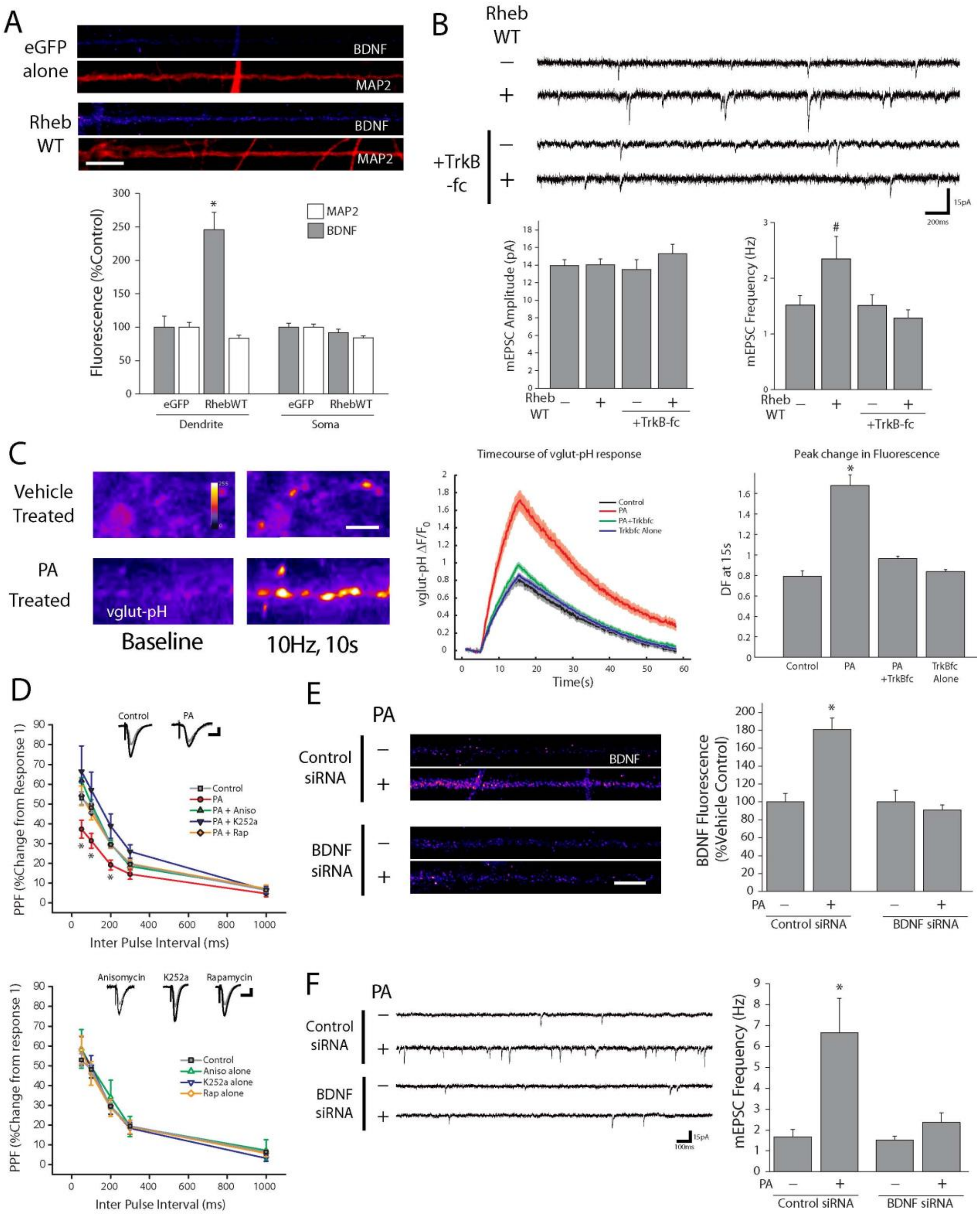
A
eGFP alone
BDNF
MAP2
Rheb WT
BDNF
MAP2
Fluorescence (%Control)
300
250
200
150
100
50
0
*
MAP2
BDNF
eGFP
RhebWT
Dendrite
eGFP
RhebWT
Soma
B
Rheb WT
—
+
+TrkB -fc
—
+
15pA
200ms
mEPSC Amplitude (pA)
18
16
14
12
10
8
6
4
2
0
Rheb WT
—
+
—
+
+TrkB-fc
mEPSC Frequency (Hz)
3
2
1
0
#
Rheb WT
—
+
—
+
+TrkB-fc
C
Vehicle Treated
PA Treated
vglut-pH
Baseline
10Hz, 10s
255
0
Timecourse of vglut-pH response
vglut-pH ΔF/F0
2
1.8
1.6
1.4
1.2
1
0.8
0.6
0.4
0.2
0
Control
PA
PA+Trkbfc
Trkbfc Alone
0
10
20
30
40
50
60
Time(s)
Peak change in Fluorescence
DF at 15s
1.6
1.4
1.2
1
0.8
0.6
0.4
0.2
0
*
Control
PA
PA +TrkBfc
TrkBfc Alone
D
Control
PA
PPF (%Change from Response 1)
90
80
70
60
50
40
30
20
10
0
Control
PA
PA + Aniso
PA + K252a
PA + Rap
*
*
*
0
200
400
600
800
1000
Inter Pulse Interval (ms)
Anisomycin
K252a
Rapamycin
PPF (%Change from response 1)
90
80
70
60
50
40
30
20
10
0
Control
Aniso alone
K252a alone
Rap alone
0
200
400
600
800
1000
Inter Pulse Interval (ms)
E
PA
Control siRNA
—
+
BDNF
BDNF siRNA
—
+
BDNF Fluorescence (%Vehicle Control)
200
180
160
140
120
100
80
60
40
20
0
*
PA
—
+
—
+
Control siRNA
BDNF siRNA
F
PA
Control siRNA
—
+
BDNF siRNA
—
+
15pA
100ms
mEPSC Frequency (Hz)
9
8
7
6
5
4
3
2
1
0
*
PA
—
+
—
+
Control siRNA
BDNF siRNA

Figure 5.1: Postsynaptic mTORC1 activation enhances presynaptic presynaptic release via synthesis of BDNF as a retrograde signal. (A) Representative images of BDNF and MAP2 expression in linearized dendritic segments, and mean (+ SEM) fluorescence intensity of MAP2 and BDNF signal in somatic and dendritic compartments normalized to average control values, in neurons treated with expression eGFP alone (n = 35 images) or in combination with RhebWT (n= 35 images). BDNF expression in dendrites was significantly (*$p < 0.05$ by Student's t-test, relative to eGFP controls) enhanced in neurons expressing RhebWT for 24 Hrs, relative to neurons expressing eGFP alone for the same duration. Scale bar represents 10μm in A. (B) Representative recordings and mean (± SEM) mEPSC amplitude and frequency in control nontransfected neurons (n = 25), as well as cells expressing RhebWT (n = 30).The top panel in (B) contains representative traces from vehicle treated group, while the lower panel contain traces from cells subject to treatment with the BDNF scavenger TrkB-fc (1μg/ml; n=12 and 10). Scavenging extracellular BDNF eliminates RhebWT induced increases in mEPSC frequency. (C) Example images of synapses expressing vglut1-pHluorin (vglut-pH) at baseline (left panel) as well as immediately after termination of a 10Hz, 10s stimulus train (right panel). Treatment with phosphatidic acid enhanced the changes in vglut-pHluorin fluorescence intensity, compared to cells treated with vehicle in response to an identical stimulus train. Scale bar represents 10mm in (C). (D) Timecourse of relative change in vglut-pHluorin fluorescence in response to a 10Hz 10s stimulus train, recorded from cells treated with vehicle, PA, TrkB-fc or TrkBfc + PA. Black bar represents onset of 10s stimulus train. Grey: Vehicle control (n = 566 synapses). Red: PA (n = 802 synapses). Green: PA+TrkB-fc (n = 652 synapses). Blue: TrkB-fc alone (n = 750 synapses). Right, mean (± SEM) change in vlgut-pHluorin fluorescence intensity from baseline recorded at the termination of a 10Hz, 10s AP train evoked by field stimulus. Evoked changes in vglut-pHluorin fluorescence intensity were significantly enhanced by treatment with PA, and this effect was blocked by pre-treatment with the BDNF scavenger TrkB-fc. (*$p<0.05$, one-way ANOVA, Tukey–Kramer post hoc) (E) Paired-pulse facilitation (PPF) in acute hippocampal slices. Treatment with phosphatidic acid (100 mM, 45 min) significantly diminished (*$p < 0.05$, relative to vehicle controls) the degree of facilitation induced by paired pulses at 50, 100 and 200 ms intervals. Pre-treatment with anisomycin, rapamycin, as well as the Trk receptor antagonist K252a, blocked this effect. Lower panel, inhibitors have no effect on their own relative to vehicle treated controls. Grey Circles: Control (n = 38 slices); Red Circles: PA (n = 10); Green closed Triangles: PA+Aniso (n = 7 slices); Blue closed triangles: PA+ K252a (n = 8 slices); Orange closed diamonds: PA+ Rap (n = 6 slices); Green open Triangles: Aniso Alone (n = 3 slices); Blue open Triangles: K252a alone (n = 9 slices); Orange open Diamonds: Rap alone (n = 8 slices). Scale bar represents 10ms and 100mV. (F) BDNF expression in linearized dendritic segments (K), and mean (+ SEM) expression BDNF in dendritic compartments normalized to average control values, in neurons subject to magnetofection plus or minus PA (100 μM, 90 min). In neurons transfected with control siRNA, treatment with PA (n = 62) significantly enhanced BDNF expression in dendrites (*$p < 0.05$) compared to vehicle treated cells (n = 55). In neurons transfected with BDNF siRNA, PA application (n = 60) failed to alter dendritic BDNF expression relative to vehicle (n = 49). Scale bar in (F) = 10 μm. (G) Representative recordings and mean (+ SEM) mEPSC frequency (N) in neurons subject to magnetofection plus or minus PA (100 μM, 90 min). Treatment with PA significantly enhanced mEPSC frequency in neurons transfected with the non-targeting control siRNA (*$p < 0.05$, t-test; n = 6) compared to

vehicle treated neurons (n = 8). In neurons transfected with BDNF siRNA, no differences were observed between cells treated with PA (n = 7) or vehicle (n = 5).

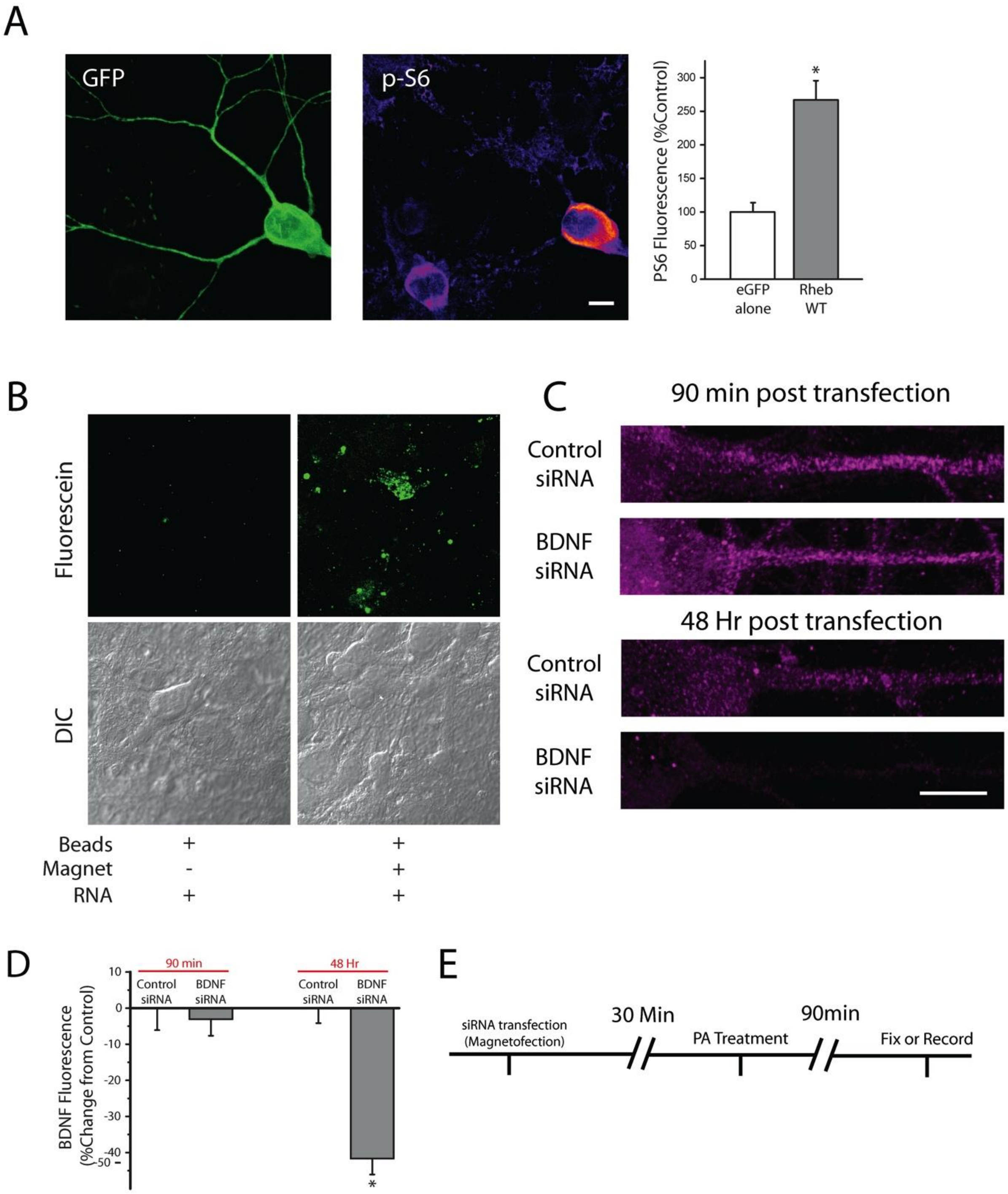
A
GFP
p-S6
PS6 Fluorescence (%Control)
300
250
200
150
100
50
0
*
eGFP alone
Rheb WT
B
Fluorescein
DIC
Beads + +
Magnet - +
RNA + +
C
90 min post transfection
Control siRNA
BDNF siRNA
48 Hr post transfection
Control siRNA
BDNF siRNA
D
90 min
48 Hr
Control siRNA
BDNF siRNA
Control siRNA
BDNF siRNA
BDNF Fluorescence (%Change from Control)
10
0
-10
-20
-30
-40
-50
*
E
siRNA transfection (Magnetofection)
30 Min
PA Treatment
90min
Fix or Record

Figure 5.2: RhebWT overexpression enhances mTORC1 activity in culture, and progressive loss of endogenous BDNF after siRNA magnetofection. (A-B) Example images (A) and mean (+SEM) normalized p-S6 expression in transfected neurons. Expression of RhebWT (n=29 cells) significantly (*p<0.05 vs EGFP alone by t test) enhanced p-S6 levels compared with transfection with EGFP alone (n= 28 cells). PS6 fluorescence intensity indicated by color look-up table. Scale bar, 10μm in (A). (B) Representative DIC and fluorescein images in cells subject to magnetofection as indicated then quenched with 0.04% Trypan blue. Trypan blue quenches extracellular fluorescein signal, indicating that magnetofection rapidly delivers fluorescein-conjugated siRNA into cells immediately after transfection. (C) Representative images of straightened somadendritic regions of cultured neurons subject to magnetofection with control or anti BDNF siRNA. Scale bar represents 10mm in (C). (D) Mean (+ SEM) expression of BDNF, normalized to average control values at identical time points, in neurons treated as indicated. While BDNF fluorescence was unaffected by magnetofection of anti-BDNF siRNA at 90 min (n = 21) compared to control siRNA transfected cells (n =33), BDNF levels were significantly (*p < 0.05, relative to control) reduced by anti-BDNF siRNA magnetofection after 48 Hrs (n=21) relative to neurons transfected with control siRNA (n=32). (E) Experimental timeline: Dissociated hippocampal cultures were transfected with siRNA against BDNF or non-targeting control via magnetofection. 30 min post transfection, cells were treated with phosphatidic acid for 90 minutes then either used for whole-cell recordings or fixed and processed for subsequent immunocytochemistry.

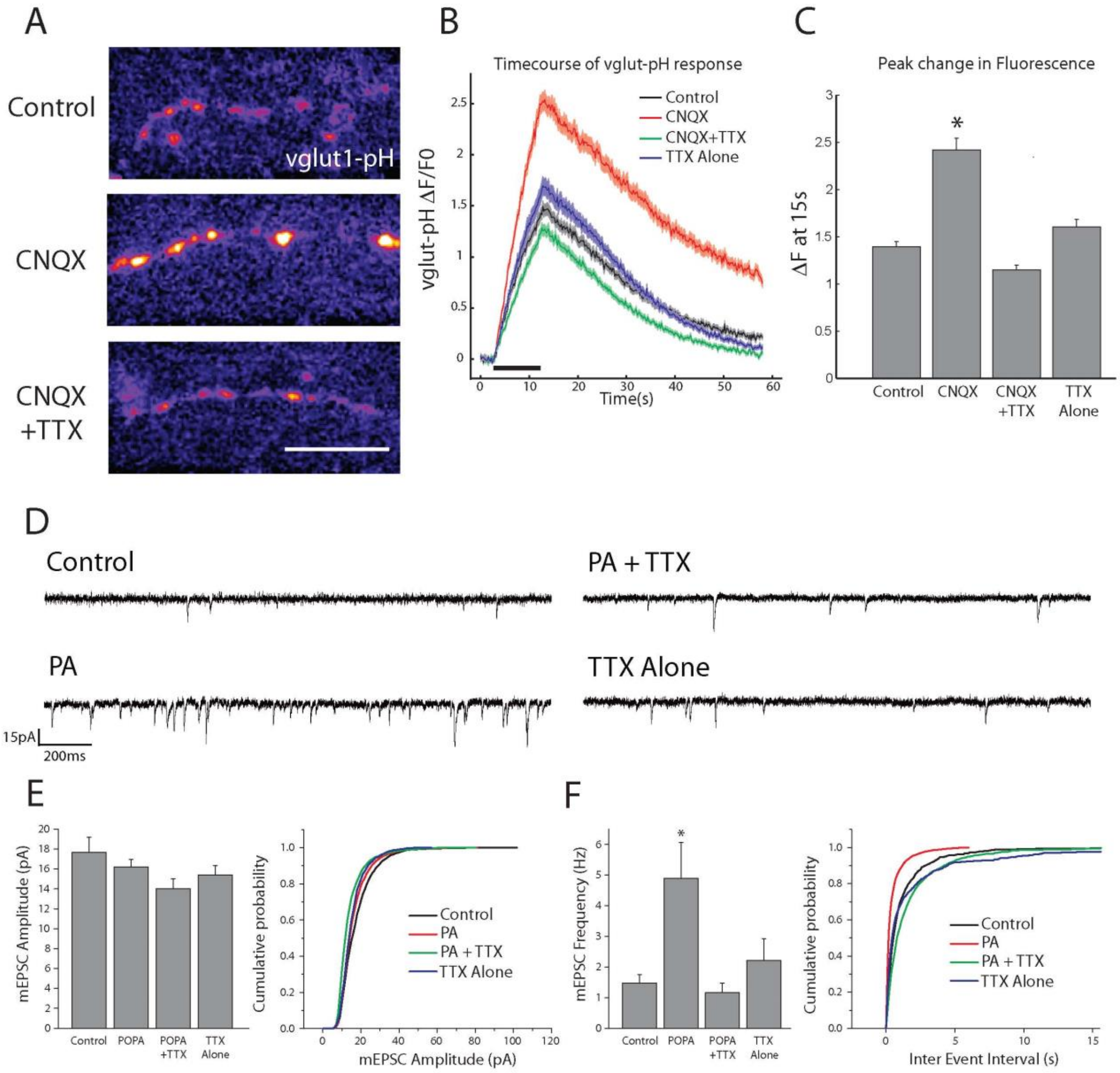
A
Control
vglut1-pH
CNQX
CNQX
+TTX
B
Timecourse of vglut-pH response
vglut-pH ΔF/F0
Control
CNQX
CNQX+TTX
TTX Alone
0
0.5
1
1.5
2
2.5
0
10
20
30
40
50
60
Time(s)
C
Peak change in Fluorescence
ΔF at 15s
*
0
0.5
1
1.5
2
2.5
3
Control
CNQX
CNQX
+TTX
TTX
Alone
D
Control
PA + TTX
PA
TTX Alone
15pA
200ms
E
mEPSC Amplitude (pA)
0
2
4
6
8
10
12
14
16
18
20
Control
POPA
POPA
+TTX
TTX
Alone
Cumulative probability
0.0
0.2
0.4
0.6
0.8
1.0
0
20
40
60
80
100
120
mEPSC Amplitude (pA)
Control
PA
PA + TTX
TTX Alone
F
mEPSC Frequency (Hz)
*
0
1
2
3
4
5
6
Control
POPA
POPA
+TTX
TTX
Alone
Cumulative probability
0.0
0.2
0.4
0.6
0.8
1.0
0
5
10
15
Inter Event Interval (s)
Control
PA
PA + TTX
TTX Alone

Figure 5.3: Shared state-dependency of presynaptic enhancement driven by acute mTORC1 activation or loss of excitatory synaptic inputs. (A-C) Example images (A) of axon terminals coexpressing mCherry-synaptophysin (mCh-Syn, top) as well as vglut-pHluorin (vglut-pH, bottom). Bottom, representative examples of synapses expressing vglut-pH after termination of a 10 Hz 10 s stimulus train. Treatment with the AMPAR blocker CNQX (40M, 3 h) enhances the changes in vglut-pHluorin fluorescence intensity, compared with cells treated with vehicle in response to an identical stimulus train. Scale bar represents 25μm. B, Relative change in vglut-pHluorin fluorescence over time in response to a 10 Hz 10 s stimulus train, recorded from cells treated with vehicle, CNQX, CNQX plus TTX, or TTX alone. Black bar represents onset of 10 s stimulus train. Black, Vehicle control (n=262 synapses). Red, CNQX (n=120 synapses). Green, CNQX plus TTX (n=349 synapses). Blue, TTX alone (n=343 synapses). Evoked changes in vglut-pHluorin fluorescence intensity were significantly enhanced by treatment with CNQX, and this effect was blocked by concurrent spike blockade with TTX. (*p<0.05, one-way ANOVA, Tukey–Kramer post hoc compared to vehicle controls at peak fluorescence levels at immediate termination of stimulus train). (D) Representative recordings in neurons treated with PA (100μm, 45 min) with or without 30 min pretreatment with TTX (1μM). (E-F) Mean (+SEM) mEPSC Amplitude (E) and Frequency (F) plus cumulative histogram of amplitude and inter-event interval of mEPSCs recorded from neurons treated with vehicle or 100 μM PA for with or wthout concurrent spike blockade via TTX as indicated: Vehicle control (n=9), PA (n=11), PA+TTX (n=13), TTX alone (n=8). (*p<0.05, one-way ANOVA, Tukey–Kramer post hoc)

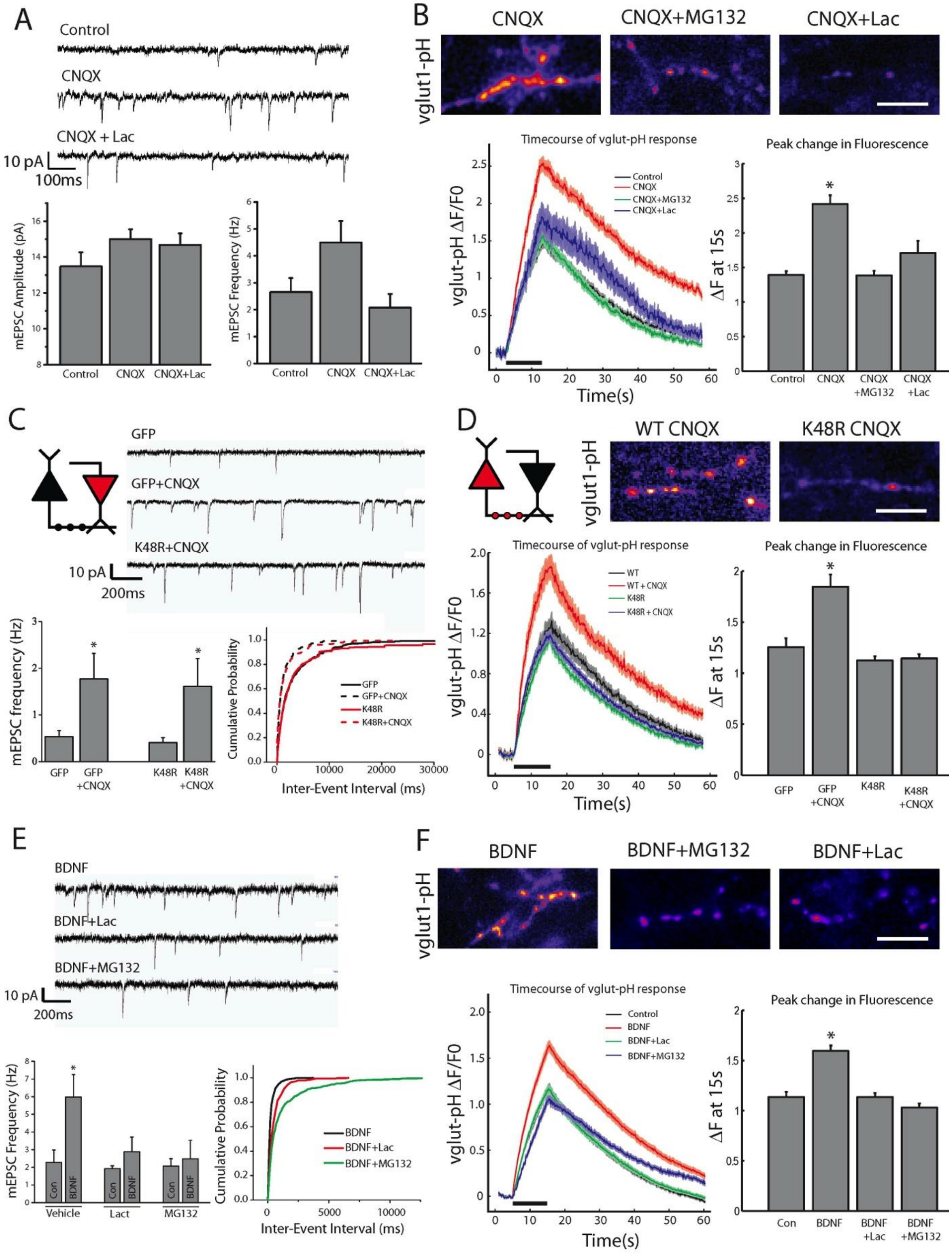
A
Control
CNQX
CNQX + Lac
10 pA
100ms
mEPSC Amplitude (pA)
mEPSC Frequency (Hz)
Control
CNQX
CNQX+Lac
B
CNQX
CNQX+MG132
CNQX+Lac
vglut1-pH
Timecourse of vglut-pH response
vglut-pH ΔF/F0
Time(s)
Control
CNQX
CNQX+MG132
CNQX+Lac
Peak change in Fluorescence
ΔF at 15s
*
Control
CNQX
CNQX +MG132
CNQX +Lac
C
GFP
GFP+CNQX
K48R+CNQX
10 pA
200ms
mEPSC frequency (Hz)
*
*
GFP
GFP +CNQX
K48R
K48R +CNQX
Cumulative Probability
Inter-Event Interval (ms)
GFP
GFP+CNQX
K48R
K48R+CNQX
D
WT CNQX
K48R CNQX
vglut1-pH
Timecourse of vglut-pH response
vglut-pH ΔF/F0
Time(s)
WT
WT + CNQX
K48R
K48R + CNQX
Peak change in Fluorescence
ΔF at 15s
*
GFP
GFP +CNQX
K48R
K48R +CNQX
E
BDNF
BDNF+Lac
BDNF+MG132
10 pA
200ms
mEPSC Frequency (Hz)
*
Con
BDNF
Vehicle
Lact
MG132
Cumulative Probability
Inter-Event Interval (ms)
BDNF
BDNF+Lac
BDNF+MG132
F
BDNF
BDNF+MG132
BDNF+Lac
vglut1-pH
Timecourse of vglut-pH response
vglut-pH ΔF/F0
Time(s)
Control
BDNF
BDNF+Lac
BDNF+MG132
Peak change in Fluorescence
ΔF at 15s
*
Con
BDNF
BDNF +Lac
BDNF +MG132

Figure 5.4: The ubiquitin proteasome system operates presynaptically to mediate increased vesicle release after exposure to retrograde signal. (A) Representative mEPSC recordings and mean (+SEM) mEPSC amplitude and frequency made from hippocampal cultures after washout of CNQX (3Hrs, 40μM) with or without Lactacystin (10μM) as indicated: Control (n=15), CNQX (n=16), CNQX + Lac (n=12). (B) Representative images (top) of vglut1-pH peak fluorescence at the termination of a 10s, 10Hz field stimulus, after washout of CNQX (40μM, 3 Hrs) with or without concurrent inhibition of the ubiquitin proteasome system with MG132 (10μM, 30 min pre-treatment) or Lactacystin (10mM, 30 min pretreatment). (bottom) Relative change in vglut1-pHluorin fluorescence over time and mean peak change in fluorescence from baseline in response to a 10 Hz 10 s stimulus train. Control (n=841), CNQX (n=407), CNQX+MG132 (n=400), CNQX + Lac (n=57). (*p<0.05 relative to vehicle controls at peak fluorescence levels at immediate termination of stimulus train). (C) Postsynaptic inhibition of proteasome function via expression of dominant negative K48R ubiquitin point mutant (red cell). Representative recordings mean mEPSC frequency recorded from cells expressing GFP alone or in combination with K48R ubiquitin, after washout of CNQX (40μM, 4Hr). Summary graphs presented on left and cumulative probability distribution shown on right. GFP (n=16), GFP+CNQX (n=14), K48R (n=10), K48R+CNQX (n=12). (D) Presynaptic inhibition of proteasome function via expression of dominant negative K48R ubiquitin point mutant (red cell) alongside vglut1-pH. Representative images of vglut1-pH peak fluorescence at the termination of a 10s, 10Hz field stimulus, after washout of CNQX (40μM, 3 Hrs) in cells expressing eiether WT or K48R ubiquitin. (bottom) Relative change in vglut1-pHluorin fluorescence over time and mean peak change in fluorescence from baseline in response to a 10 Hz 10 s stimulus train. WT(n=442 synapses), WT+CNQX (n=496 synapses), K48R (n=238 synapses), K48R+CNQX (n=792 synapses). (*p<0.05 relative to vehicle controls at peak fluorescence levels at immediate termination of stimulus train). (E) Representative mEPSC recordings and mean (+SEM) mEPSC amplitude and frequency made from hippocampal cultures after washout of BDNF (2Hrs, 250ng/ml) with or without Lactacystin (10μM) or MG132 (10μM). Control (n=7), BDNF (n=7), Control + Lac (n=5), BDNF+Lac (n=7), Control + MG132 (n=6), BDNF + MG132 (n=6). (*p<0.05 vs vehicle treated controls). (F) Representative images (top) of vglut1-pH peak fluorescence at the termination of a 10s, 10Hz field stimulus, after washout of BDNF (250ng/ml,2Hrs) with or without concurrent inhibition of the ubiquitin proteasome system with MG132 (10μM, 30 min pre-treatment) or Lactacystin (10μM, 30 min pretreatment). (bottom) Relative change in vglut1-pHluorin fluorescence over time and mean peak change in fluorescence from baseline in response to a 10 Hz 10 s stimulus train. Control (n=724), BDNF (n=808), BDNF+MG132 (n=305), BDNF+ LAc (n=715). (*p<0.05 relative to vehicle controls at peak fluorescence levels at immediate termination of stimulus train). Scale bar represents 10μm for B, D and F.

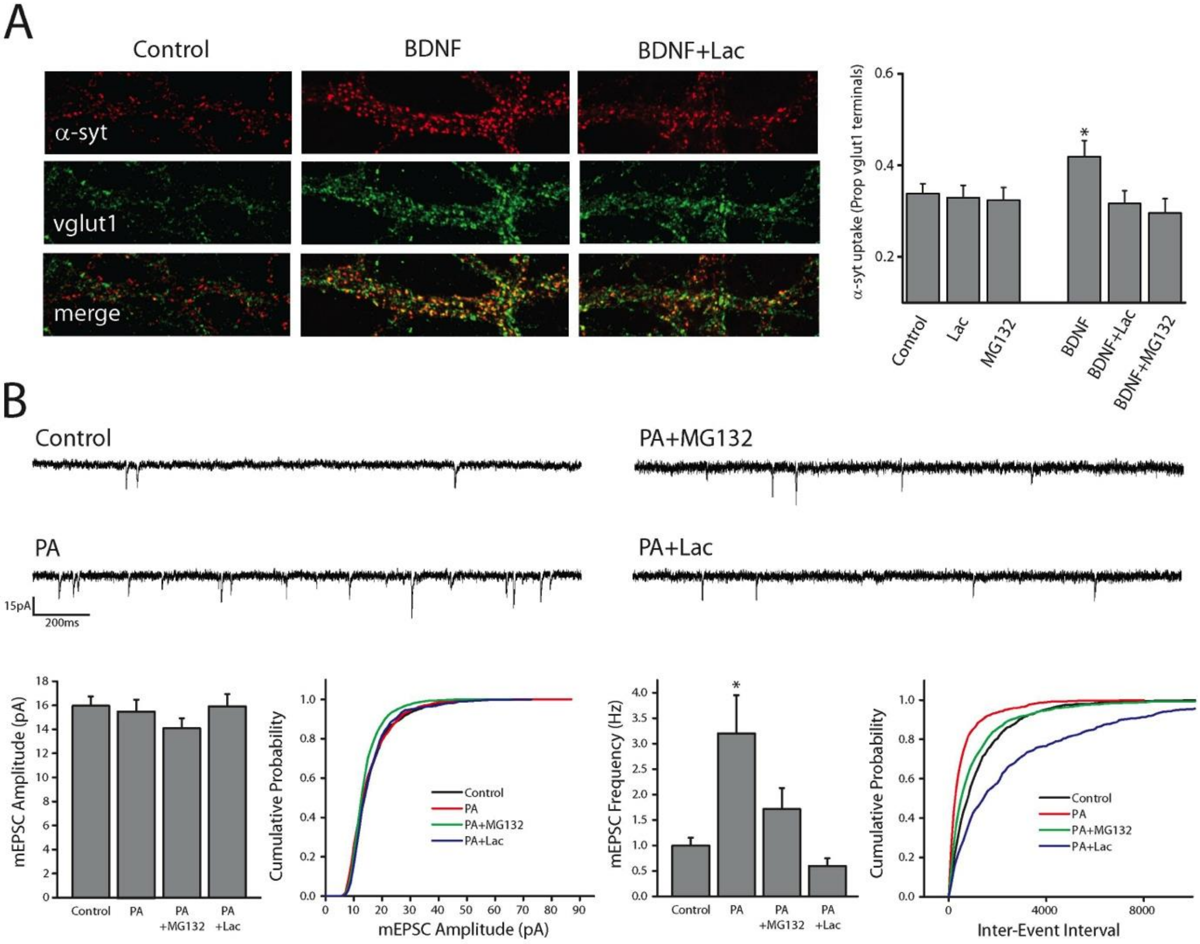
A
Control
BDNF
BDNF+Lac
α-syt
vglut1
merge
α-syt uptake (Prop vglut1 terminals)
0.6
0.4
0.2
*
Control
Lac
MG132
BDNF
BDNF+Lac
BDNF+MG132
B
Control
PA
PA+MG132
PA+Lac
15pA
200ms
mEPSC Amplitude (pA)
18
16
14
12
10
8
6
4
2
0
Control
PA
PA +MG132
PA +Lac
Cumulative Probability
1.0
0.8
0.6
0.4
0.2
0.0
0 10 20 30 40 50 60 70 80 90
mEPSC Amplitude (pA)
Control
PA
PA+MG132
PA+Lac
mEPSC Frequency (Hz)
4.0
3.5
3.0
2.5
2.0
1.5
1.0
0.5
0.0
*
Control
PA
PA +MG132
PA +Lac
Cumulative Probability
0 4000 8000
Inter-Event Interval
Control
PA
PA+MG132
PA+Lac

Figure 5.5: Pharmacological inhibition of proteasome function blocks presynaptic augmentation after BDNF exposure or acute mTORC1 activation. (A) Representative examples and mean (+SEM) syt-lum uptake from experiments where the indicated groups were treated with BDNF Alone (250ng/ml, 2Hrs) or in combination with proteasome inhibitors as indicated. Control (87=x images), Lac (n= 40 images), MG132 (n= 29 images), BDNF (n=33 images), BDNF + Lac (n=24 images), BDNF+MG132 (n=33 images). (*p<0.05, relative to control). (B) Representative recordings and mean mEPSC Amplitude and Frequency obtained from cells treated with PA (100μM, 45 min) with or without proteasome inhibitors as indicated. Summary averages presented on left and cumulative probability distributions shown on left. Vehicle control (n=10), PA Alone (n=10), PA+MG132 (n=12), PA+Lac (n=10). (*p<0.05, one-way ANOVA, Tukey–Kramer post hoc)

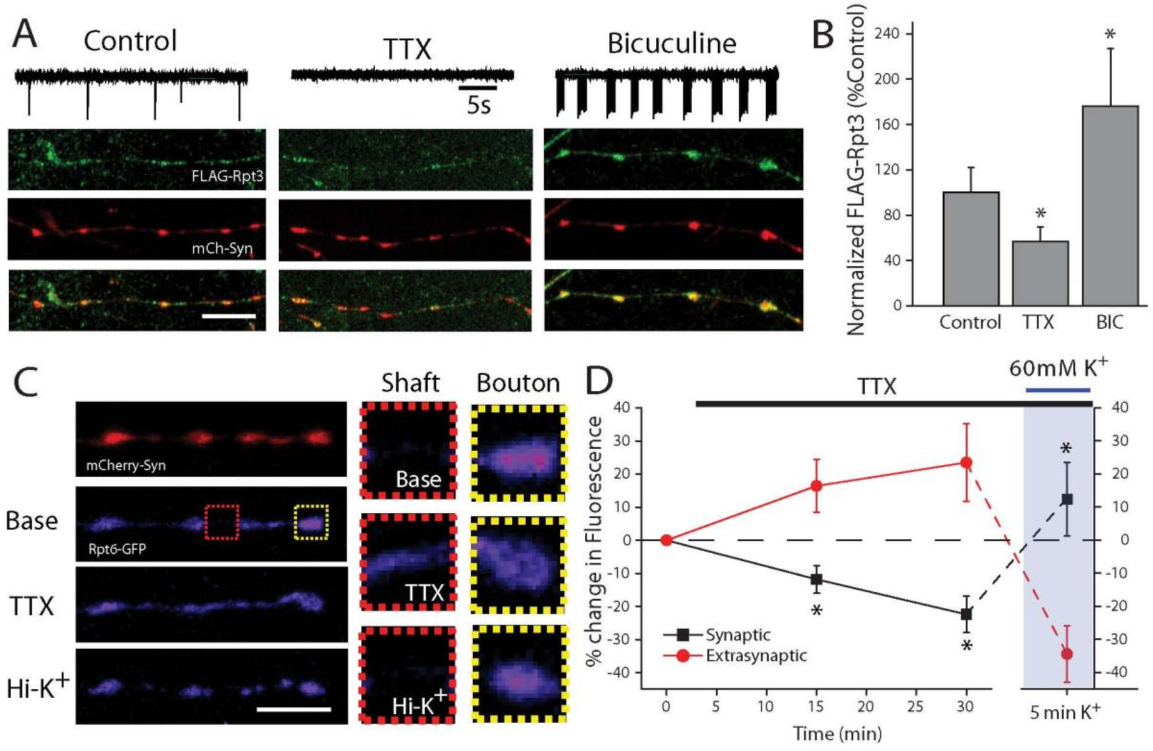
A
Control
TTX
Bicuculine
5s
FLAG-Rpt3
mCh-Syn
B
Normalized FLAG-Rpt3 (%Control)
240
200
160
120
80
40
0
*
*
Control
TTX
BIC
C
mCherry-Syn
Base
Rpt6-GFP
TTX
Hi-K+
Shaft
Bouton
Base
TTX
Hi-K+
D
TTX
60mM K+
% change in Fluorescence
40
30
20
10
0
-10
-20
-30
-40
*
*
*
Synaptic
Extrasynaptic
0
5
10
15
20
25
30
Time (min)
5 min K+

Figure 5.6: Neuronal activity drives synaptic redistribution of the proteasome in axons. (A) Effects of activity manipulation on presynaptic proteasome distribution. Top panel shows representative cell-attached recordings from cells under control conditions or after treatment with Bicuculine (10μM) or TTX (1μM) for 2Hrs. Lower panel contains representative images of axonal segments expressing Rpt3-FLAG and mCherry-Synaptophysin. (B) Group means of FLAG fluorescence intensity present in mCh-Syn positive regions under each condition: Control (n=12 images), Bic (n=11 images), TTX (n=12 images). Scale Bar represents 5μm in B. (*p<0.05 compared to controls). (C) Representative images of axonal regions expressing mCherry-Syn (top panel) as well as Rpt6-GFP (lower 3 panels). Identical set of synapses displayed in each image, under conditions of baseline images (top), after 30 min of TTX exposure (middle) and after 5min 60mM K+ (bottom). Right, enlarged sections denoting extrasynaptic ('shaft', red) or synaptic ('bouton', yellow) regions of interest under each condition. (D) Timecourse of group averages (% change in fluorescence from baseline) for extrasynaptic (black square, n=32 ROIs across 8 axons) and synaptic (red circle, n=32 ROIs across 8 axons) regions after 30 minutes of TTX treatment (1μM) followed by 5 min exposure to 60 mM K+ (blue shaded region, normalized to values at 30 min post TTX). Scale bar represents 5μm in C. (*p<0.05 compared to extrasynaptic regions at identical time point)

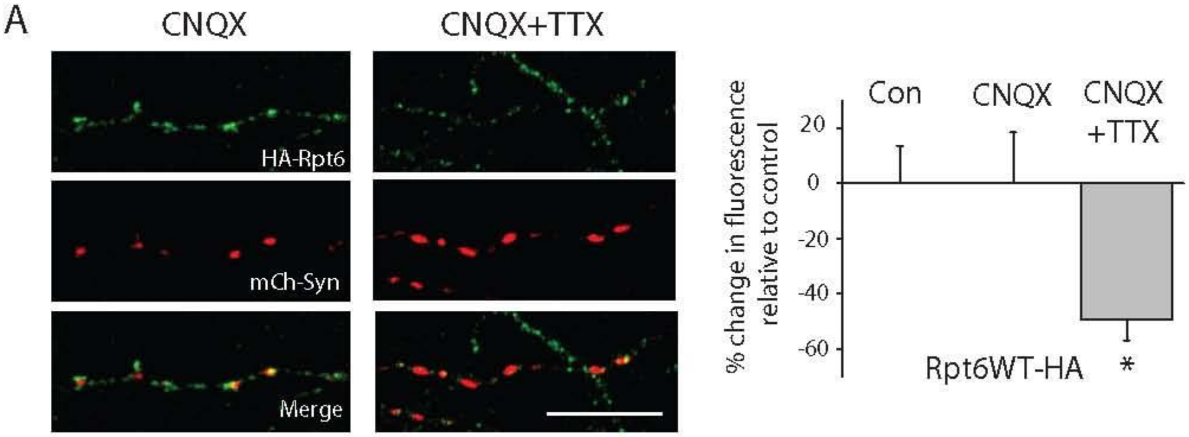
A
CNQX
CNQX+TTX
HA-Rpt6
mCh-Syn
Merge
% change in fluorescence relative to control
20
0
-20
-40
-60
Con
CNQX
CNQX +TTX
Rpt6WT-HA
*

Figure 5.7: Spike blockade eliminates association between HA-tagged proteasome subunit and marker of presynaptic boutons. Representative images of axonal segments expressing HA-Rpt6 as well as mCh-Syn, treated with CNQX alone (40μM, 3Hr) or in combination with TTX (1μM). Right, group means of % change in HA fluorescence (relative to vehicle treated controls) as indicated: Control (n=49 images), CNQX (n=55 images), CNQX+TTX (n=45 images). Spike blockade redistributed proteasome localization away from synaptic regions in the axon, regardless of presence or absence of homeostatic challenge induced by AMPAR blockade. Scale bar represents 10μm in A. (*$p<0.05$ relative to controls).

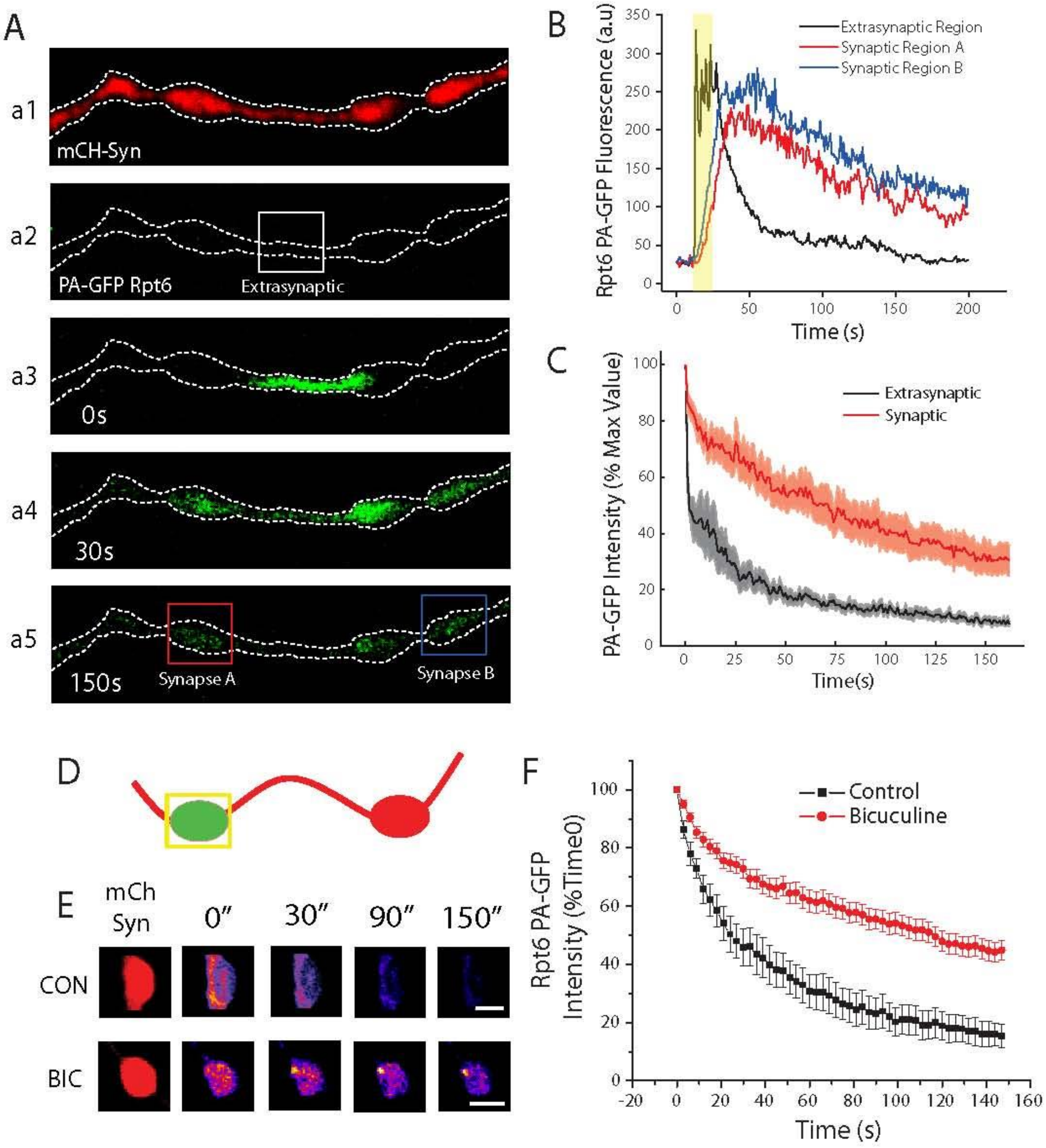
A
a1
mCH-Syn
a2
PA-GFP Rpt6
Extrasynaptic
a3
0s
a4
30s
a5
150s
Synapse A
Synapse B
B
Rpt6 PA-GFP Fluorescence (a.u)
Time (s)
Extrasynaptic Region
Synaptic Region A
Synaptic Region B
C
PA-GFP Intensity (% Max Value)
Time(s)
Extrasynaptic
Synaptic
D
E
mCh Syn
0″
30″
90″
150″
CON
BIC
F
Rpt6 PA-GFP Intensity (%Time0)
Time (s)
Control
Bicuculine

Figure 5.8: Active retention of proteasomes at presynaptic boutons (A) Example images of timelapse experiment from cells expressing mCh-Syn as well as PA-GFP Rpt6. mCh-Syn signal alone (a1), and PAGFP signal before (a2), 0s (a3), 30s (a4), and 150s (a5) after a 5s photoactivation stimulus targeted in the extraynaptic region denoted in a2 (white square). Scale bar represents xx in A. (B) Timecourse of PAGFP fluorescence values (a.u.) taken from the experiment shown in A. Traces correspond to data obtained from ROIs centered around the extrasynaptic region shown in a2 (black line), as well as two synaptic regions as highlighted in a5 (red and blue lines). (C) Timecourse of collected PAGFP fluorescence decay group means in synaptic (n= 13) and extrasynaptic (n=6) regions, normalized to peak fluorescence after photoactivation. As peak fluorescence in synaptic regions routinely occurred with a temporal delay compared to extrasynaptically photoactivated regions (as in B), peak fluorescence values were time locked to compare relative decay rates. (D) Schematic of single-synapse experiment: Individual boutons expressing mCh-Syn and PA-GFP Rpt6 were targeted for photoactivation (yellow square), then monitored to track fluorescence decay over time. (E) Example images showing mCh-Syn signal (left) and gradual loss of PAGFP fluorescence from synaptic regions after photoactivation. (F) Timecourse of collected PAGFP fluorescence decay group means in neurons treated with Bicucline (10μM for 2Hrs, n= 38) or vehicle treated controls (n=11), normalized to peak fluorescence after photoactivation. Treatment with Bicucline resulted in prolonged retention of Rpt6 PA-GFP signal at synaptic regions after photoactivation.

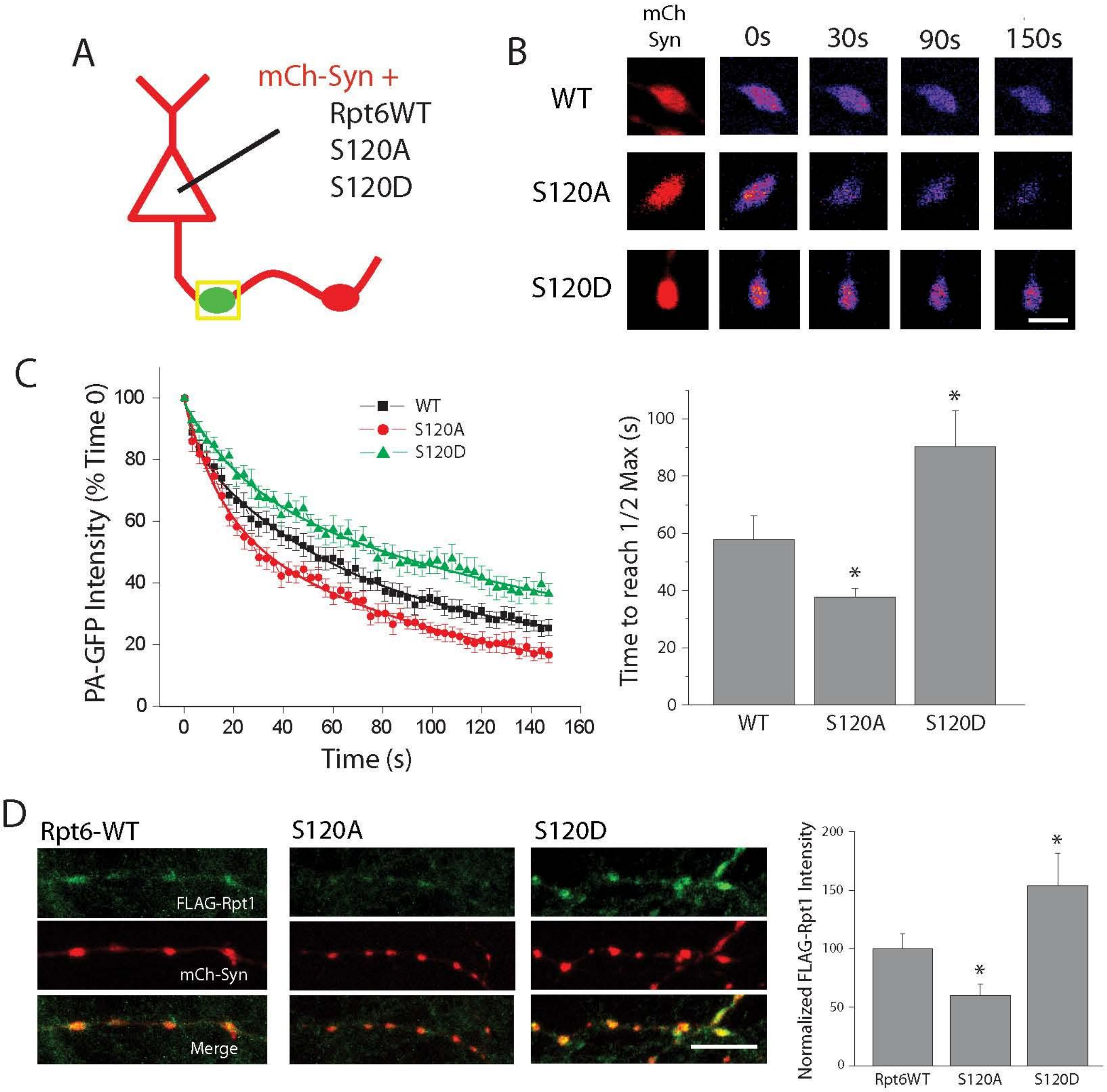
A
mCh-Syn +
Rpt6WT
S120A
S120D
B
mCh Syn
0s
30s
90s
150s
WT
S120A
S120D
C
PA-GFP Intensity (% Time 0)
100
80
60
40
20
0
0
20
40
60
80
100
120
140
160
Time (s)
WT
S120A
S120D
Time to reach 1/2 Max (s)
100
80
60
40
20
0
WT
S120A
S120D
*
*
D
Rpt6-WT
S120A
S120D
FLAG-Rpt1
mCh-Syn
Merge
Normalized FLAG-Rpt1 Intensity
200
150
100
50
0
Rpt6WT
S120A
S120D
*
*

Figure 5.9: Phosphorylation of Rpt6 at S120 alters synaptic localization of the proteasome in axons. (A) Schematic of single synapse photoactivation experiment. Neurons were transfected with mCH-Syn as well as PA-GFP tagged to WT, S120A or S120A Rpt6. Individual bouton were targeted for photoactivation (Yellow Square) then monitored to track loss of fluorescence over time. (B) Example images showing mCh-Syn signal (left) and gradual loss of PAGFP fluorescnece after photoactivation in cells expressing WT, S120A or S120D Rpt6. (C) Timecourse (left) and mean decay rates (right, quantified as time to reach ½ max) of PAGFP fluorescence decay in neurons expressing WT Rpt6 (n=15 synapses), S120A Rpt6 (n=13 synapses) or S120D Rpt6 (n=14 synapses), normalized to peak fluorescence after photoactivation. (*p<0.05 compared to Rpt6WT controls) (D) Example images of axonal regions from neurons triple transfected with mCh-SYn, FLAG-Rpt1, as well as either Rpt6-WT, Rpt67-S120A, or Rpt6-S120D. Right, group means of FLAG fluorescence intensity present in mCh-Syn positive regions under each condition as indicated: Rpt6WT (n=26 images), Rpt6-S120A (n=20 images), Rpt6 S120D (n=9 images). Scale Bar represents x in D. (*p<0.05 compared to Rpt6WT controls).

A

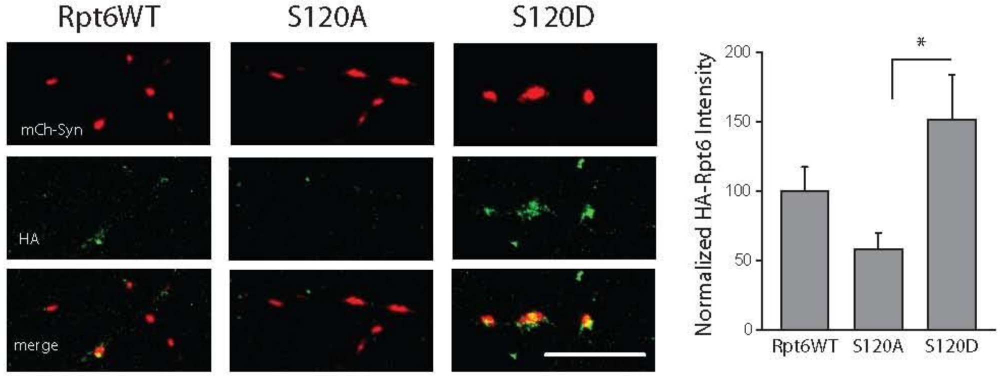
Rpt6WT
S120A
S120D
mCh-Syn
HA
merge
Normalized HA-Rpt6 Intensity
200
150
100
50
0
*
Rpt6WT
S120A
S120D

Figure 5.10: HA-tagged Rpt6 WT and point mutants display unique distribution patterns in axons. (A) Example images of axonal regions from neurons transfected with mCh-SYn, as well as HA-tagged Rpt6-WT, Rpt6-S120A, or Rpt6-S120D. Right, group means of HA fluorescence intensity present in mCh-Syn positive regions under each condition as indicated: Rpt6WT (n=30 images), Rpt6-S120A (n=30 images), Rpt6 S120D (n=20 images). Scale Bar represents 10μm in D. (*$p<0.05$).

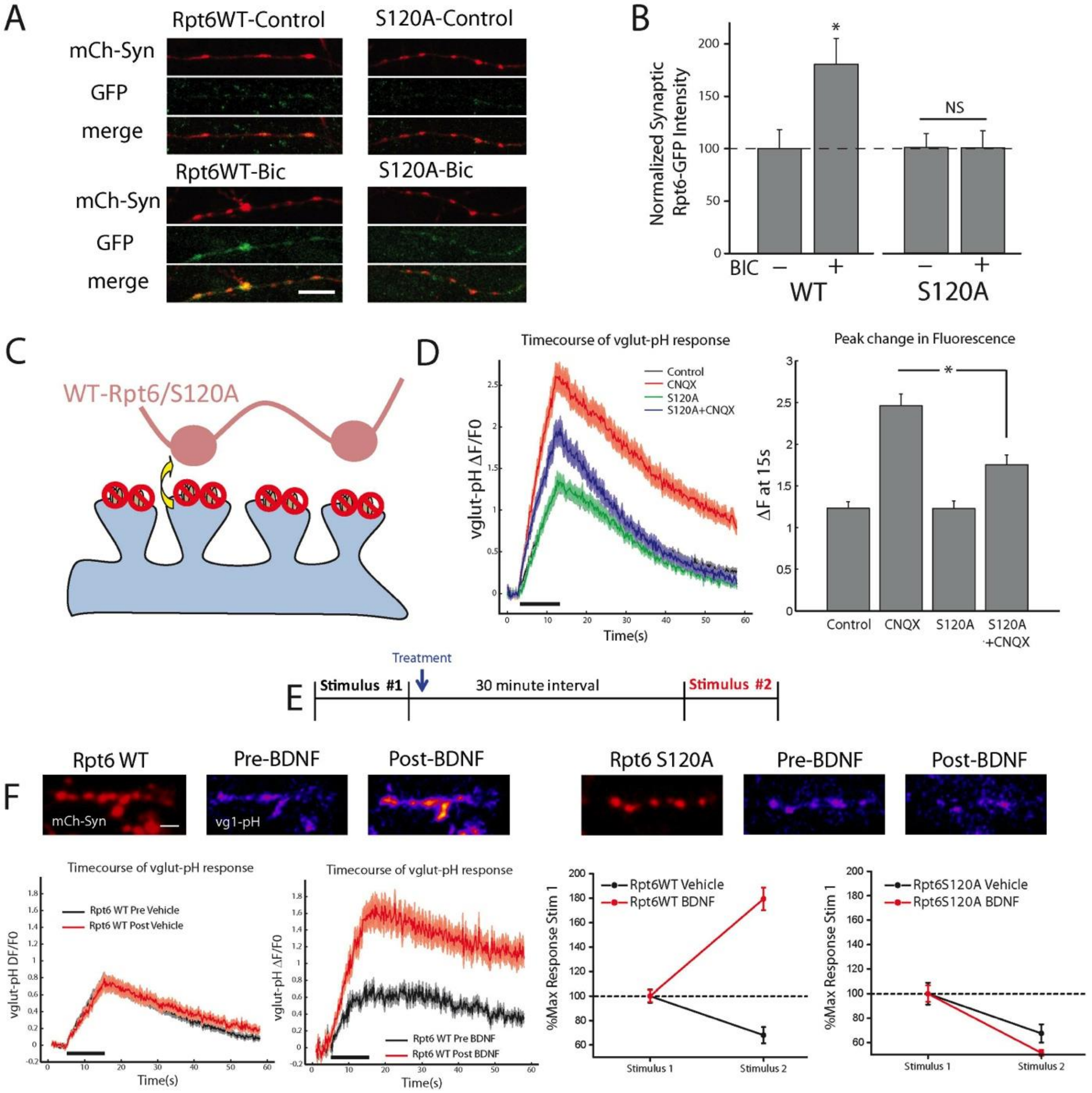
A
Rpt6WT-Control
S120A-Control
mCh-Syn
GFP
merge
Rpt6WT-Bic
S120A-Bic
mCh-Syn
GFP
merge
B
Normalized Synaptic Rpt6-GFP Intensity
0
50
100
150
200
*
NS
BIC
–
+
–
+
WT
S120A
C
WT-Rpt6/S120A
D
Timecourse of vglut-pH response
Control
CNQX
S120A
S120A+CNQX
vglut-pH ΔF/F0
Time(s)
Peak change in Fluorescence
ΔF at 15s
*
Control
CNQX
S120A
S120A +CNQX
E
Treatment
Stimulus #1
30 minute interval
Stimulus #2
F
Rpt6 WT
Pre-BDNF
Post-BDNF
mCh-Syn
vg1-pH
Rpt6 S120A
Pre-BDNF
Post-BDNF
Timecourse of vglut-pH response
Rpt6 WT Pre Vehicle
Rpt6 WT Post Vehicle
vglut-pH DF/F0
Time(s)
Timecourse of vglut-pH response
Rpt6 WT Pre BDNF
Rpt6 WT Post BDNF
vglut-pH ΔF/F0
Time(s)
Rpt6WT Vehicle
Rpt6WT BDNF
%Max Response Stim 1
Stimulus 1
Stimulus 2
Rpt6S120A Vehicle
Rpt6S120A BDNF
%Max Response Stim 1
Stimulus 1
Stimulus 2

Figure 5.11: Serine to alanine point mutation in Rpt6 eliminates activity dependent redistribution and blocks enhanced presynaptic function after loss of excitatory input or exposure to BDNF. (A) Example images of axonal regions from neurons transfected with mCh-SYn, as well as GFP-tagged Rpt6-WT or Rpt6-S120A. Cells were treated with Bicucline or vehicle after 48Hrs of expression then assessed for GFP colocalization with synaptic mCh-Syn signal. (B) Group means of GFP fluorescence intensity present in mCh-Syn positive regions under each condition as indicated: Rpt6WT Vehicle (n=10 images), Rpt6-WT Bicuculine (n=11 images), Rpt6-S120A Vehicle (n=14 images), Rpt6-S120A Bicuculine (n=16 images). Scale Bar represents x in A. (*p<0.05 compared to vehicle treated controls for each group). (C) Schematic of experiment: Neurons were transfected with vglut1-pH as in combination with either Rpt6WT or Rp6-S120A. 48Hrs later, cells were subject to AMPAR blockade with CNQX (40μM, 3Hr), then assessed for field-stimulus driven exocytosis. (D) Relative change in vglut1-pHluorin fluorescence over time and mean peak change in fluorescence from baseline in response to a 10 Hz 10 s stimulus train for groups as indicated: Control (n=248 boutons), CNQX (n=287 boutons), S120A (n=237 boutons), S120A + CNQX (n=331 boutons). (E) Experimental design for within-group assessment of the effect of acute BDNF treatment on vesicle release. Neurons expressing mCH-Syn and vglut1-pH were subject to a 10s, 10Hz field stimulus to assess initial release properties. Cells were then treated with BDNF (250ng/ml, 30min) and this same set of synapses was again stimulated using an identical spike train. (F) Example images of axonal segments depicting mCh-Syn signal, as well as peak evoked vglut1-pH fluorescence before and 30 min after application of BDNF in neurons expressing Rpt6WT (left) and Rpt6-S120A (right). (G) Examples of averaged responses from a single set of boutons expressing Rpt6WT imaged before (black) and after (red) application of either BDNF (n=31 boutons) or vehicle (n=71 boutons). (H) Collected group averages of peak vglut1-pH intensity at end of 10Hz stimulus (shown normalized to peak obtained by stimulus 1 as indicated: Rpt6 WT Vehicle (n=139 boutons), Rpt6WT BDNF (n=217 boutons), Rpt6 S120A Vehicle (n=35 boutons), Rpt6 S120A BDNF (n=363 boutons). Scale bar represents 5μm in F.

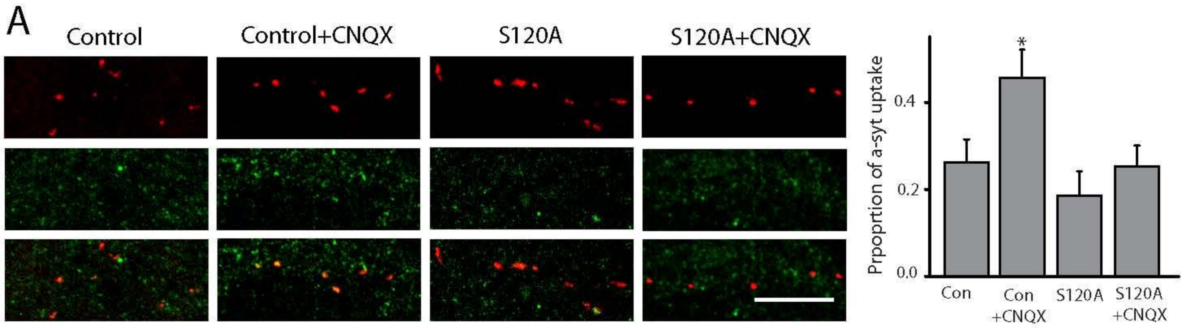
A
Control
Control+CNQX
S120A
S120A+CNQX
Prpoprtion of a-syt uptake
0.4
0.2
0.0
*
Con
Con +CNQX
S120A
S120A +CNQX

Figure 5.12: Expression of Rpt6S120 eliminates homeostatic increases in spontaneous vesicle release. Representative examples and mean (+SEM) syt-lum uptake from experiments where the indicated groups were treated with CNQX Alone (40μM, 3Hrs) or in combination with expression of Rpt6S120A as indicated: Control (n=23 images), Control+CNQX (n=23 images), S120A (n=27 images), S120A+CNQX (n=27 images). (*$p<0.05$, relative to control) Scale bar in C = 10μm.

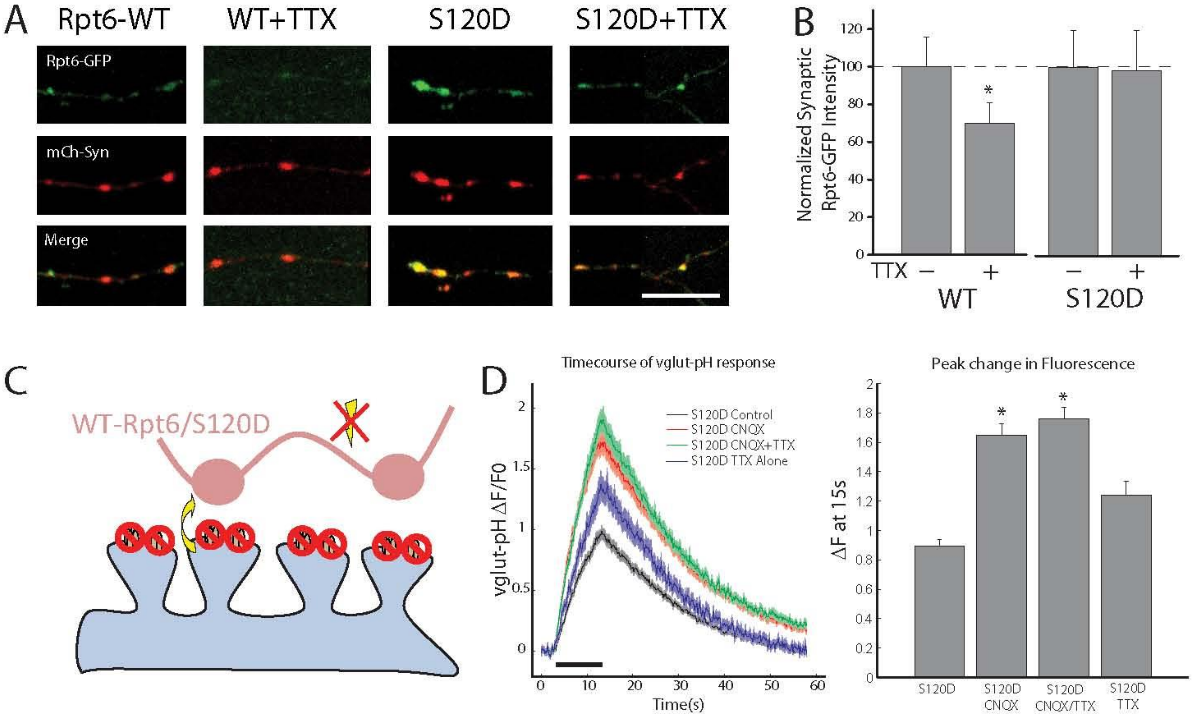
A
Rpt6-WT
WT+TTX
S120D
S120D+TTX
Rpt6-GFP
mCh-Syn
Merge
B
Normalized Synaptic Rpt6-GFP Intensity
0
20
40
60
80
100
120
*
TTX
−
+
−
+
WT
S120D
C
WT-Rpt6/S120D
D
Timecourse of vglut-pH response
vglut-pH ΔF/F0
0
0.5
1
1.5
2
S120D Control
S120D CNQX
S120D CNQX+TTX
S120D TTX Alone
0
10
20
30
40
50
60
Time(s)
Peak change in Fluorescence
ΔF at 15s
0
0.2
0.4
0.6
0.8
1
1.2
1.4
1.6
1.8
2
*
*
S120D
S120D CNQX
S120D CNQX/TTX
S120D TTX

Figure 5.13: A phosphomimetic mutation in Rpt6 is sufficient to drive the proteasome to synapses and render presynaptic compensation state-independent. (A) Example images of axonal regions from neurons transfected with mCh-SYn, as well as GFP-tagged Rpt6-WT or Rpt6-S120D. Cells were treated with TTX or vehicle after 48Hrs of expression then assessed for GFP colocalization with synaptic mCh-Syn signal. (B) Group means of GFP fluorescence intensity present in mCh-Syn positive regions under each condition as indicated: Rpt6WT Vehicle (n=14 images), Rpt6-WT TTX (n=21 images), Rpt6-S120D Vehicle (n=16 images), Rpt6-S120D TTX (n=19 images). Scale Bar represents 10μm in A. (*p<0.05 compared to vehicle treated controls for each group). (C) Schematic of experiment: Neurons were transfected with vglut1-pH in combination with either Rpt6WT or Rp6-S120D. 48Hrs later, cells were subject to AMPAR blockade with CNQX (40μM, 3Hr) and spike blockade with TTX (1μM), then assessed for field-stimulus driven exocytosis. (D) Relative change in vglut1-pHluorin fluorescence over time and mean peak change in fluorescence from baseline in response to a 10 Hz 10 s stimulus train for groups as indicated: S120D control (n=515 boutons), S120D CNQX (n=622 boutons), S120D CNQX+TTX (n=571 boutons), S120D TTX Alone (n=208 boutons). (*p<0.05 relative to vehicle treated S120D controls).

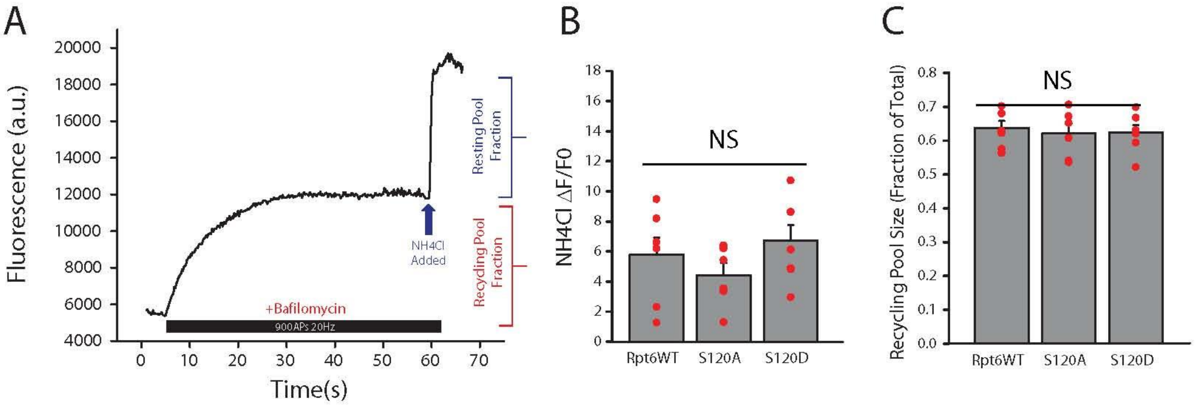
A
Fluorescence (a.u.)
20000
18000
16000
14000
12000
10000
8000
6000
4000
0
10
20
30
40
50
60
70
Time(s)
+Bafilomycin
900APs 20Hz
NH4Cl Added
Resting Pool Fraction
Recycling Pool Fraction
B
NH4Cl ΔF/F0
18
16
14
12
10
8
6
4
2
0
NS
Rpt6WT
S120A
S120D
C
Recycling Pool Size (Fraction of Total)
0.8
0.7
0.6
0.5
0.4
0.3
0.2
0.1
0.0
NS
Rpt6WT
S120A
S120D

Figure 5.14: Expression of Rpt6 point mutants on its own does not alter vesicle pool characteristics. (A) Example experimental run to assess vesicle pool fractions. Neurons were bafilomycin (1μM) then given 900APs at 20Hz to determine the recycling pool fraction of total labeled vesicles (see Ryan paper). Nh4Cl was then added to reveal the total pool of pHluorin labeled vesicles (blue arrow). (B) Group averages reveal no significant difference in the size of total vesicle pool (presented as NH4Cl-induced peak fluorescence normalized to baseline fluorescence levels) between experimental groups as indicated: Rpt6WT (n=7 experiments), Rpt6 S120A (n=6 experiments), Rpt6 S120D (n=7 experiments). (C) Group averages reveal no difference in the size of the recycling pool of vesicles (presented as fraction of fluorescence plateau reached in presence of Bafilomycin compared to total after NH4Cl) as a result of expressing Rpt6 point mutants.

5.7 Bibliography

Aravamudan B, Broadie K. (2003). Synaptic Drosophila UNC-13 is regulated by antagonistic G-protein pathways via a proteasome-dependent degradation mechanism. J Neurobiol. Feb 15;54(3):417-38.

Banko JL, Hou L, Poulin F, Sonenberg N, Klann E. (2006). Regulation of eukaryotic initiation factor 4E by converging signaling pathways during metabotropic glutamate receptor-dependent long-term depression. J Neurosci. Feb 22;26(8):2167-73.

Bayés A, van de Lagemaat LN, Collins MO, Croning MD, Whittle IR, Choudhary JS, Grant SG. (2011). Characterization of the proteome, diseases and evolution of the human postsynaptic density. Nat Neurosci. Jan;14(1):19-21.

Bingol B, Schuman EM. (2006). Activity-dependent dynamics and sequestration of proteasomes in dendritic spines. Nature. Jun 29;441(7097):1144-8

Bingol B, Wang CF, Arnott D, Cheng D, Peng J, Sheng M. (2010). Autophosphorylated CaMKIIalpha acts as a scaffold to recruit proteasomes to dendritic spines. Cell. Feb 19;140(4):567-78.

Bressloff PC, Earnshaw BA. (2007). Diffusion-trapping model of receptor trafficking in dendrites. Phys Rev E Stat Nonlin Soft Matter Phys. Apr;75(4 Pt 1):041915.

Brooks P, Fuertes G, Murray RZ, Bose S, Knecht E, Rechsteiner MC, Hendil KB, Tanaka K, Dyson J, Rivett J. (2000). Subcellular localization of proteasomes and their regulatory complexes in mammalian cells. Biochem J. Feb 15;346 Pt 1:155-61.

Brown A. (2003). Axonal transport of membranous and nonmembranous cargoes: a unified perspective. J Cell Biol. Mar 17;160(6):817-21.

Cajigas IJ, Will T, Schuman EM. (2010). Protein homeostasis and synaptic plasticity. EMBO J. Aug 18;29(16):2746-52.

Cammalleri M, Lütjens R, Berton F, King AR, Simpson C, Francesconi W, Sanna PP. (2003). Time-restricted role for dendritic activation of the mTOR-p70S6K pathway in the induction of late-phase long-term potentiation in the CA1. Proc Natl Acad Sci U S A. Nov 25;100(24):14368-73.

Chin LS, Vavalle JP, Li L. (2002). Staring, a novel E3 ubiquitin-protein ligase that targets syntaxin 1 for degradation. J Biol Chem. Sep 20;277(38):35071-9.

Coux O, Tanaka K, Goldberg AL. (1996). Structure and functions of the 20S and 26S proteasomes. Annu Rev Biochem. 65:801-47.

Deisseroth K, Bito H, Tsien RW. (1996). Signaling from synapse to nucleus: postsynaptic CREB phosphorylation during multiple forms of hippocampal synaptic plasticity. Neuron. Jan;16(1):89-101.

Deppmann CD, Mihalas S, Sharma N, Lonze BE, Niebur E, Ginty DD. (2008). A model for neuronal competition during development. Science. Apr 18;320(5874):369-73.

Djakovic SN, Schwarz LA, Barylko B, DeMartino GN, Patrick GN. (2009). Regulation of the proteasome by neuronal activity and calcium/calmodulin-dependent protein kinase II. J Biol Chem. Sep 25;284(39):26655-65.

Djakovic SN, Marquez-Lona EM, Jakawich SK, Wright R, Chu C, Sutton MA, Patrick GN. (2012). Phosphorylation of Rpt6 regulates synaptic strength in hippocampal neurons. J Neurosci. Apr 11;32(15):5126-31.

Graef IA, Wang F, Charron F, Chen L, Neilson J, Tessier-Lavigne M, Crabtree GR. (2003). Neurotrophins and netrins require calcineurin/NFAT signaling to stimulate outgrowth of embryonic axons. Cell. May 30;113(5):657-70.

Fonseca R, Vabulas RM, Hartl FU, Bonhoeffer T, Nägerl UV. (20076). A balance of protein synthesis and proteasome-dependent degradation determines the maintenance of LTP. Neuron. Oct 19;52(2):239-45.

Fenteany G, Schreiber SL. (1996). Specific inhibition of the chymotrypsin-like activity of the proteasome induces a bipolar morphology in neuroblastoma cells. Chem Biol. Nov;3(11):905-12.

Fujita Y, Shirataki H, Sakisaka T, Asakura T, Ohya T, Kotani H, Yokoyama S, Nishioka H, Matsuura Y, Mizoguchi A, Scheller RH, Takai Y. (1998). Tomosyn: a syntaxin-1-binding protein that forms a novel complex in the neurotransmitter release process. Neuron. May;20(5):905-15.

Fukuda M. (2003). Slp4-a/granuphilin-a inhibits dense-core vesicle exocytosis through interaction with the GDP-bound form of Rab27A in PC12 cells. J Biol Chem. Apr 25;278(17):15390-6.

Glickman MH, Raveh D.(2005). Proteasome plasticity. FEBS Lett. Jun 13;579(15):3214-23.

Gottschalk W, Pozzo-Miller LD, Figurov A, Lu B. (1998). Presynaptic modulation of synaptic transmission and plasticity by brain-derived neurotrophic factor in the developing hippocampus. J Neurosci. Sep 1;18(17):6830-9.

Gracheva EO, Burdina AO, Touroutine D, Berthelot-Grosjean M, Parekh H, Richmond JE. (2007). Tomosyn negatively regulates both synaptic transmitter and neuropeptide release at the C. elegans neuromuscular junction. J Physiol. Dec 15;585(Pt 3):705-9.

Hegde AN. (2010). The ubiquitin-proteasome pathway and synaptic plasticity. Learn Mem. Jun 21;17(7):314-27.

Hou L, Klann E. (2004). Activation of the phosphoinositide 3-kinase-Akt-mammalian target of rapamycin signaling pathway is required for metabotropic glutamate receptor-dependent long-term depression. J Neurosci. Jul 14;24(28):6352-61.

Hegde AN, Goldberg AL, Schwartz JH. (1993). Regulatory subunits of cAMP-dependent protein kinases are degraded after conjugation to ubiquitin: a molecular mechanism underlying long-term synaptic plasticity. Proc Natl Acad Sci U S A. Aug 15;90(16):7436-40.

Henry FE, McCartney AJ, Neely R, Perez AS, Carruthers CJ, Stuenkel EL, Inoki K, Sutton MA. (2012). Retrograde changes in presynaptic function driven by dendritic mTORC1. J Neurosci. Nov 28;32(48):17128-42.

Hoeffer CA, Klann E. (2010). mTOR signaling: at the crossroads of plasticity, memory and disease. Trends Neurosci. Feb;33(2):67-75.

Jakawich SK, Nasser HB, Strong MJ, McCartney AJ, Perez AS, Rakesh N, Carruthers CJ, Sutton MA. (2010). Local presynaptic activity gates homeostatic changes in presynaptic function driven by dendritic BDNF synthesis. Neuron. Dec 22;68(6):1143-58.

Jarome TJ, Kwapis JL, Ruenzel WL, Helmstetter FJ. (2013). CaMKII, but not protein kinase A, regulates Rpt6 phosphorylation and proteasome activity during the formation of long-term memories. Front Behav Neurosci. Aug 30;7:115.

Jiang X, Litkowski PE, Taylor AA, Lin Y, Snider BJ, Moulder KL. (2010). A role for the ubiquitin-proteasome system in activity-dependent presynaptic silencing. J Neurosci. Feb 3;30(5):1798-809.

Karpova A, Mikhaylova M, Thomas U, Knöpfel T, Behnisch T. (2006). Involvement of protein synthesis and degradation in long-term potentiation of Schaffer collateral CA1 synapses. J Neurosci. May 3;26(18):4949-55.

Lazarevic V, Schöne C, Heine M, Gundelfinger ED, Fejtova A. (2011). Extensive remodeling of the presynaptic cytomatrix upon homeostatic adaptation to network activity silencing. J Neurosci. Jul 13;31(28):10189-200.

Lessmann V, Heumann R. (1998). Modulation of unitary glutamatergic synapses by neurotrophin-4/5 or brain-derived neurotrophic factor in hippocampal microcultures: presynaptic enhancement depends on pre-established paired-pulse facilitation. Neuroscience. Sep;86(2):399-413.

Lewcock JW, Genoud N, Lettieri K, Pfaff SL. (2007). The ubiquitin ligase Phr1 regulates axon outgrowth through modulation of microtubule dynamics. Neuron. Nov 21;56(4):604-20.

Li YX, Xu Y, Ju D, Lester HA, Davidson N, Schuman EM. (1998). Expression of a dominant negative TrkB receptor, T1, reveals a requirement for presynaptic signaling in BDNF-induced synaptic potentiation in cultured hippocampal neurons. Proc Natl Acad Sci U S A. Sep 1;95(18):10884-9.

Ma T, Tzavaras N, Tsokas P, Landau EM, Blitzer RD. (2011). Synaptic stimulation of mTOR is mediated by Wnt signaling and regulation of glycogen synthetase kinase-3. J Neurosci. Nov 30;31(48):17537-46.

Marangoudakis S, Andrade A, Helton TD, Denome S, Castiglioni AJ, Lipscombe D. (2012). Differential ubiquitination and proteasome regulation of Ca(V)2.2 N-type channel splice isoforms. J Neurosci. Jul 25;32(30):10365-9.

Nayak A, Zastrow DJ, Lickteig R, Zahniser NR, Browning MD. (1998). Maintenance of late-phase LTP is accompanied by PKA-dependent increase in AMPA receptor synthesis. Nature. Aug 13;394(6694):680-3.

O'Rourke NA, Weiler NC, Micheva KD, Smith SJ. (2012). Deep molecular diversity of mammalian synapses: why it matters and how to measure it. Nat Rev Neurosci. May 10;13(6):365-79.

Ostroff LE, Fiala JC, Allwardt B, Harris KM. (2002). Polyribosomes redistribute from dendritic shafts into spines with enlarged synapses during LTP in developing rat hippocampal slices. Neuron. Aug 1;35(3):535-45.

Patapoutian A, Reichardt LF. (2001). Trk receptors: mediators of neurotrophin action. Curr Opin Neurobiol. Jun;11(3):272-80.

Rinetti GV, Schweizer FE. (2010). Ubiquitination acutely regulates presynaptic neurotransmitter release in mammalian neurons. J Neurosci. Mar 3;30(9):3157-66.

Russell SJ, Steger KA, Johnston SA. (1999). Subcellular localization, stoichiometry, and protein levels of 26 S proteasome subunits in yeast. J Biol Chem. Jul 30;274(31):21943-52.

Satoh K, Sasajima H, Nyoumura KI, Yokosawa H, Sawada H. (2001). Assembly of the 26S proteasome is regulated by phosphorylation of the p45/Rpt6 ATPase subunit. Biochemistry. Jan 16;40(2):314-9.

Scott DA, Das U, Tang Y, Roy S. (2011). Mechanistic logic underlying the axonal transport of cytosolic proteins. Neuron. May 12;70(3):441-54.

Shen H, Korutla L, Champtiaux N, Toda S, LaLumiere R, Vallone J, Klugmann M, Blendy JA, Mackler SA, Kalivas PW. (2007). NAC1 regulates the recruitment of the proteasome complex into dendritic spines. J Neurosci. Aug 15;27(33):8903-13.

Sharma M, Burré J, Südhof TC. (2011). CSPα promotes SNARE-complex assembly by chaperoning SNAP-25 during synaptic activity. Nat Cell Biol. Jan;13(1):30-9.

Spangler SA, Schmitz SK, Kevenaar JT, de Graaff E, de Wit H, Demmers J, Toonen RF, Hoogenraad CC. (2013). Liprin-α2 promotes the presynaptic recruitment and turnover of RIM1/CASK to facilitate synaptic transmission. J Cell Biol. Jun 10;201(6):915-28.

Speese SD, Trotta N, Rodesch CK, Aravamudan B, Broadie K. (2003). The ubiquitin proteasome system acutely regulates presynaptic protein turnover and synaptic efficacy. Curr Biol. May 27;13(11):899-910.

Steward O, Levy WB. (1982). Preferential localization of polyribosomes under the base of dendritic spines in granule cells of the dentate gyrus. J Neurosci. Mar;2(3):284-91.

Tang SJ, Reis G, Kang H, Gingras AC, Sonenberg N, Schuman EM. (2002). A rapamycin-sensitive signaling pathway contributes to long-term synaptic plasticity in the hippocampus. Proc Natl Acad Sci U S A. Jan 8;99(1):467-72.

Upadhya SC, Smith TK, Hegde AN. (2004). Ubiquitin-proteasome-mediated CREB repressor degradation during induction of long-term facilitation. J Neurochem. Oct;91(1):210-9.

Upadhya SC, Ding L, Smith TK, Hegde AN. (2006). Differential regulation of proteasome activity in the nucleus and the synaptic terminals. Neurochem Int. Mar;48(4):296-305.

Waites CL, Leal-Ortiz SA, Okerlund N, Dalke H, Fejtova A, Altrock WD, Gundelfinger ED, Garner CC. (2013). Bassoon and Piccolo maintain synapse integrity by regulating protein ubiquitination and degradation. EMBO J. Apr 3;32(7):954-69.

Waithe D, Ferron L, Page KM, Chaggar K, Dolphin AC. (2011). Beta-subunits promote the expression of Ca(V)2.2 channels by reducing their proteasomal degradation. J Biol Chem. Mar 18;286(11):9598-611.

Wheeler TC, Chin LS, Li Y, Roudabush FL, Li L. (2002). Regulation of synaptophysin degradation by mammalian homologues of seven in absentia. J Biol Chem. Mar 22;277(12):10273-82.

Willeumier K, Pulst SM, Schweizer FE. (2006). Proteasome inhibition triggers activity-dependent increase in the size of the recycling vesicle pool in cultured hippocampal neurons. J Neurosci. Nov 1;26(44):11333-41.

Yao I, Takagi H, Ageta H, Kahyo T, Sato S, Hatanaka K, Fukuda Y, Chiba T, Morone N, Yuasa S, Inokuchi K, Ohtsuka T, Macgregor GR, Tanaka K, Setou M. (2007). SCRAPPER-dependent ubiquitination of active zone protein RIM1 regulates synaptic vesicle release. Cell. Sep 7;130(5):943-57.

Yizhar O, Matti U, Melamed R, Hagalili Y, Bruns D, Rettig J, Ashery U. (2004). Tomosyn inhibits priming of large dense-core vesicles in a calcium-dependent manner. Proc Natl Acad Sci U S A. Feb 24;101(8):2578-83.

Zhang F, Hu Y, Huang P, Toleman CA, Paterson AJ, Kudlow JE. (2007). Proteasome function is regulated by cyclic AMP-dependent protein kinase through phosphorylation of Rpt6. J Biol Chem. Aug 3;282(31):22460-71.

Zhao Y, Hegde AN, Martin KC. (2003). The ubiquitin proteasome system functions as an inhibitory constraint on synaptic strengthening. Curr Biol. May 27;13(11):887-98.

CHAPTER VI

General Discussion

Collectively, the data collected as part of this dissertation work suggest that postsynaptic mTORC1 signaling is responsive to changes in dendritic voltage or synaptic $Ca2^+$ influx, and that blockade of AMPARs or L-type voltage gated $Ca2^+$ channels with CNQX or Nifedipine is a sufficient stimulus to drive a homeostatic shift in presynaptic function via mTOR-dependent synthesis of BDNF as a retrograde signal (Chapter 2). Work from multiple labs has suggested that retrograde control of presynaptic function may be mediated by cell-adhesion proteins (Hu et al., 2012, Futai et al, 2007) particularly in the context of homeostatic adaptation to spike blockade (Vitureira et al., 2011). Our own findings add to a growing body of evidence which supports the notion that trans-synaptically mediated homeostasis induced by loss of excitatory input (i.e. AMPAR blockade) relies instead on retrograde signaling from the post to presynaptic compartment via a diffusible signal. The data presented here is in agreement with previous reports at mammalian central synapses that have identified this retrograde signal as BDNF (Jackawhich, et al., 2010; Lindskog et al., 2010), or Nitric oxide (Lindskog et al., 2010). A similar role for postsynaptic mTORC1 in the expression of presynaptic homeostasis was recently demonstrated at the fly NMJ (Penney et al., 2012), though the molecular identity of the retrograde signal at this synapse remains unknown. An interesting feature of the work from Penney et al was the finding that postsynaptic genetic upregulation of mTORC1 activity was sufficient to induce rapid enhancement of presynaptic function. Our work at mammalian central synapses mirrors and extends these findings. Indeed, we report that this retrograde signaling mechanism appear to be an immediate effect of hyperactive mTORC1 signaling, as acute activation of mTORC1 with the lipid second messenger PA is sufficient to drive BDNF-dependent increases in presynaptic release (Chapter 3). This is notable, as it suggests that mTORC1-induced retrograde signaling may be a conserved mechanism across multiple species and synapse types to dynamically match presynaptic release to the functional properties of the postsynaptic cell. Experiments conducted at the fly NMJ have led some to posit the existence of multiple proteins operating in the postsynaptic compartment to exert and inhibitory block on mTORC1-mediated release of a retrograde signal (Frank, 2013), including dystrophin (van der Plas et al., 2006), Importin-13 (Giagtzoglou et al., 2009), and cv-c (Pilgram et al., 2011). Rather than identify postsynaptic inhibitors of mTORC1-mediated homeostasis, our work highlights a unique role for PLD1-mediated hydrolysis of the lipid second messenger PA in the activation of mTOR during activity blockade (Chapter 4). This combined pathway of PLD1-->PA-->mTOR activation appears to operate as a homeostatic sensor mechanism to detect shifts in postsynaptic activation, and, strikingly, is completely unnecessary for synaptically-driven mTORC1 activation during chemically-induced LTP. These findings suggest that unique means of mTOR activation have the potential to result in functional outcomes that are specific for the manner in which mTORC1 is activated. This could have important implications for our understanding of mTOR-related neurodevelopmental disorders, in that it may be difficult to anticipate a stereotyped functional change at the level of the synapse in response to upregulated mTOR signaling after mutations in PTEN, TSC1/2 or NF1. FInally, we identify a novel presynaptic effector mechanism at work during state-dependent homeostasis, wherein activity dependent relocalization of the UPS interacts with retrograde BDNF signaling to drive changes in presynaptic release (Chapter 5). This finding situates state-dependent presynaptic homeostasis driven by loss of excitatory input as a form of plasticity which is brought about by the coordinated regulation of local translation and targeted degradation at synapses. There are a growing number of examples of similar types of co-operative synthesis and breakdown mechanisms at work in other forms of plasticity, including during mGluR-LTD (Hou et al., 2006) and after NMDAR stimulation (Banerjee et al., 2009), though these appear to be instances of breakdown and synthesis operating in same synaptic compartment. The type of interaction we describe here is unique in that it involves coordination of degradation and translation in apposed synaptic compartments, linked by a retrograde signal.

Defining the molecular players in a homeostatic circuit at excitatory synapses

One of the defining features of a homeostatic system is that it exhibits a constant output. The acceptable range of functional output is defined as the ‘set point’, deviations from which trigger feedback mechanisms to return output levels to acceptable norms (Davis, 2006). In the case of global changes in synapse function induced by prolonged spike blockade with TTX (Ibata et al., 2008) or increased activity via CHR2 stimulation (Goold and Nicoll, 2011), it is believed that homeostatic sensors respond to abnormally high or low levels of somatic calcium influx and enact feedback mechanisms to return spike activity to within an acceptable range (Turrigiano et al., 2011). In these cases, somatically localized CamKIV and CamKK appear to act as components of a sensor mechanism which detects deviations in somatic calcium influx and implements feedback via changes in transcription. In the case of locally-mediated synaptic homeostasis, it is less clear what parameter of neuronal function is attempting to be maintained.

Stated more simply, what is the relevant 'output' measure in dendrites, deviations from which trigger spatially restricted homeostatic adaptations? It seems unlikely that a dendritic branch or individual synapse would be sensitive to changes in cell firing, though it is conceivable that back-propagating action potentials could signal this sort of information. An alternative possibility that is more parsimonious with the data presented here, is that dendrites contain sensor mechanisms which are sensitive to localized changes in voltage or $Ca2^+$ influx. The nature of the homeostatic challenges implemented in our experiments lend support to this idea, as AMPAR blockade with CNQX and voltage-gated $Ca2^+$-channel blockade with Nifedipine both undoubtedly alter steady state levels of dendritic $Ca2^+$ influx and leave the dendritic arbor in a more hyperpolarized state than it would be under normal conditions. Work from Lu Chen's lab has identified retinoic acid (RA) as a componenet of a $Ca2^+$-sensitive postsynaptic sensor crucial for implementing postsynaptic functional compensation in response to loss of excitatory input (Chen et al., 2012). Our finding that intracellular synthesis of PA is necessary for presynaptic homeostasis but not cLTP suggests that PLD1 might operate as a component of a similar $Ca2^+$ sensing mechanism operating locally in dendrites. Additional work is needed to clearly define the manner in which PLD1 respnds to changes in voltage or $Ca2^+$ influx.

Regarding effector mechanisms, our results suggest that degradation of an as yet unidentified presynaptic protein likely mediates the homeostatic changes induced by retrograde BDNF signaling (Chapter 5). Aside from this putative UPS target, the work described here does not provide additional insight into potential effectors in this homeostatic circuit. However, the type of plasticity we describe here has much in common with a commonly studied form of synaptic homeostasis characterized at the Drosophila NMJ (Frank, 2013). The genetic tractability of the fly as a model system has provided a unique opportunity to understand how synaptic homeostasis driven by loss of excitatory input is implemented at the molecular level. As previously discussed, forward genetic screens using a philanthotoxin based model of synaptic homeostasis at the fly NMJ has identified a number of presynaptic proteins which are vital for the expression of presynaptic homeostasis. Thus far, however, there have been no published hits for a protein which serves to dampen vesicle release under normal conditions, as would fit our proposed model. It would informative to use PhTx or GluAII-knockout based models of synaptic homeostasis at the fly NMJ to test for a potential role of presynaptic disinhibition mediated by degradation of a protein such as tomosyn or Slp4-A. The field of homeostatic plasticity has benefited immensely from the unique benefits provided by mammalian and invertebrate model systems, and ongoing shared effort between labs utilizing these approaches will be vital if we are to achieve a more complete understanding of the molecular players involved in state-dependent presynaptic homeostasis.

An intriguing possibility left untested by the experiments described here is that mTORC1-dependent retrograde signaling mechanisms may play a role in establishing coherence between pre and post-synaptic efficacy outside of the context of explicit deprivation of excitatory input. Evidence across multiple species and cell types demonstrates that fundamental aspects of a presynaptic terminal's function, such as release probability, are influenced by the identity and characteristics of the postsynaptic cell on which they make contact (Davis, 1995). In addition, one feature of the postsynaptic cell to which presynaptic contacts appear to be particularly sensitive is the relative degree of dendritic depolarization. Studies conducted at the drosophila neuromuscular junction (NMJ) indicate that experimentally-induced hyperpolarization of the postsynaptic membrane potential is sufficient to induce a compensatory increase in presynaptic release (Paradis et al., 2001). In the mammalian CNS, the discovery of an inverse correlation between presynaptic release probability and the number of synapses on a given dendritic branch of a pyramidal neuron has supported the idea that presynaptic efficacy homeostatically adjusts to unique levels of background synaptic activity present in any given dendrite (Branco et al., 2008). This would seem to require a mechanism responsible for integrating information about changes in levels of dendritic depolarization, and dynamically implementing feedback mechanisms to adjust presynaptic inputs accordingly. Achieving balance in pre-and postsynaptic function appears to be of fundamental importance at several types of synapses, and may be one of the most basic and widespread uses of post to pre-synaptic retrograde signaling in the nervous system (Regehr et al., 2009). Our work suggests that dendritic mTORC1 may contribute to this type of trans-synaptic homeostasis via dendritic synthesis of BDNF as a retrograde signal, through an explicit requirement for mTOR in the type of steady-state pre and postsynaptic functional matching characterized by Branco and colleagues remains to be tested.

mTORC1 dysregulation, E/I imbalance and the pathophysiology of ASD

Given its position as a central node in a rich signaling pathway with links to diverse cell functions including cell growth and division, it is perhaps unsurprising to find that dysregulated mTORC1 signaling has been implicated in multiple psychiatric and neurological conditions including Autism Spectrum Disorders (Hoeffer and Klann, 2010), epilepsy (Wong, 2010), Major Depressive Disorder (Duman et al., 2012), and neurodegenerative disorders including Alzheimer's Disease (Pei and Hugom, 2008). In the space which remains, my aim is to provide an account of how mTORC1 signaling contributes to the neuropathology of ASD, with particular emphasis on how disruptions in mTORC1-mediated homeostasis may contribute to the altered balance in excitatory and inhibitory tone common to this multifaceted disorder.

Dysreguated mTORC1 signaling in Autism Spectrum Disorders

Autism spectrum disorders (ASD) represent a heterogenous group of conditions with a triad of core diagnostic features including deficits in communication, impaired social interaction and a predisposition toward repetitive behaviors (Fombonne, 1999). Roughly 70% of autistic individuals also suffer from mental retardation. Recent advances in genomic approaches to understanding ASD have revealed a complex network of genes that may be responsible for the divergent phenotypic abnormalities present in human patients. Notably, a plurality of ASD-related mutations appear to be in genes which serve functions in chromatin remodeling, metabolism, mRNA translation, and synaptic transmission, with potential functional convergence around the maintenance of neuronal and synaptic homeostasis (Hugeut et al., 2013). The study of monogenic forms of ASD has provided valuable opportunities to try and uncover synaptic and behavioral commonalities between multiple genetic heterogeneous forms of ASD. Interestingly, many of these single-gene disorders commonly related to autism result in overactive mTORC1 signaling, leading some to posit that dysregulated translational control at synapses may be a common phenotype central to the emergence of aberrant cognitive and behavioral characteristics related to ASD (Kelleher and Bear 2008; Bourgeron, 2009; Hoeffer and Klann, 2010). Tuberous sclerosis complex and fragile X syndrome (FXS) are disorders with high rates of comorbidity with ASD. The proteins mutated in these disorders, TSC1/2 and FMRP respectively, normally act to inhibit mTORC1 activity. In addition, the genetic mutations related to Neurofibromatosis Type 1 (NF1) and PTEN hamartoma syndrome also lead to overactive translation via disinhibition of mTORC1, resulting in profound cognitive deficits and mental retardation.

mTORC1 also has an essential role in neuronal development and plasticity (Jaworski and Sheng, 2006), again suggesting a potential link in the etiology of developmental disorders such as ASD.

E/I Imbalance as general feature of ASD and Epilepsy

An important insight into a potential shared mechanism behind the sensory, cognitive, and social dysfunctions common in ASD arose from the observation that patients with ASD often exhibit characteristics of epilepsy (Tuchman and Cuccaro, 2011). Since the first reported cases of ASD by Leo Kanner in 1943, the clinical community has appreciated the high degree of co-morbidity between ASD and epilepsy (Kanner 1943). Roughly 50-70 percent of children with ASD exhibit epilepsy-elated sharp spike activity in MEG recordings during sleep (Lewine et al., 1999). In addition, a recent meta-analysis surveying all published reports from 1963-2006 showed a high degree of symptomatic overlap between the two disorders, with unique manifestations depending on the severity of the cognitive disability in ASD patients: 21.4% of ASD patients with co-morbid Intellectual disability also present with Epilepsy vs 8% observed in AD patients who carry no evidence of intellectual disability (Amiet et al., 2008).

The etiology of epilepsy is complex, with a diverse array of both genetic and environmental factors that can bias neuronal circuits toward aberrant synchronization resulting in seizures (Goldberg and Colter, 2013). However, increased mTORC1 signaling appears to be a commonly observed feature of many animal models of epilepsy, as seen after seizures induced by kainate (Zeng et al., 2009), Pilocarpine (Huang et al., 2010), and Pentylenetetrazole (Zhang and Wong, 2012). It is likely that seizure-related increases in neuronal activity drive mTOR signaling on their own, but observations from syndromic disorders characterized by unchecked mTOR kinase activity suggest that mTORC1 signaling may also play a causal role in the development or progression of epileptogenesis. Indeed, animals models exhibiting loss of PTEN or TSC1/2 function reliably develop spontaneous seizures (Ogawa et al., 2007), which can be ameliorated by treatment with rapamycin (Zhou et al., 2009, Zeng et al., 2008). Recent evidence suggests that mTORC1 dysregulation need not be system-wide for seizures to develop, as the selective deletion of the inhibitory mTOR regulator PTEN from dentate granule cells is sufficient to induce Temporal Lobe epilepsy, likely stemming from morphological changes including the aberrant growth of basal dendrites, and spine density roughly double that of normal cells (Pun et al., 2012). This study is one of several that indicate mTOR-mediated changes in dentate granule cell development and migration, including abnormal mossy fiber sprouting (Buckmaster et al., 2009), contribute to epileptogenesis. However, there is additional experimental support for a common synaptic basis of aberrant neuronal synchrony in conditions such as Tuberous Sclerosis that is mediated by elevated glutamatergic signaling (Wang et al., 2007).

There is considerable evidence for a positive relationship between the severity of cognitive impairment in ASD and prevalence of seizures (Giannotti et al., 2008; Parmeggiani et al., 2010), particularly for patients with Tuberous Sclerosis Complex (Jeste et al., 2008). In the past decade, these observations lead to the breakthrough conceptual advance that similarly unstable or noisy cortical networks may be a common feature to certain forms of epilepsy and ASD. Particularly, as originally proposed by Rubenstein and Merzenich (2003), it is possible that an imbalance in the ratio of excitatory and inhibitory tone in key brain regions which mediate sensory, language, or social behaviors could be a fundamental feature of ASD. This E/I imbalance was postulated to take the form of increased excitation, manifested via aberrantly high glutamatergic synaptic function or aberrantly low GABAergic synaptic function. A circuit-level proof of principle for this idea was performed recently, using bistable step-function opsins to chronically elevate firing activity of select populations of excitatory or PV+ inhibitory neurons in the mouse prefrontal cortex (Yizhar et al., 2011). Strikingly, a shift in E/I balance toward overexcitation resulted in deficits in episodic learning and social interactions, while comparable shifts toward increased inhibitory tone in the same brain regions produced no such effects.

There is evidence to support that this imbalance of excitation and inhibition in the brains of patients with ASD arises from disruptions in GABA mediated inhibition. For instance, removal of MecP2 specifically from GABAergic interneurons reduces inhibitory quantal size, and phenocopies many fundamental aspects of Rett syndrome seen in global MecP2 mutant Mice (Chao et al., 2010). A fascinating recent study also suggests that loss of TSC1 in GABAergic purkinje neurons of the cerebellum is sufficient to recapitulates many common ASD-like phenotypes including repetitive behaviors and impaired social interactions (Tsai et al., 2012). Though inhibitory synapse dysfunction can undoubtedly contribute to the E/I imbalance observed in ASD, there is additional evidence to support genetic links to disrupted excitatory transmission. A plurality of mutations implicated in neurodevelopmental disorders such as ASD are found in proteins localized at excitatory synapses and are integral for glutamatergic signaling at the postsynaptic density (Ebert and greenberg, 2013; Huguet et al., 2013). A unique role for altered excitatory tone in ASD is bolseted by fascinating recent work from Zylka lab, which has advanced the hypothesis that genes associated with ASD, are on average 3.7x longer than the general population of genes expressed in cortical neurons. As such, mutations with alter the transcription elongation process or topoisomerase activity in particular could have a disproportionately strong effect on the expression of ASD-related genes (King et al., 2013). The authors provide support for this model showing that pharmacological or genetic disruption in topoisomerase activity impairs the expression of 49 genes previously linked to ASD, 24 of which have previously validated roles in the development or proper function of excitatory synapses, including Cntnap2 (ref), Neurexin 3 (Aoto et al., 2013), Grid2 (Lomeli et al., 1993), IL1RAPL1 (Pavlowsky et al., 2010), PARK2 (Helton et al., 2008), Cntn5 (Toyoshima et al., 2009), Ptprt (Lim et al., 2009), Frmpd4 (Lee et al., 2008), Neurexin1 (de Wit et al., 2009), Gpc6 (Allen et al., 2012), Grm7 (Boudin et al., 2007), Nlgn1 (Irie et al., 1997), Grid1 (Roche et al., 1999), Kcnma1 (Hu et al., 2001), Grik2 (Lanore et al., 2012), Plcb1 (Spires et al., 2005), Nbea (Niesmann et al., 2011), Grm5 (Ko et al., 2012), Kalrn (Penzes et al., 2003), Robo2 (Campbell et al., 2007), Cacna1c (Obermair et al., 2004), Lrrc7 (Apperson et al., 1996), Reln (Qiu and Weber, 2007), and Nxph1 (Petrenko et al., 1996).

There is also growing support for a specific contribution of disrupted synaptic homeostatic mechanisms in the development of circuit abnormalities seen in ASD. In this model, loss of synaptic flexibility via mutations in proteins which serve vital roles in the expression of homeostatic plasticity lead to profound and progressive circuit level abnormalities. If these dysfunctional networks reside in brain regions responsible for communication, social interaction or repetitive behaviors, the behavioral phenotypes that emerge will likely be those most commonly associated with ASP patients (Ramocki and Zoghbi, 2008; Toro et al., 2010). Recent experimental evidence has shown an overlap between proteins known to be important for synaptic homeostasis and those known to be mutated in several forms of ASD. For example, loss of function in FMRP has been shown to disrupt synaptic homeostasis induced by concurrent TTX and APV treatent (Soden and Chen, 2010). Synaptic levels of SHANKs, PSD scaffolding proteins implicated in several forms of ASD (Jiang and Ehlers, 2013), have been shown to be under homeostatic control via UPS-mediated degradation (Ehlers, 2003). Additionally, multiple recent studies have found that methyl CpG binding protein 2 (MeCP2), a transcriptional repressor linked to Rett syndrome (Amir et al., 1999), is necessary for homeostatic reductions in the strength of excitatory synapses after prolonged network level activity increases (Qiu et al., 2012; Zhong t al., 2012). Our finding that mTORC1 critically regulates the synthesis of a retrograde signal at work in trans-synaptic homeostatic signaling further suggests that failure in adaptive plasticity measures may be a central feature of many forms of ASD. The type of dysregulated homeostatic measures we report here could be a contributing factor to the gradual emergence of E/I circuit level imbalances common to ASD. Mutations in proteins which normally serve to dampen mTOR function such as TSC1/2, NF1 or PTEN, would presumably limit the ability of mTORC1 to homeostatically regulate synaptic function, and may instead lead to unchecked strengthening of presynaptic connectivity via retrograde feedback mechanisms. As such, treatments that alter E/I imbalance are emerging as a promising point of therapeutic intervention in ASD, as discussed below.

Current attempts to treat mTOR-opathies and future prospects

Limited but encouraging progress has been made in recent years to correct the synaptic and behavioral deficits in mTOR-related neurodevelopmental disorders. Of particular interest have been attempts to modify mTORC1 signaling specifically, or translational regulation in general, to ameliorate abnormal phenotypes in ASD mouse models (Delorme et al., 2013). Multiple mouse models of ASD with disruptions in mTORC1 signaling have been shown to benefit from rapamycin treatment. TSC2-/- mice, for example, show improvements in L-LTP and spatial learning after receiving 5 days of rapamycin injections (Ehninger et al., 2008). Rapamycin treatment also improved deficits in social interactions and anxiety-like behaviors in a mouse model of PTEN Hamartoma Syndrome (Zhou et al., 2009). An alternate mTOR inhibitor temsirolimus has been shown to reduce the threshold for audiogenic seizures and correct deficits in object recognition memory in Fmr1 knockout mice (Busquets-Garcia et al., 2013). These data from mouse models of ASD, combined with emerging reports of reduced seizure frequency in human patients with TSC or PMSE (polyhydramnios, megalencephaly, and symptomatic epilepsy syndrome) after treatment with rapamycin or the rapalog everolimus (Kreuger et al., 2013; Parker et al., 2013), are remarkable in that they suggest that reduction in dysregulated mTORC1 signaling is perhaps sufficient to correct behavioral phenotypes in animals for which the major steps of neuronal circuit development have already occurred. This is not a finding shared by all attempted interventions in animals models of neurodevelopmental disorders. Mutations in SynGAP1, for example, disrupt the maturation of excitatory synapses and lead to ASD-like phenotypes. If this mutation is corrected before a critical period of circuit formation, the associated behavioral phenotype is eliminated (Clement et al, 2012). If interventions are made after this developmental window, however, no correction in ASD-like behaviors are observed, suggesting that disrupted circuit formation itself is the central cause of phenotypic dysfunction observed in this form of ASD, which is perhaps not that case for conditions linked to mTOR dysfunction.

Recalling the earlier stated hypothesis of E/I imbalance as a central feature of ASD, exciting recent work has provided initial indications that increasing systemic inhibitory tone could be a useful alterntive strategy for correcting the maladaptive phenotypes associated with certain forms of ASD. As a truly inspiring example of “bench-to-bedside” science at work, a group from Seaside therapeutics has recently used the GABA-B receptor agonist Arbaclofen to correct the abnormal protein synthesis, increased dendritic spine density, seizure frequency and instances of repetitive behavior in fmr1 knockout mice (Henderson et al., 2012). This opens an exciting possibility for potential therapeutic interventions in mTOR-opathies such as PTEN Hamartoma syndrome and Tuberous Sclerosis. There is evidence for hyperactive mTOR signaling in both fmr1-knockout animals (Sharma et al., 2010) and in fragile x patients (Hoeffer et al, 2012), and recent work suggests that impaired inhibitory synaptic function is an early to emerge feature of hyperactive mTORC1 activity in TSC1 knockout neurons (Bateup et al., 2013). Additional work is necessary to determine if a similar approach targeted at elevating inhibition would be equally efficacious in forms of ASD with specific links to dysregulated mTORC1 activity. The work collected here identifies BDNF-mediated augmentation of presynaptic signaling as an immediate consequence of hyperactive mTORC1 signaling. This presynaptic enhancement requires the presence of the UPS at synaptic terminals, the distribution of which can be altered by diminished spike activity. As such, increasing inhibitory tone using an approach similar to that taken by Henderson and colleagues could serve to reduce proteasome accumulation at synaptic boutons, thereby potentially mitigating the effects of hyperactive mTOR at the network level.

Bibliography

Allen NJ, Bennett ML, Foo LC, Wang GX, Chakraborty C, Smith SJ, Barres BA. (2012). Astrocyte glypicans 4 and 6 promote formation of excitatory synapses via GluA1 AMPA receptors. Nature. May 27;486(7403):410-4.

Amiet C, Gourfinkel-An I, Bouzamondo A, Tordjman S, Baulac M, Lechat P, Mottron L, Cohen D. (2008). Epilepsy in autism is associated with intellectual disability and gender: evidence from a meta-analysis. Biol Psychiatry. Oct 1;64(7):577-82.

Amir RE, Van den Veyver IB, Wan M, Tran CQ, Francke U, Zoghbi HY. (1999). Rett syndrome is caused by mutations in X-linked MECP2, encoding methyl-CpG-binding protein 2. Nat Genet. Oct;23(2):185-8.

Apperson ML, Moon IS, Kennedy MB. (1996). Characterization of densin-180, a new brain-specific synaptic protein of the O-sialoglycoprotein family. J Neurosci. 1996 Nov 1;16(21):6839-52.

Auerbach BD, Osterweil EK, Bear MF. (2011). Mutations causing syndromic autism define an axis of synaptic pathophysiology. Nature. 2011 Nov 23;480(7375):63-8.

Banerjee S, Neveu P, Kosik KS. (2009). A coordinated local translational control point at the synapse involving relief from silencing and MOV10 degradation. Neuron. 2009 Dec 24;64(6):871-84.

Bateup HS, Johnson CA, Denefrio CL, Saulnier JL, Kornacker K, Sabatini BL. (2013). Excitatory/inhibitory synaptic imbalance leads to hippocampal hyperexcitability in mouse models of tuberous sclerosis. Neuron. May 8;78(3):510-22.

Béïque JC, Na Y, Kuhl D, Worley PF, Huganir RL. (2011). Arc-dependent synapse-specific homeostatic plasticity. Proc Natl Acad Sci U S A. Jan 11;108(2):816-21.

Boudin H, Doan A, Xia J, Shigemoto R, Huganir RL, Worley P, Craig AM. (2000). Presynaptic clustering of mGluR7a requires the PICK1 PDZ domain binding site. Neuron. Nov;28(2):485-97.

Bourgeron T. (2009). A synaptic trek to autism. Curr Opin Neurobiol. Apr;19(2):231-4.

Branco T, Häusser M. (2010). The single dendritic branch as a fundamental functional unit in the nervous system. Curr Opin Neurobiol. Aug;20(4):494-502.

Buckmaster PS, Ingram EA, Wen X. (2009). Inhibition of the mammalian target of rapamycin signaling pathway suppresses dentate granule cell axon sprouting in a rodent model of temporal lobe epilepsy. J Neurosci. Jun 24;29(25):8259-69.

Busquets-Garcia A, Gomis-González M, Guegan T, Agustín-Pavón C, Pastor A, Mato S, Pérez-Samartín A, Matute C, de la Torre R, Dierssen M, Maldonado R,Ozaita A. (2013). Targeting the endocannabinoid system in the treatment of fragile X syndrome. Nat Med. May;19(5):603-7.

Campbell DS, Stringham SA, Timm A, Xiao T, Law MY, Baier H, Nonet ML, Chien CB. (2007). Slit1a inhibits retinal ganglion cell arborization and synaptogenesis via Robo2-dependent and -independent pathways. Neuron. 2007 Jul 19;55(2):231-45.

Chao HT, Chen H, Samaco RC, Xue M, Chahrour M, Yoo J, Neul JL, Gong S, Lu HC, Heintz N, Ekker M, Rubenstein JL, Noebels JL, Rosenmund C, Zoghbi HY. (2010). Dysfunction in GABA signalling mediates autism-like stereotypies and Rett syndrome phenotypes. Nature.Nov 11;468(7321):263-9.

Chen L, Lau AG, Sarti F. (2012). Synaptic retinoic acid signaling and homeostatic synaptic plasticity. Neuropharmacology. 2012 Dec 25. pii: S0028-3908(12)00597-7.

Clement JP, Aceti M, Creson TK, Ozkan ED, Shi Y, Reish NJ, Almonte AG, Miller BH, Wiltgen BJ, Miller CA, Xu X, Rumbaugh G. (2012). Pathogenic SYNGAP1 mutations impair cognitive development by disrupting maturation of dendritic spine synapses. Cell. 2012 Nov 9;151(4):709-23.

Corner MA, Baker RE, van Pelt J. (2006). Homeostatically regulated spontaneous neuronal discharges protect developing cerebral cortex networks from becoming hyperactive following prolonged blockade of excitatory synaptic receptors. Brain Res. 2006 Aug 23;1106(1):40-5.

Davis GW. (2006). Homeostatic control of neural activity: from phenomenology to molecular design. Annu Rev Neurosci. 2006;29:307-23.

de Wit J, Sylwestrak E, O'Sullivan ML, Otto S, Tiglio K, Savas JN, Yates JR 3rd, Comoletti D, Taylor P, Ghosh A. LRRTM2 interacts with Neurexin1 and regulates excitatory synapse formation. Neuron. 2009 Dec 24;64(6):799-806.

Delorme R, Ey E, Toro R, Leboyer M, Gillberg C, Bourgeron T. (2013). Progress toward treatments for synaptic defects in autism. Nat Med. Jun;19(6):685-94.

Duman RS, Li N, Liu RJ, Duric V, Aghajanian G. (2012). Signaling pathways underlying the rapid antidepressant actions of ketamine. Neuropharmacology. Jan;62(1):35-41.

Ebert DH, Greenberg ME. (2013). Activity-dependent neuronal signalling and autism spectrum disorder. Nature. 2013 Jan 17;493(7432):327-37.

Ehlers MD. (2003). Activity level controls postsynaptic composition and signaling via the ubiquitin-proteasome system. Nat Neurosci. 2003 Mar;6(3):231-42.

Ehninger D, Han S, Shilyansky C, Zhou Y, Li W, Kwiatkowski DJ, Ramesh V, Silva AJ. (2008). Reversal of learning deficits in a Tsc2± mouse model of tuberous sclerosis. Nat Med. Aug;14(8):843-8.

Feng P, Huang C. (2013). Phospholipase D-mTOR signaling is compromised in a rat model of depression. J Psychiatr Res. May;47(5):579-85.

Frank CA. (2013). Homeostatic plasticity at the Drosophila neuromuscular junction. Neuropharmacology. Jun 24. pii: S0028-3908(13)00283-9.

Fombonne E. (1999) The epidemiology of autism: a review. Psychol Med. Jul;29(4):769- 86.

Giagtzoglou N, Lin YQ, Haueter C, Bellen HJ. (2009). Importin 13 regulates neurotransmitter release at the Drosophila neuromuscular junction. J Neurosci. Apr 29;29(17):5628-39.

Giannotti F, Cortesi F, Cerquiglini A, Miraglia D, Vagnoni C, Sebastiani T, Bernabei P. (2008). An investigation of sleep characteristics, EEG abnormalities and epilepsy in developmentally regressed and non-regressed children with autism. J Autism Dev Disord. 2008 Nov;38(10):1888-97.

Goldberg EM, Coulter DA. (2013). Mechanisms of epileptogenesis: a convergence on neural circuit dysfunction. Nat Rev Neurosci. May;14(5):337-49.

Goold CP, Nicoll RA. (2010). Single-cell optogenetic excitation drives homeostatic synaptic depression. Neuron. Nov 4;68(3):512-28.

Helton TD, Otsuka T, Lee MC, Mu Y, Ehlers MD. (2008). Pruning and loss of excitatory synapses by the parkin ubiquitin ligase. Proc Natl Acad Sci U S A. Dec 9;105(49):19492-7.

Henderson C, Wijetunge L, Kinoshita MN, Shumway M, Hammond RS, Postma FR, Brynczka C, Rush R, Thomas A, Paylor R, Warren ST, Vanderklish PW,Kind PC, Carpenter RL, Bear MF, Healy AM. (2012). Reversal of disease-related pathologies in the fragile X mouse model by selective activation of GABAB receptors with arbaclofen. Sci Transl Med. Sep 19;4(152):152ra128.

Hoeffer CA, Sanchez E, Hagerman RJ, Mu Y, Nguyen DV, Wong H, Whelan AM, Zukin RS, Klann E, Tassone F. (212). Altered mTOR signaling and enhanced CYFIP2 expression levels in subjects with fragile X syndrome. Genes Brain Behav. Apr;11(3):332-41.

Hoeffer CA, Klann E. (2010). mTOR signaling: at the crossroads of plasticity, memory and disease. Trends Neurosci. Feb;33(2):67-75.

Hou L, Antion MD, Hu D, Spencer CM, Paylor R, Klann E. (2006). Dynamic translational and proteasomal regulation of fragile X mental retardation protein controls mGluR-dependent long-term depression. Neuron. Aug 17;51(4):441-54.

Hu H, Shao LR, Chavoshy S, Gu N, Trieb M, Behrens R, Laake P, Pongs O, Knaus HG, Ottersen OP, Storm JF. (2001). Presynaptic $Ca2^+$-activated K+ channels in glutamatergic hippocampal terminals and their role in spike repolarization and regulation of transmitter release. J Neurosci. Dec 15;21(24):9585-97.

Huang X, Zhang H, Yang J, Wu J, McMahon J, Lin Y, Cao Z, Gruenthal M, Huang Y. (2010). Pharmacological inhibition of the mammalian target of rapamycin pathway suppresses acquired epilepsy. Neurobiol Dis. Oct;40(1):193-9.

Huguet G, Ey E, Bourgeron T. (2013). The genetic landscapes of autism spectrum disorders. Annu Rev Genomics Hum Genet.;14:191-213.

Ibata K, Sun Q, Turrigiano GG. (2008). Rapid synaptic scaling induced by changes in postsynaptic firing. Neuron. Mar 27;57(6):819-26.

Irie M, Hata Y, Takeuchi M, Ichtchenko K, Toyoda A, Hirao K, Takai Y, Rosahl TW, Südhof TC. (1997). Binding of neuroligins to PSD-95. Science. Sep 5;277(5331):1511-5.

Jaworski J, Sheng M. (2006). The growing role of mTOR in neuronal development and plasticity. Mol Neurobiol. Dec;34(3):205-19.

Jeste SS, Sahin M, Bolton P, Ploubidis GB, Humphrey A. (2008). Characterization of autism in young children with tuberous sclerosis complex. J Child Neurol. May;23(5):520-5.

Jernigan CS, Goswami DB, Austin MC, Iyo AH, Chandran A, Stockmeier CA, Karolewicz B. (2011). The mTOR signaling pathway in the prefrontal cortex is compromised in major depressive disorder. Prog Neuropsychopharmacol Biol Psychiatry. Aug 15;35(7):1774-9.

Jiang YH, Ehlers MD. (2013). Modeling autism by SHANK gene mutations in mice. Neuron. Apr 10;78(1):8-27.

Kanner L. (1943). Autistic disturbances of affective contact. Nervous Child 2, 217-250

Kelleher RJ 3rd, Bear MF. (2008) The autistic neuron: troubled translation? Cell. Oct 31;135(3):401-6

King IF, Yandava CN, Mabb AM, Hsiao JS, Huang HS, Pearson BL, Calabrese JM, Starmer J, Parker JS, Magnuson T, Chamberlain SJ, Philpot BD, Zylka MJ. (2013). Topoisomerases facilitate transcription of long genes linked to autism. Nature. Sep 5;501(7465):58-62.

Ko SJ, Isozaki K, Kim I, Lee JH, Cho HJ, Sohn SY, Oh SR, Park S, Kim DG, Kim CH, Roche KW. (2012). PKC phosphorylation regulates mGluR5 trafficking by enhancing binding of Siah-1A. J Neurosci. Nov 14;32(46):16391-401.

Krueger DA, Wilfong AA, Holland-Bouley K, Anderson AE, Agricola K, Tudor C, Mays M, Lopez CM, Kim MO, Franz DN. (2013). Everolimus treatment of refractory epilepsy in tuberous sclerosis complex. Ann Neurol. Jun 24. doi: 10.1002/ana.23960.

Lanore F, Labrousse VF, Szabo Z, Normand E, Blanchet C, Mulle C. (2012). Deficits in morphofunctional maturation of hippocampal mossy fiber synapses in a mouse model of intellectual disability. J Neurosci. Dec 5;32(49):17882-93.

Lee HW, Choi J, Shin H, Kim K, Yang J, Na M, Choi SY, Kang GB, Eom SH, Kim H, Kim E. (2008). Preso, a novel PSD-95-interacting FERM and PDZ domain protein that regulates dendritic spine morphogenesis. J Neurosci. 2008 Dec 31;28(53):14546-56.

Lewine JD, Andrews R, Chez M, Patil AA, Devinsky O, Smith M, Kanner A, Davis JT, Funke M, Jones G, Chong B, Provencal S, Weisend M, Lee RR, Orrison WW Jr. (1999). Magnetoencephalographic patterns of epileptiform activity in children with regressive autism spectrum disorders. Pediatrics. Sep;104(3 Pt 1):405-18.

Li N, Lee B, Liu RJ, Banasr M, Dwyer JM, Iwata M, Li XY, Aghajanian G, Duman RS. (2010). mTOR-dependent synapse formation underlies the rapid antidepressant effects of NMDA antagonists. Science. 2010 Aug 20;329(5994):959-64.

Lim SH, Kwon SK, Lee MK, Moon J, Jeong DG, Park E, Kim SJ, Park BC, Lee SC, Ryu SE, Yu DY, Chung BH, Kim E, Myung PK, Lee JR. (2009). Synapse formation regulated by protein tyrosine phosphatase receptor T through interaction with cell adhesion molecules and Fyn. EMBO J. 2009 Nov 18;28(22):3564-78.

Liu RJ, Fuchikami M, Dwyer JM, Lepack AE, Duman RS, Aghajanian GK. GSK-3 inhibition potentiates the synaptogenic and antidepressant-like effects of subthreshold doses of ketamine. Neuropsychopharmacology. 2013 Oct;38(11):2268-77.

Lomeli H, Sprengel R, Laurie DJ, Köhr G, Herb A, Seeburg PH, Wisden W. (1993). The rat delta-1 and delta-2 subunits extend the excitatory amino acid receptor family. FEBS Lett. 1993 Jan 11;315(3):318-22.

Niesmann K, Breuer D, Brockhaus J, Born G, Wolff I, Reissner C, Kilimann MW, Rohlmann A, Missler M. (2011). Dendritic spine formation and synaptic function require neurobeachin. Nat Commun. Nov 22;2:557.

Meikle L, Talos DM, Onda H, Pollizzi K, Rotenberg A, Sahin M, Jensen FE, Kwiatkowski DJ. (2007). A mouse model of tuberous sclerosis: neuronal loss of Tsc1 causes dysplastic and ectopic neurons, reduced myelination, seizure activity, and limited survival. J Neurosci. May 23;27(21):5546-58.

Obermair GJ, Szabo Z, Bourinet E, Flucher BE. (2004). Differential targeting of the L-type Ca2$^+$ channel alpha 1C (CaV1.2) to synaptic and extrasynaptic compartments in hippocampal neurons. Eur J Neurosci. Apr;19(8):2109-22.

Ogawa S, Kwon CH, Zhou J, Koovakkattu D, Parada LF, Sinton CM. (2007). A seizure-prone phenotype is associated with altered free-running rhythm in Pten mutant mice. Brain Res. Sep 7;1168:112-23.

Parmeggiani A, Barcia G, Posar A, Raimondi E, Santucci M, Scaduto MC. (2010). Epilepsy and EEG paroxysmal abnormalities in autism spectrum disorders. Brain Dev. Oct;32(9):783-9.

Pavlowsky A, Gianfelice A, Pallotto M, Zanchi A, Vara H, Khelfaoui M, Valnegri P, Rezai X, Bassani S, Brambilla D, Kumpost J, Blahos J, Roux MJ, Humeau Y,Chelly J, Passafaro M, Giustetto M, Billuart P, Sala C. (2010). A postsynaptic signaling pathway that may account for the cognitive defect due to IL1RAPL1 mutation. Curr Biol. Jan 26;20(2):103-15.

Parker WE, Orlova KA, Parker WH, Birnbaum JF, Krymskaya VP, Goncharov DA, Baybis M, Helfferich J, Okochi K, Strauss KA, Crino PB. (2013). Rapamycin prevents seizures after depletion of STRADA in a rare neurodevelopmental disorder. Sci Transl Med. Apr 24;5(182):182ra53.

Pei JJ, Hugon J. (2008). mTOR-dependent signalling in Alzheimer's disease. J Cell Mol Med.Dec;12(6B):2525-32.

Penzes P, Beeser A, Chernoff J, Schiller MR, Eipper BA, Mains RE, Huganir RL. (2003). Rapid induction of dendritic spine morphogenesis by trans-synaptic ephrinB-EphB receptor activation of the Rho-GEF kalirin. Neuron. Jan 23;37(2):263-74.

Petrenko AG, Ullrich B, Missler M, Krasnoperov V, Rosahl TW, Südhof TC. (1996). Structure and evolution of neurexophilin. J Neurosci. Jul 15;16(14):4360-9.

Pilar-Cuéllar F, Vidal R, Díaz A, Castro E, dos Anjos S, Pascual-Brazo J, Linge R, Vargas V, Blanco H, Martínez-Villayandre B, Pazos Á, Valdizán EM. (2013). Neural plasticity and proliferation in the generation of antidepressant effects: hippocampal implication. Neural Plast. 2013:537265.

Pilgram GS, Potikanond S, van der Plas MC, Fradkin LG, Noordermeer JN. (2011). The RhoGAP crossveinless-c interacts with Dystrophin and is required for synaptic homeostasis at the Drosophila neuromuscular junction. J Neurosci. 2011 Jan 12;31(2):492-500.

Potter WB, Basu T, O'Riordan KJ, Kirchner A, Rutecki P, Burger C, Roopra A. (2013). Reduced juvenile long-term depression in tuberous sclerosis complex is mitigated in adults by compensatory recruitment of mGluR5 and Erk signaling. PLoS Biol. Aug;11(8):e1001627.

Pun RY, Rolle IJ, Lasarge CL, Hosford BE, Rosen JM, Uhl JD, Schmeltzer SN, Faulkner C, Bronson SL, Murphy BL, Richards DA, Holland KD, Danzer SC. (2012). Excessive activation of mTOR in postnatally generated granule cells is sufficient to cause epilepsy. Neuron.Sep 20;75(6):1022-34.

Qiu S, Weeber EJ. (2007). Reelin signaling facilitates maturation of CA1 glutamatergic synapses. J Neurophysiol. Mar;97(3):2312-21.

Qiu Z, Sylwestrak EL, Lieberman DN, Zhang Y, Liu XY, Ghosh A. (2012). The Rett syndrome protein MeCP2 regulates synaptic scaling. J Neurosci. Jan 18;32(3):989-94.

Ramocki MB, Zoghbi HY. (2008). Failure of neuronal homeostasis results in common neuropsychiatric phenotypes. Nature. Oct 16;455(7215):912-8.

Roche KW, Ly CD, Petralia RS, Wang YX, McGee AW, Bredt DS, Wenthold RJ. (1999). Postsynaptic density-93 interacts with the delta2 glutamate receptor subunit at parallel fiber synapses. J Neurosci. 1999 May 15;19(10):3926-34.

Rubenstein JL, Merzenich MM. Model of autism: increased ratio of excitation/inhibition in key neural systems. Genes Brain Behav. 2003 Oct;2(5):255-67.

Sharma A, Hoeffer CA, Takayasu Y, Miyawaki T, McBride SM, Klann E, Zukin RS. Dysregulation of mTOR signaling in fragile X syndrome. J Neurosci. 2010 Jan 13;30(2):694-702.

Spires TL, Molnár Z, Kind PC, Cordery PM, Upton AL, Blakemore C, Hannan AJ. (2005). Activity-dependent regulation of synapse and dendritic spine morphology in developing barrel cortex requires phospholipase C-beta1 signalling. Cereb Cortex. Apr;15(4):385-93.

Toyoshima M, Sakurai K, Shimazaki K, Takeda Y, Nakamoto M, Serizawa S, Shimoda Y, Watanabe K. (2009). Preferential localization of neural cell recognition molecule NB-2 in developing glutamatergic neurons in the rat auditory brainstem. J Comp Neurol. Apr 1;513(4):349-62.

Tsai PT, Hull C, Chu Y, Greene-Colozzi E, Sadowski AR, Leech JM, Steinberg J, Crawley JN, Regehr WG, Sahin M. (2012). Autistic-like behaviour and cerebellar dysfunction in Purkinje cell Tsc1 mutant mice. Nature. Aug 30;488(7413):647-51.

Tuchman R, Cuccaro M. (2011). Epilepsy and autism: neurodevelopmental perspective. Curr Neurol Neurosci Rep. Aug;11(4):428-34.

van der Plas MC, Pilgram GS, Plomp JJ, de Jong A, Fradkin LG, Noordermeer JN. (2006). Dystrophin is required for appropriate retrograde control of neurotransmitter release at the Drosophila neuromuscular junction. J Neurosci. Jan 4;26(1):333-44.

Wang Y, Greenwood JS, Calcagnotto ME, Kirsch HE, Barbaro NM, Baraban SC. (2007). Neocortical hyperexcitability in a human case of tuberous sclerosis complex and mice lacking neuronal expression of TSC1. Ann Neurol. Feb;61(2):139-52.

Wong M. (2010). Mammalian target of rapamycin (mTOR) inhibition as a potential antiepileptogenic therapy: From tuberous sclerosis to common acquired epilepsies. Epilepsia.Jan;51(1):27-36.

Yizhar O, Fenno LE, Prigge M, Schneider F, Davidson TJ, O'Shea DJ, Sohal VS, Goshen I, Finkelstein J, Paz JT, Stehfest K, Fudim R, Ramakrishnan C,Huguenard JR, Hegemann P, Deisseroth K. (2011). Neocortical excitation/inhibition balance in information processing and social dysfunction. Nature. Jul 27;477(7363):171-8.

Zeng LH, Xu L, Gutmann DH, Wong M. (2008). Rapamycin prevents epilepsy in a mouse model of tuberous sclerosis complex. Ann Neurol. Apr;63(4):444-53.

Zeng LH, Rensing NR, Wong M. (2009). The mammalian target of rapamycin signaling pathway mediates epileptogenesis in a model of temporal lobe epilepsy. J Neurosci. May 27;29(21):6964-72.

Zhang B, Wong M. (2012). Pentylenetetrazole-induced seizures cause acute, but not chronic, mTOR pathway activation in rat. Epilepsia. Mar;53(3):506-11.

Zhong X, Li H, Chang Q. (2012). MeCP2 phosphorylation is required for modulating synaptic scaling through mGluR5. J Neurosci. Sep 12;32(37):12841-7.

Zhou J, Blundell J, Ogawa S, Kwon CH, Zhang W, Sinton C, Powell CM, Parada LF. (2009). Pharmacological inhibition of mTORC1 suppresses anatomical, cellular, and behavioral abnormalities in neural-specific Pten knock-out mice. J Neurosci. Feb 11;29(6):1773-83.

CHAPTER VII

Materials and Methods

BDNF shRNA Transfection: U6 promotor-driven scrambled and BDNF shRNA-expressing plasmids were obtained from OriGene Technologies (Rockville, MD); BDNF shRNA 1: 5′-TGTTCCACCAGGTGAGAAGAGTGATGACC-3, BDNF shRNA 2: 5′-GTGATGCTCAGCAGTCAAGTGCCTTTGGA-3′, scrambled: 5′-GCACTACCAGAGCTAACTCAGATAGTACT-3′. Each plasmid additionally contains a tRFP expression cassette driven by a distinct (pCMV) promoter. Neurons were transfected with 0.5 μg of total DNA with the CalPhos Transfection kit (ClonTech; Mountain View, CA) according to the manufacturer's protocol. All experiments were performed 24 hr after transfection.

Cell culture: Dissociated hippocampal neuron cultures were prepared according to previously published methods (Banker and Goslin, 1990). Briefly, hippocampi from Sprague–Dawley rat pups (P1–P3) were dissected in cold dissociation media (DM; 82 mM Na2SO4, 30 mM K2SO4, 5.8 mM MgCl2–6H2O, 252 μM CaCl2–2H2O, 1 mM HEPES, 200 mM glucose, 0.001% w/v phenol red), and transferred to a 15 ml conical tube. Dissociation media (DM) was gently removed (save roughly 500 μl covering the tissue itself) and replaced with 5 ml of pre-warmed (37 °C) cysteine-activated papain solution (3.2 mg l-cysteine (Sigma-Aldrich, Saint Louis, MO, USA) with 500 μl papain (Sigma-Aldrich, Saint Louis, MO, USA) in 10 ml DM, pH ~7.2). The tissue was then incubated in activated papain solution for 15 min at 37 °C to allow for tissue digestion. The tube was inverted ~2–3 times after 7 minutes of incubation. Papain inactivation was achieved via two washes in ice-cold DM containing 12.5% v/v fetal bovine serum, followed by two washes in DM alone. Dissociated cells were then washed 2× in chilled normal growth medium [NGM; Neurobasal A (Gibco, Grand Island, NY, USA) supplemented with 2% v/v B27 (Invitrogen, Carlsbad, CA, USA) and 1% v/v Glutamax (Invitrogen, Carlsbad, CA, USA)], then titurated ∼10–15 times in 5 ml NGM to obtain a single cell suspension. This single cell suspension was incubated on ice for ∼3–5 min. 4.5 ml of the cell suspension was then transferred to a new 15 ml tube and centrifuged at 67×g (0.5×1000 rcf) at 4 °C. For plating, 50–70 K cells (in a volume of 150 μl) were dispensed onto poly-d-lysine-coated glass-bottom petri dishes (Mattek, Ashland, MA, USA) and maintained at 5% CO2/37 °C. Roughly 4 h after plating, cells were supplied with 2 ml of NGM-GC (NGM supplemented with 15% v/v glial conditioned media and 10% v/v cortical conditioned media). 24Hr after plating, cells were fed by replacing 50% of the total volume with fresh NGM-GC and every 4 days thereafter by replacing 25% of the total volume with fresh media. Cells were maintained for 14 days with NGM-GC supplementation, then fed every 4 days thereafter with NGM alone. All neurons used for experiments were allowed to mature to an age of ≥21 DIV, unless otherwise noted.

Chemical LTP protocol: Pharmacological induction of LTP in cultured hippocampal neurons was achieved using one of two stimulus solutions, designated cLTP1 or cLTP2. cLTP1 stimulus consisted of the following: 0.2mM Glycine, 0.02mM Bicuculline, and 0.003mM Strychnine in a Mg2+-free extracellular solution. The cLTP2 stimulus also used Mg2+-free extracellular solution as a base but contained 50μM Forskolin and 0.1μM Rolipram. Both means of cLTP induction followed a similar protocol: Dissociated cultures (DIV 21 or older) were removed from the incubator and place on bench top for 10 min to acclimate to room temperature. Neuronal media from then removed from each dish and replaced with 2mls cLTP1 or cLTP2 solution. Neurons were incubated in cLTP solution for 10 min at room temp. After 10 min, cLTP solution was removed and cells were washed 2x with neuronal media. Dishes were then allowed to recover at 37^{o}C for 2 Hr before use in subsequent electrophysiology or imaging experiments.

Electrophysiology: Whole-cell patch-clamp recordings were made with an Axopatch 200B amplifier from cultured hippocampal neurons bathed in HEPES-buffered saline (HBS) containing (in mM) the following: 119 NaCl, 5 KCl, 2 $CaCl_2$, 2 $MgCl_2$, 30 Glucose, 10 HEPES, pH 7.4. Whole-cell pipette had resistances ranging from 3 to 6 MΩ. Internal solution contained (in mM) the following: 100 cesium gluconate, 0.2 EGTA, 5 $MgCl_2$, 2 adenosine triphosphate, 0.3 guanosine triphosphate, 40 HEPES, pH 7.2. mEPSCs were recorded at −70 mV from neurons with a pyramidal-like morphology in the presence of 1 μM TTX and 10 μM bicuculline and analyzed off-line using Synaptosoft minianalysis software. sEPSCs in active networks were recorded at −70 mV in modified HBS (as above, except with 0.5 mM $CaCl_2$ and 3.5 mM $MgCl_2$) without TTX or bicuculline. mIPSCs were recorded at -70mV in the presence of 1μM TTX, 10μM CNQX and 50 μM DL-APV. Internal solution contained (in mM) the following: 135 CsCl, 1 EGTA, 10 HEPES, 5 $MgCl_2$, 4 Mg-ATP, and 1 Li-GTP, pH 7.2. During loose-patch recordings, neurons were bathed in HBS lacking pharmacological inhibitors to permit recording of background spike activity. Pipette solution contained extracellular solution.

For current clamp recordings, changes in intrinsic excitability were assessed in neurons subject to pharmacological isolation via 10μM CNQX, 50 μM DL-APV, and 10 μM bicuculline. Internal solution contained (in mM) the following: 120 K-$MeSO_4$, 20 KCl, 0.2 EGTA, 10 HEPES, 2 $MgCl_2$, 4 Mg-ATP, 0.3 Na-GTP, and 7 phosphocreatine, pH 7.2. A series of 500 ms current injections were used to depolarize the soma from resting membrane potential in step-wise increments of 100pA. Series resistance was compensated for by >80%. Neurons which had a resting membrane potential above -55 mV were not included in further analysis. Membrane hyperpolarization in response to a -25 pA current step was used to measure input resistance. Action potential properties and spike frequency data were analyzed using Clampfit 10.0 (Molecular Devices). Statistical differences between experimental conditions were determined by ANOVA followed by Fisher's LSD post hoc tests

Total excitatory synaptic input onto recorded neurons was assessed by computing charge transfer >30 randomly selected 1 s intervals for each recording. NMDAR EPSCS were recorded in HBS with 0 $MgCl_2$ and were evoked with a bipolar stimulating electrode positioned close to the recorded neuron. Once a stable response was obtained to stimuli delivered at 0.33 Hz, MK801 (20 μM) was applied to the bath for 5 min without stimulation. Following wash in, 200 stimulations were delivered in the presence of MK801. The peak of the NMDAR current was measured for each and normalized to the first response. Group comparisons are presented as the normalized mean peak NMDAR current as a function of number of stimulations in the presence of MK801. Statistical differences between experimental conditions were determined by ANOVA and post hoc Fisher's least significant difference (LSD) test, unless otherwise indicated.

$Ca2^+$ phosphate transfection: To achieve sparse expression, neurons were transfected with 0.5 μg of total DNA using the $Ca2^+$ phosphate CalPhos Transfection kit (ClonTech) according to the manufacturer's protocol. Unless otherwise indicated, all experiments were performed 24 h post-transfection.

DNA Constructs: Plasmids encoding TSC1, TSC2, RhebWT, and RhebQ64L were used as previously described (Inoki et al., 2002, 2003). vglut-pHluorin was provided by Robert Edwards (UCSF). Human HA-PLD1, human HA-PLD2, rat HA-PLD2, and pEGFP-Spo20PABD-WT were provided by Dr. Michael Frohman (SUNY Stony Brook). GFP-Rap1-

PABD was provided by Dr. Frank Schmitz (Universität des Saarlandes Medizinische Fakultät). Rapamycin-resistant (S2035T) and Rapamycin/Phosphatic acid resistant (32035T/R2109A) mTOR point mutants were provided by Dr. Jie Chen (University of Illinois at Urbana-Champaign). FLAG-Rpt3, HA-Rpt6, GFP-Rpt6, HA-Rpt6 S120A, HA-Rpt6 S120D, PAGFP-Rpt6 WT, PAGFP-Rpt6 S120A, and PAGFP-Rpt6 S120D were all prpvided by Dr. Gentry Patrick (USCD).

Hippocampal slice electrophysiology: Transverse hippocampal slices (400 μm) were prepared with a Stoelting tissue chopper from P18-24 Sprague Dawley rats, and allowed to recover at room temperature in a humidified interface chamber saturated with 95% O_2 5% CO_2 for at least 2 hours prior to experiments. Slices were then transferred to a separate submersion chamber containing the appropriate treatment dissolved in 80ml artificial cerebrospinal fluid (aCSF) containing, in mM: 120NaCl, 2.5 KCl, 2.5 $CaCl_2$, 1.3 $MgCl_2$, 26.2 $NaHCO_3$, 1 NaH_2PO_4, 11 glucose, pH 7.4 saturated with 95% O_2 5% CO_2. For recording, slices were transferred to a submerged recording chamber and continuously perfused at a rate of ~ 3 ml/min with aCSF saturated with 95% O_2 5% CO_2. Recordings were made at 28-29ºC, with bath temperature maintained using an in-line temperature controller (Warner Instruments). Extracellular field potentials were recorded with glass micropipettes filled with 3 M NaCl (filled either with 3 M NaCl) placed in the middle of stratum radiatum of area CA1. Pairs of cathodal stimuli (0.1 ms pulse width) were delivered to the commissural/Schaffer collateral afferents by bipolar stainless steel electrodes (FHC, Brunswick, ME) at intervals of 50, 100, 200, 300, and 1000 ms, with stimulus intensity set to evoke fEPSPs 50% of their maximal amplitude.

Immunocytochemisty and microscopy: Except for experiments involving vglut-pHluorin, all imaging was performed on an inverted Olympus FV1000 laser-scanning confocal microscope using a Plan-Apochromat 63×/1.4 oil objective with 1× or 2× digital zoom. Alexa 488 was excited with the 488 nm line of an argon ion laser and emitted light was typically collected between 500 and 530 nm with a tunable emission filter. Alexa 555/568 were excited with a 559 nm diode laser and emitted light was typically collected between 570 and 670 nm. Before image collection, the acquisition parameters for each channel were optimized to ensure a dynamic signal range and to ensure no signal bleed-through between detection channels. For every experiment, identical parameters were used for each treatment option. We verified that no detectable staining was observed in control samples incubated in the absence of primary antibody (but otherwise processed identically).

For BDNF and phospho-S6 (PS6) staining, cells were treated in conditioned media as indicated, then fixed at room temperature for 20 min with 4% paraformaldehyde (PFA)/4% sucrose in PBS with 1 mM MgCl2 and 0.1 mM CaCl2 (PBS-MC). After washing in PBS-MC (5 min), cells were permeabilized (0.1% Triton X in PBS-MC, 5 min), blocked with 2% bovine serum albumin in PBS-MC for 30 min, and labeled with a rabbit polyclonal antibody against BDNF (Santa Cruz Biotechnology, 1:100), or a rabbit polyclonal S235/236 phosphospecific antibody (Cell Signaling Technology; 1:50); for each, colabeling and a mouse monoclonal antibody against MAP2 (Sigma-Aldrich, 1:5000) for either 60 min at room temperature or overnight at 4°C. Alexa 555-conjugated goat anti-rabbit (1:500) and Alexa 635-conjugated goat anti-mouse (1:500) secondary antibodies (each 60 min at room temperature) were used to visualize BDNF/PS6 and MAP2 staining, respectively. To ensure blind sampling of BDNF/PS6 expression, neurons with a pyramidal-like morphology were selected for imaging by epifluorescent visualization of MAP2 staining. Analysis of expression in somatic or dendritic neuronal compartments was performed on maximal intensity z-compressed image stacks.

Dendrites were linearized and extracted from the full-frame image using the straighten plug-in for ImageJ. For both somatic and dendritic signal, expression was estimated by the average nonzero pixel intensity for each compartment. To analyze dendritic BDNF expression, dendrites were linearized and extracted from the full-frame image using the straighten plug-in for ImageJ. To combine data across multiple experimental runs of the same experiment, expression in each image was normalized against the average nonzero pixel intensity for the respective control group. In experiments where BDNF or PS6 were assessed in transfected cells, neurons were also colabeled with a chicken polyclonal antibody against GFP (Millipore, 1:1000) and an Alexa 488-conjugated goat anti-chicken secondary antibody. Statistical differences were assessed by ANOVA, followed by Fisher's LSD post hoc tests.

To assess presynaptic UPS levels in neurons subject to pharmacological activity manipulations, neurons were transfected with mCh-Syn as well as FLAG-Rpt3, FLAG-Rpt1, HA-Rpt6 WT, HA-Rpt6 S120A, HA-Rpt6 S120D. 48Hrs post transfection, neurons were fixed and permeabilized as described previously, then blocked in 2% BSA prior to staining with a mouse monoclonal primary antibody against HA (1:500 in 2% BASA, 1Hr at RT, Cell Signaling, Danvers MA) or a rabbit polyclonal primary antibody against FLAG (1:500 in 2% BSA, 1Hr at RT, Sigma). Following incubation in primary antibody, neurons were washed 3x with RT PBS-MC and incubated with a goat anti mouse or goat anti rabbit Alexa 488 secondary antibody (1:500 in 2% BSA, 1Hr at RT, Molecular Probes, Eugene, OR). Neurons were imaged on an inverted confocal microscope (Olypus FV1000) using a Plan-Apochromat 63x/1.4 oil objective with 2x digital zoom, as described earlier. Regions of interest were selected based on epifluorescent visualization of mCH-Syn expression to ensure blind sampling of HA or FLAG staining. Analysis of expression in presynaptic compartments was performed on maximal intensity z-compressed image stacks. Axons were linearized and extracted from the full-frame image using the ‘straighten’ plug-in for ImageJ. For analysis, the integrated intensity of HA or FLAG fluorescence that co-localized with regions of high mCH-Syn expression was quantified using custom written analysis routines. To control for differences in reporter expression across cells, levels of HA or FLAG intensity in somatic regions were used to normalize presynaptic HA/FLAG levels within each neuron. A similar approach was used to quantify changes in presynaptic GFP fluorescence intensity under conditions of GFP-Rpt6 WT, GFP-Rpt6 S120A, or GFP-Rpt6 S120D expression.

For analysis of surface GluA1 expression, neurons were live-labeled with a rabbit polyclonal antibody recognizing a surface epitope of GluA1 (10 μg/ml, EMD Biosciences) for 15 min at 37°C, followed by fixation (2% PFA in PBS-MC for 15 min at room temperature), and immunocytochemical labeling with a mouse monoclonal anti-PSD95 antibody (1:1000, Millipore Bioscience Research Reagents) as described above. Alexa 488-conjugated goat anti-mouse (1:500) and Alexa 555-conjugated goat anti-rabbit (1:500) secondary antibodies (each 60 min at room temperature) were used to visualize PSD95 and GluA1 staining, respectively. Neurons were selected based on PSD95 epiflourescence to ensure blind sampling of surface GluA1. For analysis, “synaptic” GluR1 was defined as a particle that occupied >10% of the area defined by a PSD95 particle, and the average integrated intensity (total number of nonzero pixels times intensity) of synaptic GluR1 particles was calculated using custom written analysis routines for ImageJ. Analysis was performed on both full-frame images as well on dendrites straightened and extracted from the full-frame image, where “n” equals the number of images or number of dendrites, respectively. Both analysis methods yielded similar results. Statistical differences were assessed by ANOVA, followed by Fisher's LSD post hoc tests.

Optical analysis of presynaptic function used live-labeling with an Oyster 550-conjugated rabbit polyclonal antibody against the lumenal domain of synaptotagmin 1 (syt-lum; 1:100, Synaptic Systems). Before labeling, neurons were treated with 2 μM TTX for 15 min to isolate spontaneous neurotransmitter release. Neurons were then labeled with anti-syt-lum for 5 min at room temperature, washed, fixed with 4% PFA/4% sucrose in PBS-MC, permeabilized, and blocked as above, then labeled with a guinea pig polyclonal anti-vglut1 antibody (1: 2500, Millipore Bioscience Research Reagents). The intrinsic fluorescent signal of the anti-syt-lum at synaptic sites was amplified by an Alexa 555-conjugated goat anti-rabbit (1:500) secondary antibody. An Alexa 488-conjugated goat anti-guinea pig (1:250) secondary antibody (each for 60 min at room temperature) was used to visualize vglut1 staining. Neurons were selected based on vglut1 epiflourescence to ensure blind sampling of syt-lum expression. For analysis, a "synaptic" syt-lum particle was defined as a particle that occupied >10% of the area defined by a vglut1 particle, and the proportion of vglut1 particles containing synaptic syt-lum particles was calculated using custom written analysis routines for ImageJ. Statistical differences were assessed by ANOVA, followed by Fisher's LSD post hoc tests.

Local perfusion: All local perfusion experiments were performed on an inverted Olympus FV1000 laser-scanning confocal microscope using Plan-Apochromat 40×/0.95 air (for live imaging) and Plan-Apochromat 40×/1.0 oil (for retrospective imaging) objectives. Stable microperfusion was achieved by use of a dual micropipette delivery system, as described previously (Sutton et al., 2006). The delivery micropipette was pulled as a typical whole-cell recording pipette with an aperture of ~0.5 μm. The area of dendrite targeted for local perfusion was controlled by a suction pipette, which was used to draw the treatment solution across one or more dendrites and to remove the perfusate from the bath. A cell-impermeant fluorescent dye

(Alexa 488, 1 µg/ml) was included in the perfusate to visualize the affected area. In all local perfusion experiments, the bath was maintained at 37°C and continuously perfused at 1.5 ml/min with HBS.

For analysis, the size of the treated area was determined in each linearized dendrite based on Alexa 488 fluorescence integrated across all images taken during local perfusion. Adjacent nonoverlapping dendritic segments, 25 µm in length, proximal (i.e., toward the cell soma) and distal to the treated area were assigned negative and positive values, respectively. To examine localized changes in syt-lum uptake, 2 µM TTX was bath applied for 10 min to isolate spontaneous neurotransmitter release immediately following local perfusion. Neurons were then live-labeled with syt-lum for 5 min at room temperature, and processed for immunocytochemistry as described above. To assess relative changes in syt-lum and vglut1 staining in perfused dendrites, the average nonzero pixel intensity was calculated for each dendritic segment. The average value in untreated segments was assigned a value of 1, which was then used to normalize vlgut and syt-lum intensity in all segments (including the treated area). Statistical differences in these measurements between syt and vglut at each segment were assessed by Student's t test.

Magnetofection-based siRNA delivery: BDNF siRNA or non-targeting control siRNA were purchased from Dharmacon (siGENOME SMARTpool, M-080046, Thermo Fisher Scientific., Lafayette, CO.). To favor rapid translational knockdown, a combination of four BDNF-targeting siRNAs were pooled: (1): Sense = 5'-UCGAAGAGCUGCUGGAUGAUU-3', Antisense = 5'-UCAUCCAGCAGCUCUUCGAUU-3'; (2): Sense = 5'UAUGUACACUGACCAUUAAUU-3', Antisense: 5'-UUAAUGGUCAGUGUACAUAUU-3'; (3): Sense: 5'-GAGCGUGUGUGACAGUAUUUU-3', Antisense: 5'-

AAUACUGUCACACACGCUCUU-3'; (4): Sense: 5'-GAACUACCCAAUCGUAUGUUU-3', Antisense: 5'- ACAUACGAUUGGGUAGUUCUU-3'; Control siRNA: Sense: 5'-UAAGGCUAUGAAGAGAUACUU-3'; Antisense: 5'-GUAUCUCUUCAUAGCCUUAUU-3'. Each annealed double-stranded RNA oligonucleotide contained 3'-UU overhangs, a single isomer 6-FAM on the 5'- end of the sense strand, and a 5'-phosphate on the antisense strand. For rapid siRNA transfection, siRNA (67.5 µg in 100 µl media) was combined with 3.5 µl neuromag transfection reagent (Oz Biosciences, France). After a 20 minute incubation period, cultured neurons were bathed in the Neuromag/siRNA mix, and then placed on the manufacturer supplied magnet for 15 min at 37°C. After magnetofection, cells were immediately treated with PA or vehicle, and used in experiments as described.

Preparation of PA vesicles: The lipid second messenger phosphatidic acid (PA) was acquired from Avanti Polar Lipids (Alabaster, Alabama), and was prepared according to previously described methods (Yoon et al., 2011). PA lipids in chloroform were dried under a stream of nitrogen gas in a 20ml glass scintillation vial. Dried lipids were reconstituted in a buffer of 150 mM NaCl and 10 mM Tris-Cl (pH8.0), to a concentration of 6mM. The solution was briefly vortexed, then subjected to bath sonication for a period of 5min, resulting in a homogenous solution of unilaminar vesicles (15-50nm in diameter). PA vesicles were added directly to cell media to produce a concentration of 100µM. Lipid vesicles were made fresh at the start of each experiment.

vglut1-pHluorin imaging: Cultured hippocampal neurons were transfected at DIV 14–16 with vglut-pHluorin as well as mCherry-synaptophysin to aid in visual identification of terminal boutons. Experiments were conducted 2–3 d post-transfection in HBS containing 10 µM CNQX and 50 µM DL-APV. Action potentials were evoked via a Grass stimulator unit using a custom fabricated electric field stimulator, which was inserted into each dish just before start of an experiment. Each stimulus consisted of a 2 ms 10 V potential difference between platinum-iridium wires 6 mm apart. To observe changes in evoked release, we recorded the change in vglut-pHluorin fluorescence intensity elicited by delivering stimulus repetitions at 10 Hz for 10 s, which has been shown to provide a measure of exocytosis undiluted by signal degradation due to endocytosis or reacidification (Kim and Ryan, 2009). Each stimulus train was delivered three times for each set of synapses, with a 5 min interval separating each train. Images were taken using a Hammamatsu EM-CCD camera mounted on an inverted microscope (Olympus IX8) using a 40× 1.3 NA oil-immersion objective (Olympus). The filter set consisted of a 472/30 excitation filter, a 495 edge dichroic mirror, and a 520/30 emission filter. Illumination was achieved via a Sutter Lambda LS/OR30 300 W xenon bulb control by a Sutter Lambda 10 shutter (Sutter Instrument). All images were captured at a depth of 16 bits to a Dell Optiplex computer using MetaMorph software (Molecular Devices). Full frame (512 × 512, 16 μm pixels) imaging sequences were acquired at a rate of 5 Hz using 50 ms exposure for vglut-pHluorin. Image sequences were analyzed using the “time series” plug-in for ImageJ (http://rsb.info.nih.gov/ij/plugins/time-series.html). Active synapses were identified for each experiment by subtracting the signal before the initiation of each stimulus train from the peak increase in vglut-pHluorin signal elicited by the train. Rectangular ROIs (1.55 × 1.55 μm) were placed over each of the resulting puncta in the “difference image.” The time-lapse plug-in was then used to measure average fluorescence for each ROI over time. To correct for photobleaching during image series acquisition, an identically sized ROI was positioned in a nonsynaptic region adjacent to an identified release site. Measurements obtained from this nonsynaptic ROI were fit with a biexponential decay function, and these values were then subtracted from the data traces associated with active release sites. Automated image analysis and photobleaching correction was performed in MATLB (see Appendix 2). Fluorescence signals were quantified as $\Delta F/F0$, where F0 is defined as the average of five sequential images recorded before the onset of stimulation for each ROI.

Western blotting: Samples were collected in lysis buffer containing 100 mM NaCl, 10 mM $NaPO_4$, 10 mM $Na_4P_2O_7$, 10 mM lysine, 5 mM EDTA, 5 mM EGTA, 50 mM NaF, 1 mM $NaVO_3$, 1% Triton-X, 0.1% SDS, and 1 tablet Complete Mini protease inhibitor mixture (Roche)/7 ml, pH 7.4. Equal amounts of protein for each sample were loaded and separated on 12% polyacrylamide gels, then transferred to PVDF membranes. Blots were blocked with Tris-buffered saline containing 0.1% Triton-X (TBST) and 5% nonfat milk for 60 min at room temperature, and incubated with a rabbit polyclonal primary antibody against BDNF (Santa Cruz Biotechnology, 1: 200) for either 60 min at room temperature or overnight at 4°C. After washing with TBST, blots were incubated with HRP-conjugated anti-rabbit or anti-mouse secondary antibody (1:5000; Jackson Immunoresearch), followed by enhanced chemiluminescent detection (GE Healthcare). All blots were probed with a mouse monoclonal antibody against α-tubulin (1:5000, Sigma-Aldrich) to confirm equal loading. Band intensity was quantified with densitometry with NIH ImageJ and expressed relative to the matched control sample. Statistical differences between treatment conditions and control were assessed first by an overall nonparametric ANOVA (Kruskal–Wallis test) followed by a post hoc Wilcoxon signed rank test for individual comparisons.

APPENDIX I:

A Fragile Balance at Synapses: New Evidence Supporting a Role for FMRP in Homeostatic Plasticity

Homeostatic synaptic scaling operates in tandem with forms of neuronal plasticity such as long-term potentiation and long-term depression to maintain neural circuit activity within a stable range. Experimentally, homeostatic adaptations at synapses are usually induced by prolonged spike blockade [with tetrodotoxin (TTX)], yielding a form of synaptic scaling thought to involve cell-wide, transcription-dependent changes that affect every synapse on a given neuron (Turrigiano, 2008). However, more recent evidence has also identified locally mediated adaptive mechanisms that allow spatially discrete synaptic compensation within a neuron's highly compartmentalized dendritic arbor (Sutton et al., 2006; Rabinowitch and Segev, 2008). Early work in this area demonstrated that concurrent action potential and NMDA receptor (NMDAR) blockade (TTX + the NMDAR antagonist APV) promotes dendritic translation of GluA1 AMPAR subunits, leading to localized enhancement of synaptic strength (Sutton et al., 2006). Other work demonstrated that TTX and APV treatment drives intracellular synthesis of retinoic acid (RA), which reduces the association of the RNA-binding protein RARα with select mRNAs such as GluA1, thereby removing their translational block (Aoto et al., 2008).

Another RNA-binding protein that regulates dendritic translation is the fragile X mental retardation protein (FMRP) (Zalfa et al., 2003; Muddashetty et al., 2007). As evidenced by the devastating symptoms in fragile X syndrome (FXS), mutations in the Fmr1 gene result in severe disruptions in cognitive and social abilities, suggesting a pivotal role for FMRP in basic learning and memory processes (Bassell and Warren, 2008). In a recent article published in The Journal of Neuroscience, Soden and Chen (2010) demonstrate that FMRP is directly involved in homeostatic plasticity, and provide evidence to support it acting within dendrites to regulate the translation of specific mRNAs in response to increases in RA signaling.

To investigate a potential role for FMRP in local synaptic scaling, Soden and Chen first examined the effects of prolonged action potential and NMDAR blockade (36 h TTX + APV) in organotypic hippocampal slices prepared from wild-type (WT) or Fmr1 knock-out (KO) mice. Whereas CA1 pyramidal neurons exhibited enhanced mEPSC amplitude following TTX+APV treatment, no such scaling response was evident in CA1 neurons from Fmr1 KO mice (their Fig. 1). Because this group had previously shown a role for RA in homeostatic scaling induced by TTX+APV treatment (Aoto et al., 2008), the authors next examined whether FMRP was required upstream or downstream of activity-dependent RA synthesis. Using a fluorescent reporter in which three tandem retinoic acid response elements (RAREs) control GFP transcription, the authors found that cultured WT and Fmr1 KO hippocampal neurons displayed equivalent levels of RARE-GFP reporter expression after TTX+APV treatment (their Fig. 2). However, the protein synthesis-dependent increase in mEPSC amplitude induced by direct RA treatment (4 h) was lost in Fmr1 KO neurons. In addition, Soden and Chen found that RA application induced a translation-dependent increase in the levels of GluA1, GluA2, and eEF2 in synaptoneurosomes in organotypic slices from WT, but not Fmr1 KO, slices (their Fig. 5). Finally, in studies where specific proteins were immunoprecipitated following metabolic labeling with radiolabeled amino acids, the increase in GluA1 synthesis driven by RA treatment was also lost in Fmr1 KO neurons. Together, these results suggest that FMRP plays a role downstream of RA in dendritic protein synthesis, where it is required for the translation of specific mRNAs in response to RA signaling.

Although Soden and Chen (2010) demonstrated a critical role for FMRP in homeostatic plasticity dependent on RA synthesis, interestingly, they found that neither FMRP nor RA was required for homeostatic enhancement of synaptic strength induced by TTX alone [Soden and Chen (2010), their Fig. 4]. In WT and Fmr1 KO neurons, 60 h of TTX treatment induced a similar increase in mEPSC amplitude, and in each case the enhanced mEPSCs were resistant to inhibition with the polyamine philanthotoxin, which targets GluA2-lacking AMPARs. In contrast, scaled mEPSCs following TTX+ APV treatment are specifically reversed by polyamine toxins [Sutton et al. (2006); Aoto et al. (2008); Soden and Chen (2010), their Fig. 2]. These observations underscore the notion that multiple forms of homeostatic plasticity exist in hippocampal neurons, and suggest that FMRP plays a specific role in synaptic adaptations that require local translation near synaptic sites.

Rescue experiments using viral expression of FMRP in organotypic hippocampal slices from Fmr1 KO mice indicated that proper RA-induced scaling in CA1 neurons can be restored by returning FMRP to appropriate levels (their Fig. 7). That acute restoration of FMRP expression can restore RA-induced scaling argues against the possibility that defects in synapse development or maturation in Fmr1 KO neurons accounts for the absence of homeostatic control, and supports a specific requirement for FMRP in RA-induced scaling. To elucidate FMRP's mechanism of action in RA-induced scaling, Soden and Chen assessed the efficacy of two FMRP mutants in additional rescue experiments. One mutant, FMRPΔRGG, lacked the RGG box necessary for binding to G-quartet structures on select target mRNAs. The other mutant, FMRP(I304N), carried a point mutation in a crucial KH domain necessary for binding to mRNAs with a “kissing complex” motif. Neither of these mutants had an effect on AMPAR levels or basal synaptic transmission when expressed in WT neurons (their supplemental Fig. 5). Likewise, expression of FMRPΔRGG-GFP in slices from Fmr1 KO mice had no effect on baseline mEPSC amplitude (their Fig. 7) or GluA1 levels as assessed via Western blotting (their Fig. 8). In contrast, expression of FMRP(I304N)-GFP decreased basal mESPC amplitude and reduced GluA1 protein levels in Fmr1 KO cells (their Fig. 7, Fig. 8). Given previous work showing an interaction between FMRP and GluA1 mRNA in synaptoneurosomes (Muddashetty et al., 2007), these results raise the possibility that FMRP may normally associate with and suppress the translation of GluA1 mRNA via its RGG box and not its KH domain, though Soden and Chen did not directly examine the mRNA binding properties of either mutant. Importantly, neither mutant rescued scaling induced by RA or TTX+APV treatment, indicating that recovery of FMRP's ability to suppress GluA1 synthesis may not be sufficient to restore its role in RA-induced dendritic translation.

The differential effect of the FMRP mutants on baseline mEPSC amplitude and GluA1 levels suggests that their inability to rescue synaptic scaling results from distinct impairments. The inability of FMRPΔRGG to rescue synaptic scaling in Fmr1 KO cells may stem from the possibility that the RGG box is necessary for FMRP's interaction with GluA1 mRNA. If this is the case, why then is expression of the FMRP(I304N) mutant, which contains an intact RGG box and clearly exerts a suppressive effect on GluA1 expression, not successful in restoring RA-induced scaling? Previous reports have shown that this mutation blocks the ability of FMRP to associate with translating polyribosomes, as well as with its autosomal paralog FXR2P (Feng et al., 1997). It may be that mRNP particles containing FMRP must be associated with actively translating ribosomes for RA-induced translational regulation to occur, so disrupting this interaction renders FMRP(I304N) unable to rescue the scaling effect in Fmr1 KO cells. On the other hand, given recent data suggesting that FMRP and FXR2P play unique roles during the expression of mGluR-LTD (Zhang et al., 2009), it is possible that FXR2P may also serve an important function during RA-induced synaptic scaling, and that this function requires its interaction with FMRP. Future experiments should clarify the precise aspect of FMRP function that is necessary for homeostatic plasticity.

In the experiments detailed above, Soden and Chen have provided compelling evidence that FMRP plays an important role in RA-induced synaptic scaling. However, one remaining unanswered issue concerns the mechanism by which FMRP regulates the effects of RA on dendritic protein synthesis. In coimmunoprecipitation studies, Soden and Chen found no evidence for a direct physical interaction between FMRP and RARα (their Fig. 6), yet FMRP was clearly required for increased translation signaled through RARα. The authors suggest that FMRP and RARα need to be bound to the same mRNAs for RA-induced translational changes to occur. Indeed, two of the RARα targets highlighted in this study, GluA1 and GluA2 mRNA, are also known targets of FMRP (Muddashetty et al., 2007), suggesting that combinatorial action of these two RNA-binding proteins might be responsible for mediating the specific alterations in translational efficiency necessary for local homeostatic plasticity. While this idea is attractive, it is also possible that FMRP is necessary for the appropriate targeting of GluA1 mRNA to specific RA-response sites near synapses. Another possibility is that FMRP, through an allosteric mechanism, operates in concert with RA to induce the conformational changes in RARα necessary for translational disinhibition of specific mRNAs. In the Chen laboratory's initial series of studies of RA-induced synaptic scaling, they found that treatment with the RARα-specific agonist AM580 was sufficient to stimulate local synthesis of GluA1 and cause an enhancement of mEPSC amplitude (Aoto et al., 2008). Although the authors clearly demonstrate that scaling induced by direct RA application is lost in FMR1 KO neurons, it would be informative to know whether this same effect is observed following RARα activation with AM580.

Although a number of important questions remain, Soden and Chen's work clearly establishes a role for FMRP in homeostatic control of excitatory synapse function and serves to further our understanding of the synaptic etiology of FXS. To this point, the abnormal mGluR-LTD observed in FMR1 KO mice has received considerable attention as a potential link to the cognitive dysfunction associated with this disorder. These new results raise the intriguing possibility that dysfunctional homeostatic regulation, perhaps in concert with defects in mGluR-dependent signaling in neurons, plays an important role in the devastating symptoms of FXS. The extent to which altered homeostatic plasticity contributes to the pathogenesis of FXS and other such disorders is an important area of future study.

Acknowledgments

This chapter has been published (see citation below) and permission was received from the editors to use this work as part of a dissertation:

Henry FE. (2011). A fragile balance at synapses: new evidence supporting a role for FMRP in homeostatic plasticity. J Neurosci. 2011 May 4;31(18):6617-9.

Bibliography

Aoto J, Nam CI, Poon MM, Ting P, Chen L (2008) Synaptic signaling by all-trans retinoic acid in homeostatic synaptic plasticity. Neuron 60:308–320.

Bassell GJ, Warren ST (2008) Fragile X syndrome: loss of local mRNA regulation alters synaptic development and function. Neuron 60:201–214.

Feng Y, Absher D, Eberhart DE, Brown V, Malter HE, Warren ST (1997) FMRP associates with polyribosomes as an mRNP, and the I304N mutation of severe fragile X syndrome abolishes this association. Mol Cell 1:109–118.

Muddashetty RS, Kelić S, Gross C, Xu M, Bassell GJ (2007) Dysregulated metabotropic glutamate receptor-dependent translation of AMPA receptor and postsynaptic density-95 mRNAs at synapses in a mouse model of fragile X syndrome. J Neurosci 27:5338–5348.

Rabinowitch I, Segev I (2008) Two opposing plasticity mechanisms pulling a single synapse. Trends Neurosci 31:377–383.

Soden ME, Chen L (2010) Fragile X protein FMRP is required for homeostatic plasticity and regulation of synaptic strength by retinoic acid. J Neurosci 30:16910–16921.

Sutton MA, Ito HT, Cressy P, Kempf C, Woo JC, Schuman EM (2006) Miniature neurotransmission stabilizes synaptic function via tonic suppression of local dendritic protein synthesis. Cell 125:785–799.

Turrigiano GG (2008) The self-tuning neuron: synaptic scaling of excitatory synapses. Cell 135:422–435.

Zalfa F, Giorgi M, Primerano B, Moro A, Di Penta A, Reis S, Oostra B, Bagni C (2003) The fragile X syndrome protein FMRP associates with BC1 RNA and regulates the translation of specific mRNAs at synapses. Cell 112:317–327.

Zhang J, Hou L, Klann E, Nelson DL (2009) Altered hippocampal synaptic plasticity in the FMR1 gene family knockout mouse models. J Neurophysiol 101:2572–2580.

.

APPENDIX II:

Matlab as a tool for automated data analysis after optical assessment of presynaptic function

A2.1. Abstract

Deep insights into the functional consequences of perturbing particular components of the presynaptic molecular machinery have been difficult to acquire. Over the past decade, exciting advances using newly developed optical tools to read out presynaptic function have allowed large scale investigation of multiple aspects of presynaptic function in the context of intact cellular circuitry. The resulting data from these types of experiments can be extremely large and is well suited to automated analysis. Here, the matlab programming environment was utilized for the purposed of large-scale, fast, and accurate analysis of data acquired from live-imaging investigations of presynaptic function using pH-sensitive variants of GFP.

A2.2 Introduction

The synapse, defined as the unique site of cellular contact and communication between neuronal cells, is the fundamental element of the nervous system (Shepherd and Erulkar, 1997). In the adult human, the number of synaptic connections in the vastly complex information processing network of the mature brain is thought to number in the trillions (Pakkenberg et al., 2003). The synapse is comprised of a pre and a post synaptic compartment, each containing a unique set of molecular machinery suited to its particular role in synaptic communication (Chua et al, 2010). The presynaptic compartment is generally suited to converting the electrical signal of an action potential into a chemical signal via the release of chemical neurotransmitters such as glutamate, while the postsynaptic compartment has evolved to reconvert the chemical message back into an electrical signal via activation of ligand-gated ion channels embedded in the postsynaptic membrane. This is a highly simplified view of chemical neurotransmission, focusing on a single aspect of excitatory signalling in the central nervous system, but will serve well for the purposes of this text, as glutamatergic signalling at excitatory synapses in the mammalian central nervous system is the topic of study in the experiments described herein. While the molecular mechanisms of postsynaptic signalling and plasticity have received much attention over the past several decades, delving into the physiology of the presynaptic terminal is much more difficult owing to the small size of the sites of vesicular release. Presynaptic machinery is extraordinarily complex, though biochemical and genetic approaches have yielded great insight into much of the molecular components at work (Jahn and Fasshauer 2012). Deep insights into the functional consequences of perturbing particular components of the presynaptic molecular machinery have been harder to acquire, however. Historically, efforts to understand the functional aspects of the presynaptic release machinery have been guided largely through the use of electrophysiological experiments, which can relay a great deal of information regarding the function of a large number of synapses (Katz, 1971). Over the past decade, however, exciting advances using newly developed optical tools to readout presynaptic function have allowed large scale investigation of multiple aspects of presynaptic function in the context of intact cellular circuitry (Dreosti and Lagnado, 2011). These experimental advances allow unprecedented analysis of vesicle release properties on a synapse by synapse basis, but the resulting data set from live-imaging experiments is so large as to be unwieldy using conventional manual analysis strategies. Thus, the goal of this project was to utilize the matlab programming environment to automate and systematize analysis of live imaging data for experiments investigating various functional aspects of presynaptic release. It is essential to gain a better understanding of the mechanisms involved in presynaptic vesicle release, as many neurological and psychiatric disorders have a presynaptic locus (Waites and Garner, 2011).

A2.3 Results

The overall workflow of data analysis for vglut1-pHluorin live imaging experiments is shown in Figure 1. After determining sites of active presynaptic release, labeling and saving these regions of interest (ROIs), and obtaining fluorescence intensity measurements at each time point for each synapse in a given run, the data stored in an excel file for subsequent automated processing in Matlab. It appears possible to port some aspects of these initial steps into a setup acting via matlab (see discussion), but for ease of immediate use with current data sets these initial processing steps were performed outside the matlab environment. After organizing the raw data in excel files in a centralized location, the task accomplished using matlab proceeds as such: 1) Import data from excel files into matlab and concatenate data across separate trails into a single variable for processing, 2) correct distortions that result from photobleaching that is unavoidable over the course of the imaging session, 3) normalize the resulting bleach-corrected data to either a mean level of baseline (pre-stimulus onset) fluorescence or to the peak level of fluorescence intensity achieved after stimulus and 4) graph up the resulting timecourse plots and any other relevant features able to be extracted from the data.

The first three of these tasks (collect, correct, normalize) have been accomplished using a combination of multiple custom-written functions aligned together in a single script entitled “phluorin_group_collect” (see Script 1 in supplemental material). This script begins by using the xlsread function to import data from a specified folder denoted by a directory change command. The data in these files are assigned to variable names according to experimental group and order in which the data was collected (e.g. ‘Control1’,’bdnf3’,etc.). After data import, experimental trails are subject to photobleach correction. Due to a combination of factors (the compound phenol-red in cell culture media, high levels of autofluorescence in the monolayer of astrocytes and glia on which the neurons are plated, etc.) there is an unavoidable level of photobleaching inherent in these live imaging experiments. An example of this phenomenon may be seen in Figure 2, wherein the same point on the image yields a significant reduction (~30%) in fluorescence measured in arbitrary units (a.u.) when comparing frames taken at the start and end of a 60s imaging session. The function ‘bleach_correct_func’ was constructed to automate the task of photobleach correction (see Function 1 in supplemental material). This function receives as input a matrix of raw data pulled directly from the ‘timeseries’ ImageJ plugin used in the initial analysis steps. As the first 4 columns of the resulting matrix do not carry information regarding the synaptic ROIs image in that experiment, the bleach corrector function first creates a separate variable containing columns solely related to synaptic ROIs (termed ‘data_act’). All rows from this dataset are then averaged, and the resulting mean synaptic timecourse (‘mean_data’) is then plotted to provide the user an account of the raw data trace (Figure 3, top panel, ‘synaptic raw data’). The bleach corrector function next uses information regarding background photobleaching (taken as the fluorescence timecourse from a non-synaptic ROI placed in a background region of the imaging field) to construct a photobleach decay curve (Figure 3, middle panel, 'bleach timecourse and curve fit'). The general strategy was to fit a polynomial function to the fluorescence decay timecourse provided by the non-synaptic ROI and then subtract these values from each point in the synaptic ROIs in the dataset. The success of the strategy can be seen by comparing the top and bottom panels in Figure 3. Note that in the top panel, the stimulus-induced increase in fluorescence is imposed on an overall downward slope in fluorescence levels. The bottom panel, in contrast, shows a stable baseline, characteristic stimulus-induced increase in fluorescence and stable return roughly to baseline levels by the end of the trial. Occasionally the background ROI selected to provide information regarding the general photobleaching trend for a given trial will be contaminated by increases in fluorescence emanating from nearby synaptic regions. The resulting decay curve will contain a stimulus artifact which obstructs proper curve fitting (see top panel of Figure 4). To overcome this artifact, a linear interpolation was fit between the timecourse points immediately preceding and following the stimulus bout (occurring from 5 – 20 seconds in the trail). These interpolated points were then introduced in place of the artifactual points in the bleach decay curve. Note the difference in curve fit between the uncorrected (top panel) and artifact-corrected (bottom panel) bleach decay curves in Figure 4.

After correcting for photobleaching, experimental trails are subject to two forms of normalization: normalization to baseline levels of fluorescence, or normalization to peak levels of fluorescence. Each of these normalization strategies serves a particular purpose. Baseline normalization is useful for comparing differences in the peak intensity and rate of change in pHluorin signal intensity induced by the stimulus train. Higher peak levels and faster rate of fluorescence change are generally thought to reflect changes in vesicular release probability, a fundamental aspect of presynaptic function subject to several multifaceted forms of plasticity. The function ‘base_norm_func is utilized as part of the phluorin_group_collect script, and subtracts the value of baseline fluorescence (established as the mean of the 10 frames directly proceeding onset of stimulus train) from each point in the time series. The results of a baseline normalized experimental trail can be seen in Figure 5, with DF/F0 in the y axis representing the change in fluorescence levels at each time point compared to fluorescence levels at time 0. Once the data has been baseline normalized, relevant features are then extracted for additional analysis including average peak values for each experimental group, as well as average rate of exocytosis, defined as the slope of the line starting from stimulus onset to peak change in fluorescence levels (see Figure 6 for illustration of this analysis for two experimental groups). These features are extracted and plotted alongside the combined timecourse for each experimental group by using the function entitled ‘phluporin_graph_func’. An example of the result of applying this function to a set of four experimental groups can be seen in Figure 7.

Parallel to baseline normalization, the resulting dataset from photobleach correction is also subject to peak normalization, wherein each trial is normalized such that the baseline levels of fluorescence is defined as 0 while peak levels of fluorescence is defined as 1 (see Function 3 ‘peak_norm_func’ in supplemental material). This is not particularly useful for comparing overall changes in exocytosis levels, but can potentially be used to provide information about changes in endocytosis, which is the process of vesicular reassembly and repositioning after a membrane fusion event. Because the fluorescence signal of pHlouorin depends fundamentally on the slightly acidic environment of the intravesicular lumen, changes in fluorescence back to baseline levels after cessation of the stimulus train can be used to provide information about changes in the endocytotic machinery. Tau values for endocytosis are generally accepted to be the point at which fluorescence levels retune to ~37% of peak levels. Proper comparison between groups, however, required normalizing each experimental condition to its own max fluorescence levels, which is achieved by the peak_norm_func. Figure 8 shows the same data set used for baseline normalization in Figure 5, now subject to peak normalization. After peak normalization, a double exponential decay curve is fit to the region following stimulus offset and continuing to the end of the imaging session. Tauendo values are calculated for the mean peak normalized trace for each experimental condition and plotted. An example of this analysis strategy for determining tau values for endocytosis for on ‘control’ trail can be seen in Figure 9. The comprehensive endocytosis plot created by the function entitled phluorin_endograph_func, containing mean peak normalized timecourses, extracted endocytosis subsections for the timecourse with labeled tau values, as well as tau values represented as text can be seen in Figure 10.

A2.4 Discussion

In a given experimental run for these types of live imaging experiments, the number of synapses imaged in a given trial may range from 25 to 150. Thus by imaging at an acquisition frequency of 5Hz for a period of 60s, a single imaging session can yield a data set between 7,500 and 45,000 unique data points. When all experiments of a group are concatenated into a single file, the size of the data set becomes even more intimidating. For example, the experimental “Control” group shown in Figure 7 contained timecourse data for 750 synapses, resulting in a dataset containing 225,000 points. The size and iterative nature of certain aspects of the analysis involved in these experiments (normalization, correction, averaging, plotting) is ideally suited to some degree of automation using Matlab, as has been demonstrated. Comparison between the automated analysis performed using the functions and script described in this text were remarkably similar to results from manual analysis performed on the same data set (manual analysis not shown), confirming the efficacy of the automation for use in future experiments. Differences between analysis performed using the automated process described here and manual analysis performed previously are potentially due to particular aspect of the photobleach correction process. The stimulus artifact correction shown in Figure 5 was not performed in the manual analysis, which limited the goodness-of-fit able to be applied to the bleach decay curve. Additionally, unlike the manual analysis performed previously, the bleach decay curve used in the automated analyses described here was fit with a 6th degree polynomial, which was empirically determined to yield optimal results. The most salient effect of these features is that the baseline period in the 5s prior to stimulus train onset is notably more flat and stable than it appears after manual analysis.

As it currently stands, some degree of manual processing appears unavoidable for these experiments. For instance, though the act of determining active number of synapses proceeds very quickly using the ‘diffimage’ plugin tool for ImageJ, actual selection of synaptic ROIs requires user input to define each region. Some attempts have been made to automate this process using tools in the ImageJ suite, though none have been satisfactory. Future use of matlab for imaging analysis in these experiments might be well suited to defining regions of high signal intensity compared to surrounding regions, which could in principle be used to define active synaptic puncta. In addition, automatic statistical comparison between experimental groups is not currently a feature of the automation process described here. Future efforts will be made to include this feature as part of the automated workflow. Finally, though the process described here is extremely effective in automating data analysis for the set of experiments they were designed for (imaging at 5Hz, 60s experiment duration, 10s stimulus, stim train onset at 5s, etc), the code is not robust with respect to altering any of the experimental parameters. In order to facilitate ease of use in other types of experiments (as well as by other members of the imaging community), future versions will ideally include user-defined input variables that will allow a greater range of experimental conditions to be processed and analysed.

A2.5 Conclusion

In sum, optical readouts of presynaptic function such as the use of pH-sensitive variants of GFP used to vesicular proteins have promoted significant progress in our understanding of basic presynaptic function over the past decade. Automation of the large datasets acquired from such experiments not only saves the experimenter valuable time, but provides more biologically accurate depictions of the data, particularly through the use of the enhanced photobleach correction features described above. Additional work is needed to make the automation described herein as user friendly as possible, but this initial work was completely successful in accomplishing the predetermined goal of largely automated analysis of synaptic data acquired from live imaging experiments.

A2.6 Bibliography

Chua JJ, Kindler S, Boyken J, Jahn R. The architecture of an excitatory synapse. J Cell Sci. 2010 Mar 15;123(Pt 6):819-23.

Dreosti E, Lagnado L. Optical reporters of synaptic activity in neural circuits. Exp Physiol. 2011 Jan;96(1):4-12.

Jahn R, Fasshauer D. Molecular machines governing exocytosis of synaptic vesicles. Nature. 2012 Oct 11;490(7419):201-7

Jakawich SK, Nasser HB, Strong MJ, McCartney AJ, Perez AS, Rakesh N, Carruthers CJ, Sutton MA. Local presynaptic activity gates homeostatic changes in presynaptic function driven by dendritic BDNF synthesis. Neuron. 2010 Dec 22;68(6):1143-58.

Katz B. Quantal mechanism of neural transmitter release. Science. 1971 Jul 9;173(3992):123-6.

Kim SH, Ryan TA. CDK5 serves as a major control point in neurotransmitter release. Neuron. 2010 Sep 9;67(5):797-809

Pakkenberg B, Pelvig D, Marner L, Bundgaard MJ, Gundersen HJ, Nyengaard JR and Regeur L. Aging and the human neocortex. Experimental Gerontology. 2003, 38(1-2):95-9.

Shepherd GM, Erulkar SD. Centenary of the synapse: from Sherrington to the molecular biology of the synapse and beyond. Trends Neurosci. 1997 Sep;20(9):385-92.

Waites CL, Garner CC. Presynaptic function in health and disease. Trends Neurosci. 2011 Jun;34(6):326-37.

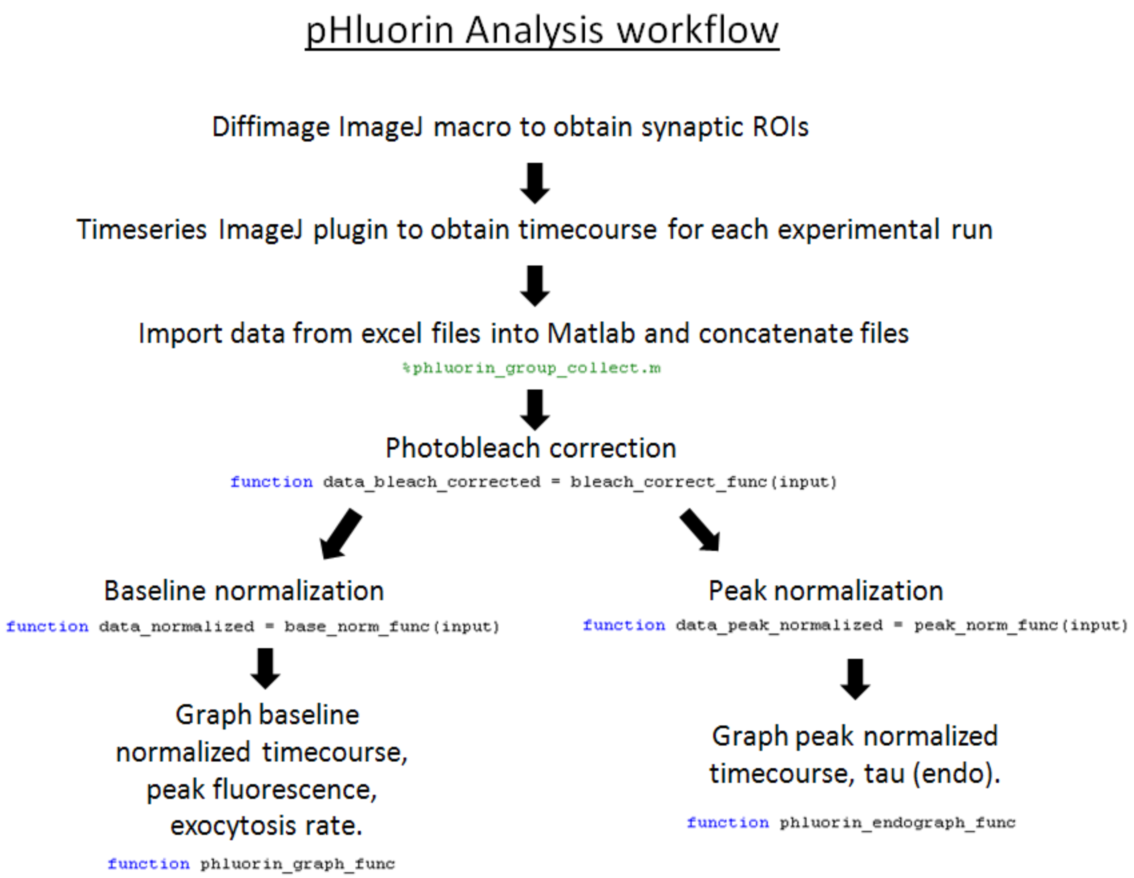
pHluorin Analysis workflow
Diffimage ImageJ macro to obtain synaptic ROIs
Timeseries ImageJ plugin to obtain timecourse for each experimental run
Import data from excel files into Matlab and concatenate files
Photobleach correction
Baseline normalization
Peak normalization
Graph baseline normalized timecourse, peak fluorescence, exocytosis rate.
Graph peak normalized timecourse, tau (endo).

```
%phluorin_group_collect.m
function data_bleach_corrected = bleach_correct_func(input)
function data_normalized = base_norm_func(input)
function data_peak_normalized = peak_norm_func(input)
function phluorin_graph_func
function phluorin_endograph_func
```

Figure A2.1: Workflow of imaging analysis

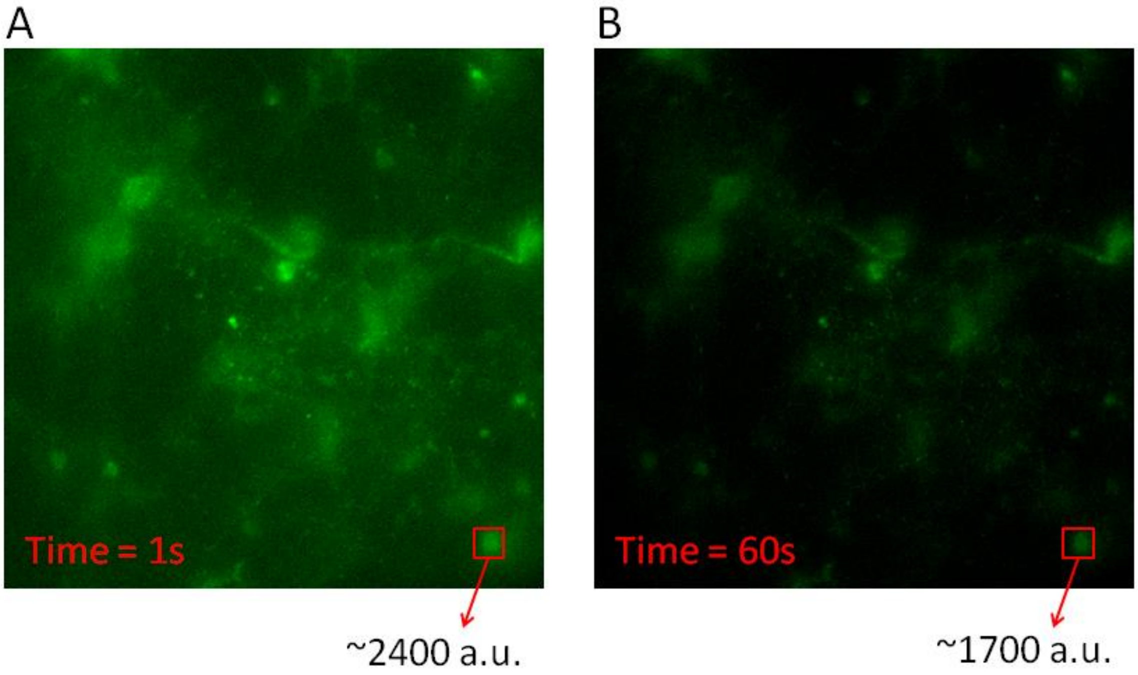
A
B
Time = 1s
Time = 60s
~2400 a.u.
~1700 a.u.

Figure A2.2: Example images of photobleaching apparent over a single 60s imaging session

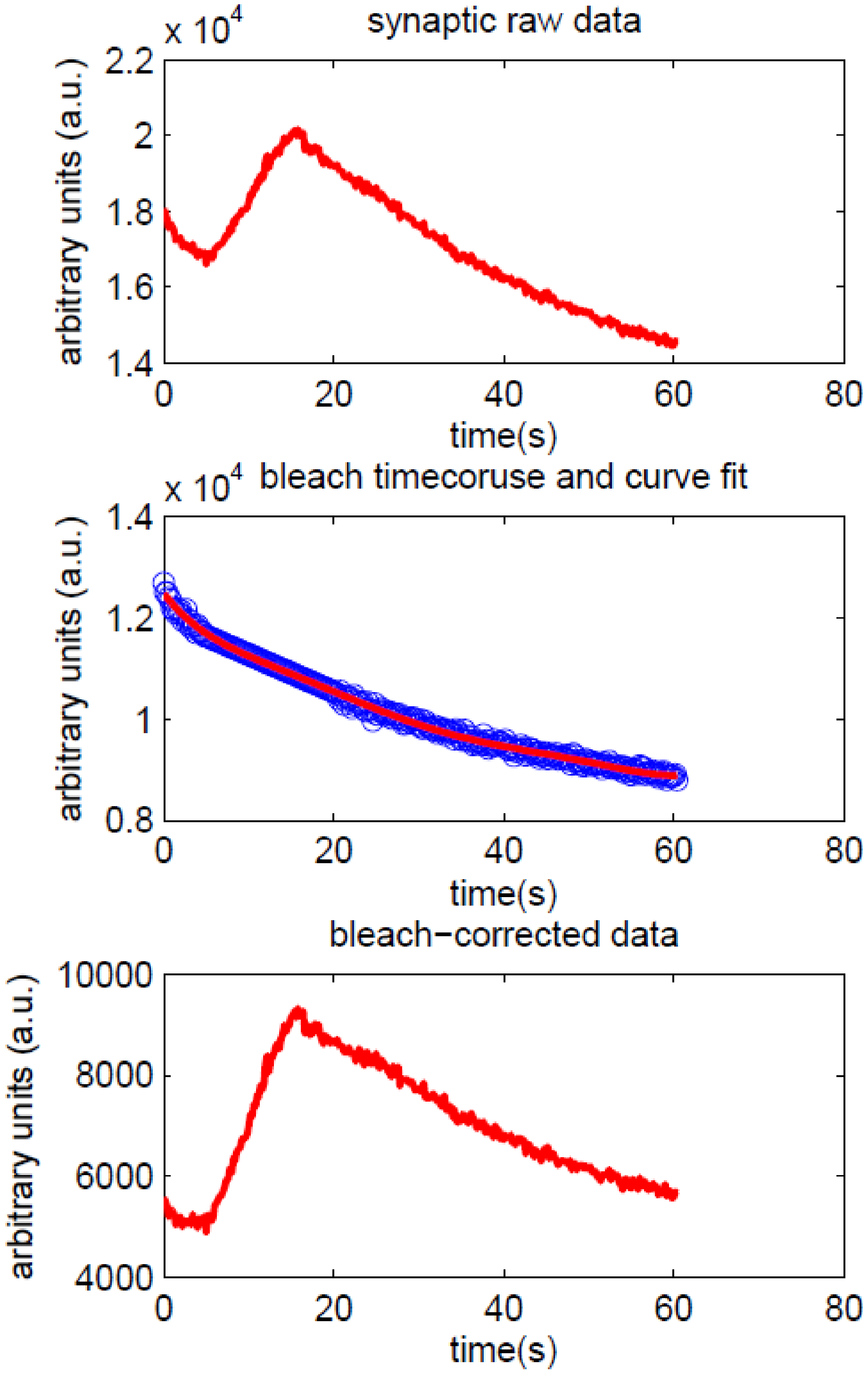

Figure A2.3: Example of plot produced by the function 'bleach_correct_func'.

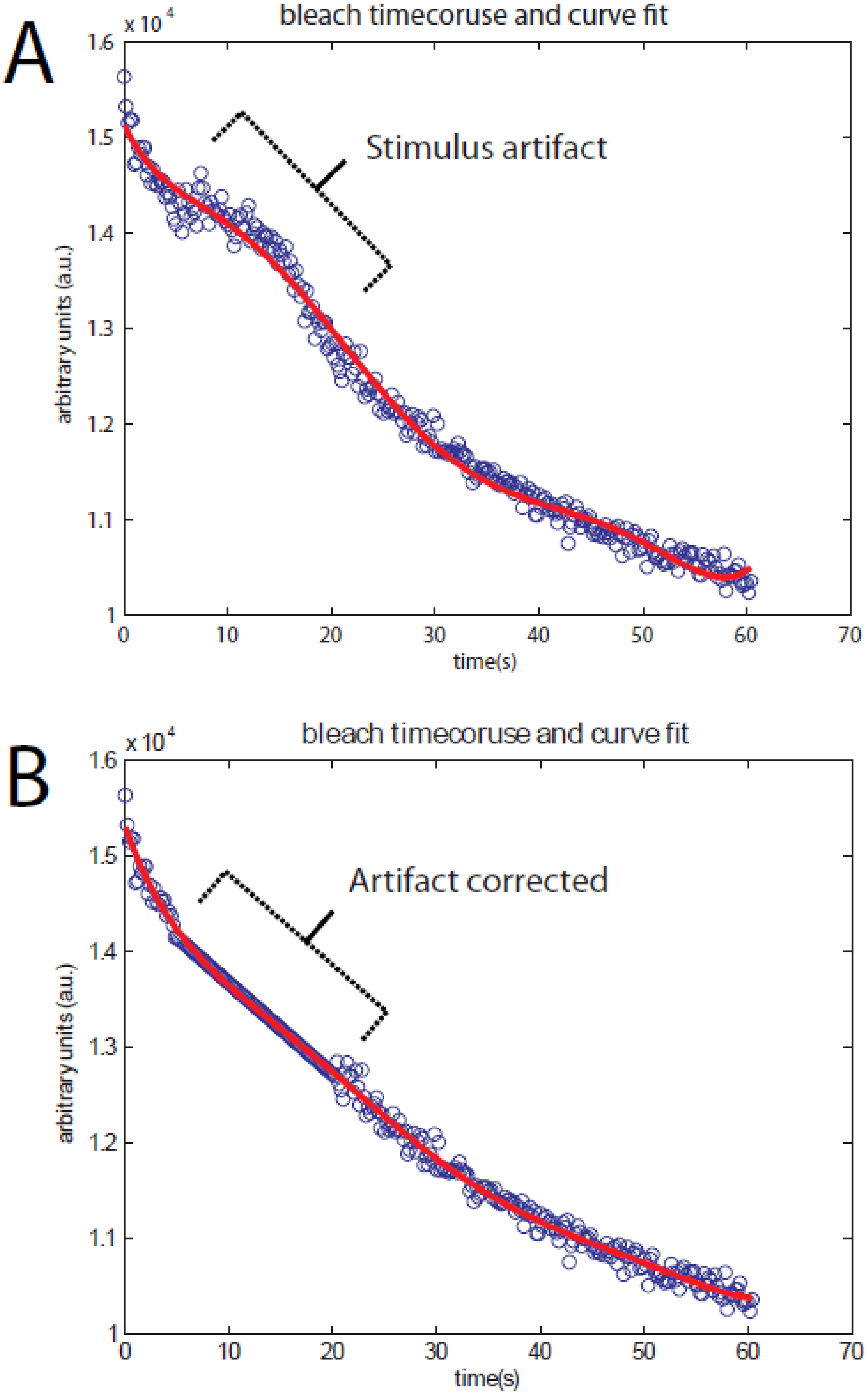

Figure A2.4: Comparison of artifact-corrected and uncorrected photobleaching timecourses.

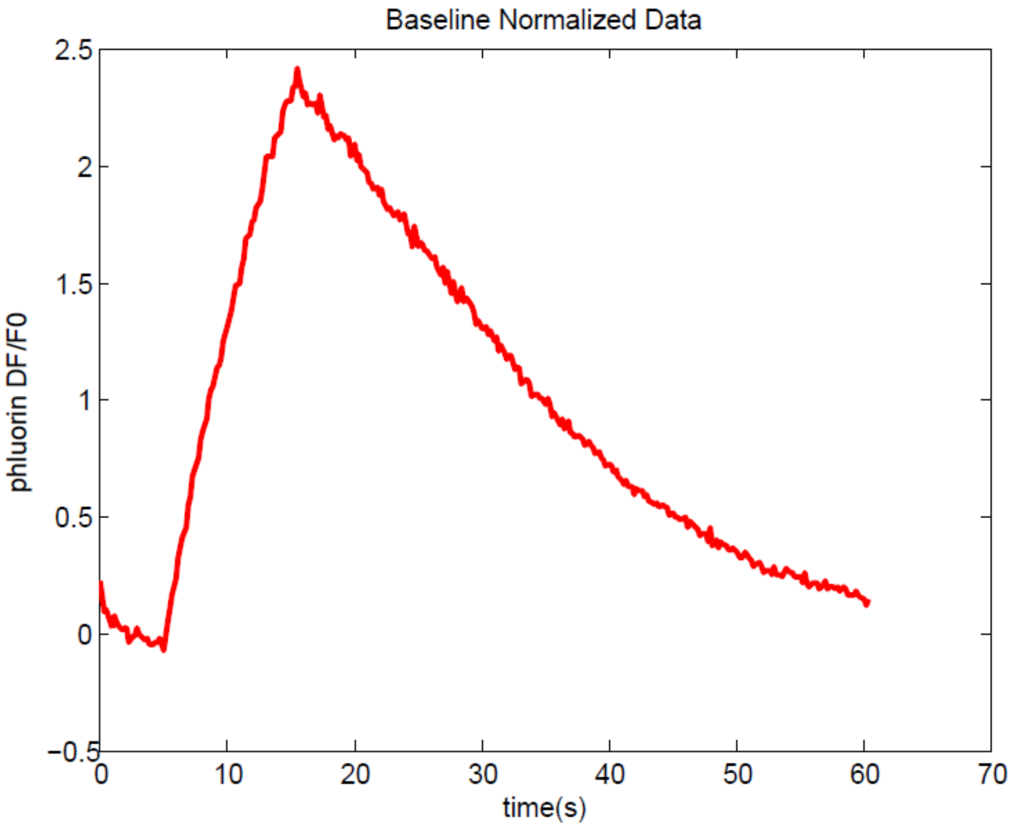

Figure A2.5: Example of plot produced by the function 'base_norm_func'.

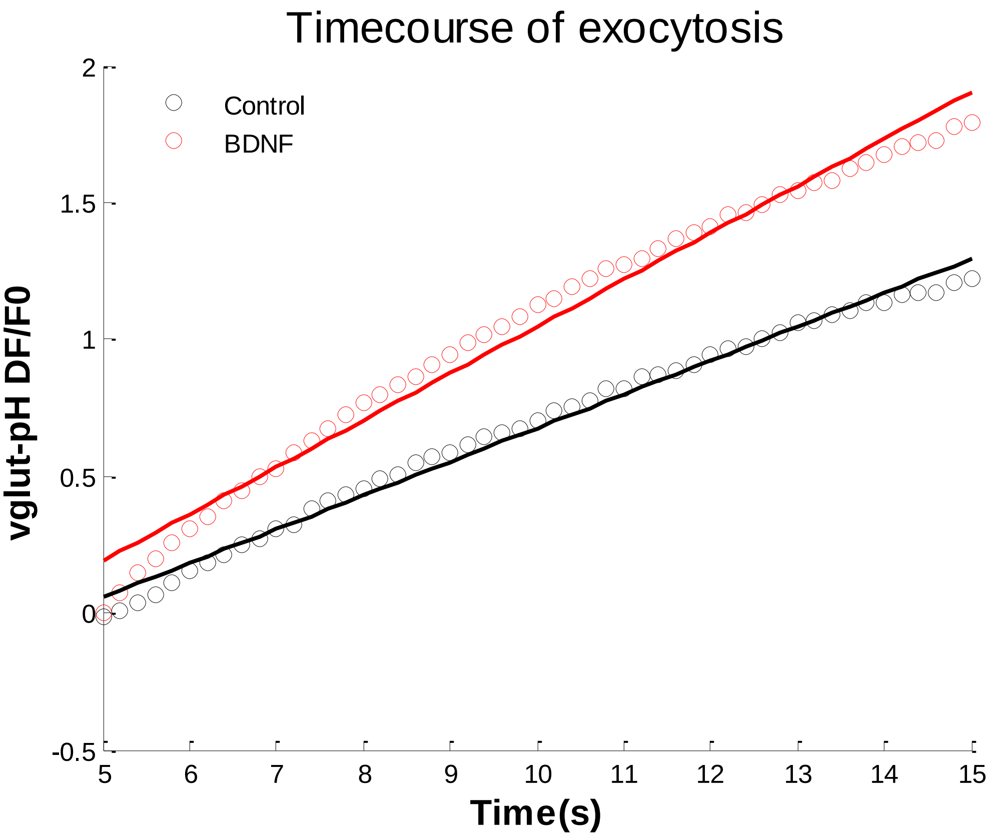

Figure A2.6: Illustration of process used to determine rate of exocytosis

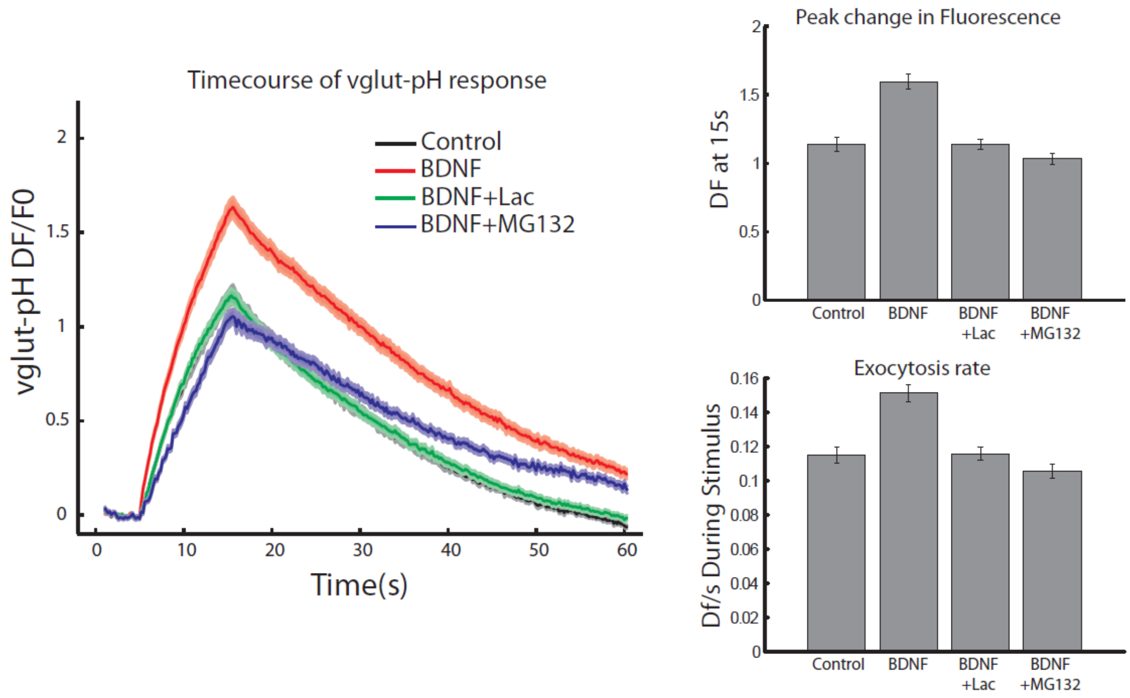

Figure A2.7: Example of plot produced by the function 'phluorin_graph_func'.

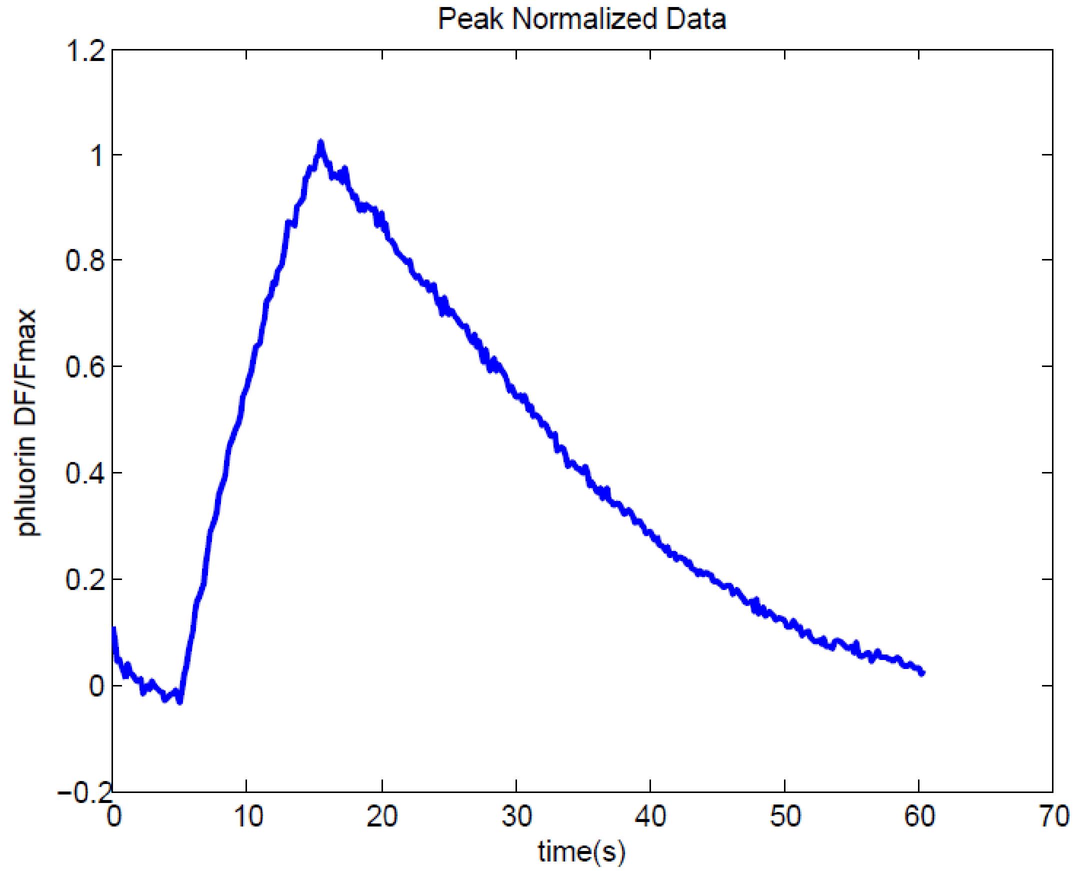

Figure A2.8: Example of plot produced by the function 'peak_norm_func'.

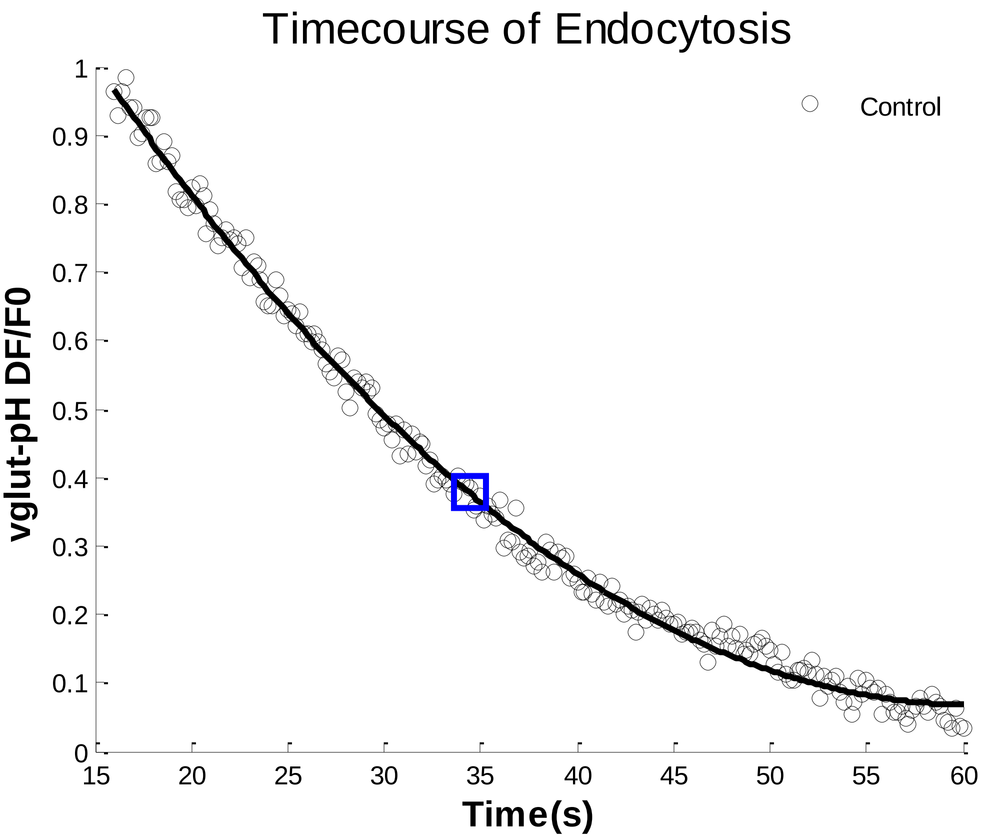

Figure A2.9: Illustration of process used to determine tau values for endocytosis

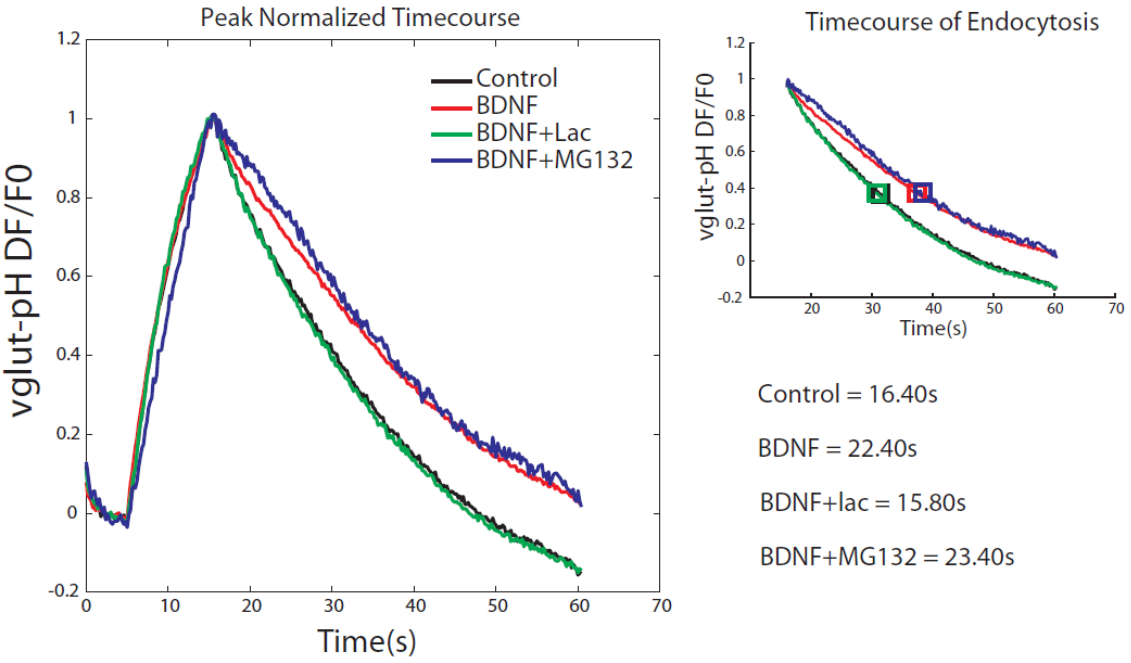

Control = 16.40s

BDNF = 22.40s

BDNF+lac = 15.80s

BDNF+MG132 = 23.40s

Figure A2.10: Example of plot produced by the function ‘phluorin_endograph_func’.